2017

Seismic design study of concentrically braced frames with and without buckling-controlled braces

Seyedbabak Momenzadeh
Iowa State University

Seismic design study of concentrically braced frames with and without buckling-controlled braces

by

Seyedbabak Momenzadeh

A dissertation submitted to the graduate faculty

in partial fulfillment of the requirements for the degree of

DOCTOR OF PHILOSOPHY

Major: Civil Engineering (Structural Engineering)

Program of Study Committee:
J. Jay Shen, Major Professor
Jon M. Rouse
Behrouz Shafei
Jeramy C. Ashlock
Alan Russell

Iowa State University

Ames, Iowa

2017

DEDICATION

This study is dedicated to my mom and dad who have always been supportive even when I decided to pursue my education thousands of miles away from them. I could not have made any accomplishments if it was not for their endless sacrifices.

TABLE OF CONTENTS

NOMENCLATURE

AISC	American Institute of Steel Construction
ASTM	American Society for Testing and Materials
BC	Buckling Controller
BCB	Buckling-Controlled Brace
BCBF	Buckling-Controlled Braced Frame
BR	Buckling-Restrainer
BRB	Buckling-Restrained Brace
BRBF	Buckling-Restrained Braced Frame
CBF	Concentrically Braced Frame
CHS	Circular Hollow Section
FE	Finite Element
FEM	Finite Element Method
FEMA	Federal Emergency Management Agency
HSS	Hollow Structural Section
MF	Moment Frame
ODR	Overall Drift Ratio
RHS	Rectangular Hollow Section

SCBF	Special Concentrically Braced Frame
SDR	Story Drift Ratio
SMRF	Special Moment Resisting Frame
TSXBF	Two-Story X-Braced Frame

ACKNOWLEDGEMENTS

I would like to express my sincere gratitude to my adviser, Dr. Jay Shen, who provided me with the opportunity to join his research group and patiently advised me throughout all the stages of my Ph.D. research.

I also want to thank Dr. Onur Seker for mentoring me in my research. I am always grateful for his support and encouragement in various circumstances.

Special thanks to the faculty members who served on my committee: Dr. Rouse, Dr. Shafei, Dr. Ashlock, and Dr. Russel.

This research is partially supported by the American Institute of Steel Construction (AISC) and Iowa State University (ISU). The opinions expressed in this study are solely those of the author and do not necessarily reflect the views of AISC, ISU, or other agencies and individuals whose name appear in this document.

ABSTRACT

Special concentrically braced frames (SCBFs) have become more popular as lateral load resisting systems after disappointing performance of special moment resisting frames (SMRFs) in the 1994 Northridge earthquake. SCBFs dissipate earthquake energy through buckling of compressive braces and yielding of tensile braces. V-type, inverted V-type, and two-story X-bracing are three major categories of SCBF bracing configurations. According to the current design approach implemented in AISC 341-10, beams and columns in SCBFs shall be designed based on the capacity of the braces to keep the beams and columns in the elastic region. However, a limited number of studies have shown that braced-intersected girders in two-story X-braced frames do not always remain elastic during an earthquake, violating current design code assumptions. Inelastic behavior in girders is due to the unsymmetrical cyclic behavior of the braces that creates a considerable unbalanced force. In an attempt to achieve symmetrical behavior, buckling-restrained braces (BRBs) superior to conventional braces in terms of ductility and cyclic behavior have been developed, but the majority of the developed BRBs are relatively complex and costly, resulting in hesitancy in the engineering community to accept them as a proper substitute for conventional braces. The present study is intended to investigate whether SCBFs designed based on current design codes meet the current design codes requirements. A newly developed buckling-controlled brace (BCB) is also introduced and the effect of such braces on the seismic demand of SCBFs is studied. For this purpose, three SCBFs with different beam sizes and bracing configurations were designed in accordance with current design codes and a group of earthquake ground motions was applied to them to investigate their seismic responses. Conventional braces of these frames were also replaced with BCBs to evaluate the influence of the new developed

braces on the seismic response of the SCBFs. The results point out that girders and columns in TSXBFs yield under earthquake ground motions, while they are designed for the capacity of the braces and are expected to remain elastic. In addition, SCBF seismic demand is substantially reduced by replacing the conventional braces with BCBs, so it seems that BCBs would be a suitable substitute for conventional braces.

CHAPTER 1. INTRODUCTION

1.1. Background

Special moment resisting frames (SMRFs) were among popular lateral load resisting systems that had been broadly used before 1994, but severe damage observed after the 1994 Northridge earthquake and the 1995 Hyogo-ken Naubu (Kobe) earthquake caused the engineering society to be hesitant to use this type of system. After the discouraging SMRF performance, concentrically braced frames (CBFs) became more popular to engineers. Because of the more stringent requirements and restrictions now required for SMRFs, heavier beams and columns must be used in these systems, resulting in complex connection details and high labor costs. Conversely, special concentrically braced frames (SCBFs) are relatively easy to construct and cost-effective, making them advantageous over SMRFs. SCBFs are lateral load resisting systems that dissipate earthquake energy through buckling of compressive braces and yielding of tensile braces. V-type, inverted V-type (chevron) and X-type were three different bracing configurations that were commonly used in SCBFs, but X-type gradually became a rarely-used bracing type because of its additional connection costs. On the other hand, seismic design of brace-intersected girders in V-type and chevron frames usually led to deep girders that were also not desirable, so in an attempt to reduce girder size, engineers have been using two-story X-bracing systems that consist of V-type and inverted V-type bracing in alternating stories. As a result, V-type, inverted V-type and two-story X-bracing, shown in Figure 1, are the three major categories of bracing configuration currently used in SCBFs. During the past two decades, while extensive studies have been performed on the seismic behavior of the SCBFs, with the majority of these studies focused on the behavior of the braces, investigations regarding the beams and columns have been scattered and

scarce, even though study of the performance of braces, beams and columns that interrelate with one another as single systems seems necessary and important.

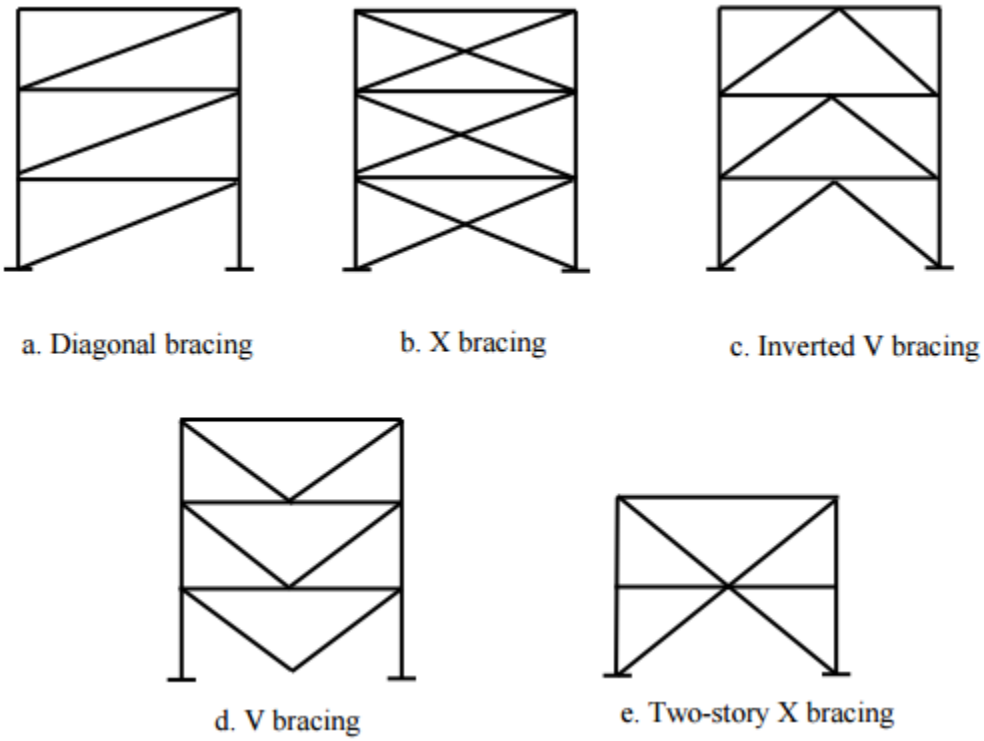

Figure 1: Typical Bracing configurations in SCBFs.

According to the AISC 341-10 [AISC, 2010], beams and columns must remain elastic during an earthquake. To fulfill this requirement, the demand in these members are calculated by three structural analysis cases, and the most critical one should be chosen for the design. Although it may have seemed sufficient to use current criteria to design the SCBFs, recent research has shown that a more thorough study is required to develop a better understanding regarding the demand in SCBFs [Uriz and Mahin, 2008].

1.2. Motivation

SCBFs have been widely used around the world, especially in the aftermath of the 1994 Northridge earthquake. Damages observed in such frames in past earthquakes, such as the 1985 Mexico [Osteraas and Krawinkler, 1989], the 1989 Loma Prieta [Kim and Goel, 1992], the 1994 Northridge [Tremblay, et al., 1995; Krawlinkler, et al., 1996] and the 1995 Hyogo-ken Naubu (Kobe) [AIJ/Kinki Branch Steel Committee, 1995; Hisatoku, 1995; Tremblay, et al., 1996], warned engineers to use caution in utilizing such systems. Figure 2 shows a fracture in a column that was initiated in the flange and developed further into the web during the Hyogo-ken Nanbu (Kobe) earthquake in 1995.

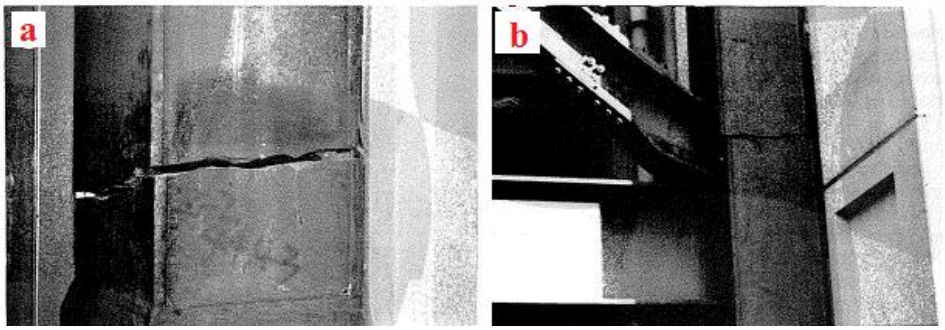

Figure 2: Column fracture in Hyogo-ken Nanbu (Kobe) earthquake (Tremblay et al., 1995).

To restore the confidence of engineers in using SCBFs, procedures specified in design codes have been changing over the past decades. According to the latest design code [AISC 341-10], braces should be designed as a "column" member to resist equivalent seismic forces calculated based on ASCE7-10. In addition, beams and columns must remain elastic and be designed based on the capacity of the braces. For this purpose, all tensile braces should be replaced by their expected tension capacity and all compression braces should be replaced by: 1) their expected buckling capacity; 2) their expected post-buckling capacity, as shown in Figure 3. The standard also states that braced frames must

be designed for the first mode loading pattern (Figure 4) and all tension and compression braces would reach their capacity simultaneously, even though recent studies have shown that this loading pattern is only one of the multiple possible patterns that might occur and the one chosen represents an optimistic case for frame design [Shen, et al., 2014]. In addition, according to AISC 341, even though designers are permitted to neglect the bending moment in the columns that should be designed under a compression force derived from structural analysis of the frame at the governed case, studies have demonstrated that flexural demand in columns caused by non-uniform story drifts [Koboevic and Redwood, 1997; Sabelli et al., 2003] would have a substantial effect on frame behavior and it is not safe for it to be neglected.

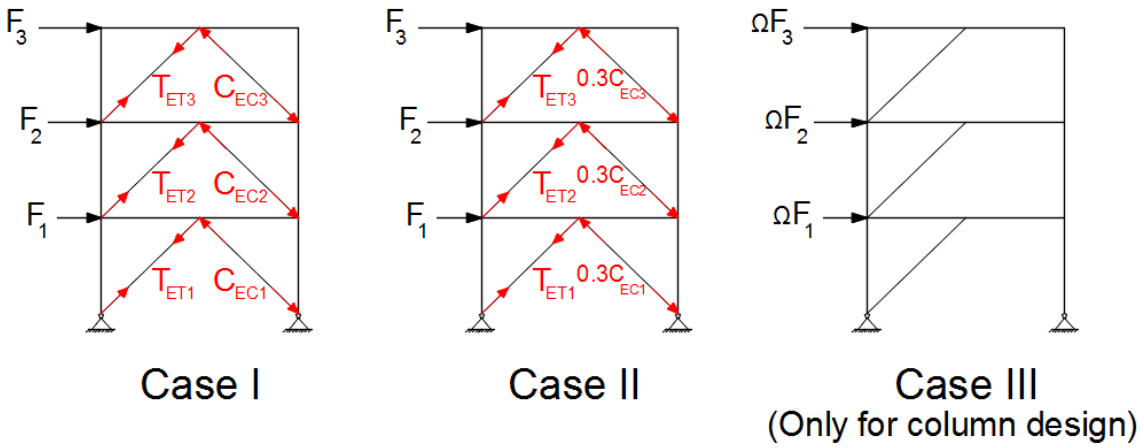

Figure 3: Three analysis cases.

In Figure 3:

T_{ET}: Expected tensile capacity of the braces.

C_{EC}: The smaller of {T_{ET}, 1.14×expected compression capacity of the braces}.

Ω: Over strength factor which can be considered equal to 2 for SCBFs [ASCE7-10].

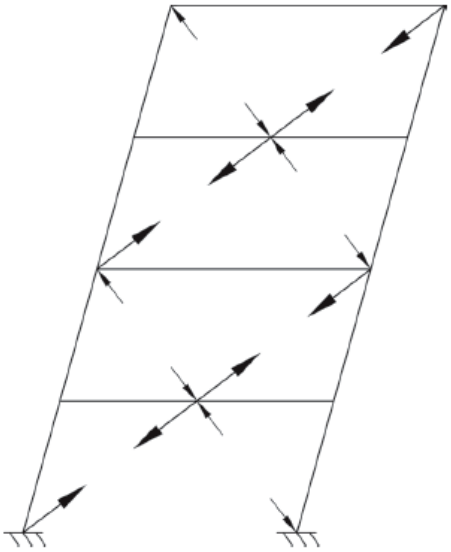

Figure 4: Anticipated braced frame mechanism (AISC341-16).

In summary, it seems that there are still some issues in SCBFs that should be addressed:

- Previous experimental studies on SCBFs have shown that columns are susceptible to fracture at about 2.8% story drift ratio (SDR) [Uriz, 2005; Uriz and Mahin, 2008]. This is an issue of special concern because of the fact that columns are the most important members in a frame. The premature fracture described earlier was mainly due to the shortage of knowledge regarding the column demands.
- Although extensive research has been carried out on inelastic behavior of steel braces, the effect of brace performance on column demand is still unclear. It is also worth mentioning that braces in different configuration have different effects on column demand. Since the evaluation of these effects is missing in the current literature, this study aims to cover these issues.

- While researchers have previously used pin beam-to-column connections in their simulations for studying the behavior of braced frames, the rigidity of these connections have a direct impact on the bending moment transferred from beam to column, so the connection type will have a significant effect on the column demand and there is a need to evaluate whether or not the pin connection assumption is sufficiently accurate.

In addition to the above issues, despite the fact that engineers believed that the bending moment in the columns in SCBFs is negligible, premature column fracture in recent experimental studies have demonstrated that there is a considerable demand (flexural and axial) on the columns, especially after 1% SDR. Although empirical methods have been proposed to estimate flexural demands in columns in SCBFs [MacRae, et al., 2004], the relationship between the flexural demand on the column and brace behavior is still only vaguely known.

In conclusion, all the previously mentioned issues clearly indicate the necessity of a thorough study on the seismic demand of SCBFs.

1.3. Problem Statement and Objectives

Extensive and unexpected damages observed in various experimental studies [Uriz and Mahin, 2008; Lai and Mahin, 2010] demonstrate that, while SCBFs are useful as lateral load resisting systems, there are some inconsistencies in current design methods that may lead to severe damage to the frames. As mentioned earlier, various analysis cases required by AISC for designing SCBFs show that there are some issues in predicting the actual required axial force in the column

(P_r) and amendment to this provision seems inevitable. Moreover, substantial flexural demand on columns in SCBFs can result in their early fracture [Uriz and Mahin, 2008], mainly because of premature fracture of the braces and framing action that in turn may produce a substantial demand on the columns. The aforementioned complex behavior and tedious design procedures are mainly because of difficult to predict nonlinear behavior of the buckled braces.

Use of buckling-restrained braces (BRBs) has become popular among the engineers in recent years, mainly because of the large hysteretic loops exhibited by BRBs when compared with conventional braces. Buckling-controlled braces (BCBs) that perform similar to BRBs are bracing members newly-developed by the current research group. Preliminary analyses of BCBs have shown that they can be an effective substitute for conventional braces because of their stable and symmetrical cyclic behavior and cost-effectiveness. Although inelastic cyclic behavior of the isolated brace specimens has been experimentally and numerically studied, there remains a need for comparing the seismic demand of BCBFs with that of SCBFs, so there is a need to assess the influence of BCBs on the demand on the members used in SCBFs. In summary, the objectives of the present study are to:

- Assess the reliability of current design procedure for SCBFs and make recommendations for improving frame performance.
- Investigate the behavior of BCBs under different loading types to study the impact of different parameters on the overall response of the braces.
- Study the effect of the brace section on BCB performance.
- Assess the effect of beam strength and bracing configuration on the demands on members of SCBFs.

- Investigate the effect of incorporating the newly-developed BCBs on the seismic behavior of SCBFs.

1.4. Organization of the Dissertation

Chapter 2 provides an extensive literature survey related to (1) experimental tests on SCBFs; (2) analytical studies on SCBFs; (3) experimental and analytical studies on single isolated braces and brace ductility in SCBFs; (4) seismic demand on beams in SCBFs; (5) seismic demand on columns in SCBFs; and (6) experimental and analytical studies on buckling restrained braces and an introduction to buckling-controlled braces.

Chapter 3 presents an introduction to BCBs and effect of using different cross sections on the behavior of braces is assessed under both monotonic and cyclic loading. In addition, impact of the BCBs on the behavior of the SCBFs is studied through finite-element simulations.

Chapter 4 presents seismic response of a 9-story steel braced frame under twenty earthquake ground motions. Three different bracing configurations are studied and their performance is compared in terms of brace ductility and beam and column seismic demand. Moreover, influence of the strength of the brace-intersected beams on the seismic response of the SCBFs is investigated.

Chapter 5 presents the seismic response of SCBFs incorporating BCBs. Seismic behavior of a 9-story BCB-frame is compared with a conventional frame and effect of beam strength on BCBF response is evaluated using nonlinear dynamic analyses.

Chapter 6 presents the impact of the different loading patterns on the behavior of SCBFs. Four different loading patterns are extracted from the deformation of the 9-story frame simulated

in Chapter 4. The loading patterns are applied to a two-story X-braced frame and the beam and column response is studied through extensive finite-element simulations.

Chapter 7 summarizes the results obtained in this investigation and provides important conclusions. Recommendations for future studies related to the seismic behavior of steel braced frames are also discussed.

CHAPTER 2. LITERATURE REVIEW

2.1. Introduction

SCBFs have been among the most interesting lateral load resisting systems studied by structural researchers over the past two decades. Braced frames currently comprise about 40 percent of the buildings in California and the trend for their use is believed to be increasing [Chen, 2010]. Extensive experimental and analytical studies have been conducted on the performance of the braces [Tremblay, 2002; Lee and Bruneau, 2005; Yang and Mahin, 2005, Tremblay, et al., 2008, Fell, et al., 2009, Nip, et al., 2010], gusset plates [Roeder, et al., 2006; Chambers and Ernst, 2005, Roeder, et al., 2010] and frames [Khatib, et al., 1987; Tremblay, et al., 1995; Sabelli, 2000; Sabelli and Mahin, 2003; Tremblay, et al., 2003, Uriz and Mahin, 2008, Shen et al., 2014; Shen et al., 2015]. In this chapter, previous studies related to the present investigation are reviewed and necessary comments are made regarding these results. This chapter can be divided into five sections:

i. Studies on experimental tests on SCBFs.
ii. Analytical studies on SCBFs.
iii. Experimental and analytical studies of single braces and brace ductility in SCBFs.
iv. Seismic demand on beams in SCBFs.
v. Seismic demand on columns in SCBFs.
vi. Experimental and analytical studies on buckling-restrained braces.

2.2. Experimental tests on SCBFs

2.2.1. Experimental Test Carried out by Uriz and Mahin in 2008 at UC-Berkeley

A full-scale test on a chevron frame was carried out in 2001 by Uriz and Mahin at UC Berkeley. That test can be considered to be the starting point of an era in which researchers realized that full-scale tests were required for enhancing our knowledge regarding the behavior of structures, with this frame being one of the first tested full-scale steel frames. The frame was designed based on the AISC seismic provision 1997 and was comprised of two 9 ft stories and one 20 ft bay with chevron bracing in both of stories. Cyclic loading was applied to the roof through a loading beam as shown in Figure 5.

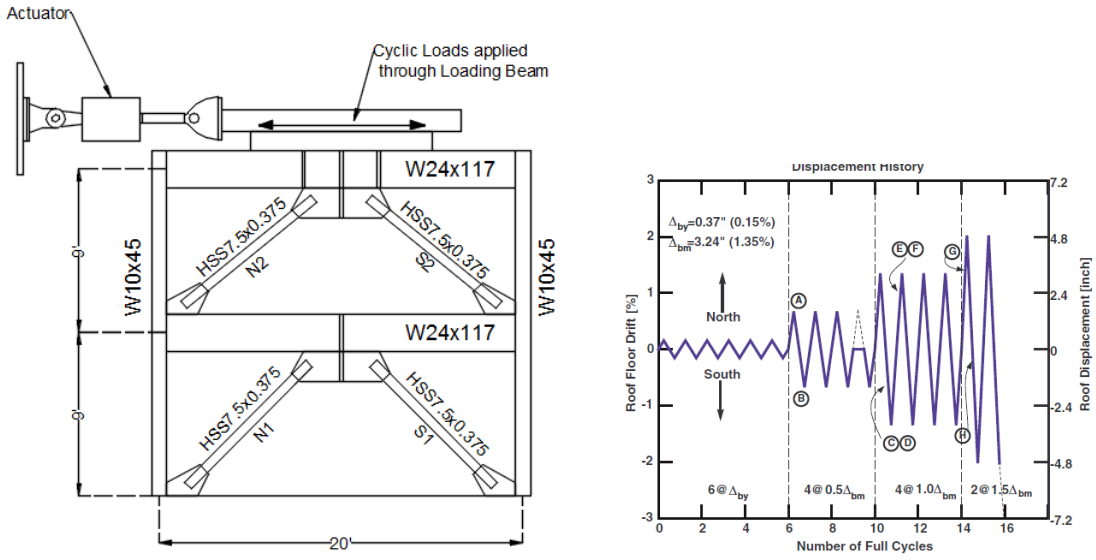

a) Elevation of the Tested Frame b) Loading Protocol

Figure 5: Tested frame by Uriz and Mahin (2008).

The key observations of this study can be summarized as follows:

- The first story braces began out-of-plane buckling at 0.67% overall drift ratio (ODR) and the deformation of the frame was concentrated in the first story, while the second story of the frame remained almost un-deformed. The ODR can be calculated by dividing the roof displacement of the frame-by-frame height.
- An early brace fracture occurred at 1.35% ODR, as can be seen in Figure 6 and, as a consequence, beams and columns contributed to resisting the applied load, leading to column fracture as well.
- It should be mentioned that the column used in this frame satisfies the requirements of the current design code (based on the calculations of the author) and the early fracture in the column (Figure 6) was mainly due to the unpredicted large demand on the column.

a) Fracture in the brace at 1.35% ODR b) Fracture in column at 1.35% ODR

Figure 6: Fracture at 1.35% ODR in Uriz and Mahin test (2008).

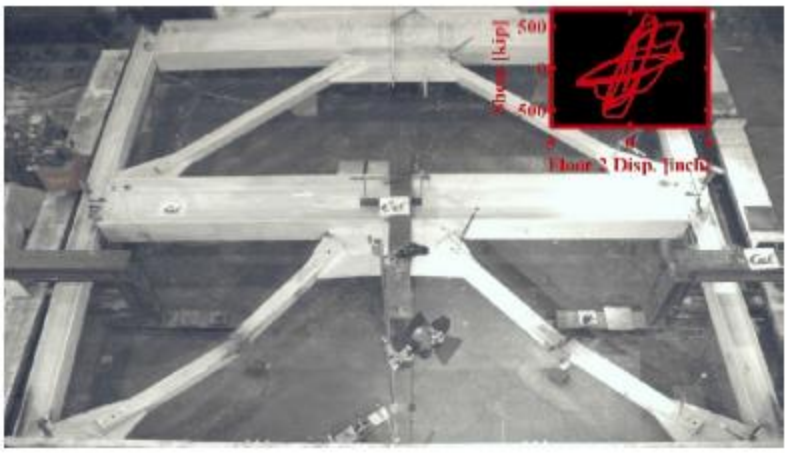

Figure 7: Deformation of the frame at the end of the test (Uriz and Mahin 2008).

2.2.2. Experimental Test Carried out by Lai and Mahin in 2013 at UC-Berkeley

A full-scale test on an SCBF was performed in 2013 in the UC-Berkeley laboratory by Lai and Mahin. A two-story steel frame with one bay was tested for four different brace sections, the first two of which are of interest in this study. The frame was constructed with a story height of 9 ft and a 20 ft spacing between columns. V-type braces were employed in the first story of the frames and inverted V-type braces were used for the second story. A linear lateral force was applied at the floor levels of the frame using two actuators at each level. Figure 8 shows the second specimen constructed in the lab.

Figure 8: Test specimen constructed in UC-Berkeley by Lai and Mahin in 2013.

The frame was designed according to the AISC seismic provisions [AISC 2005b] and ASCE-7 [2005]. Table 1 provides the member sizes used in this investigation.

Table 1: Member sizes used in experimental study by Lai and Mahin in 2013.

	First Story			Second Story		
	Columns	Beam	Braces	Columns	Beam	Braces
Specimen 1	W12x96	W24x68	HSS6x6x3/8	W12x96	W24x117	HSS5x5x5/16
Specimen 2	W12x96	W24x68	HSS6x0.5	W12x96	W24x117	HSS5x0.5

The experimental process was divided into several sets of loading steps, each consisting of two complete cycles except for the first loading step that had six complete cycles. Details of the loading sequence are presented in Figure 9.

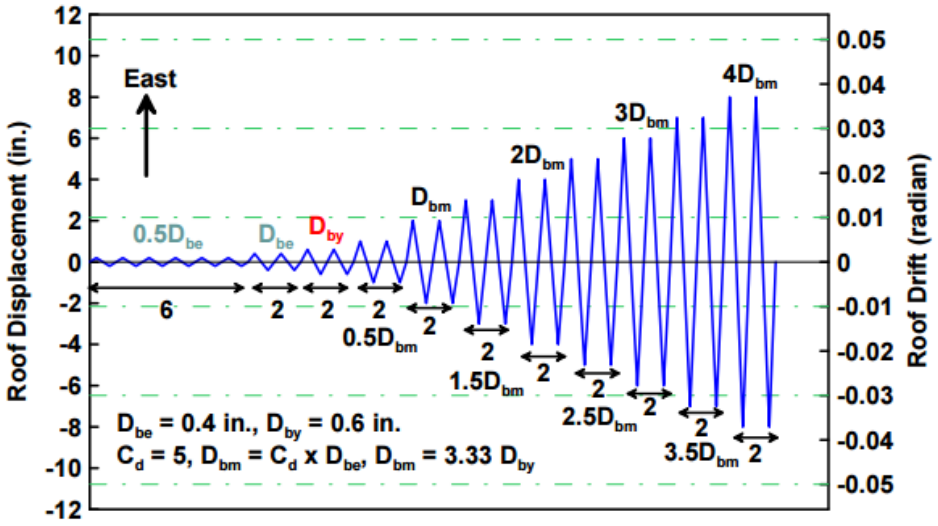

Figure 9: Loading sequence used in an experimental test by Lai and Mahin in 2013.

The key observations of this study can be summarized as follows:

- Braces in both of the specimens experienced out-of-plane global buckling in both stories at about 0.5% ODR.
- Local buckling at the end of the first story beam in both specimens was observed at 1.4% ODR, as can be seen in Figure 10a. It is worth mentioning that each beam in both of the stories in the tested specimens were required to be designed as a beam-column member in conformance with AISC 341-10, while neither beam used in these frames satisfied the compressive member compactness requirement defined by AISC341-10. The early local buckling in the beams could have been avoided if proper sections had been used.
- Square braces in the first story of the first specimen fractured at 1.9% ODR (Figure 10b), while no cracks were observed in the round braces used in the second specimen. It should be noted that, although the braces were properly working at this stage, the first-story beam in specimen 2 fractured at this drift value (Figure 10c). These results might have produced a major concern to the researchers because other studies have shown that drift demand in

the SCBFs might exceed even 4% with a 2% probability of exceedance in 50 years [Uriz 2005, McCormick et al. 2007].

- Columns in both of the specimens yielded at 1.4% ODR, with yielding in the top portion of the columns in specimen 1 and a vertical yielding line in the column in specimen 2 observed. Figure 11 presents the P-M interaction curves of the columns in the tested frames that clearly demonstrate that the columns yielded during the test. This is an important result for the current study because, as mentioned earlier, columns are required to remain elastic and should not experience any yielding during the earthquake. It seems that the seismic demand on the columns in SCBFs is somewhat underestimated in the current design code.

a) Local Buckling in top flange b) Brace Fracture c) Beam Fracture

Figure 10: Test results provided by Lai and Mahin (2013).

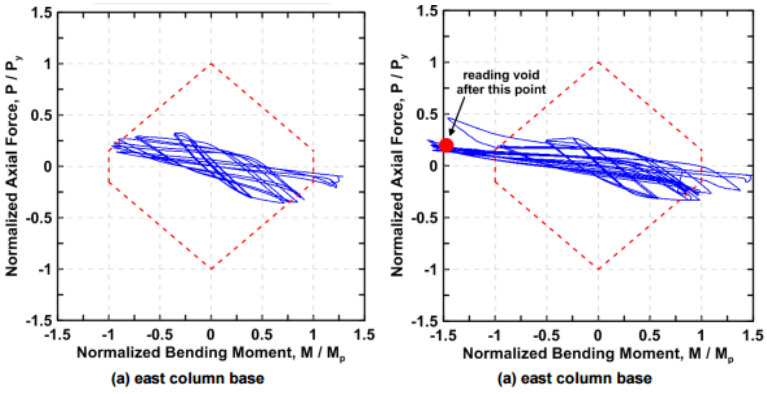

a) P-M Interaction in 1st Spec. b) P-M Interaction in 2nd Spec.

Figure 11: Column results provided by Lai and Mahin (2013).

2.3. Analytical studies on SCBFs

Shen, et al., (2015) carried out numerous dynamic time history analyses and finite-element based simulations to investigate the behavior of two-story X-braced frames. 6- and 12-story buildings were simulated in RUAUMOKO and 20 ground motions were applied to the frames. A two story X-braced frame was then simulated in ABAQUS. Based on their results, the following conclusions were drawn:

- The first-mode mechanism is an optimistic case to occur in the two-story X-braced frames, and it leads to design of shallow beams for braced-intersected beams, even though the current design code clearly states that SCBFs should be designed based on the first mode deformation, a recommendation that seems insufficient. Deformation of the simulated frame a under first-mode loading pattern is presented in Figure 12, and severe deformation in the second-story beam can be observed in this figure.

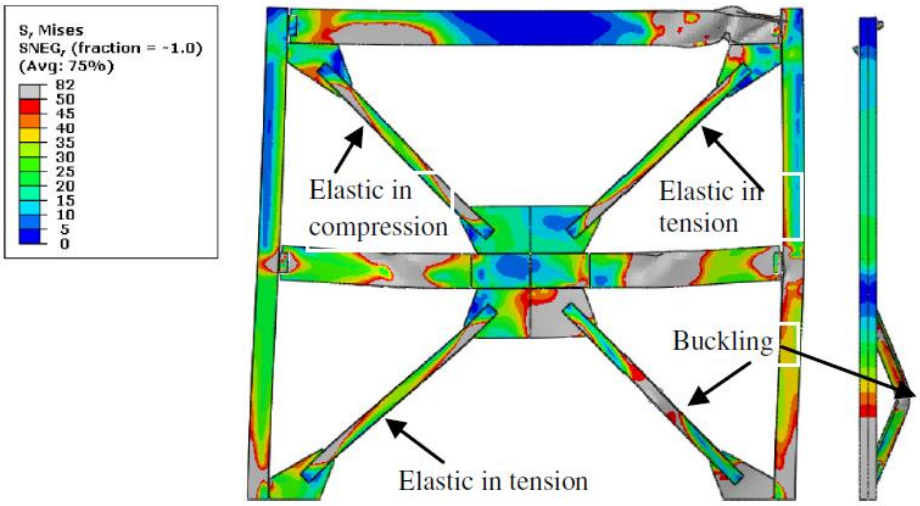

Figure 12: Deformation of the frame under first-mode loading pattern at 4% 1st SDR (Shen et al. 2015).

- Large inelastic vertical deflection occurs in the brace-intersected beams after the beam yields, inducing additional demand in the braces and connections. Because pin

connection performance in actual structures closely resembles that of rigid connections, it can be assumed that the additional demand in the connections will be transferred to the columns as well.

Kumar, et al., (2017) performed dynamic analysis in Perform-3D to study the seismic response of steel braced frames and they consequently proposed a new design approach taking into account the flexural demand on columns. They proposed three different limit states (P_1 through P_3) for braced-frame design, but it seems difficult to utilize this design approach in practice. In the first limit state, the frame should be designed according to the current design code and based on the member sections, critical axial force, and bending moment of each member can be achieved. Then, as a second try, based on the calculated forces, new sections would be designed. This method can be so time-consuming and it may need several attempts before the convergence is reached. In the third limit state, it is assumed that two plastic hinges will form at the top and bottom of each column and the columns would be designed based on their flexural capacity. Although this approach might be useful for lower stories in high-rise buildings, there is not sufficient information in that paper to determine how many stories should be designed based on this approach. It is obvious that this method will lead to over-designed sections in the top stories and that design will be too conservative. Another shortcoming of that study could be the sections used for the columns, with the proposed method leading to heavy sections such as W40×397, not practical for use in real structures. It therefore seems that a comprehensive research study is required to determine the demand on the columns in SCBFs and compensate for the aforementioned shortcomings.

2.4. Studies on brace ductility in SCBFs

Various studies have investigated the behavior of single braces under cyclic loading. Nip, et al., (2010) carried out an experimental test on 16 small HSS sections (HSS40x40 mm^2 and HSS60x60 mm^2). Based on the section size and length, brace ductilities varying from 4 to 10 were achieved in the test. Figure 13a shows the result of a test on the specimen for which the ductility was around 10. Brace ductility can be calculated by dividing the maximum axial displacement of the brace prior to fracture by the yielding displacement. It should be noted that brace ductility depends on different parameters such as section size, specimen length, etc. Regarding the fact that larger sections are usually used in real structures, the calculated ductility might not be applicable to practical cases. In an attempt to investigate the behavior of a more practical section, Fell, et al., (2009) performed an experimental test on eighteen braces in which seven cases out of eighteen were conventional HSS sections. They tested HSS4x4 sections that were still smaller than the braces usually used in the steel structures, but the slenderness ratio was roughly 77, close to that of the real braces. All the braces fractured at about 2.5% SDR (Figure 13b), similar to the test results provided by Uriz and Mahin (2008) and Lai and Mahin (2010).

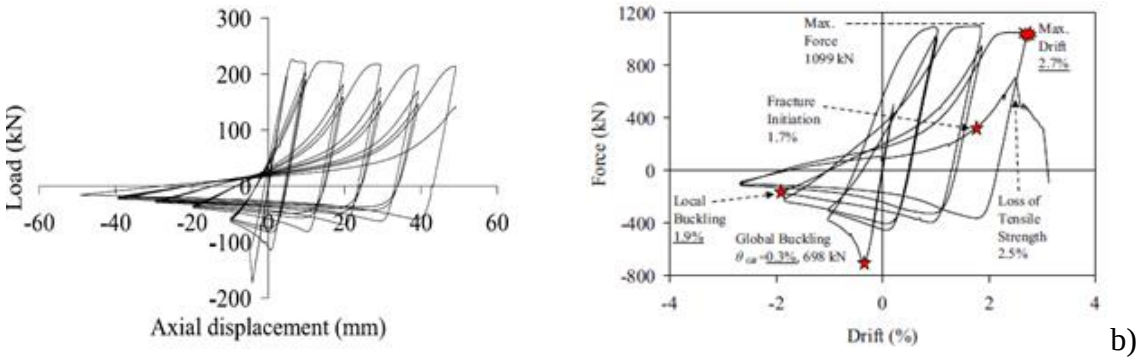

a) Nip et al. test (2010). b) Fell et al test (2009).

Figure 13: Experimental test results on HSS braces.

In 2008, an experimental test by Tremblay, et al., was performed on isolated single specimens in the Hydro-Quebed structural engineering laboratory at Ecole Polytechnique of Montreal. (2008). The importance of this study can be summarized in two observations: 1) they used large sections like those commonly used in steel structures; 2) unsymmetrical gusset plates were used in the test to reflect the authentic behavior of braces in a frame. Three rectangular hollow sections (RHS) and two circular hollow sections (CHS) were tested in this study and the following conclusions were made:

- The maximum SDR reached by the specimens were about 2%, as shown in Figure 14.
- By decreasing the width-to-thickness ratio of the section, fracture in the braces can be postponed.
- Both RHS and CHS specimens fractured before reaching the current SDR demand described in various studies [Uriz 2005, McCormick et al. 2007].

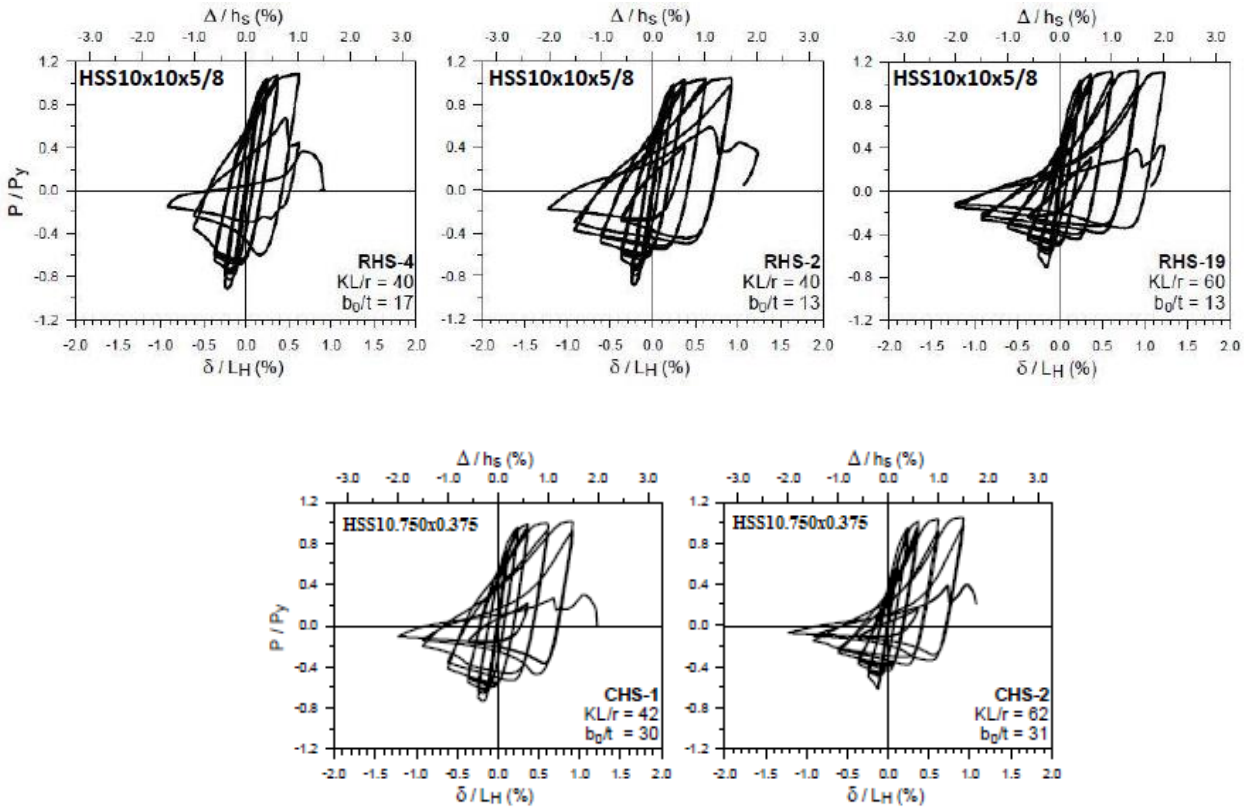

Figure 14: Specimens tested by Tremblay et al. (2008).

Table 2 summarizes the results of the studies related to peak brace ductility. As can be seen in this table, the maximum ductility capacity of HSS sections is about 10.

Table 2: Peak brace ductilities of the recently tested tubular bracings.

Item	Test ID	Brace Member (mm × mm × mm)	b/t or D/t	KL/r	Peak Brace Ductility (μ)*	Reference
1	S85-14	HSS100×100×6	13.7	85	10.00	Han et al. (2007)
2	HSS1-1	HSS102×102×6.4	14.2	77	8.90	Fell et al. (2009)
3	3B	HSS127×127×8.0	15.0	65	6.00	Shaback and Brown (2003)
4	2B	HSS152×152×9.5	12.1	52	7.00	
5	RHS19	HSS254×254×15	14.2	60	8.00	Tremblay et al. (2008)
6	RHS2	HSS254×254×15	14.2	40	6.00	
7	CHS2	HSS273×9.5	30.8	62	10.00	
8	CHS1	HSS273×9.5	30.8	42	8.50	
9	2050-CS-HR	HSS40×40×3	13.3	135	10.00	Nip et al. (2010)

*The given ductility ratios are estimated from the published plots.

2.5. Seismic demand on beams in SCBFs

Shen, et al., (2014) simulated six SCBFs in RUAUMOKO-2D to investigate seismic demand on brace-intersected beams. A 6- and a 12-story frame were simulated with two different types of bracing configurations (Two-story X-bracing (TSXBF) and chevron) to compare the beam demand in different types of frames. In addition, two different design approaches were used for each TSXBF, producing both a strong and a weak brace-intersected beam. The latter was designed based on current design codes and the former designed similarly to chevron frames. Incremental dynamic analyses (IDA) were performed on each frame under ten pairs of ground motions and the intensity of the ground motions were increased until peak SDR in the frame reached 6%. Key observations of that study can be summarized as follows:

- Brace ductility increases substantially after brace-intersected beam yielding in weak beam frames, mainly due to the vertical displacement of the beam, as can be seen in Figure 15.
- SDR, used in the current design code to represent the seismic response of a structure, is not a proper index to be used in SCBFs. With respect to the vertical displacement of the yielded braced-intersected beam, brace ductility demand increases dramatically and could be close to the fracture point even for an SDR smaller than 2%, as can be seen in Figure 16a and Figure 16b. When S_a is equal to 1.5 in the weak beam frame (type B), SDR is smaller than 2% while brace ductility demand is roughly 10.

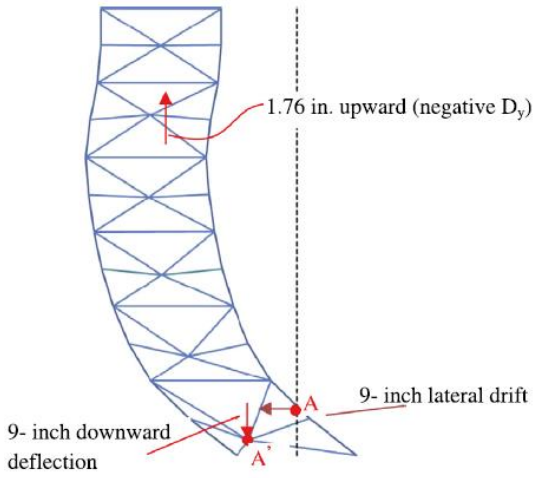

Figure 15: Deformation of the 12-story frame type B [Shen et al. 2014].

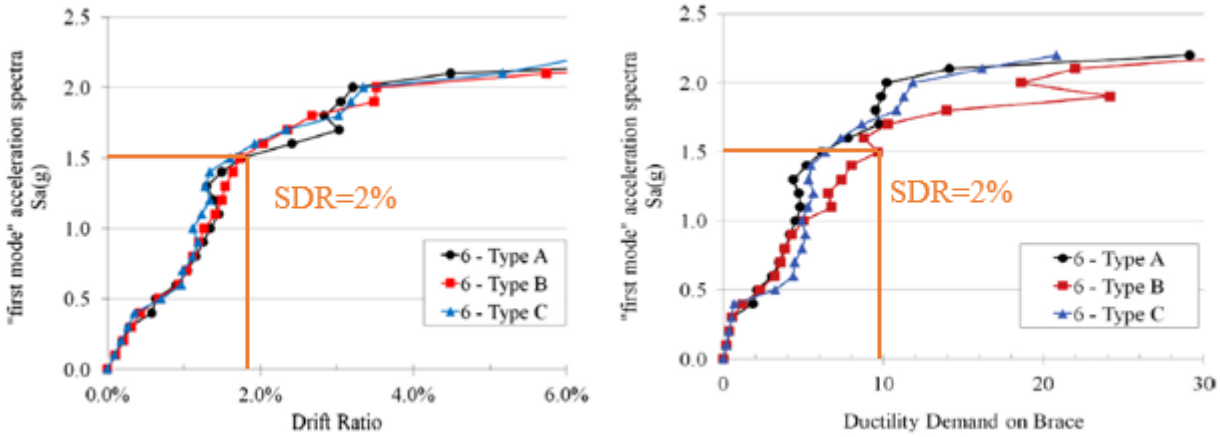

i. Sa[T_1] vs. SDR ii. Sa[T_1] vs. Brace ductility demand

Figure 16: Seismic response of 12-story frame [Shen et al. 2014].

2.6. Seismic demand on columns in SCBFs

Flexural demand on the columns in SCBFs is predominantly due to the non-uniform SDR along the height of the frame [Sabelli, et al., 2003]. The change in the SDRs in alternate stories represents the need for the column to bend. Although the SDR in the frames can be readily calculated, a method for relating the SDR to the flexural demand on the columns remains vague. In an attempt to resolve this issue, MacRae, et al., (2004) proposed an empirical formula shown as

Equation 1 to take into account the effect of the SDR on the bending moment demand on the columns.

$$M_{c,max} = M_{c,mech}(\frac{\Delta_t}{\Delta_{tm}})^{0.65} \leq M_{c,mech} \qquad \text{Equation 1}$$

In the above formula:

$M_{c,max}$=Maximum column moment;

$M_{c,mech}$=Maximum column moment in the frame at mechanism formation;

Δ_t=roof displacement;

Δ_{tm}=roof displacement at mechanism formation.

Although the above formula can be a helpful step towards implementing the flexural demand in the design process, there are some issues of concern in this study that must be considered. Although most of the results presented in this paper (including the above formula) are derived based on a drift concentration factor (DCF) defined in the study, it seems that DCF is not a proper index to be used for evaluation of the braced frame response. Although different parameters such as brace ductility help us to understand at what stage the structure is, DCF does not seem to be helpful. It also seems clear that any approach for designing the columns should include performance of the braces, so this formula can be valid only if the braces do not fracture. All of these limitations show that a new approach for solving the column design issue is still needed.

Newell and Uang (2006) conducted an experimental and numerical study to investigate seismic demand on steel columns. Their study was done in three phases. In the first phase, they applied twenty ground motions to simulated columns using DRAIN 2DX and, based on the story drift time histories of columns, they developed a loading sequence for their experimental test; the proposed loading protocol is presented in Figure 17. In the second phase, they conducted an

experimental test and applied the proposed loading protocol to the steel columns in the University of California San Diego laboratory. In the third phase, they simulated the tested columns in ABAQUS and verified their simulation with the test results. Their simulation results led to the conclusion that steel columns experience yielding as seen in Figure 18, that shows the result for one of the columns under three different axial load ratios. This result demonstrated once again that current design provisions cannot be met by steel columns during an earthquake, and some design modifications are necessary.

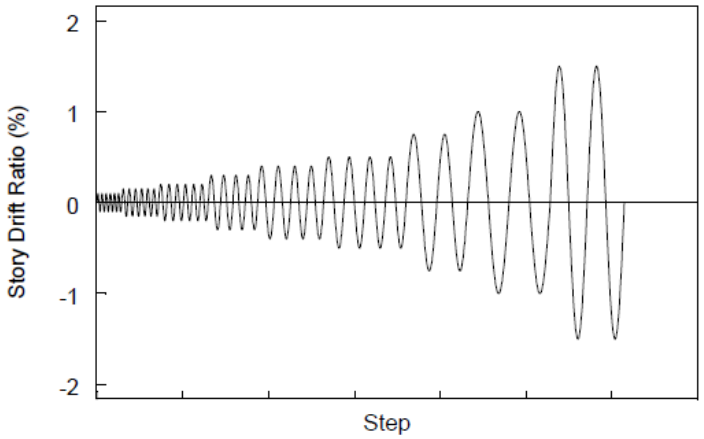

(a) Lateral Deformation

Figure 17 : Loading sequence developed by Newell and Uang (2006).

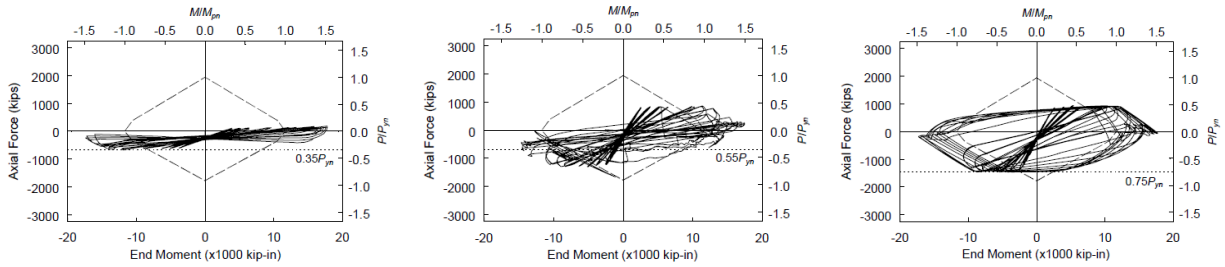

a) 35% P_y b) 55% P_y c) 75% P_y

Figure 18: P-M interaction in columns [Newell and Uang 2006].

Recently, Richards (2009) used RUAUMOKO-2D to investigate the seismic demand on columns in special braced frames. He simulated 36 frames with three different heights (3-, 9- and

18 stories), three different bracing types (BRBFs, SCBFs, eccentrically braced frames (EBFs)) and four different strength levels for each frame. He concluded that column axial demand in the upper stories of tall braced frames could be more than two times higher than those commonly used in the design, and maximum column axial demand at the base of the 9- and 18-story BRBFs and EBFs were only 55-70% of the demand commonly used in design. In addition, the study stated that braces do not reach their capacities in tension and compression at the same time, so the mechanism suggested by current design code is unlikely to happen. Although some of these conclusions might be correct, there are certain issues that cast doubt on the accuracy of the results, including:

- Based on the current design code, brace-intersected beams should be designed for gravity loads as "beam" members, while beams in the other stories should be designed for both gravity and seismic loads as "beam-column" members, so it seems that different beam sizes should be used for alternate stories, even though identical beam sections were used for all the stories in this study.
- W16x40 is used for the beams in even stories, even though it is not a compact section and is prohibited for uses in "beam-column" members, so it seems that beams were not properly designed in the study.
- Effects of the bending moment on column demand is neglected in this study even though they make a major contribution in the column demand and might affect the conclusions.

In 2010, Chen carried out several numerical analyses to assess the seismic demand of SCBFs. He simulated three SCBFs and three BRBFs with different heights using OpenSees (the Open System for Earthquake Engineering Simulation) and applied a suite of ground motions to the frames, and P-M interaction of the first story columns in each frame is presented in Figure 19.

As can be seen in the top row, almost all the columns in the SCBFs experienced yielding. In addition, interaction curves in the bottom row which representing the BRBFs prove that they performed slightly better than conventional frames but they are also still close to yielding [Chen, 2010]. With respect to the data provided, the following comments can be made on the results:

- Yielding patterns in the 3- and 6-story SCBFs were similar to one another with flexural demand predominant in these cases. However, in the 16-story frame the yielding pattern completely changes and the axial force ratio is dominant in this case. This phenomenon can be explained by taking into account the effect of the higher mode deformation that can produce the maximum axial force in the column while the bending moment is small. In the shorter frames this effect is negligible and flexural demand has the major contribution in the demand on the columns.
- The behavior of TSXBF was evaluated in this study and there remains a need to assess the applicability of the provided result to the chevron frames, another common bracing configuration in steel structures.

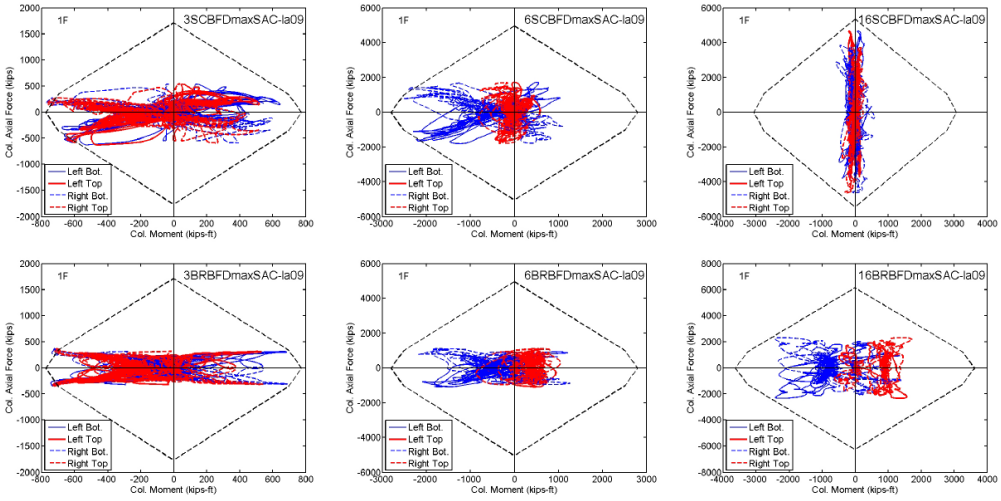

Figure 19: P-M interaction in first story column [Chen 2010].

2.7. Studies on all-steel buckling restrained braces

While Hollow Structural Sections (HSS) are the most popular shapes utilized in Special Concentrically Braced Frames (SCBFs) construction because of their large strength-to-weight ratios and construction simplicity, premature failure potential and unsymmetrical hysteretic behavior of such braces may trigger non-uniform distribution of the plastic deformations (vertically and horizontally), as well as negatively affecting ductile (special) CBFs in terms of overall energy dissipation capability.

A ductile CBF dissipates the major portion of the seismic energy input through buckling and yielding of braces that would undergo large ductility demands, on the order of 10 to 25 [Shen, et al., 2014 and 2017], when subjected to severe earthquake ground motions, as shown in Figure 20.

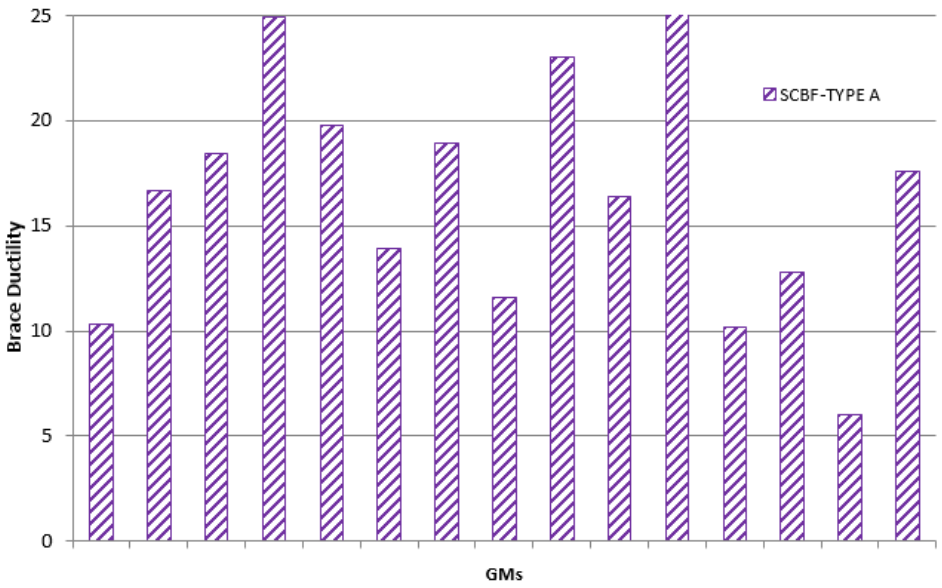

Figure 20: Brace ductility demand under different ground motions [Shen et al. 2017].

Several evaluations of seismic demands in ductile CBFs [Uriz, 2005; Sabelli and Chunho, 2001; McCormick, et al., 2007] indicated that mean peak inter-story drift demands on CBFs may

reach nearly 4% [Sabelli, et al., 2007] and perhaps even up up to 5.7% [Uriz, 2005]. Recent experimental studies [Uriz and Mahin, 2008; Park, et al., 2004; Nip, et al., 2010; Fell, et al., 2009; Shaback and Brown, 2003; Goggins, et al., 2006; and Tremblay, et al., 2008], on the other hand, have shown that a few cycles with relatively large plastic amplitudes can lead to local buckling-induced fracture in HSS braces, possibly in turn precipitating torsional irregularities and inelastic deformations (or even fracture) in columns [Uriz and Mahin, 2008] due to framing action subsequent to brace fracture, as it can be seen in Figure 21.

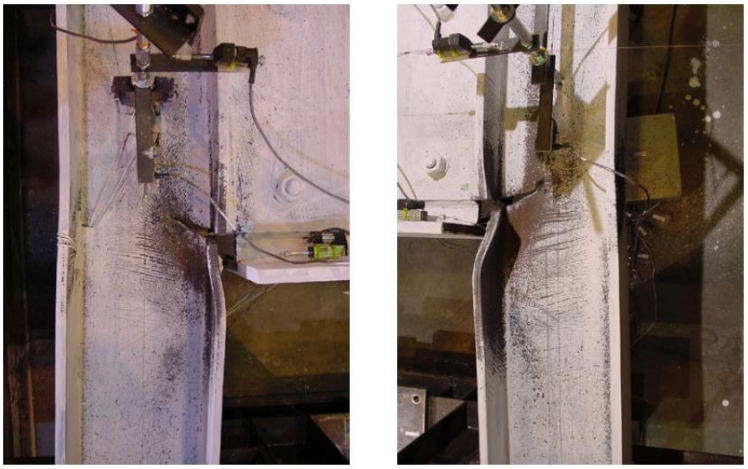

Figure 21: Column fracture subsequent to brace fracture [Uriz and Mahin, 2008].

Moreover, as mentioned in the previous chapters, experimental studies on isolated steel brace specimens have demonstrated that brace fracture is likely to occur prior to attaining a peak brace ductility of 6 [Shaback and Brown, 2009; Tremblay, et al., 2008] to 10 [Tremblay, et al., 2008; Han, et al., 2007], corresponding to an equivalent inter-story drift angle of 0.015 to 0.025. This large discrepancy between the anticipated ductility capacity of ductile CBFs and the seismic demand on the structure may be attributable to early experimental data obtained from testing of small-size conventional braces made of double angles [Jain, et al., 1987; Black and Wegner, 1980; Astaneh Asl, et al., 1985], double channels [Black and Wegner, 1980], W- and WT-shapes [Black

and Wegner, 1980; Leowardi and Walpole. 1996], that usually exhibit longer fracture life than tubular braces.

Furthermore, conventional buckling braces exhibit unstable and unsymmetrical inelastic cyclic behavior due to strength degradation following brace buckling. This abrupt change in compressive strength not only imposes large unbalanced brace forces [Tremblay and Nobert, 2000] on brace-intersected girders and columns in braced bays, but also significantly amplifies the possibility of weak story formation [Sabelli, et al., 2003] in conventional CBFs. Although recent advances in seismic design provisions [i.e., AISC 341-10 and Eurocode 8 (EC8)] have resulted in more stringent design requirements for ductile CBFs with the purpose of enhancing their relatively lesser ductile behavior, researchers have addressed issues associated with non-dissipative structural member design, which are designed to remain elastic, such as girders [Shen, et al., 2014 and 2015] and columns [Brandonisio, et al., 2012; Marino 2014] in ductile CBFs. For example, Brandonisio, et al., (2012) proposed an alternative approach to the one stipulated in EC8 in which the authors modified the over-strength factor and slenderness limitations given by EC8 to reduce the overall structural weight and obtain a more uniform plastic deformation distribution along with satisfactory overall nonlinear behavior. Similarly, Bosco, et al., (2014) studied the seismic response of columns in 4- and 8-story CBFs with diagonal braces by means of non-linear dynamic analyses using five sets of ground motions. Their results indicated that both gravity columns and columns in braced bays designed according to EC8 experienced yielding (or buckling) before diagonal braces attained their assumed ductility limits.

Efforts to mitigate seismic hazards in CBFs have resulted in numerous concrete-encased and all-steel buckling restrained braces (BRBs) [Zhao, et al., 2011; Usami, et al., 2011; Ma, et al., 2011; Razavi, et al., 2012; Clark, et al. 1999]. All-steel BRBs are comprised of a steel core that

carries the applied load and a restraining system that prevents buckling of the main core. Although all-steel BRBs have been increasingly attracting more attention from researchers, the extreme complexity [Zhao, et al., 2011; Usami, et al., 2011] of all-steel BRB configurations are among the drawbacks of such braces (Figure 23), making the engineering community hesitant to employ them as an effective substitute for conventional steel braces in an actual CBF construction.

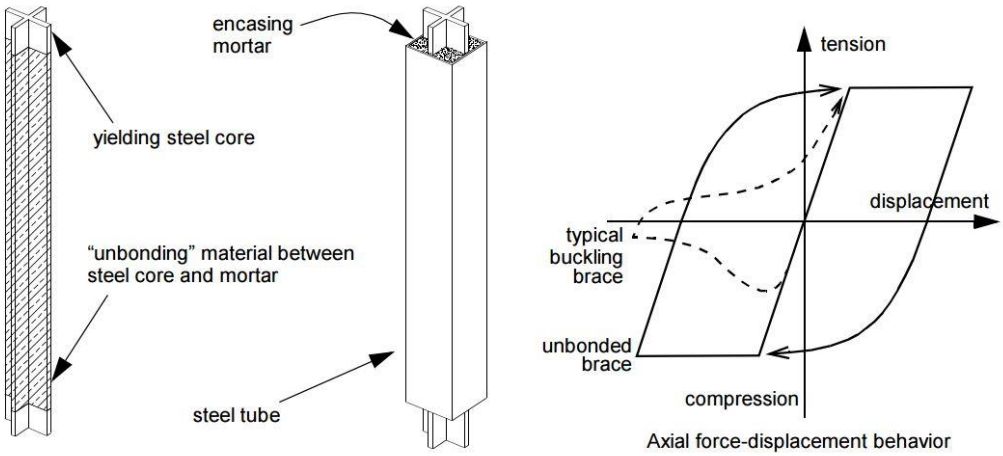

Figure 22: Assembly and hysteretic behavior of a typical concrete-encased BRB (Clark et al. 1999).

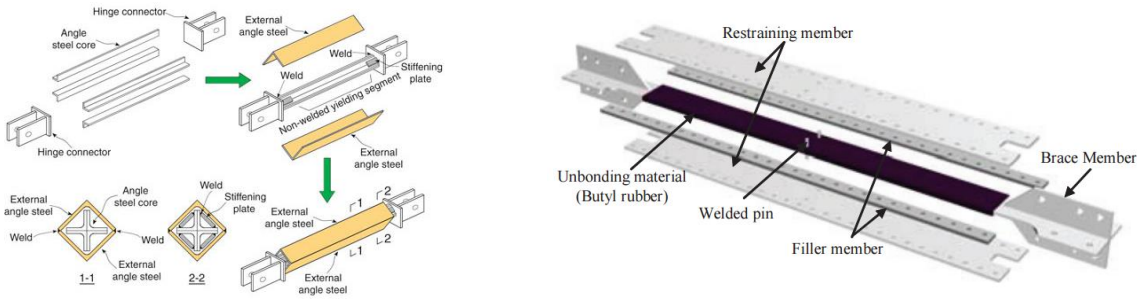

a) All-steel BRB configuration (Zhao et al. 2011)

b) All-steel BRB assembly (Ma et al. 2011)

Figure 23: Complex assembly of conventional all-steel BRBs.

For the purpose of avoiding such complexity, instead of using a combination of filler plates, channels, and HSS along with bolted or welded attachments as a buckling restraining mechanism,

Shen, et al., (2017) introduced a simple and promising buckling-control concept without compromising the intended performance goals and practicality. As illustrated in Figure 24, a Tube-in-Tube buckling-controlled brace (TinT-BCBs) consists of a load-bearing tube (main brace) providing resistance to seismic forces, encased in another tube (controlling section) of circular or rectangular HSS that controls both global and local buckling of the main brace by providing continuous lateral support along the brace length. Note that the gap between the tubes is provided to limit the contribution of the outer tube to the axial load-carrying system. A FEM-based numerical study performed by Shen, et al., (2017) has discussed the influential parameters, i.e., the gap between the tubes, the relative outer tube thickness and the coefficient of friction, using built-up HSS with square-in-square bracing configuration to establish a conceptual foundation for cyclic behavior of TinT-BCBs. Their study implied that TinT-BCBs are promising both in terms of economy and in overcoming the aforementioned issues related to seismic performance of ductile braced frames.

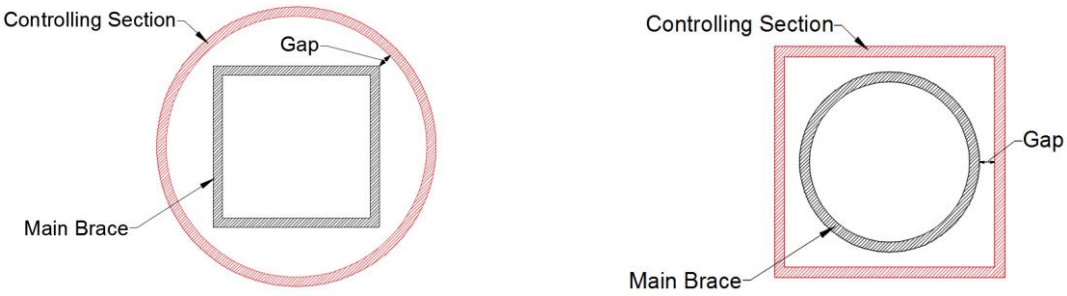

a) Square-in-round b) Round-in-square

Figure 24: Scheme of TinT-BCBs.

In summary, while various studies have either experimentally or numerically investigated the behavior of the SCBFs, there are still some gaps in the current literature that should be addressed. Some of the major missing parts are as follows:

- It is still difficult to understand the relationship between the bending moment demands on the columns and brace ductility in SCBFs.
- It is important to understand how different bending moment in the column could be achieved by changing the bracing configurations in the braced frames.
- It is necessary to evaluate the rigidity of the beam-to-column connections and assess its impact on the flexural demand on the members.
- It seems important to study the effect of the variation in cross-section on the performance of the BCBs.
- The effect of the BCBs on seismic demand of SCBFs with different bracing configuration should be investigated.

CHAPTER 3. BUCKLING-CONTROLLED BRACES

3.1. Introduction

While Special Concentrically Braced Frames (SCBFs) are widely used globally in earthquake resisting systems because of their simplicity in construction and design, premature brace failure in CBFs is one of the main issues of such system and researchers have been trying to find a solution to this problem. In an attempt to overcome this issue, engineers have developed buckling-restrained braces (BRBs) to increase the ductility of the braces and to postpone fractures. BRBs are composed of a structural steel cores that bear the loads and a system that restrains the steel core from buckling [AISC 341-10]. All-steel and concrete-encased BRBs are two different types of BRBs that have been developed in recent years. Various configurations for all-steel BRBs [Zhao et al., 2011; Usami, et al., 2011; Ma, et al., 2012; and Razavi, et al., 2012] and concrete-encased BRBs [Tremblay, et al., 2006; Park, et al., 2009; Lin, et al., 2012] have been developed to effectively restrain the buckling of braces and reach stable and symmetrical hysteretic behavior. Although performance of BRBs is considerably superior to that of conventional braces, there are still some issues that make the engineering community hesitant to accept them as an effective replacement for conventional steel braces. For example, among the drawbacks of these braces are the complex and expensive configurations of some of the developed BRBs. In addition, compression strength adjustment factor, calculated by dividing the compressive strength by tensile strength, can be as large as 1.5 in some of the BRBs [Palmer, et al. 2014], and this difference can lead to significant unbalanced forces in CBFs, so it seems that there is a need to develop a new brace that not only exhibits symmetrical hysteretic behavior but also is cost-effective and easy to

construct. To address this issue, a new all-steel buckling-controlled brace (BCB) has been developed in the present study.

This chapter investigates the relative effectiveness of TinT-BCBs with Round-in-Square and Square-in-Round configurations with an emphasis on the efficiency and applicability of the developed TinT-BCBs composed of HSS that can be employed in an actual CBF construction. The results are evaluated in terms of hysteretic response of bracings and global response of braced frames both with and without a buckling-controller by means of both testing and Finite-Element (FE) simulations. For this purpose, the behavior of a set of isolated TinT-BCBs with round-in-square and square-in-round configurations was first compared through FE simulations under uniaxial and cyclic loading. Subsequently, response of the braced frames that incorporate conventional braces and TinT-BCBs are compared with respect to plastic deformation distribution on structure, braces, and girders. Finally, two round-in-square type BCB specimens have been tested to validate the observations carried out in the model-based study.

3.2. FEM-based evaluation of TinT-BCBs

A FEM-based parametric study was performed on several BCBs with different sections, gap sizes, and friction coefficients to evaluate the comparative efficiency of round-in-square and square-in-round TinT-BCBs. The general scheme of the simulations described in this chapter can be summarized as follows:

i. Investigating the behavior of isolated BCBs under monotonic compression.
ii. Examining the influence of connection design on the behavior of BCBs.
iii. Studying the cyclic behavior of the developed BCB.

3.2.1. Isolated BCBs under monotonic compression

In the first phase of the model-based study, an ensemble of isolated TinT-BCBs with round-in-square (RS) and square-in-round (SR) configurations were subjected to monotonic loading to better comprehend and assess the influence of each configuration (RS and SR). Table 3 summarizes influential design parameters, i.e., the ratio of the outside tube thickness to the main tube's, the coefficient of friction between the outer surface of the inside tube (main brace) the inner surface of the outer tube (buckling-controller), and the initial gap between the tubes. As illustrated in Figure 24, the initial gap is defined as the minimum distance between the inner and outer tubes.

The gap amplitudes varied from a small gap of 0.017" to a relatively large gap of 0.1765". Two different friction coefficients were considered for each main brace-buckling controller couple (Table 3). Friction coefficients of 0.3 and 0.1 were selected to represent bare steel and lubricated steel surfaces, respectively. Simulation cases were divided into SR and RS groups, , based on their cross-sectional configurations. As given in Table 3, SR group represents BCBs with a square load-bearing tube encased in a round outer tube, while the RS group included models comprised of a round inside tube and a square outer tube. In addition to the TinT-BCB models, for the sake of the comparison, a conventional brace simulation was also performed for each simulation group (SR and RS). Note that the main brace (load-bearing tube) section was identical for all models in the same simulation group.

All models were analyzed using a general-purpose finite-element software package, ABAQUS (Hibbit et, al., 2001). Values of modulus of elasticity and Poison's ratio were assumed to be 29,000 ksi and 0.3, respectively. Nominal material properties with kinematic hardening rules were used for non-linear material definition of all models.

Table 4 shows the material properties adopted for the simulation cases. Since initial imperfections could have a substantial impact on the buckling load and hysteretic behavior, a two-step analysis was conducted on each model to properly represent initial deflections. In the first step, an elastic buckling analysis was conducted to obtain the buckling modes of each model. Subsequent to the buckling analysis, an imperfection of 1/1,000 of the brace length was applied to the models, considering the first buckling mode of the member. In the second step, a large-displacement static analysis was carried out to analyze each model under compression force. This approach allowed the static analyses to begin from a zero-stress condition. The dissipated energy fraction was set to 2e-4 in the automatic stabilization method to lessen convergence problems during the analyses. A full Newton method was utilized as the solution technique and geometric nonlinearities were taken into account in the analyses. A 3D 8-node linear brick element with reduced integration was employed to mesh the members (C3D8R). Care was taken in the modeling of the contact elements.

A hard contact method was used for the interactions normal to the surfaces to prevent any penetration, while the penalty method was used to describe friction formulation for the tangential interaction between inner and outer tubes. A fixed boundary condition was applied to one end, while relative axial displacements were applied from the other end of the specimens. A mesh size of 0.5 inches was used along the main brace length except for the locations that are expected to experience local deformations. A finer mesh was employed in critical sections like the mid-length of the conventional bracing. Two elements were also defined in the thickness of the gusset plates, inner, and outer tubes to properly capture the anticipated local deformations. Figure 25 shows the meshing for the one of the cases. Small circles and squares next to each member represent number of nodes and elements in the member, respectively.

Table 3: Properties of simulation cases.

Name*	Main Brace (in x in)	Length (in)	Controlling Section (in x in)	Friction Coefficient	Gap (in)	Thickness ratio
SR	Square HSS6x6x3/8	113.63	Conventional Buckling Brace			
SR1A			HSS10x0.625	30 %	0.1765	1.67
SR1B			HSS10x0.625	10 %	0.1765	1.67
SR2A			HSS9.625x0.5	30 %	0.105	1.33
SR2B			HSS9.625x0.5	10 %	0.105	1.33
RS	Round HSS7.5x0.375	113.63	Conventional Buckling Brace			
RS1A			HSS8x8x1/4	30 %	0.017	0.67
RS1B			HSS8x8x1/4	10 %	0.017	0.67
RS2A			HSS8x8x1/8	30 %	0.134	0.33
RS2B			HSS8x8x1/8	10 %	0.134	0.33
RS3A			HSS8x8x3/16	30 %	0.076	0.5
RS3B			HSS8x8x3/16	10 %	0.076	0.5
RS4A			HSS9x9x5/8	30%	0.169	1.67
RS4B			HSS9x9x5/8	10%	0.169	1.67

*SR: Square-in-round tube. RS: Round-in-square tube.

Table 4: Nominal material properties.

	F_y (ksi)	F_u (ksi)
Square Tubes	46	58
Round Tubes	42	58
Plates	36	58

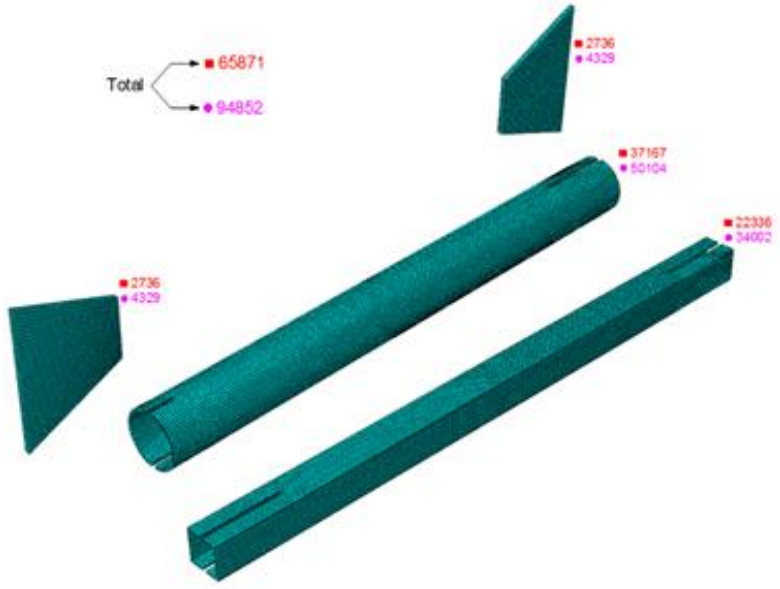

Figure 25: Number of elements and nodes in each member.

3.2.2. Results of SR and RS simulation groups

Simulation results of the first simulation group (square-in-round) are presented in terms of axial load-deformation relationships as well as deformed shapes, along with relative stress distributions. Figure 26 and Figure 27 present the axial force versus axial displacement of square-in-round (SR) models, and the comparison between the deformed shapes of the conventional brace (without an encasing tube) and a typical SR type TinT-BCB, respectively.

Global buckling of the conventional brace took place at an equivalent story drift ratio (drift angle) of about 0.25% when the compressive strength was 65% of the yielding strength. Following global buckling, the conventional brace experienced local buckling (Figure 27c) and gradually lost 65% of its compressive strength capacity, as indicated in Figure 26. TinT-BCBs, on the other hand, never buckled in the traditional manner throughout the analysis. As shown in Figure 26, the first contact between the two tubes was observed soon after 0.25% story drift ratio (SDR) was reached, resulting in stiffness reduction. It should be noted that the slight difference between SR1 and SR2 specimens (Figure 26) in terms of the stiffness change was due to variation in gap amplitudes. Subsequent to the first contact between the two tubes, all TinT-BCBs experienced strength degradation before attaining the tensile strength capacity of the inside tube. A strength degradation of about 15% with respect to the tensile capacity occurred in all cases in the SR simulation group after a drop at 0.5% SDR. This can be attributed to the rotation of the brace end, as illustrated in Figure 27b. Although the outer tubes controlled the global buckling of the main braces until a certain deformation level, the main brace eventually suffered local plastic deformations (Figure 27d) through the initiation of global instability (Figure 27b). Note that the gusset plates were designed to allow out-of-plane rotations, a factor that induced an additional flexural demand on the brace assemblies. As indicated in Figure 26, there was a slight drop in the strength after

formation of the local deformations, and consequently the contact between the tubes became more substantial in the vicinity of the local plastic deformations (Figure 27d), so the compressive strength was increasing for a while after the contact owing to the friction force transfer. It is also noteworthy that neither friction coefficient nor the section properties of the buckling-controllers had a significant impact on the behavior of SR cases, since the brace assemblies were not capable of controlling the flexural demand imposed by end rotations.

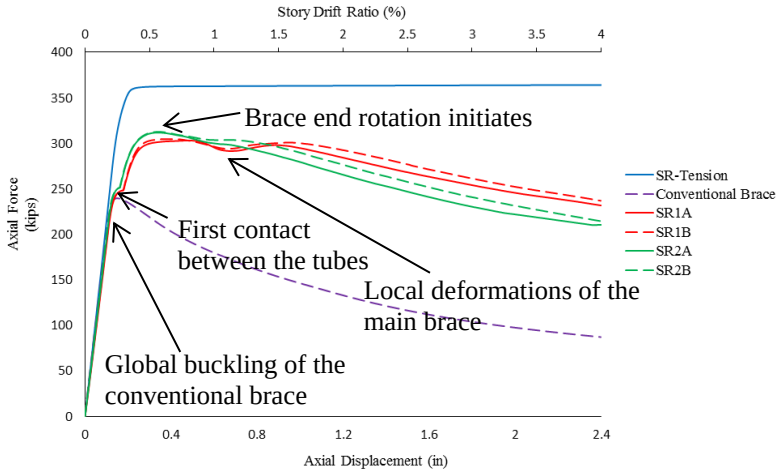

Figure 26: Axial force vs. axial displacement of SR cases.

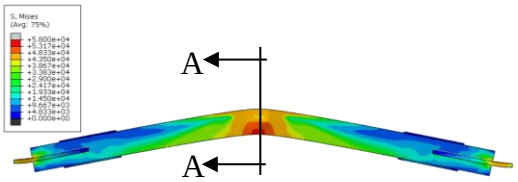

a) Global buckling of the conventional brace.

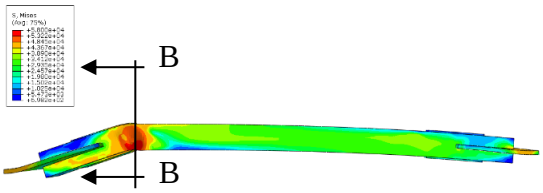

b) Typical deformation of square-in-round BCBs.

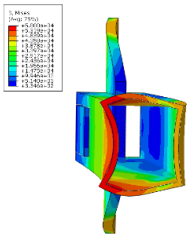

c) Sec A-A

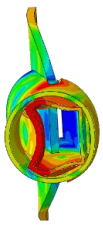

d) Sec B-B

Figure 27: Deformed shapes of the conventional brace and a typical Square-in-Round TinT-BCB at 4% SDR.

Figure 28 and Figure 29 present the axial force versus axial displacement and deformed shapes of RS simulation group, respectively. As expected, the conventional brace buckled globally at about 0.25% SDR and lost 60% of its compression strength when the brace attained an axial deformation quantity corresponding to 4% SDR. The impact of encasing on the brace behavior, however, differed from one case to another based on the properties of the controlling section.

The RS1 and RS3 cases experienced global instability, with the RS3 cases, in particular, exhibiting a trend similar to that of the conventional brace with a larger compressive strength. The behavior of the RS2 and RS4 cases, on the other hand, were governed by local deformation formation, in contrast to the RS1 and RS3 cases. As shown in Figure 28, the strength deterioration became substantial after 1.5% SDR for RS1 and RS2, while the RS4 cases remained stable until an equivalent SDR of 3.5%. Since the outer tube thickness of RS4 was larger than that of the inside tube, local deformations of the inner tube is successfully controlled (Figure 29e) with virtually the same strengths in compression and tension (Figure 28). The deformation pattern shown in Figure 29d demonstrates that the outer tube of RS2 did not effectively control the lateral thrust force imposed by the inner tube. In other words, when end rotations were not substantial, regardless of the gap amplitude and the friction coefficient, the simulation cases with an outer tube thickness less than that of the inside tube were not capable of controlling formation of local deformations in the main brace (Figure 28).

Variations in the friction coefficient did not play an important role on the behavior of the braces when severe local buckling occurred in the members, as observed in RS2 (Figure 29d). However, when the buckling of the inner tube was controlled by the outer tube, the smaller friction coefficient led to less compression overstrength. Even though the difference was not substantial, comparing RS4A with RS4B indicates that the case with a friction coefficient of 0.1 (RS4B)

followed a trend virtually identical to the tensile strength, while the compression strength of RS4A case was slightly larger than the tensile strength.

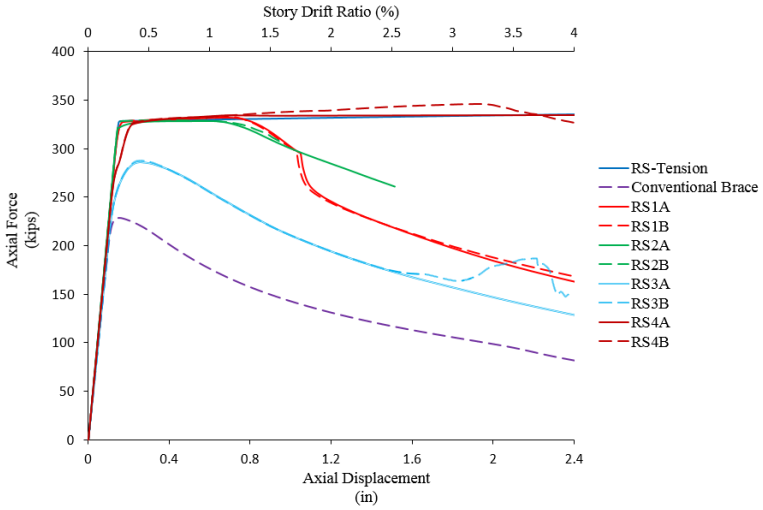

Figure 28: Axial force vs. axial displacement of RS cases.

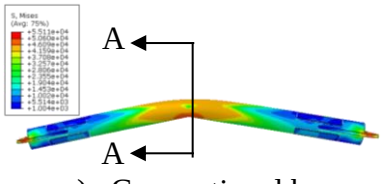

a) Conventional brace.

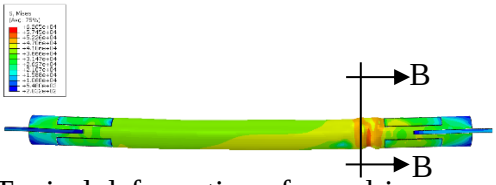

b) Typical deformation of round-in-square BCBs.

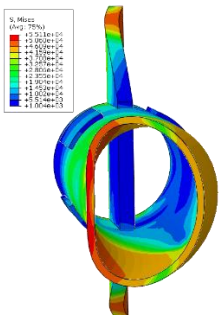

c) Sec A-A

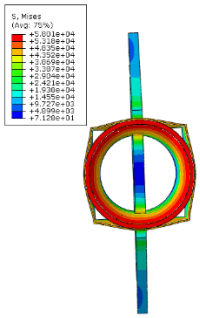

d) Sec B-B in RS2A

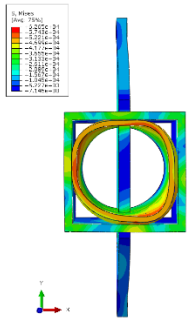

e) Sec B-B in RS4A.

Figure 29: Comparison of deformation of conventional braces and SR-BCBs at 4% SDR.

3.2.2.1. Key observations

Based on the FEA results and deformation patterns obtained from SR and RS simulation groups, the following observations can be made:

i. Similar deformation patterns in terms of the location of the localized plastic deformations were observed in both SR and RS cases. Encasing the conventional braces with an outer tube led the plastic region of the braces to be shifted from the middle portion to the loading end.

ii. The flexural demands imposed by the end rotations, more or less, affected the overall behavior as well as axial force-displacement relationship of the BCBs. It seems that the deformation that initiates end rotations and the severity of the impact were determined by the efficiency of the buckling controllers. Given that both SR and RS simulation groups possess comparable gap amplitudes and relative outer tube thicknesses, the distinction between their behaviors regarding the governing limit states (i.e. global instability or formation of local plastic deformations) can be attributable to the difference between the confinement provided by the circular- and square-shaped buckling controllers.

iii. In contrast to the observed deformation patterns in SR simulation group, the limit states of the TinT-BCBs in RS simulation group were not predominantly governed by global instability due to end rotations. The behavior of the braces in the RS group in certain cases was governed by the inside-tube to outer-tube thickness ratio. The larger the relative outer tube thickness, the less likely strength degradation occurred.

iv. The effect of the coefficient of friction on the force-deformation relationship was not noticeable unless the outer tube successfully controlled the local and global deformations of the inside tube.

3.2.2.2. Impact of enhanced connections

Simulation results presented in the previous section have demonstrated that connection design has a determining impact on brace behavior. Even though utilizing particular parameters successfully prevented BCBs from experiencing global instability (e.g. RS4), in seismic design practice, allowing such rotational demands might not be practical, so in this section an enhanced gusset plate design, presented in Figure 30, has been developed to maximize the effectiveness of BCBs with any design parameters. To investigate the impact of the new gusset plate configuration, the SR2 and RS1 cases, that experienced a significant strength loss in the previous section, are simulated once again with the enhanced connections. In addition to the models that underwent global instability (SR2 and RS1), the gusset connections of RS4, that appeared to be the optimal case among the others, was also enhanced. As shown in Figure 30, the gusset plates were stiffened with four tapered rather than rectangular stiffeners to minimize the additional steel weight as well as to provide a constraint against the end rotations.

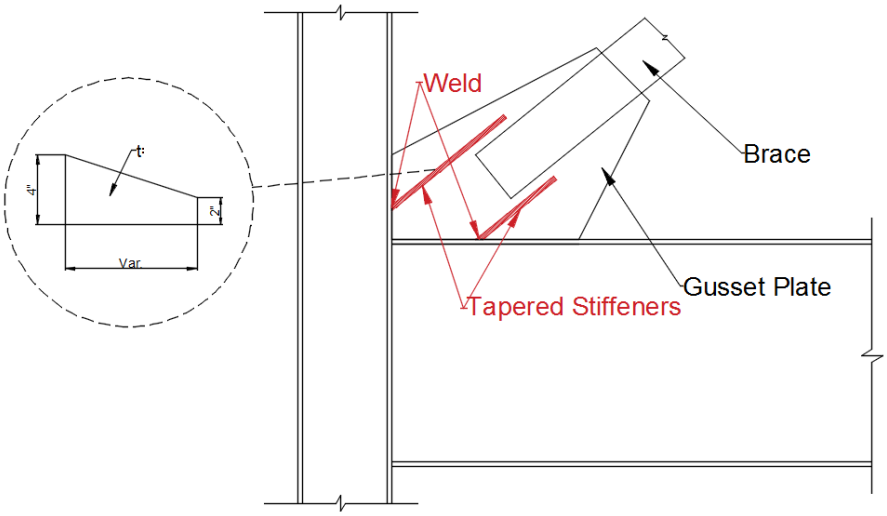

Figure 30: Enhanced gusset plate details.

All numerical parameters and materials used in this section were identical to those used in the previous cases. A fixed end boundary condition is applied to the stiffeners to represent the constraint provided by the flanges of the beam and the column in an actual structure. Figure 31 shows the FE model of RS1A case after adding both the stiffeners and the applied boundary conditions. Note that RS1A-S accounts for the RS1 model with enhanced connections.

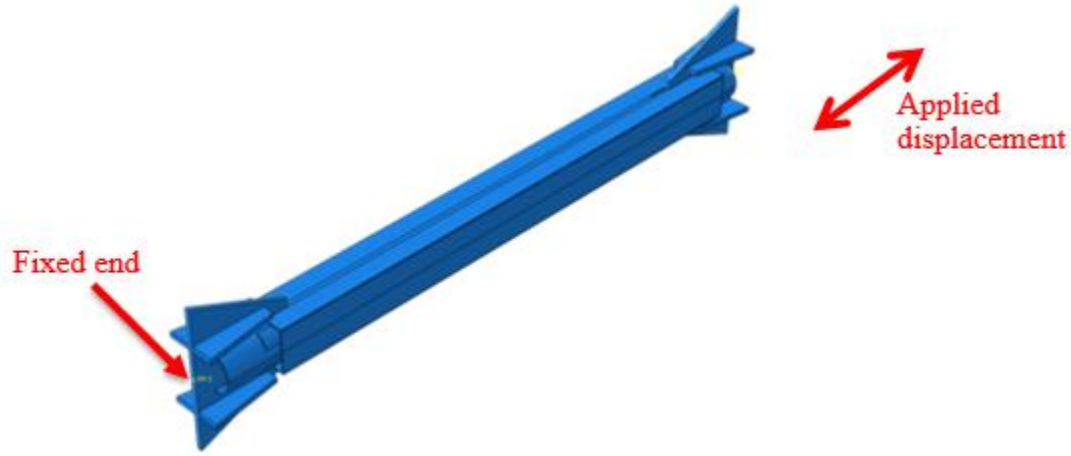

Figure 31: RS1A-S case (RS1A with stiffeners).

Figure 32, Figure 33, and Figure 34 compare the relative efficiencies of the TinT-BCBs with and without stiffeners in terms of axial force-deformation relationships and deformed shapes at 4% SDR. The following can be observed:

i. As can be seen in Figure 32 and Figure 33a, irrespective of cross-sectional shapes, introducing stiffeners to the gusset plates significantly improved the BCB performance in terms of plastic deformation capability without significant strength loss because the limit state that triggers the strength loss was altered with the enhanced connections in both the SR2 and the RS1 cases.

ii. It seems that the level of improvement was more substantial in the SR2 cases than in the RS1 cases. Although both cases attained the same deformation level without

significant strength or stiffness loss, as illustrated in Figure 32 and Figure 33a, the flexural constraint provided by the stiffeners postponed the occurrence of strength loss from 1.5% SDR to 2.5% SDR in the RS1 cases and eliminated the strength loss in the SR2 cases. It should, however, be noted that the difference between the level of enhancements achieved by SR2 and RS1 cases might not be due only to the rotational constraint provided by the stiffeners. In fact, the observed strength deteriorations in RS1 and SR2 cases had two discrete causes:

a) The outer tube thickness in RS1 case was not sufficient to control the lateral expansion of the inside tube, as indicated in Figure 33a. Considering the fact that the lateral thrust force can be associated with the applied axial compressive force and the gap amplitude, the likelihood of premature strength loss for the RS case can be reduced by introducing a thicker outer tube capable of mitigating the severity of the local deformations while resisting the lateral thrust force. Note that the gap amplitude was as small as possible (0.017") in the RS1 specimen.

b) The strength loss in the SR2 case, conversely, appeared to be more conceptual than the design deficiency observed in the RS1 case. As shown in Figure 32, while the local stiffness provided by the outer tube was sufficient, due to the cross-sectional shape of the two tubes in RS1, the large gap between the flat portions of the square inside tube and the round outer tube allowed the flat portions to deform in a concave manner, a situation that could not be avoided by altering the buckling-controller properties like increasing the outer tube thickness or reducing the initial gap. However, by diminishing the end rotations,

the local deformation severity alleviates and, when combined with the presence of a thick outer tube, SR2 performance improved, as can be seen in Figure 32.

iii. Comparing RS1A and RS1B indicates that employing a smaller friction coefficient tends to reduce the rate of strength loss in the BCBs, as shown in Figure 33a. On the other hand, the SR cases with stiffeners (SR2A-S and SR2B-S) were not sensitive to alterations in the friction coefficient (Figure 32); this can be explained by the relatively small contact area that limits the shear force transfer between the tubes.

iv. Because of the consistency of the governing limit states, the impact of the enhanced connections was relatively less substantial in the RS4 and RS4-S cases, as seen in Figure 34. The influence of the friction coefficient, in contrast, was more significant in the RS4 cases than in the RS1 cases, since buckling of the inner tube is effectively controlled.

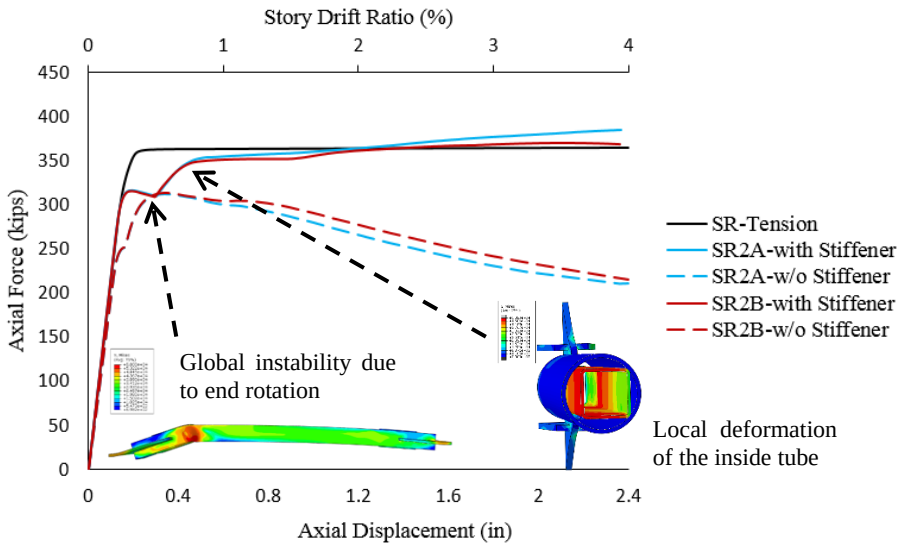

Figure 32: Comparison of SR2 cases w/ and w/o stiffeners.

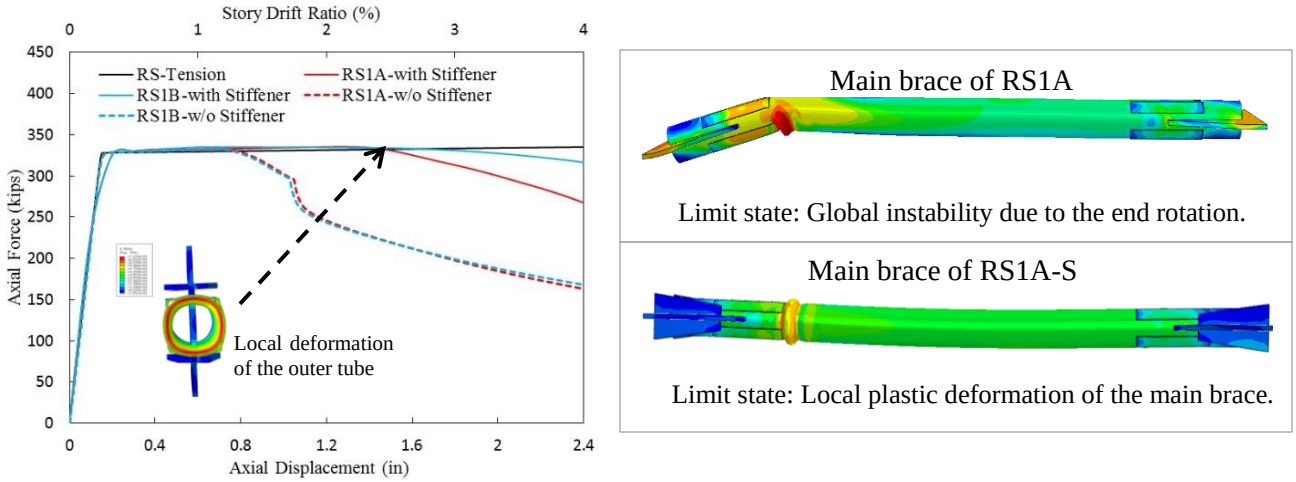

a) Axial force vs. axial displacement b) Deformed shape of RS1A and RS1A-S at 4% SDR

Figure 33: Comparison of RS1 cases with and w/o stiffener.

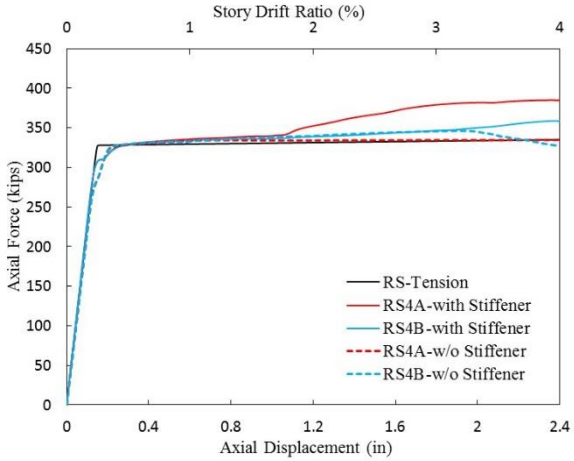

Figure 34: Comparison of deformation of RS4 cases.

3.2.3. Isolated BCBs under cyclic loading

In previous sections the performance of newly developed all-steel BCBs was investigated under monotonic loading. It can be concluded that in RS cases either the outer tube to inner tube thickness ratio should be greater than one or an enhanced gusset plate should be utilized to achieve stable behavior under monotonic compressive loading. On the other hand, in SR cases, it is necessary to limit the brace ends rotation due to concave deformation of the inside tube, so an enhanced gusset plate should be used in SR cases. In this section, the hysteretic behavior of RS4,

RS4-S, RS1-S, and SR2-S cases under cyclic loading will be evaluated. A static cyclic analysis was carried out on each brace under the loading sequence presented in Figure 35. Mesh size, element type, and interactions used in this section are similar to those used in the previous section.

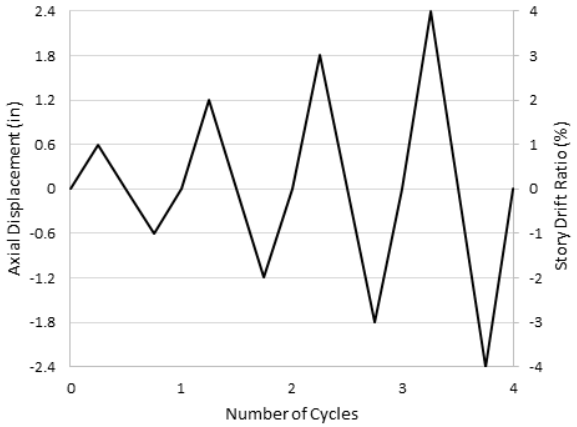

Figure 35: Loading sequence.

Table 5: Simplified loading sequence.

Cycle #	Axial disp. (in)	SDR (%)
1	±0.6	1
2	±1.2	2
3	±1.8	3
4	±2.4	4

Hysteretic responses of the above-mentioned cases are presented in Figure 36. A stable and symmetrical cyclic response was observed for each case until 3% SDR. It is evident that BCBs are capable of dissipating a greater amount of energy than conventional braces due to the larger enclosed area of hysteretic response, and there is no significant difference between RS and SR cases under cyclic loading. In addition, symmetrical behavior of BCBs leads to a smaller unbalanced force applied to brace-intersected girders in CBFs. Table 6 describes the amount of reduction in unbalanced force for each case for different cycles. It can be concluded that utilizing BCBs results in a significant decrease in unbalanced force, so a shallower brace-intersected girder can be employed. In this table, P_c, P_y and F_v represent compression capacity, tensile capacity, and vertical unbalanced force, respectively.

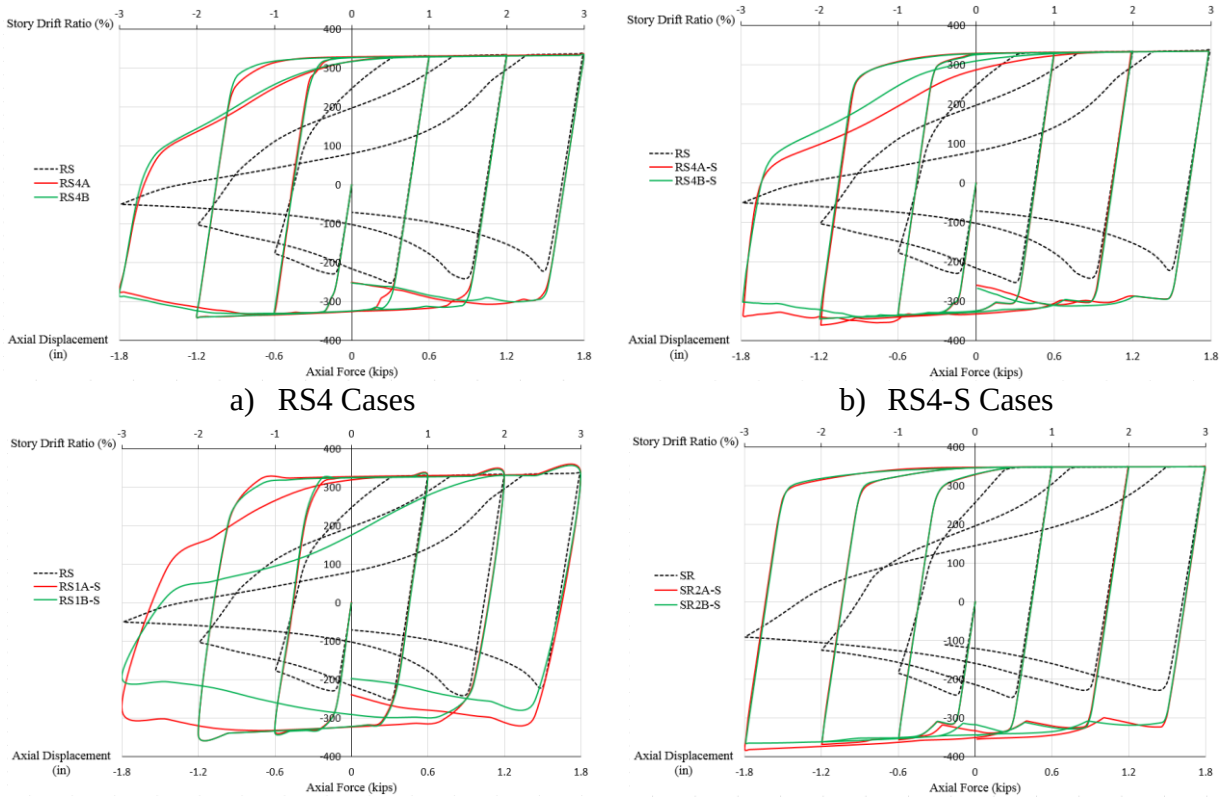

a) RS4 Cases b) RS4-S Cases

c) RS1-S Cases d) SR2-S Cases

Figure 36: Cyclic Behavior of the BCBs with round-in-square configuration.

Table 6: Unbalanced force reduction in each case.

Name	1% SDR			2% SDR			3% SDR		
	P_c/P_y	F_v/P_y	Reduction (%)	P_c/P_y	F_v/P_y	Reduction (%)	P_c/P_y	F_v/P_y	Reduction (%)
RS	0.54	0.33	N.A.	0.32	0.48	N.A.	0.15	0.60	N.A.
SR	0.53	0.33	N.A.	0.36	0.45	N.A.	0.26	0.52	N.A.
RS4A	1.00	0.00	100	1.03	0.02	96	0.83	0.12	80
RS4B	1.00	0.00	100	1.03	0.02	96	0.86	0.10	83
RS4A-S	1.01	0.00	100	1.09	0.06	88	1.01	0.00	100
RS4B-S	1.01	0.00	100	1.07	0.05	90	0.91	0.06	89
RS1A-S	1.00	0.00	100	1.04	0.03	94	0.82	0.13	78
RS1B-S	1.01	0.00	100	1.03	0.02	96	0.58	0.30	50
SR2A-S	1.02	0.01	97	1.04	0.03	93	1.10	0.07	87
SR2B-S	1.01	0.00	100	1.04	0.03	93	1.06	0.04	92

3.3. Testing of Round-in-Square BCBs (Seker, 2016)

Simulation results have demonstrated, while RS cases exhibit stable and symmetrical behavior when the thickness ratio of the outer tube to the inner tube is greater than one or when enhanced connections are utilized, SR cases have promising behavior only when the gusset plates are reinforced with stiffeners, so round-in-square BCB was chosen for experimental study to permit study of a pair of comparable specimens both with and without enhanced gusset plates. Two identical round-in-square (RS) type BCB specimens with conventional and enhanced gusset connections were tested by Seker in 2016 at the Iowa State University structural laboratory (Seker, 2016). Since the primary objective of this testing was to examine the validity of the detailed observations carried out in the numerical portion of the study, the design parameters adopted for the test specimens, such as initial gap amplitude and relative thickness of the outer tube, were determined by considering the range employed in the FEM-based study. Note that the experimental portion does not intend to compare the efficiency of round-in-square and square-in-round BCBs. Table 7 summarizes the main brace and outer tube sections, gap amplitudes, and connection types of the tested specimens.

Table 7: Section properties of the Round-in-Square BCB specimens (Seker, 2016).

Test Name	Circular Main Brace (in x in)	Square Controlling Section (in x in x in)	Enhanced Connections	Gap* (in)
RS#1	HSS 1.900x0.125	HSS 2 ½ ×2 ½ × 1/8	No	0.175
RS#2		HSS 2 ½ ×2 ½ × 1/8	Yes	

RS-BCB specimens were shop-fabricated using round and square hollow sections with gusset assemblies at their ends. Side and sectional views of the first and second specimen are shown in Figure 37(a) and (b), respectively. The main brace section was determined by considering the available loading capacity of the test equipment. The specimens were composed of a round HSS1.900x0.125, eight 3/16”-thick net section reinforcing plates, a square HSS2 ½ x 2 ½ x 1/8

section and 3/8” thick gusset plates. RS#1 and RS#2 designs were identical except for their connections, and the RS#1 specimen were designed to be ductile. The gusset assembly of RS#2 consisted of a 3/8” thick gusset plate, four ¼” thick stiffeners, two horizontal supporting plates and two vertical supporting plates, as shown in Figure 37(b).

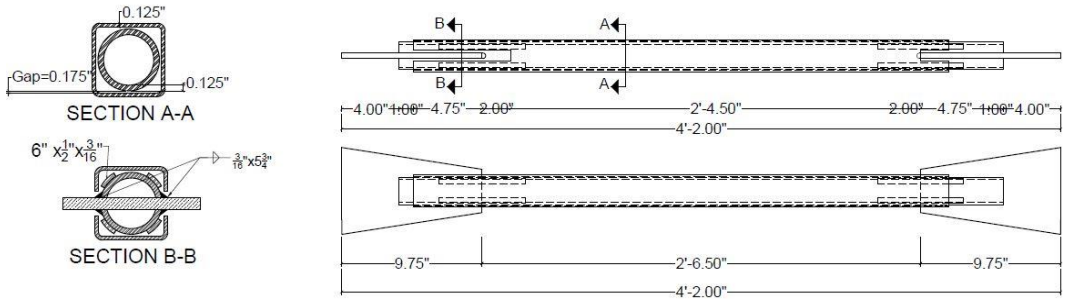

a) RS#1

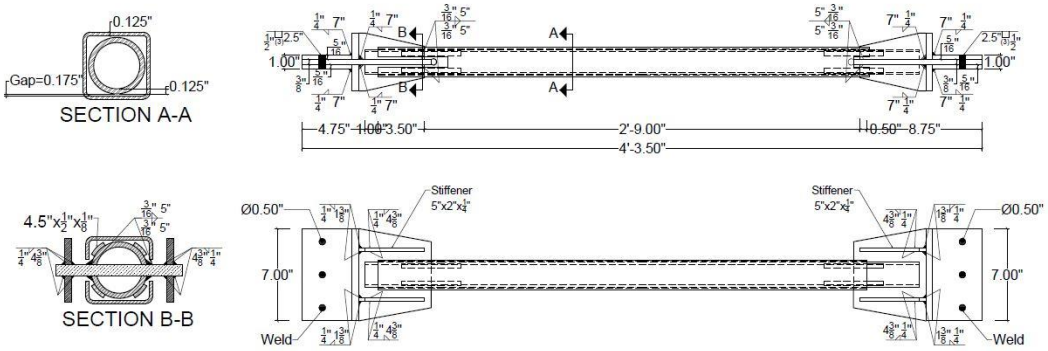

b) RS#2

Figure 37: Shop drawings of BCB specimens (Seker, 2016).

RS-BCB specimens were subjected to displacement-control incremental cyclic loading. A modified version of the loading protocol given in AISC Seismic Provisions (AISC341-10) was adopted for the tests. In this study, the design story drift was conservatively assumed to be 2% of story height for all specimens. The test setup and loading protocol are given in Figure 38.

a) Test Setup

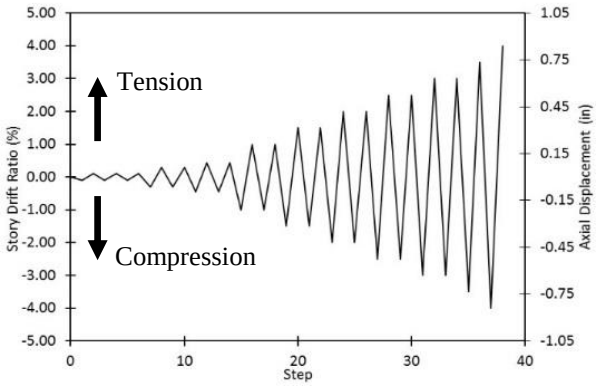

b) Loading protocol used in the tests

Figure 38: Test setup and loading protocol (Seker, 2016).

3.3.1. Test results

The hysteretic responses of the specimens are presented in Figure 39. The RS#1 specimen exhibited a stable and symmetrical response until it reached a ductility of 4, corresponding to an equivalent story drift ratio of 1.0%. Nevertheless, during the subsequent inelastic cycle to 2% SDR compression, the RS#1 specimen exhibited global instability. As indicated in Figure 39, fracture initiation in RS#1 was observed at the corner of the slotted end of the outer tube at a ductility value of about 7. The excessive flexural deformation imposed by the out-of-plane rotation of the gusset plate stimulated the fracture of the slotted portion of the outer tube to the loading end (Figure 40a). The end rotation-induced global instability led to significant strength loss, on the order of 50% of the initial strength, in the following cycle. The test was terminated during the second compression cycle to 2% SDR due to severe outer-tube deformation. The peak ductility value attained by the RS#1 specimen was about 8.5.

In the second test (RS#2), the gusset plates of RS#1 specimens were reinforced with stiffeners and subjected to cyclic loading. It seemed that introducing vertical stiffeners to the connections not only substantially improved the overall hysteretic response (Figure 39) but also

altered the governing limit state (Figure 40). The first significant strength deterioration took place during the first compression cycle of 3%. Local deformation of the outer tube in the RS#2 specimen was noticeable at 2.0% SDR in compression during the first compression cycle at a story drift ratio of 3.5% (Figure 40b). The strength in compression dropped to 55% of the initial yield strength at 3.5% SDR. The inside tube fractured during the tension cycle to 3.5% SDR. The peak ductility attained by RS#2 specimen was 13.9.

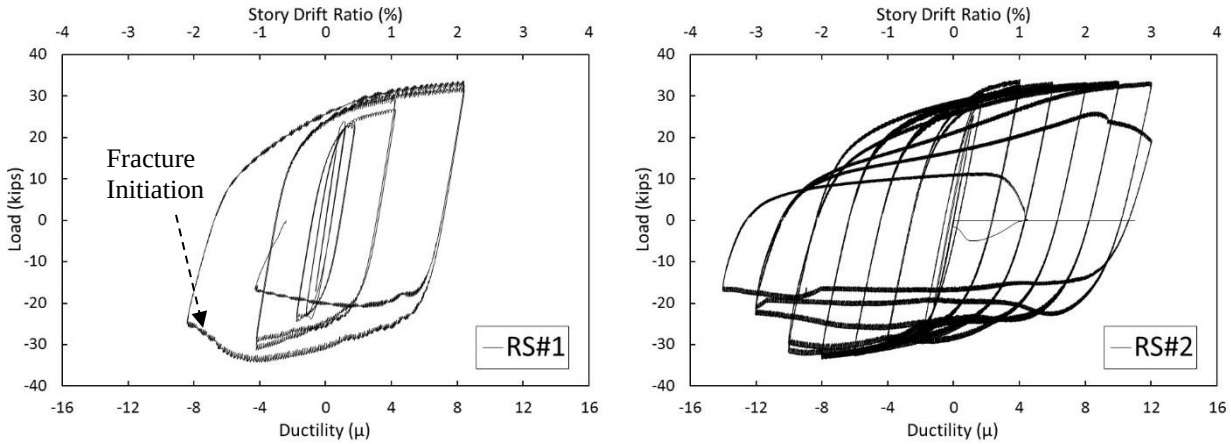

Figure 39: Hysteretic response of the test specimens (Seker, 2016).

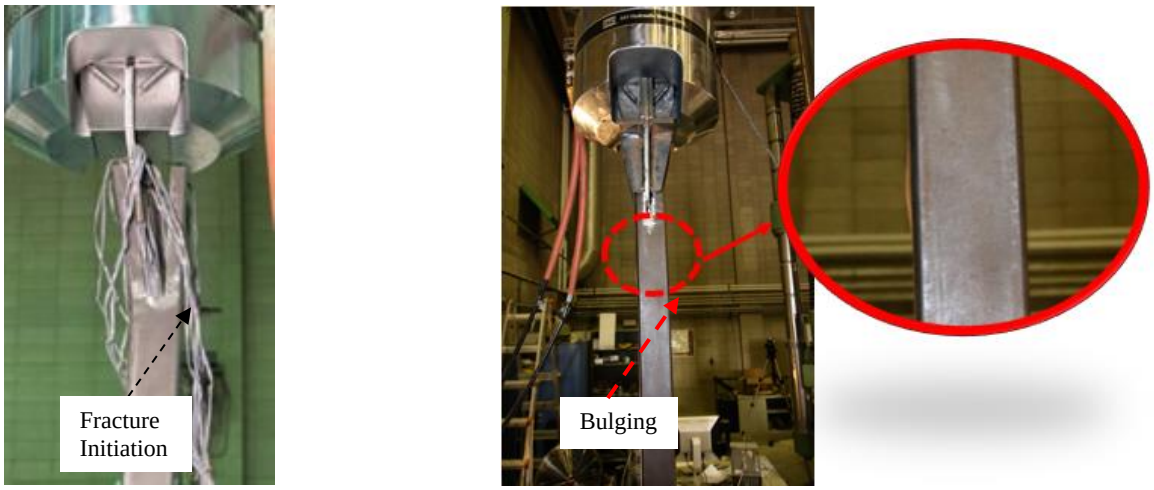

a) Fracture initiation at the outer tube in RS#1. b) Local deformation of outer tube in RS#2.

Figure 40: Deformation of RS#1 and RS#2 specimens (Seker, 2016).

Overall, the findings of the experimental portion provided compelling evidence to substantiate that inelastic cyclic behavior of the tested specimens was quite consistent with the observed deformation patterns in the simulation-based study. In fact, the deformation patterns obtained from the simulated BCBs and the tested BCB specimens were governed by two major limiting conditions: (1) Global instability of the entire assembly due to small ratio of outer tube to inner tube thickness; and (2) Local deformation of the outer tube due to local plastic deformation of the inside tube. Hysteretic responses of the RS#1 specimen, comprised of conventional gusset plates designed for ductile CBFs, were controlled by end rotation-induced global instability, so premature fracture of the outer tube did not allow the plastic deformation capability of the inside tube to be fully utilized. The RS#2 specimen, on the other hand, had shown stable hysteretic response, ability to control global and local deformations up to a 0.025 inter-story drift ratio, as well as dissipation of a greater amount of energy compared to both the RS#1 specimen and conventional braces. It is also noteworthy that the outer tube of RS#2 was not thick enough to resist the lateral thrust induced by the lateral expansion or potential local deformation of the inside tube, so bulging of the outer tube of RS#2 specimen resulted in significant gradual strength degradation, as observed in the numerical study.

3.4. Cyclic Behavior of CBFs incorporating BCBs

The behavior of the RS cases was studied and described experimentally and numerically in previous sections. In this section a tested ductile CBF specimen was first simulated, then the previously calibrated conventional CBF model was modified by introducing buckling-controllers to determine their effects on frame behavior.

3.4.1. Calibration of FE Model

A full-scale experimental test was performed in 2008 by Uriz and Mahin (2008) at the University of California, Berkeley (Uriz and Mahin, 2008). The tested frame was the two-story nearly full-scale CBF with inverted V-type braces shown in Figure 41. A general-purpose finite-element (FE) software tool, ABAQUS 6.13.3 (Hibbitt, et al., 2001), was used for simulating the tested frame. A reduced integrated three-dimensional eight-node solid-element configuration (C3D8R) was employed in the models and the coupon test results provided in (Uriz and Mahin, 2008) were used for the material properties provided in Table 8. Lateral supports were also applied to the middle of both the beams and the beam-to-column connections of the first story.

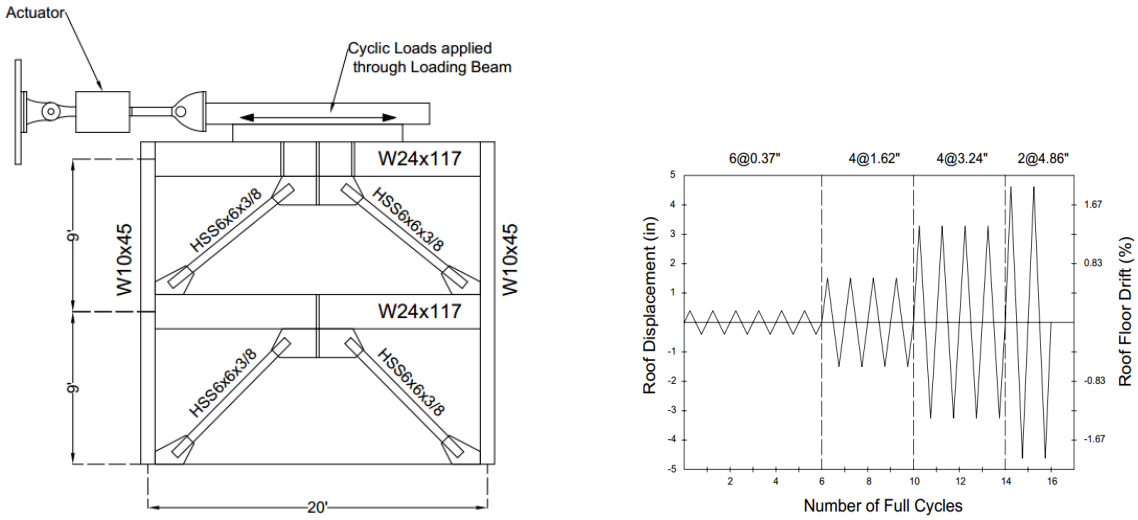

Figure 41: Tested Frame by Uriz and Mahin (2008) and Loading Sequence.

Table 8: Material Properties.

Member	ASTM Grade	Nominal Stress		Coupon Test	
		F_y (ksi)	F_u (ksi)	F_y (ksi)	F_u (ksi)
Beams and Columns	A993	50	65	55	74
Braces	A500 Grade B	46	58	60.6	65.9
Gusset Plates and Plate Stiffeners	A36	36	58	56	78

A gap was introduced in the flanges and some portion of the web of the beams in the beam-to-column connections (Figure 42) to simulate the behavior of the actual connections constructed with shear tabs. Using such a gap would produce results for the tested and simulated frames similar to one another except for the local behavior of the beam adjacent to the connection, an area not within the scope of this study. A simulated frame was analyzed under simplified version of cyclic loading applied to the tested frame. The lateral force versus roof displacement of the actual frame and simulated frame using the coupon test results and nominal material properties are compared in Figure 43. The simulation successfully predicted the global response of the frame along with the out-of-plane rotation of the gusset, stress concentration of the column, and local buckling of braces until fracture, as shown in Figure 44 and Figure 45.

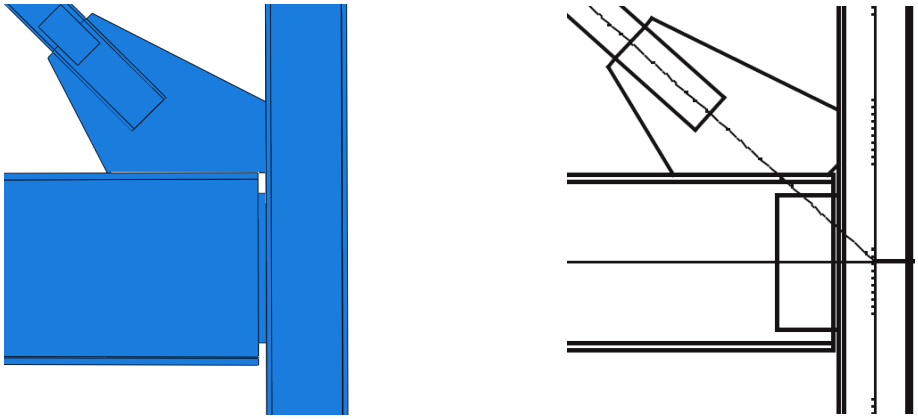

Figure 42: Simulated Connection and Layout of Constructed Connection (Uriz and Mahin, 2008).

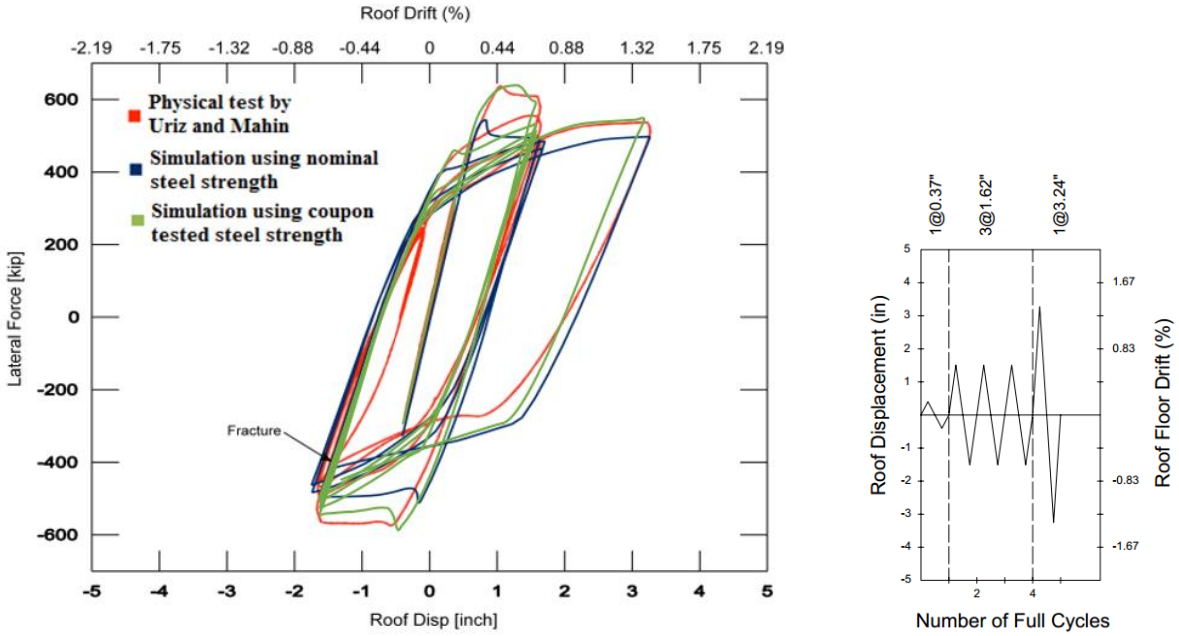

Figure 43: Simulation and test results under major portion of the cyclic loading sequence (Uriz and Mahin, 2008).

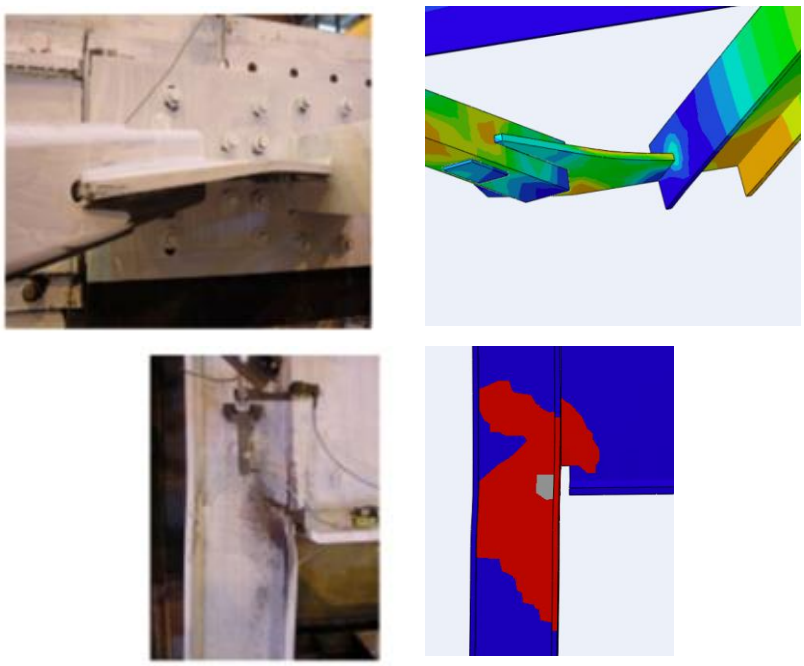

Figure 44: Local behavior of the members in tested and simulated frames (Uriz and Mahin, 2008).

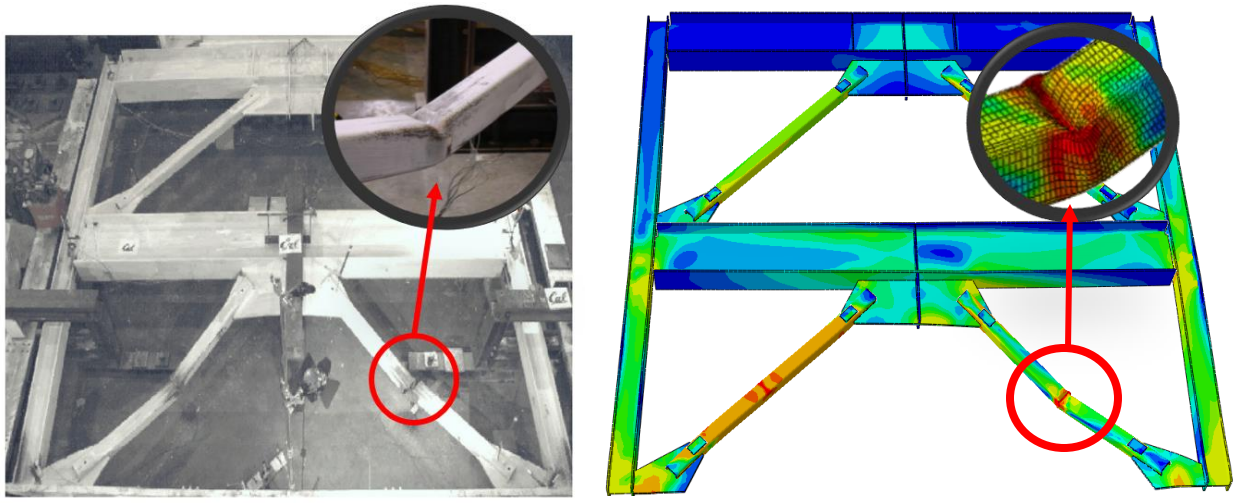

Figure 45: Comparison of the deformed shapes of tested (Uriz and Mahin, 2008) and simulated frames.

3.4.2. Cyclic response of ductile CBFs with buckling controllers

Based on the cyclic response of the isolated BCBs, stable and symmetrical hysteretic behavior of these braces can substantially improve the performance of CBFs. To further investigate their impact, the RS4 and RS1-S cases (one case with and one without stiffener) were incorporated into the chevron CBF, respectively. The original FE model of the tested frame, previously presented in the verification study, was simulated once again using HSS7.5x0.375 sections as bracing members to enable comparison of the conventional frame with the BCB frame. Note that both the square tubes incorporated in the tested CBF specimen and their circular substitutes possess comparable compressive and tensile strengths.

Nominal material strength was used for the brace members to make the two frames comparable. Mesh size of 2 inches was adopted for all members except for the braces. An additional seed was used for the outer and inner tubes to capture potential local deformations of the braces accurately. A reduced integrated 3D 8-node linear brick element configuration (C3D8R) was employed for the simulation of the members. Static general analysis was utilized for analyzing the frames and a dissipated energy fraction of 3e-4 was used for automatic stabilization to help

with convergence. A penalty method was used for the tangential surface-to-surface interaction between the inner and outer tube to simulate the actual behavior of the tube in tube braces.

3.4.2.1. Cyclic response of the frames

Figure 46 shows the dimensions of the simulated frame, lateral supports, and the displacement-type loading applied on the top flange of the roof girder. The simplified loading sequence used in the frame simulations is presented in Figure 35.

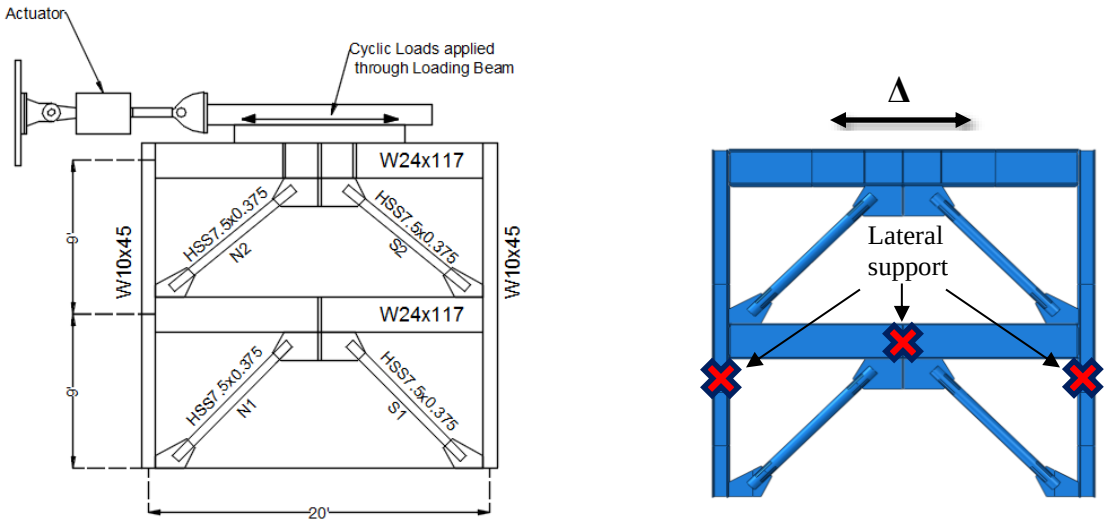

Figure 46: Simulated conventional CBF with circular bracings.

Numerous experimental investigations (Nip, et al., 2010; Fell, et al., 2009; Tremblay, et al., 2008; Han, et al., 2007) on inelastic cyclic behavior of HSS braces have demonstrated that the peak ductility that can be attained by cold-formed tubes varies depending on the width-to-thickness (b/t or D/t) ratio (Fell, et al., 2009; Black and Wegner, 1980) and slenderness ratio (Tremblay, et al., 2008) of specimens. Based on the aforementioned experimental data, conventional steel HSS braces, either rectangular or circular, with realistic width-to-thickness ratios, are most likely to fracture prior to attaining a brace ductility of 10, so in the present study, two distinct measures were assumed for both conventional CBFs and BCB frames as the governing limit states: (1) In light of the experimental data, it was conservatively assumed that conventional braces reach their

fracture-resistant limit during the first tension cycle subsequent to attaining a ductility of 10 in compression; (2) BCB frames are subjected to cyclic loading until significant strength degradation occurs either in tension or compression.

Figure 47 presents a comparison between the hysteretic responses of S1 braces (the brace in the first story to the south) in the conventional and BCB frames. Figure 48 and Figure 49 present the deformation of the frame and stress distribution, respectively, in the first story gusset plates. The following observations can be made:

i. A BCB frame successfully reached 3.2% SDR, while braces in the conventional frame fracture about 2% SDR. Peak brace ductility attained by BCBs without any strength degradation is at least 1.3 times larger than that of conventional braces. Note that BCB are not necessarily fractured after 3.2% SDR.

ii. BCBs in both stories yielded in both tension and compression. Stable and symmetrical hysteretic behavior of BCBs until 3.2% SDR, presented in Figure 47, results in significantly larger energy dissipation than with a conventional frame.

iii. The braces in the first and second stories of BCB frames exhibited a similar hysteretic response, but the cyclic response of the braces in the conventional CBF widely differed from one story to another. As indicated in Figure 48(a), the first story braces experienced in-plane and out-of-plane buckling simultaneously and eventually reached their fracture-resistant limit, while the inelastic deformation in the roof story was minor.

iv. Lateral displacement of the conventional frame accumulated in the first story of the frame due to formation of a soft story subsequent to buckling of the conventional braces, as shown in Figure 48(a). While this abrupt change in strength and stiffness

might simultaneously trigger torsional irregularities and amplify the impact of P-Δ effects significantly, incorporating BCBs led to a uniform lateral displacement distribution along the height of the frame, as shown in Figure 48(b).

v. The first story gusset plates of the conventional frame suffered large stresses, shown in Figure 49a, due to the bending moment induced by out-of-plane buckling of the braces. Introducing buckling-controllers resulted in a significant decrease in the stress level of gusset plates, even without enhanced connections (Figure 49b). As presented in Figure 49(c), utilizing stiffeners in the gusset connections further reduced the stress of the gusset plates.

vi. Although utilizing BCBs substantially improves the cyclic behavior of the CBFs in terms of energy dissipation and ductility, large stress distribution in the columns of both conventional and BCB frames could be a major concern that should be addressed in future studies.

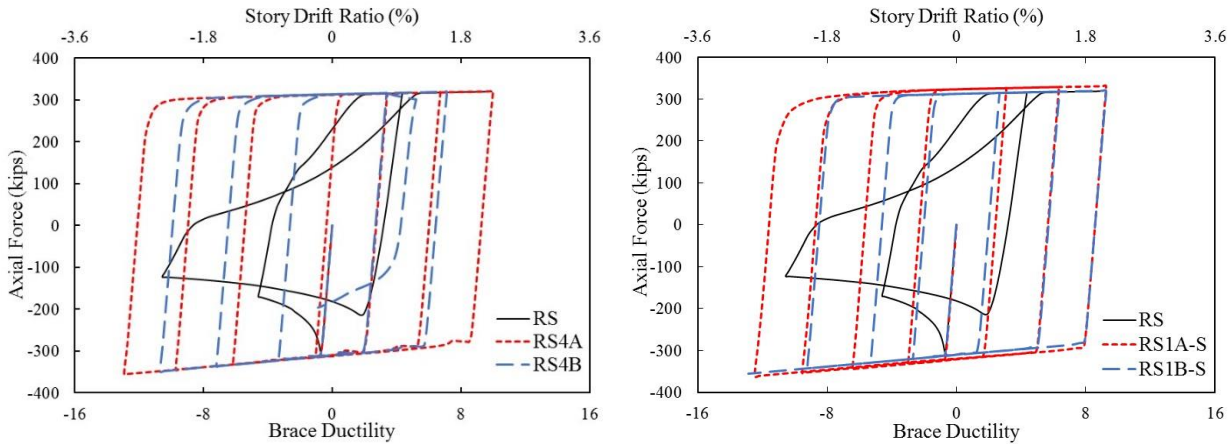

a) RS vs. RS4 cases b) RS vs. RS1-S cases

Figure 47: Hysteretic response of S1 brace.

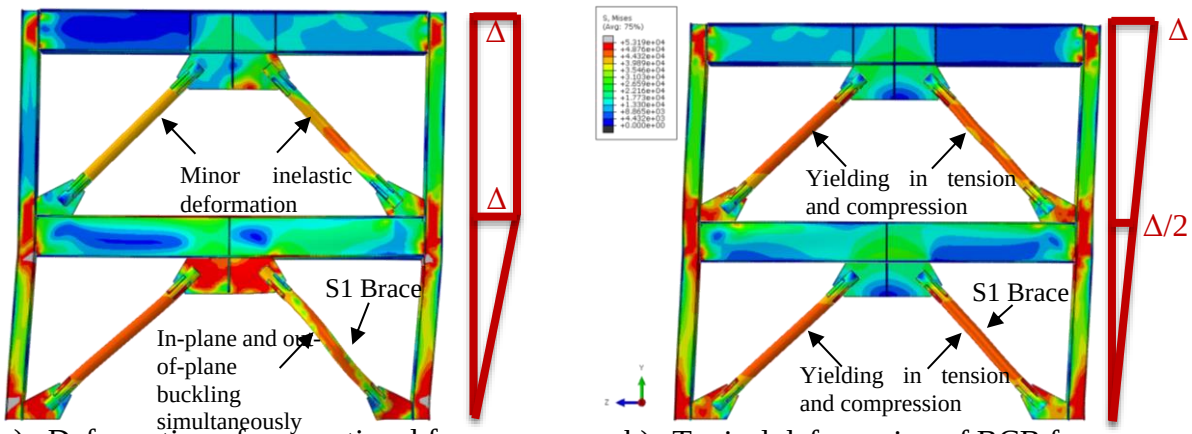

a) Deformation of conventional frame b) Typical deformation of BCB frame

Figure 48: Comparison of the deformation of conventional and BCB frame.

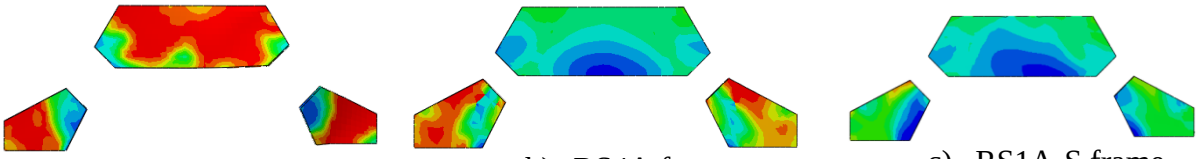

a) Conventional frame b) RS4A frame c) RS1A-S frame

Figure 49: Stress distribution in the first story gusset plates.

3.5. Conclusions

This chapter discussed investigation of the performance of a newly developed all-steel buckling-controlled brace with different cross sections. Cyclic behavior of these braces was evaluated through finite-element analysis in terms of ductility and energy dissipation. Performance of CBFs incorporating BCBs was then compared with conventional CBFs. The major objectives of this chapter were (1) to compare the performance of two BCB configurations; and (2) to reveal the advantages of developed BCBs compared with conventional braces. The major conclusions of this chapter are as follows:

i) The thickness ratio of the outer tube to the inner tube should be greater than one to effectively control local buckling of the main brace.

ii) Although round-in-square BCBs exhibit desirable performance either when the thickness ratio of the outer tube to the inner tube is greater than one or when an enhanced gusset plate is employed, regardless of the thickness ratio in square-in-round BCBs, it is necessary to utilize an enhanced gusset plate to achieve promising results.

iii) Experimental and numerical results demonstrate stable and symmetrical hysteretic behavior of BCBs until 3% SDR. It can be observed that BCBs are significantly more ductile than conventional braces and the larger enclosed area of the cyclic loops in BCBs results in greater energy dissipation compared to that of conventional braces.

iv) The symmetrical cyclic behavior of BCBs results in substantial reduction in unbalanced force applied to brace-intersected girders. It can be observed that this reduction can be as large as 80% at a 3% story drift ratio.

v) While early buckling of conventional braces can potentially lead to a soft/weak story in braced frames, thereby accumulating a lateral displacement of the frame in such a story, incorporating BCB efficiently causes a linear distribution of lateral displacement along the height of the frame.

vi) Incorporating BCBs results in a significant decrease in gusset-plate stress. Controlling the out-of-plane buckling of the braces eliminates the flexural demand on the gusset plate and diminishes the stresses. In addition, utilizing enhanced gusset plate further reduces gusset-plate stress.

CHAPTER 4. SEISMIC BEHAVIOR OF SCBFs UNDER EARTHQUAKE GROUND MOTIONS

4.1. Introduction

AISC341-16 categorizes CBFs into two groups of ordinary concentrically braced frames: (OCBFs) and special concentrically braced frames (SCBFs). OCBFs are expected to provide limited inelastic deformation capacity in their members and connections, so in such frames braces should be designed as moderately ductile members and beams and their connections should be determined using over-strength seismic loads. On the other hand, SCBFs are expected to provide significant inelastic deformation capacity primarily through brace buckling and yielding of braces in tension, so columns, beams, and braces in these frames are required to satisfy the restrictions of highly ductile members (AISC341-16). Also, the required strength of columns, beams, and connections in SCBFs should be determined using a capacity-limited seismic load effect to ensure that they remain elastic during an earthquake. However, limited number of recent investigations have shown that beams and columns might experience yielding during an earthquake (Shen et al. 2015) and therefore deviate from the current design code.

In this chapter, seismic behavior of a 9-story SCBF is investigated under an ensemble of earthquake ground motions to assess whether current provisions are met. At the beginning of this chapter, a building description is presented with one of its braced frames designed based on three approaches:

i) A Two-Story X-Braced frame is used as the lateral load resisting system. This frame is designed in conformance with the current design code.

ii) A Two-Story X-Braced frame is used as the lateral load resisting system. In this frame, the effects of the V-braces in even stories are neglected in the design procedure and brace-intersected beams similar to chevron (inverted V) frames are used.

iii) A Chevron frame is used as the lateral load resisting system. This frame is designed in conformance with the current design code.

In the second part of this chapter, the group of 20 earthquake ground motions used in this study is presented, followed by investigation of the effect of the gusset plates on the behavior of the shear connections through finite-element simulations; the conclusions drawn from the finite element simulation are utilized in modeling the 9-story frame. In the last part of this chapter, seismic behavior of designed braced frames are studied through a non-linear dynamic time history analyses.

4.2. Building Description

In the present study, three different braced frames were designed and their seismic behavior were investigated under various ground motions. Typical floor plans shown in Figure 50 present the orientation of the secondary beams and bay widths in each direction. It can also be seen that the SCBFs are located in the perimeter frames to resist lateral forces. The two different types of bracing configurations used in this study are presented in Figure 51. Perimeter frames are assumed to carry a small portion of gravity loads based on their tributary area and half the lateral force in each direction is transferred to every SCBF as well. Interior beams and columns are designed based on the gravity load applied in their tributary areas.

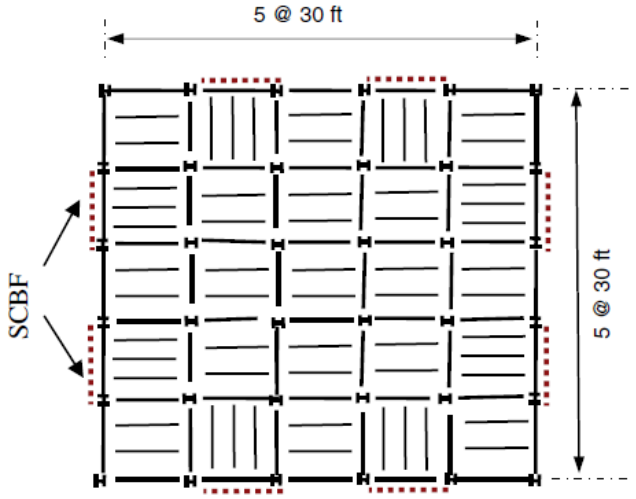

Figure 50: Typical floor plan with locations of SCBFs.

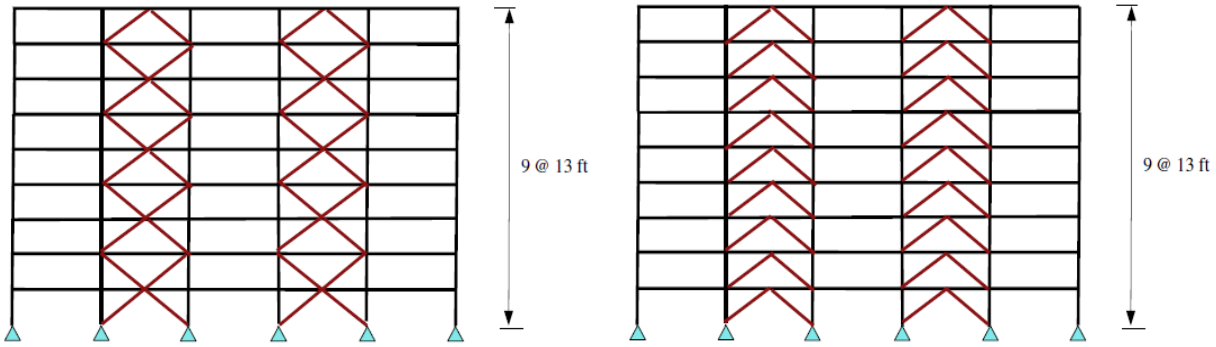

a) TSXB configuration. b) Chevron bracing configuration.

Figure 51: Elevation of designed frames.

Assumed dead and live loads of 80 psf and 50 psf, respectively, are applied on 3-1/2 in. thick concrete constructed on a metal deck with steel shear studs welded to the beams on each floor. The roofing system provides a non-flexible diaphragm that transfers lateral forces to the SCBF. The building is designed in conformance with the provisions of ASCE7-10 for required design strength and AISC 341-10 for seismic design requirements, and the building is assumed to be located on a site with S_s and S_1 equal to 2.0 and 1.0, respectively. As the base shear, 22% of the building weight is applied to the building in each direction, and each braced bay is designed based on a quarter of the total base shear. The loading combination governing design of the braces is

$(1.2+0.2S_{DS})DL+1.0LL+\rho Q_E$, where ρ (the redundancy factor) is assumed to be 1.3. Identical brace sizes are used for every two consecutive stories and brace sections are selected by considering the strength, slenderness ratio, and ductility criteria specified in AISC 341-16. Moreover, Beams and columns are designed based on the capacity of the braces according to the provisions of AISC 341-16 with highly ductile and moderately ductile sections selected for columns and beams, respectively, to satisfy the current design code requirement. Round or rectangular HSS sections are chosen for braces, while W sections are used for beams and columns. In addition, gravity beams and columns are designed based on the load acting on their tributary area.

In addition to following this frame design, an additional design approach has been taken into account. Previous studies have shown that current design codes have not been able to predict the proper required beam size in TSXBFs (Shen, et al., 2015), mainly because the unbalanced force from the braces applied to the beam would be zero if the same section was used for braces in alternating stories. In other words, the beams will not be designed for seismic loads which is not conservative. To overcome this issue, an additional frame has been designed by removing the V-type braces in the upper story of the brace intersected beams, leading to a strong beam similar to those usually used in chevron frames. The two different design approaches are presented in Figure 52. For simplicity in comparing the results, the TSXBF with strong beams will be referred to simply as "Frame S" and the regular TSXBF that is designed according to the current design code [AISC 341-10, ASCE 7-10] will be designated as "Frame W", and the chevron frame will be designated as "Frame C". Table 9 shows the summary of the section sizes used for each member.

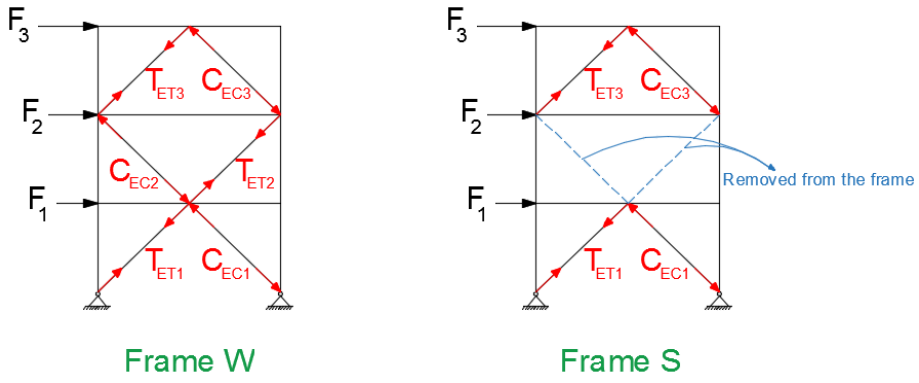

Figure 52: Two approaches for designing braced-intersected beams.

Table 9: Member sizes of the 9-Story Braced Frame

Level	Braces	Columns in braced bays	Beams			Gravity Columns	Gravity Beams
			Frame W	Frame S	Frame C		
9	HSS 8.625×0.375 (KL/r = 81, D/t = 24.7)	W14×48	W30×211	W30×211	W30×211	W10×33	W18×65
8	HSS 10×0.625 (KL/r = 71.1, D/t =17.2)	W14×132	W18×86	W18×86	W33×318	W10×33	
7			W18×65	W30×326			
6	HSS 10×10×5/8 (KL/r = 62.5, b/t = 14.2)	W14×233	W21×93	W21×93	W36×395	W10×33	
5			W18×65	W33×387			
4	HSS 14×0.625 (KL/r = 50, D/t = 24.1)	W14×370	W21×111	W21×111	W36×395	W10×33	
3			W18×65	W36×395			
2	HSS 14×0.625 (KL/r = 50, D/t = 24.1)	W14×550	W21×111	W21×111	W36×395	W10×33	
1			W18×65	W36×395			

4.3. Earthquake Ground Motions

Ten pairs of earthquake ground motions compatible with site class D have been used in this investigation. Ground motions are selected from the PEER ground motion data base using S_{DS}=1.333(g), S_{D1}=1.000(g), and T_L=12.0 s. Response spectra of the ground motions are represented in Figure 53 as black solid lines, and not more than two of the ground motions are taken from any one earthquake to avoid event bias. The target design spectrum achieved from ASCE7-10 is also represented in this figure by a blue line. The period of the first mode of the frame is shown with a purple dashed line in Figure 53. Detailed information on these ground motions is summarized in Table 10, and ground-motion time histories are presented in Appendix A.

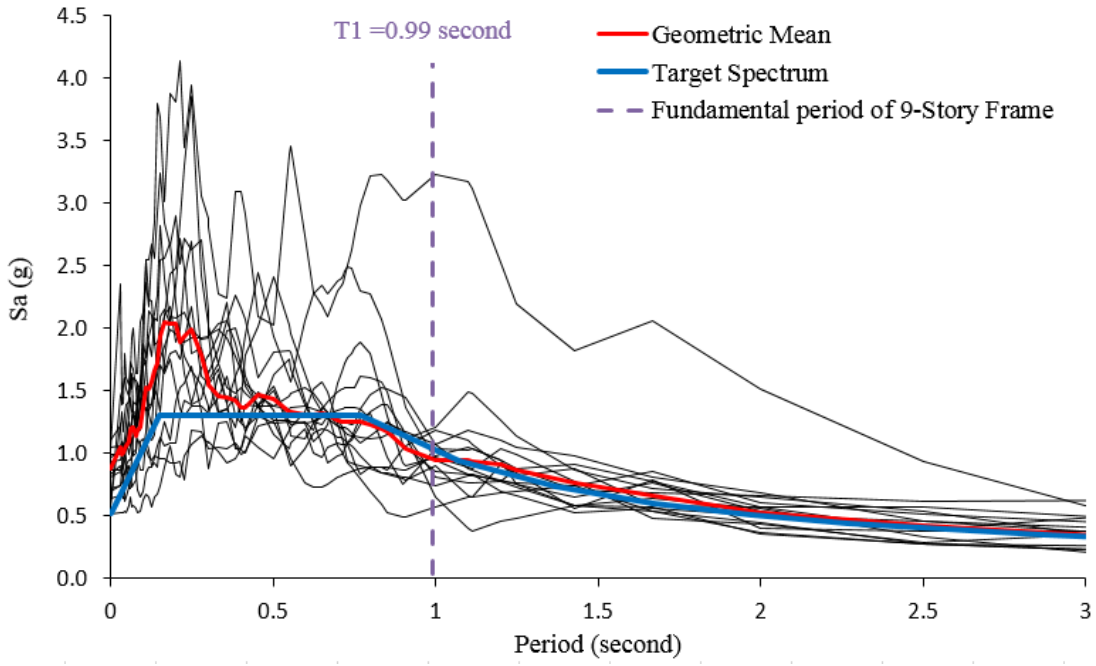

Figure 53: Response spectra of twenty ground motions used in this study.

Table 10: Ground motions used in this study.

ID no.	NGA#	Sc. factor	Event	Year	Mag	Duration(s)	PGA(g)	PGV(in./s)
GM01	1085	1.1675	Northridge	1994	6.69	40	0.979	53.5
GM02							0.578	36.0
GM03	1489	2.8835	Chi-Chi-Taiwan	1999	7.62	90	0.810	50.8
GM04							0.718	65.0
GM05	1515	2.5841	Chi-Chi-Taiwan	1999	7.62	90	0.643	57.1
GM06							0.513	50.2
GM07	1009	3.8019	Northridge	1994	6.69	55.33	1.041	48.4
GM08							0.985	36.8
GM09	726	6.5733	Superstition Hills	1987	6.54	21.89	0.817	20.3
GM10							1.059	46.1
GM11	179	1.9573	Imperial valley	1979	6.53	39	0.699	60.0
GM12							0.929	30.9
GM13	802	2.3023	Loma Prieta	1989	6.93	39.955	0.835	50.3
GM14							0.866	39.2
GM15	779	1.0816	Loma Prieta	1989	6.93	25.005	1.021	41.3
GM16							0.581	30.7
GM17	722	4.8465	Superstition Hills	1987	6.54	21.98	0.512	27.2
GM18							0.669	63.1
GM19	1148	7.2093	Kocaeli-Turkey	1999	7.51	30	1.566	57.2
GM20							1.098	109.4

Note: NGA# - sequential number in PEER strong ground motion database.

4.4. Effect of the Gusset Plates on the Behavior of Shear Connections

Girders in braced frames are usually connected to columns with shear connections. Two types of such shear connections are used in the TSXBFs, as can be seen in Figure 54. The connections in the odd stories can be assumed to be pin connections since a negligible bending

moment is transferred from the beam to the column, so researchers usually simulate the beams as pin-pin members, even though in even stories adding two gusset plates to the top and bottom of the shear connections makes this assumption questionable.

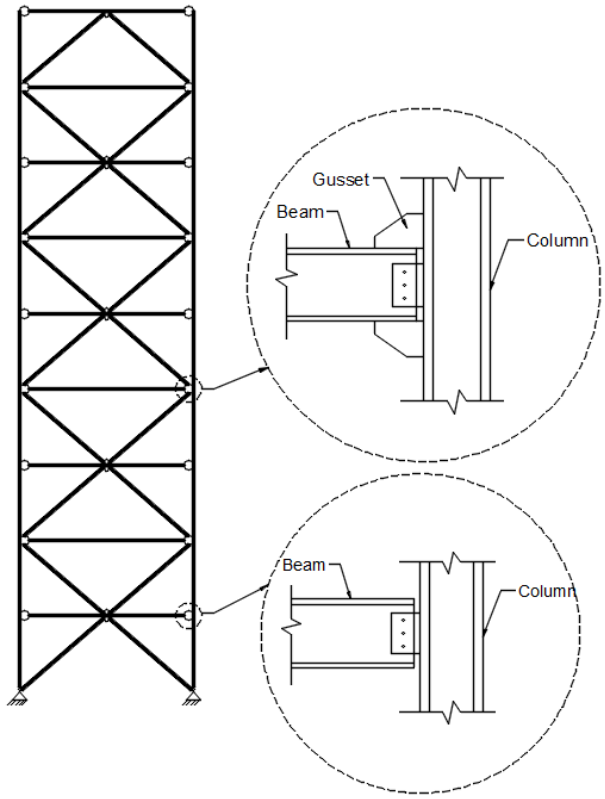

Figure 54: Two types of shear connections in a TSXBF.

To assess the rigidity of the aforementioned shear connections, the frame shown in Figure 55 was simulated in ABAQUS with two types of connections: 1) with gusset plate and 2) without gusset plate. Lateral displacement is applied to the beams at both stories to represent first-mode deformation of the frame.

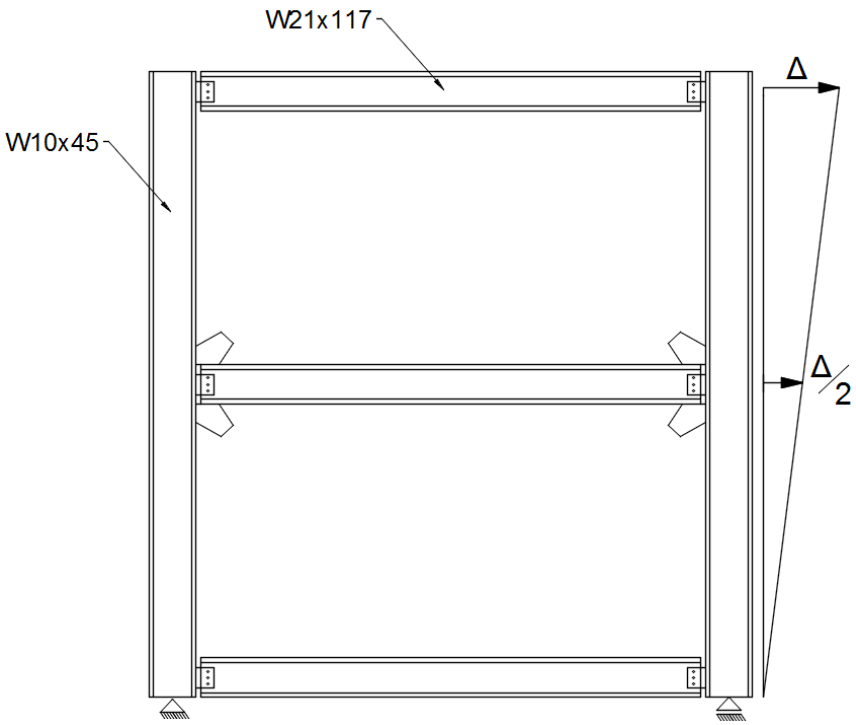

Figure 55: Simulated frame in ABAQUS for connection rigidity study.

Because local behavior of the connection is important for assessing the rigidity of a beam-to-column connection, an authentic shear tab connection was simulated in the frames. A Pl 19×7×5/8 in^3 and six 3/4" A325 bolts were used for the shear tab connection simulation, as can be seen in Figure 56 (the shear tab is removed from this figure). Materials presented in Table 11 were used for the members and C3D8R elements were used for meshing the parts. A 1/16" tolerance was defined between the bolt and hole edge from constructability considerations. Two general static steps were defined in the software for analyzing the frame. In the first step, a pre-tensioning load was applied to the bolts while the lateral displacement of the frame was still zero. In the second step, a pushover analysis was performed on the frame. A hard surface-to-surface interaction was defined between the bolts and the holes to prevent any penetration while the gusset plates were tied (welded) to the beam and columns.

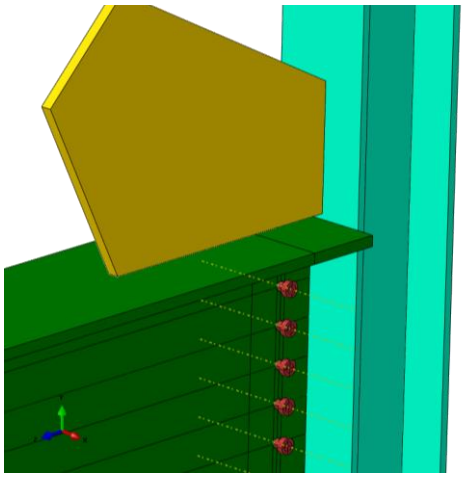

Figure 56: Details of the shear connection simulated in ABAQUS.

Table 11: Material properties [Uriz (2005)].

Member	ASTM Grade	Nominal Stress		Coupon Test	
		F_y (ksi)	F_u (ksi)	F_y (ksi)	F_u (ksi)
Beams and Columns	A993	50	65	55	74
Braces	A500 Grade B	46	58	60.6	65.9
Gusset Plates and Plate Stiffeners	A36	36	58	56	78

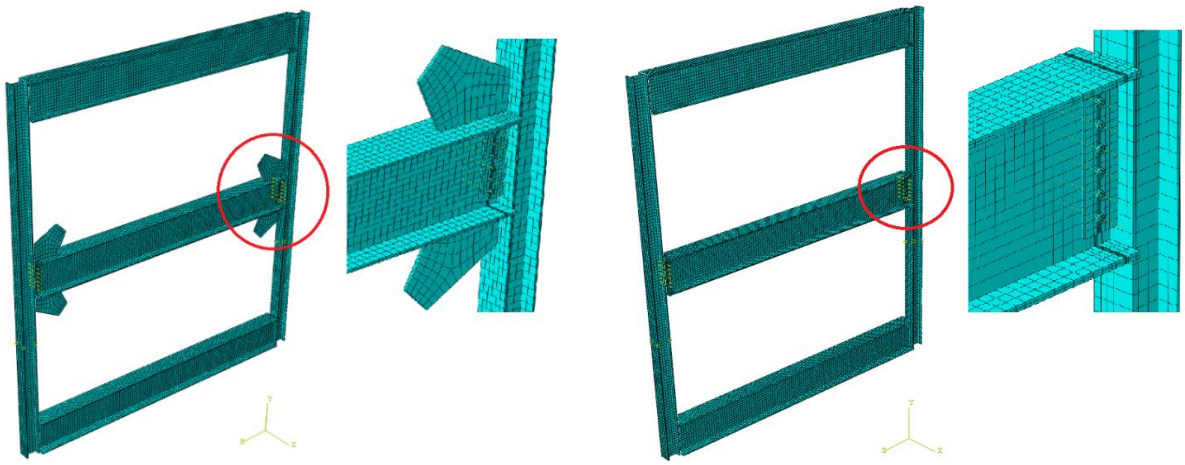

a) Connection with gusset plate b) Connection w/o gusset plate

Figure 57: Simulated frame in ABAQUS.

Relative rotation of the beam and column is measured in this study to evaluate the rigidity of the connection. The angle between the beam and column with a fully rigid connection remains 90º, so the relative rotation (called connection rotation in this study) between these two members is zero. However, in a shear connection, a beam and a column can rotate independently, so the smaller the connection rotation becomes, the more rigid the connection. Rotation of the members can be calculated by subtracting the displacements of the top and bottom nodes of the section and dividing the result by the depth of the section. Figure 58 shows a comparison of the connection rotation between two cases. As can be seen in Figure 58, at 1.5% SDR the connection rotation in the frame without a gusset plate is much larger than for the other case.

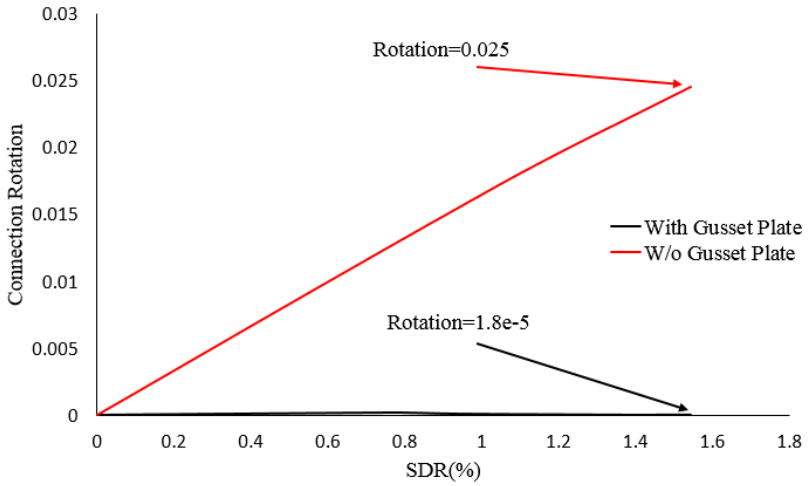

Figure 58: Comparison of connection rigidity between with and w/o gusset plate cases.

The difference between connection rotations can also be seen in Figure 59. The angle between the beam and column in the "with gusset" case is almost 90º, while in the other case, the beam and the column rotate independently. It seems that gusset plates play an important role in stiffening the connections.

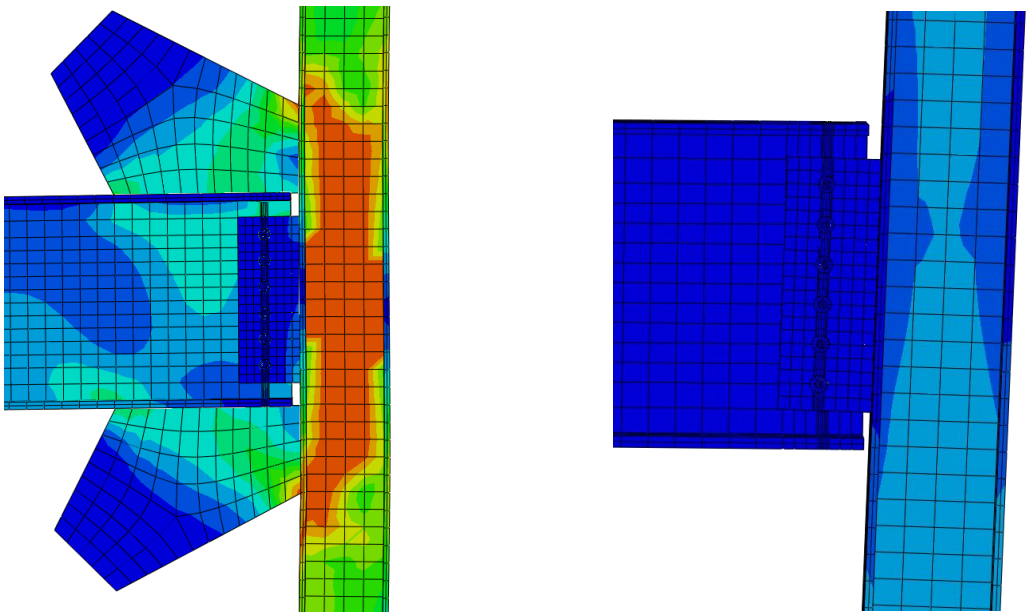

a) Model with gusset plate. b) Model w/o gusset plate.

Figure 59: Finite element result at 1.5% SDR.

Although connections with no gusset plate performed similarly to expectations, it seems that by adding the gusset plates to the connections, the behavior of the connections become more like a rigid connection. It is worth mentioning that the rotation calculation is only valid in the elastic range, and after the yielding point, it is hard to estimate the exact rotation of the members due to the complex inelastic local behavior of sections. In conclusion, in the current study, connections with two gusset plate welded to the beam and column are simulated as a rigid connection to increase the accuracy of the results. Conversely, other connections (without any gusset plates) are modeled as pin connections to simulate the actual behavior of the frame.

4.5. Verification of RUAUMOKO-2D Model

Dynamic time history analyses of the current study have been carried out using a two-dimensional software tool, RUAUMOKO-2D, developed by Carr at the University of Canterbury, New Zealand (Carr, 2004). Since a major aspect of inelastic behavior of steel braced frame is due to buckling and yielding of the braces, it was necessary to use an accurate model that suitably

predicts the performance of the braces. In this study, the REMENNIKOV model was utilized for simulation of the braces. Figure 60 represents the verification performed by Carr in 2004 of the REMENNIKOV steel brace member (Carr, 2004).

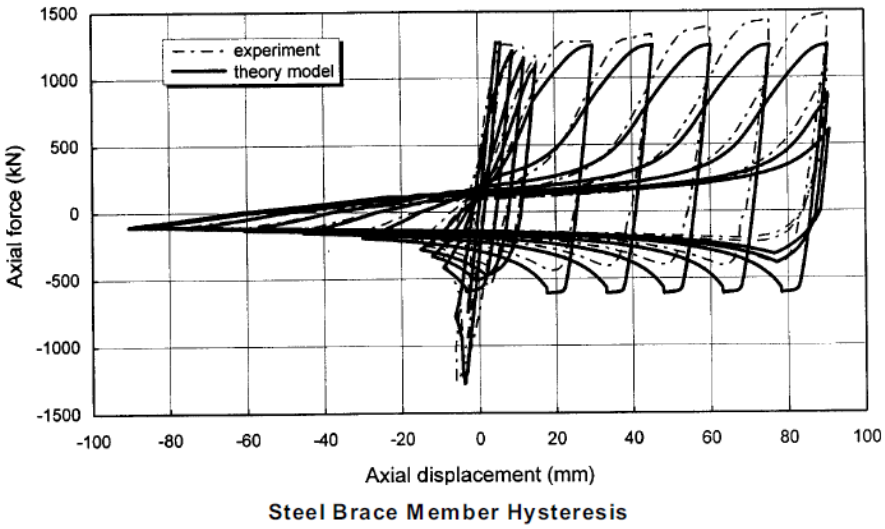

Figure 60: REMENNIKOV steel brace member verification (Carr, 2004).

Five parameters had to be calibrated to accurately simulate the behavior of the braces, and experimental tests on three isolated single members and one tested steel braced frame were simulated in RUAUMOKO-2D to calibrate the parameters of the REMENNIKOV member. Results of the aforementioned simulations are presented in following subsections.

4.5.1. Experimental test by Fell et al. (2009)

In order to evaluate the accuracy of the the simulations and calibrate the brace model, one of the specimens tested by Fell, et al., (2009) was chosen for verification. Figure 61 presents the tested specimen, boundary conditions and loading protocol used in the test.

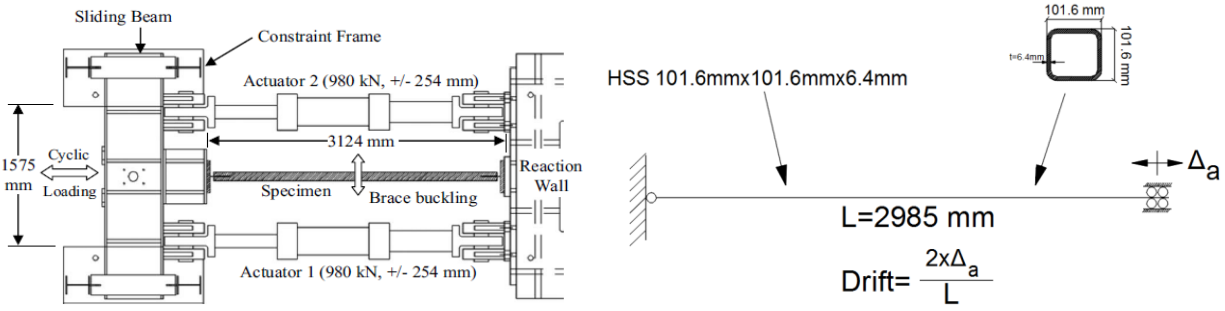

a) Test setup [Fell et al. (2009)]. b) Simulated member.

Standard Cyclic		
#cycles	Δ_a (mm)	Drift (%)
6	1.0	0.08
6	1.5	0.10
6	2.3	0.15
4	3.0	0.20 – B
2	15.5	1.03
2	27.9	1.85
2	40.4	2.68
2	59.9	4.00 - MCE
2+n	75.9	5.00

c) Loading protocol.

Figure 61: Tested specimen by Fell et al. (2009).

An inelastic analysis was performed in RUAUMOKO-2D applying the static displacement loading protocol shown in Figure 61. A time step of 5e-5 was chosen to ensure the accuracy of the results and properly capture the buckling of the braces. A beam-column element was employed in the simulation and coupon test results shown in Table 12 were assigned to the element.

Table 12: Coupon test results (Fell et al., 2009).

	E (ksi)	Fy (ksi)	ν
Material Properties	29000	74	0.3

Figure 62 shows a comparison between experimental and simulation results in which a simulated member has accurately captured the buckling point, maximum story drift, and the peak tension force, and the overall test results also were satisfactorily predicted by the numerical model as well.

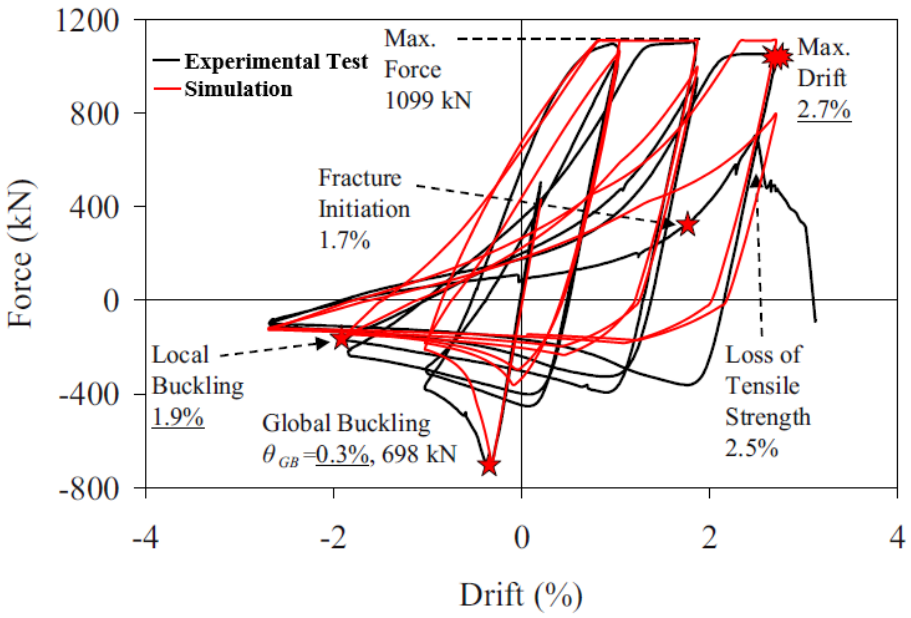

Figure 62: Comparison of simulation and experimental results.

Table 13 presents the parameters employed for simulating the experimental test.

Table 13: Employed Parameters in RUAUMOKO-2D.

k	E1	E2	E3	E4
0.7	0.2	0.95	1.2	0.25

4.5.2. Experimental test by Tremblay, et al., (2008)-RHS 19

A series of experimental tests were performed in 2009 on rectangular and circular hollow sections (RHS and CHS) at the Hydro-Quebec Structural Engineering Laboratory at Ecole Polytechnique of Montreal by Tremblay, et al. Figure 63 shows the testing setup and end

connection attachment. Unsymmetrical gusset plates used in this test provide the real boundary condition of braces employed in steel frames.

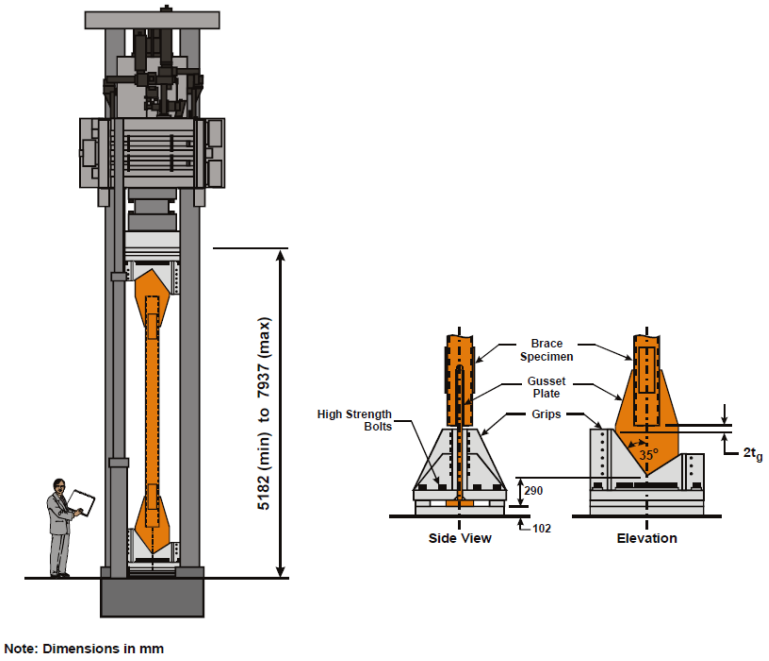

Figure 63: Test setup of experimental tests carried out by Tremblay, et al. (2009).

Figure 64 presents the loading protocol applied to HSS 10×10×5/8 (RHS19) in the experimental test. The length of the specimen was 228 in and slenderness ratio was 60. Material properties are given in Table 14.

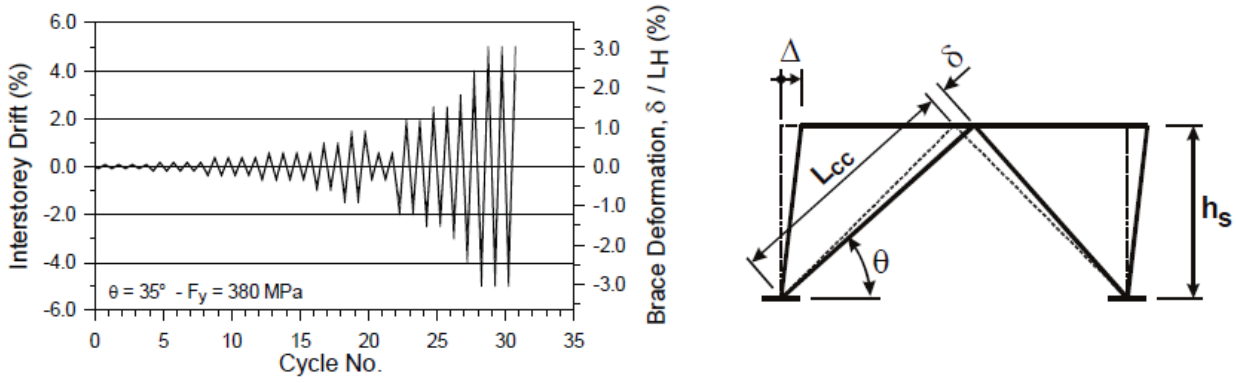

Figure 64: Loading protocol used in experimental test by Tremblay et al. (2009).

Table 14: Material properties used in experimental test by Tremblay et al. (2009).

	E (ksi)	Fy (ksi)	ν
Material Properties	29000	50	0.3

Figure 65 provides a comparison between the simulated and experimental results. As can be observed in this figure, simulation has successfully predicted the buckling of the actual brace and overall behavior of the model is in good agreement with experimental testing.

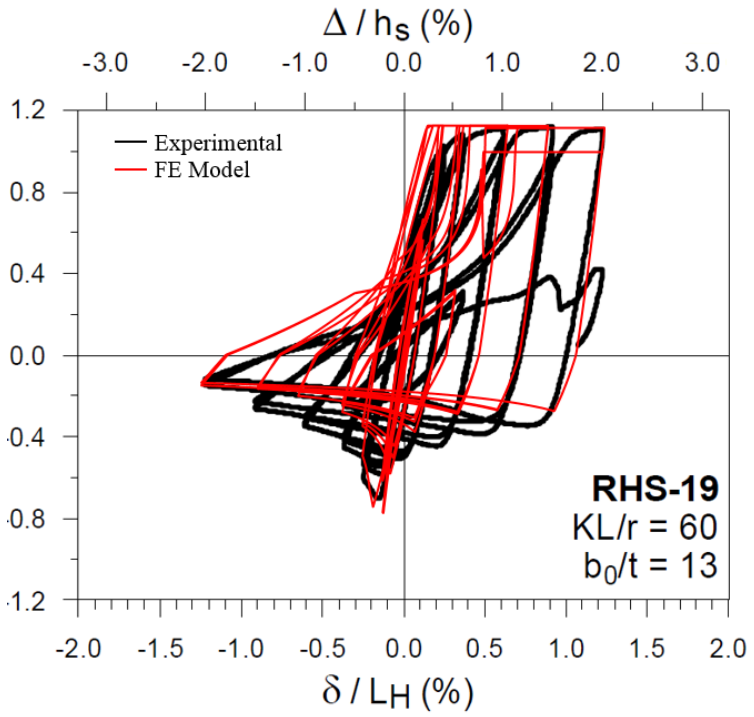

Figure 65: Comparison of simulation and experimental results.

Table 15 presents the brace parameters that were employed in RUAUMOKO-2D to capture the brace behavior.

Table 15: Employed Parameters in RUAUMOKO-2D.

k	E1	E2	E3	E4
0.7	0.2	0.25	1.2	1.4

4.5.3. Experimental test by Tremblay et al. (2009)-RHS2

HSS 10×10×5/8 was tested again using the same loading protocol and test setup described in the previous section, with length of the specimen reduced to 152 in to evaluate the performance of the braces with different slenderness ratios; the slenderness ratio of this specimen was 40. Figure 66 provides a comparison between the simulated and experimental results.

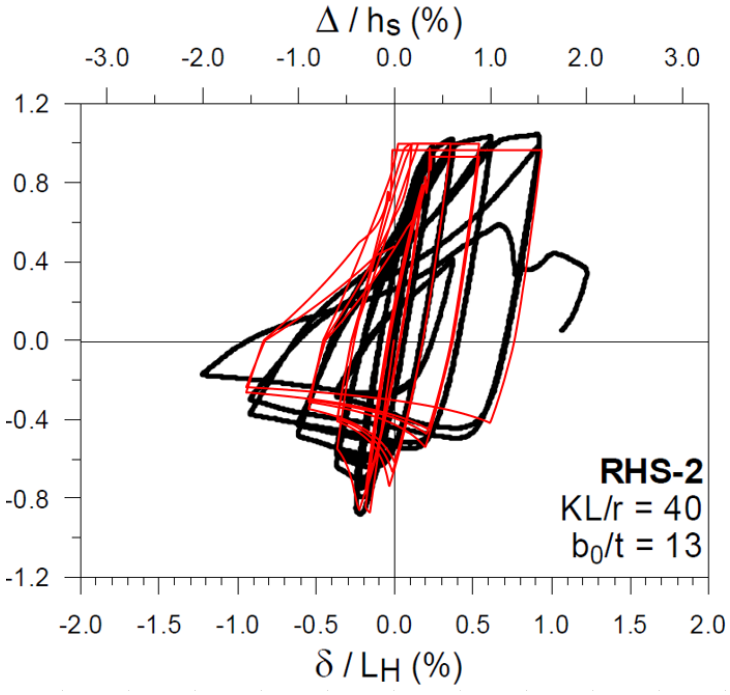

Figure 66: Comparison of simulation and experimental results.

Table 16 shows the parameters utilized in modeling of the RHS2 brace in RUAUMOKO-2D.

Table 16: Employed Parameters in RUAUMOKO-2D.

k	E1	E2	E3	E4
0.7	0.2	0.25	1.2	1.4

4.5.4. Experimental test by Uriz and Mahin (2008)

A full-scale chevron frame tested by Uriz and Mahin (2008) was modeled in RUAUMOKO-2D to evaluate the accuracy of the brace behavior in a steel frame using test setup, loading protocol, and boundary conditions described in previous sections. Figure 67 shows the node and element numbers used in RUAUMOKO. Details of the frame simulation are provided in Appendix B.

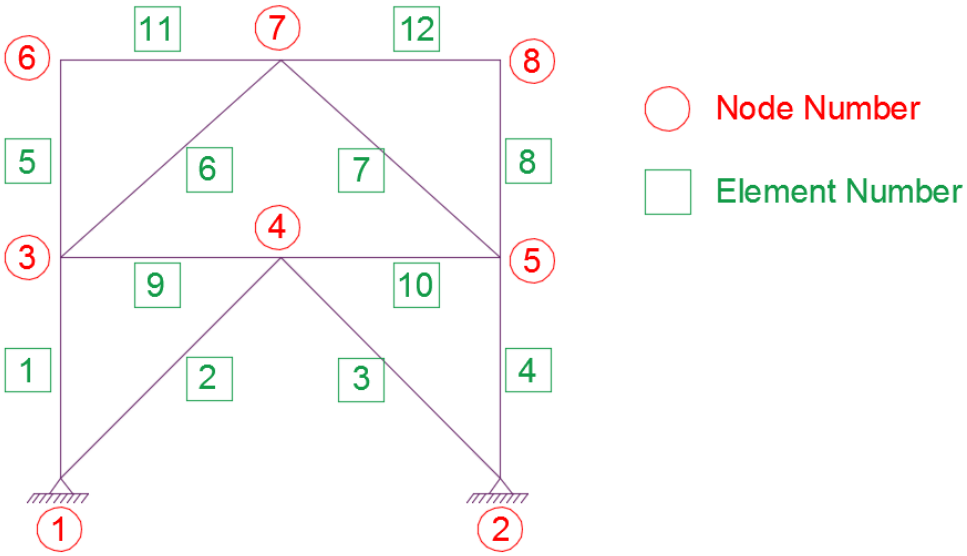

Figure 67: Uriz and Mahin tested frame (2008) simulated in RUAUMOKO-2D.

Figure 68 provides a comparison between the experimental and simulation results. As can be seen, overall behavior of the frame is accurately captured by the model and cyclic performance of the frame prior to the fracture and strength loss of the experimental results is in good agreement with the simulation results.

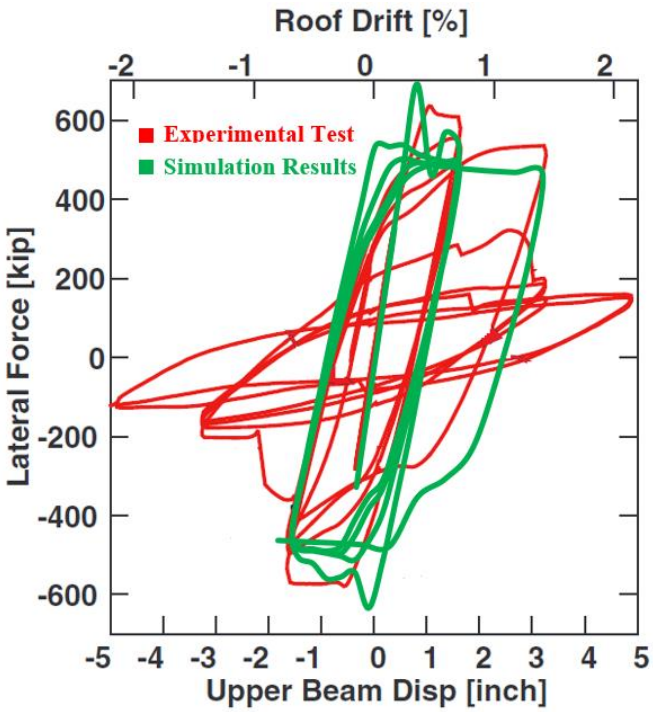

Figure 68: Comparison of simulation and experimental results.

Table 17 provides the calibration parameters utilized in modeling of the braces of the frame in RUAUMOKO-2D.

Table 17: Employed Parameters in RUAUMOKO-2D.

k	E1	E2	E3	E4
0.7	0.2	0.25	1.2	1.4

According to the provided results, a REMENNIKOV member can successfully predict the actual behavior of the steel braces if proper parameters are employed in the simulation. Considering the simulation results provided in this section, brace parameters can be divided into two groups based on the slenderness ratio of the section, and Table 18 presents different values for the parameters based on the slenderness ratio of the braces.

Table 18: Brace parameters achieved from verification of models with experimental results.

Kl/r	k	E1	E2	E3	E4
40-65	0.7	0.2	0.25	1.2	1.4
65-80	0.7	0.2	0.95	1.2	0.25

Since slenderness ratio of the braces used in the 9-story frame varies between 50 and 80, values of the brace parameters presented in Table 18 will be used in the simulation of braces in this study.

4.6. Frame Simulation Description

One of the braced bays of the perimeter frames was simulated in RUAUMOKO to study the nonlinear behavior of the braced frames under earthquake ground motions. Two different bracing configurations, a TSXBF and a chevron frame, were modeled in RUAUMOKO as presented in Figure 69. Frames consist of nine 13-ft stories with a bay width of 30 ft.

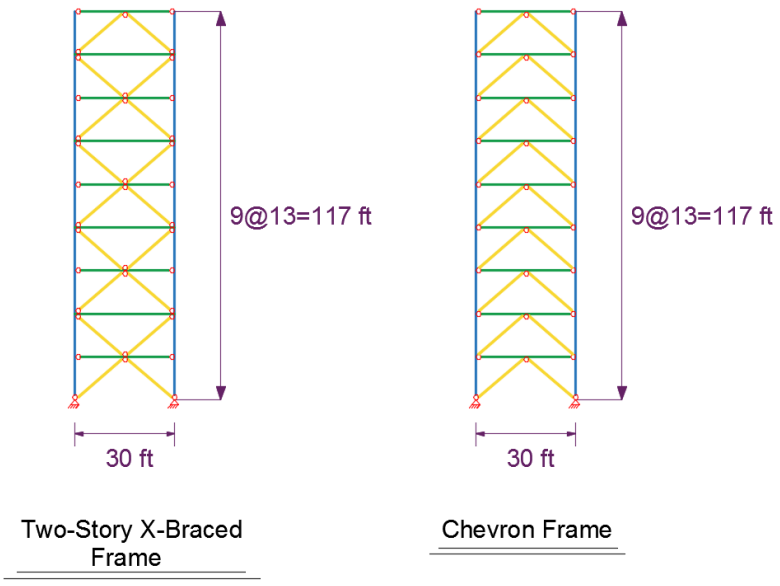

Figure 69: Simulated frames in RUAUMOKO-2D.

A REMENNIKOV steel brace was used to simulate the brace behavior and similar parameters used in the verification model were utilized to successfully predict the buckling and yielding of the braces. A steel beam-column element was also utilized to simulate the girders and columns. A dummy column is connected to the main frame through rigid beams to account for the P- Δ effects. Each column of the main bay carried a gravitational load based on its tributary area, and a quarter of the weight of each floor was applied to the dummy column with one-eighth of the mass of each floor put on each column in the braced bay, as is shown in Figure 70.

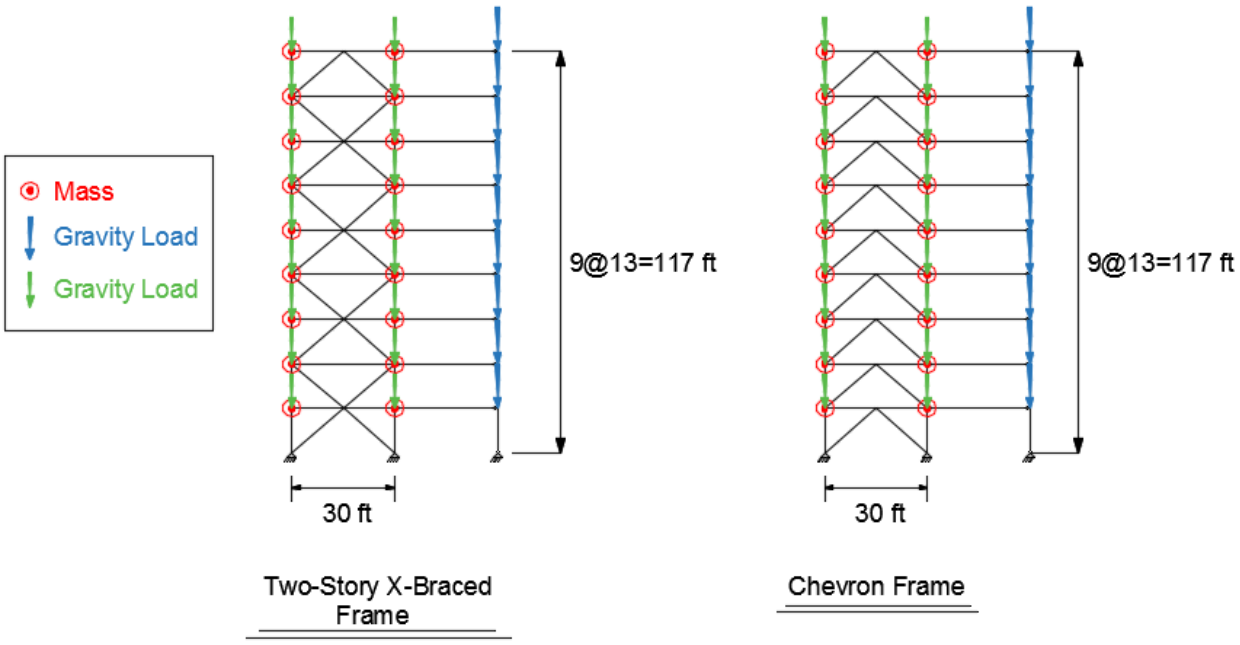

Figure 70: Loads and masses applied to the simulated frames.

All the joints in each floor were horizontally tied to one another to account for the effect of the concrete deck, but intersecting points of the braces and the beams are released from the aforementioned constraint to accomplish a non-zero axial force in the girders. In addition, rigid blocks are defined at locations where gusset plates are welded to the beams/columns. The rigid blocks perform like a rigid element and shorten the flexible length of the members, a condition

closer to the actual beams and columns. Rigid blocks are shown in red color in Figure 71. Details of the 9-story frame simulation in RUAUMOKO are provided in Appendix B.

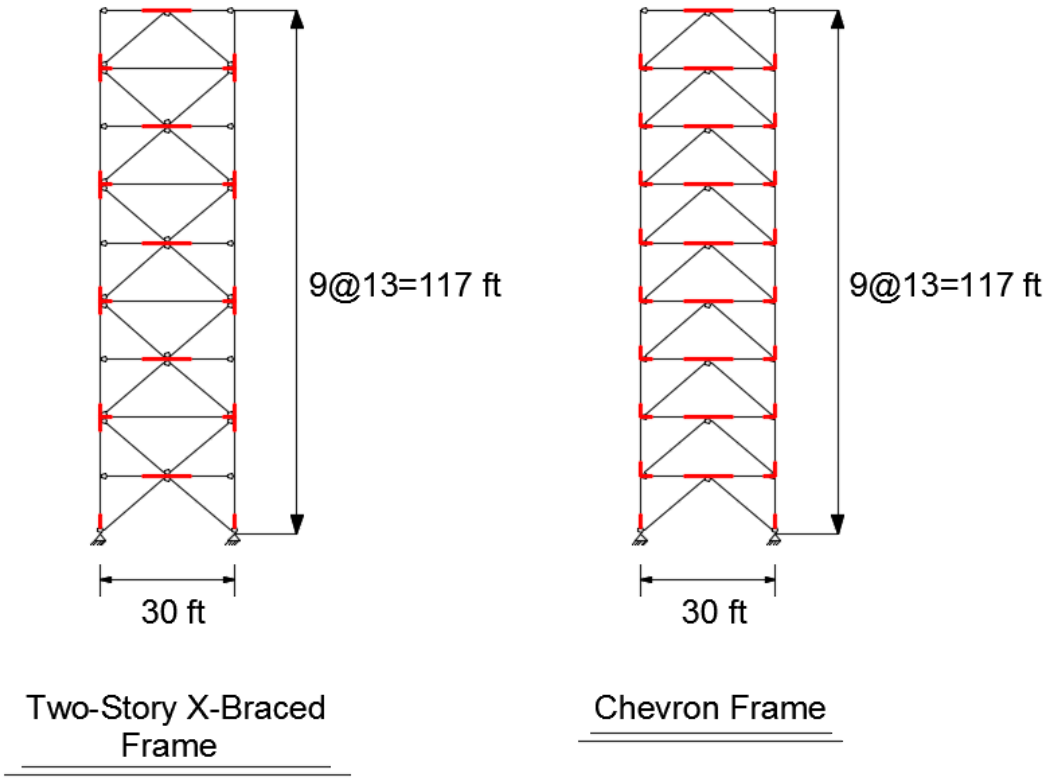

Figure 71: Rigid block used in the simulation of the frames.

4.7. Results of the Time History Analyses under GM11

Seismic performance of the 9-story frames under GM11 is studied in this section. The Imperial Valley earthquake (GM11) was a 39 s long earthquake with a peak ground acceleration (PGA) of 0.699g, as is shown in Figure 72. The response spectrum of this earthquake ground motion and the target design spectrum are shown in Figure 72.

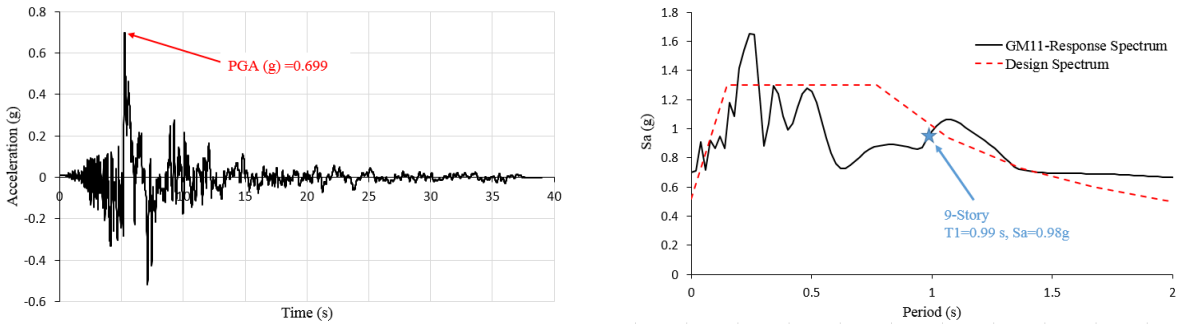

a) GM11 b) GM11 Response spectrum

Figure 72: Imperial Valley earthquake ground motion (GM11).

4.7.1. Frame Response in terms of SDR and Members' Ductility

Incremental dynamic analyses (IDA) were performed on frames W, S, and C under GM11 and the results of these analyses are discussed in this section. Intensity of the ground motions are increased until peak story drift ratio in the frame reaches 4%. Figure 73 shows the spectral acceleration of the frame versus the peak story drift ratio. It can be observed that beam strength has no significant effect on the story drift of the frame. In addition, changing the bracing configuration has no impact on the lateral displacement of the frame. It should be noted that SDR values of the three frames are very similar prior to the design limit (2% SDR).

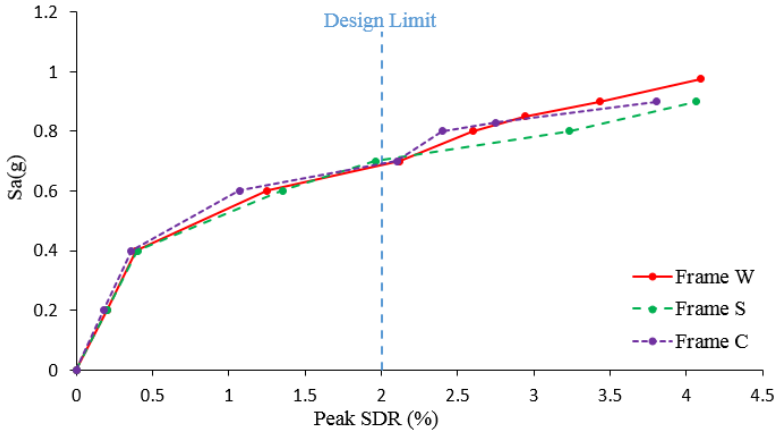

Figure 73: Spectral acceleration versus peak SDR under GM11.

Spectral acceleration versus peak brace ductility of the frame is presented in Figure 74. Previous experimental studies have demonstrated that peak brace ductility capacity of the HSS braces is between 10 and 16, so based on these results, the responses of brace ductility of the frame are divided into three regions:

i) Brace ductility $\leq 10 \rightarrow$ Braces are less likely to experience fracture.

ii) $10 <$ Brace ductility $\leq 16 \rightarrow$ Braces are likely to experience fracture.

iii) Brace ductility $> 16 \rightarrow$ Braces are even more likely to experience fracture.

From Figure 74 and consideration of these three regions, the following conclusions can be made:

i) Peak brace ductility in frame W is significantly greater than for the other two frames at 4% SDR. It can be seen that braces in the frame W are more likely to experience fracture compared with the other frames.

ii) Beam strength plays an important role in reducing the ductility demand of the braces. As can be seen in Figure 74, peak brace ductility in frame S falls into the second region, while ductility of the braces in the frame W falls into the third region and prone to fracture, so it seems that increasing the beam strength results in reducing the brace ductility.

iii) Comparison of the results for frames S and C leads us to the conclusion that bracing configuration has no significant effect on the ductility of the braces, and as long as similar beams, in terms of strength, are used in the frames, peak brace ductility of the frames will be close to one another.

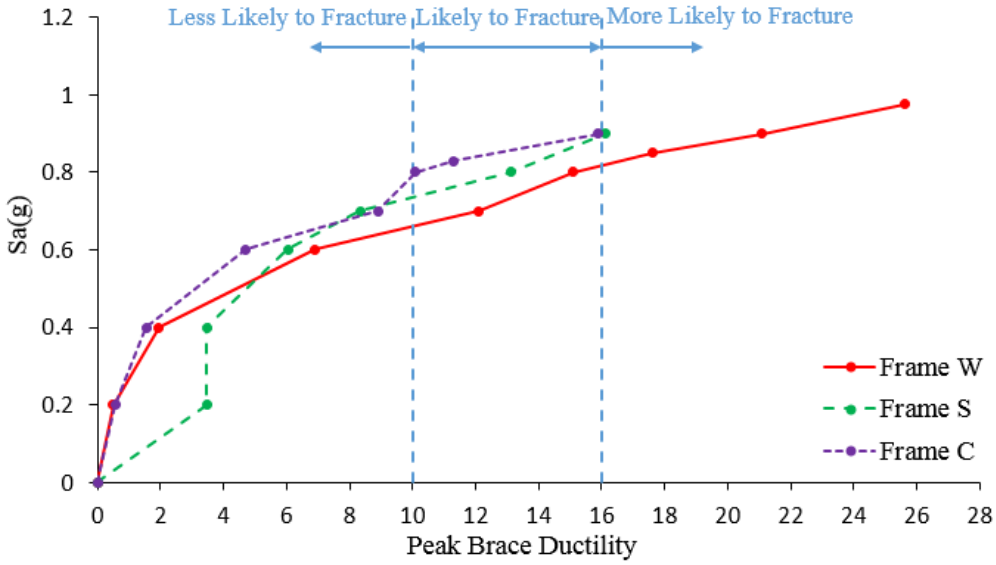

Figure 74: Spectral acceleration vs. peak brace ductility under GM11.

Figure 75 presents the spectral acceleration versus peak beam ductility of the frame. Beam ductility can be calculated by dividing the vertical displacement of the beam by its yielding displacement. According to the Figure 75, following observations can be made:

i) While ductility of the 1st level beam in frame W is greater than one at 4% SDR, meaning that the beam is yielding, according to AISC341-10, beams should remain elastic during the earthquake. It seems that the braced-intersected beam designed based on the current design code does not meet the required criteria.

ii) Comparison of the results for frames S and C shows that bracing configuration does not have a considerable effect on beam ductility. Since a deep beam is used in both frame C and frame S, the brace-intersected girders do not experience yielding in these frames. It should be noted that the vertical deflection of the beams in frame C and frame S is 260% smaller than the one in frame W.

iii) As can be seen in Figure 75, the IDA curve of frame W is comprised of two portions: 1) before yielding; 2) after yielding, and the slope of the IDA curve

decreases when the beam yields. From an engineering point of view, this means that a small increase in the intensity of aground motion results in a larger rise in the beam ductility demand after the beam experiences yielding.

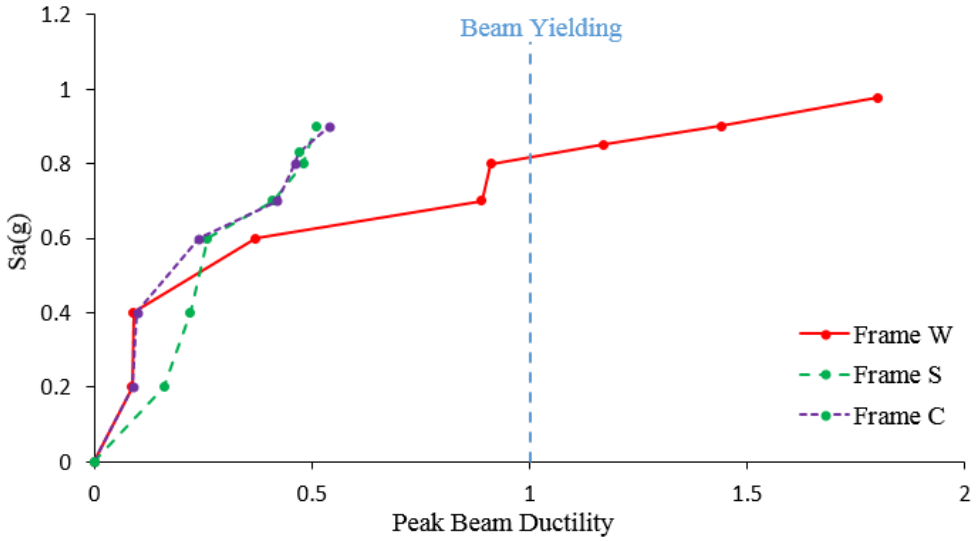

Figure 75: Spectral acceleration vs. peak beam ductility under GM11.

Figure 77 plots the peak SDR of the frame vs. its peak brace ductility. Based on the response of the frames provided in this figure, the following conclusions can be drawn:

i) A significant difference between the brace ductility of frame W and frame S, mainly due to the yielding of the braced-intersected girders, can be observed in this figure. The blue dashed line in Figure 77 presents the relationship between SDR and brace ductility of the first story of the frame. It should be noted that this relationship, valid if the vertical displacement of the girder is neglected, can be derived as follows:

$$SDR = \frac{\Delta}{h} \times 100 = \frac{\Delta}{13 \times 12} \times 100 \rightarrow \Delta = 1.56 \times SDR$$

$$\Delta_{brace} = \Delta \times \cos 41 = (1.56SDR) \times cos41 = 1.18SDR$$

$$Brace\ Ductility = \frac{\Delta_{brace}}{\Delta_y} = \frac{1.18SDR}{\left(\frac{F_y L}{E}\right)} = \frac{1.18SDR}{0.32} = 3.7SDR$$

→ SDR=0.27×Brace Ductility

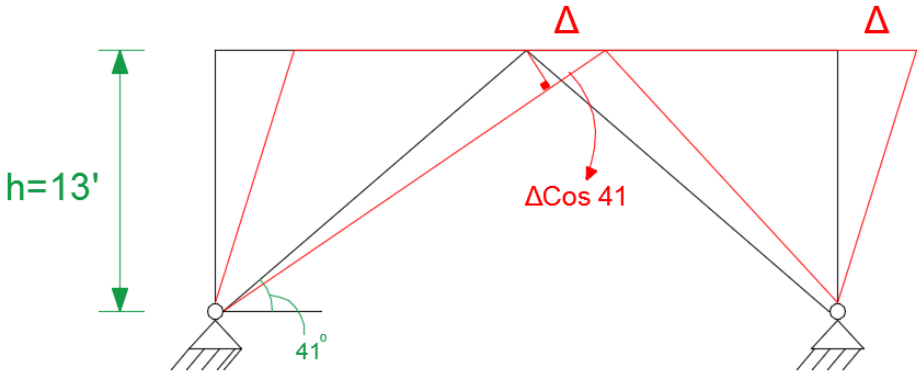

Figure 76: Deformation of a frame under lateral force.

ii) Comparison of the results for frame S and frame C demonstrates that utilizing a strong beam leads to smaller brace ductility and response of the frames are closer to the blue dashed line that represents the linear relationship between the SDR and brace ductility that represents an ideal case. Figure 77 also shows that if a strong brace-intersected girder is used, responses of the frames are close to one another regardless of the bracing configuration. Figure 78 presents the effect of the vertical displacement of the girder on brace ductility.

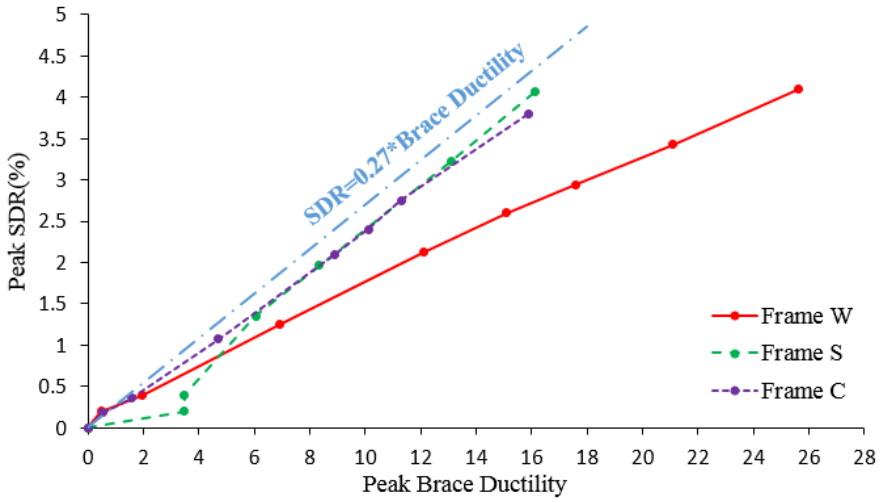

Figure 77: Peak SDR vs. peak brace ductility of the frame.

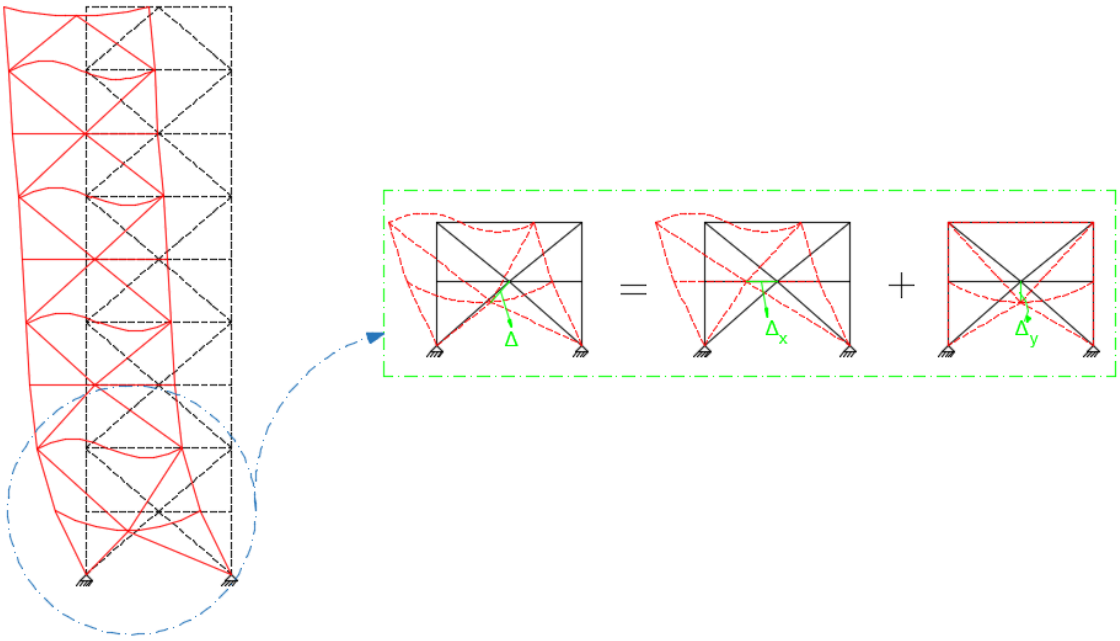

Figure 78: Deformation of frame W when peak brace ductility occurs at 4% SDR.

Figure 79 presents peak SDR versus peak beam ductility of the frames. It can be observed that braced-intersected girders in the first story of frame W almost yielded at SDR of about 2%, the design level. It should be emphasized that, based on the current design code (AISC341-10), beams and columns are assumed to remain elastic during an earthquake but beams experience yielding even at the design level that is unexpected.

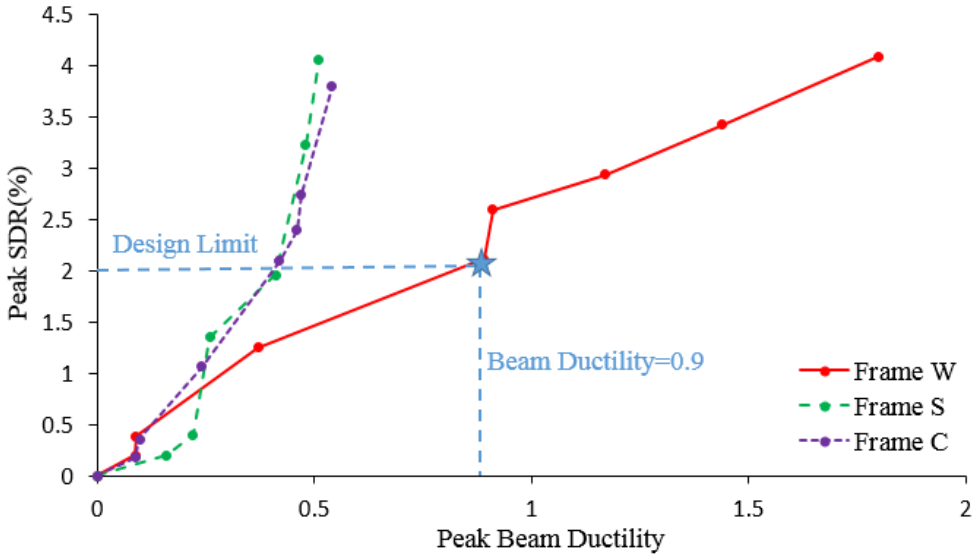

Figure 79: Peak SDR vs. peak beam ductility under GM11.

4.7.2. Seismic Demand on the Girders

Axial force, bending moment, and total demand/capacity of the girders of frames W, S, and C are provided in Figure 80, Figure 81, and Figure 82. P_c can be calculated by multiplying the gross area (A_g) of the section by the critical stress (F_{cr}) and M_c can be calculated by multiplying the plastic modulus of the section (Z_x) by yielding stress (F_y). From these figures, the following conclusions can be drawn:

i) Axial force demand in the girders in frames S and C are similar to one another and bracing configuration has no significant impact on the axial force demand in SCBFs. However, it can be observed that axial force demand/capacity on beams in frame W is slightly greater than that for other frames, with the difference mainly due to the smaller capacity of the beams in frame W.

ii) It is interesting to mention that increasing the SDR has no considerable impact on the axial force demand on the beams and the beams demand is almost constant for different SDRs.

iii) Increase in the lateral displacement of the frame has a negligible effect on the flexural demand of the beams, as can be seen in Figure 80, Figure 81, and Figure 82.

iv) By comparing the results for frames W, S, and C, it can be observed that flexural demand on the girders in frame W is greater than for other frames. This can be explained by investigating the behavior of braces intersecting the beams. While it has been demonstrated in previous figures that brace ductility demand in frame W is substantially larger than for frames S and C, flexural demand on the beams depends on unbalanced forces shown in Figure 83, and results from the difference in the axial force of the braces, so larger unbalanced forces acting on the girders in frame W coupled with the smaller capacity of the beams leads to large flexural demand ratio in the beams.

v) Although behavior of frames S and C is similar in some aspects, flexural demands on the girders in even stories are significantly different, mainly due to the girder end connections in these frames. Rigid connections are utilized in frame S because of the gusset plates welded to the beam and column. Due to the rigid connections in frame S and lateral displacement of the frame, a large bending moment is applied to the beam, substantially increasing the demand on the girders.

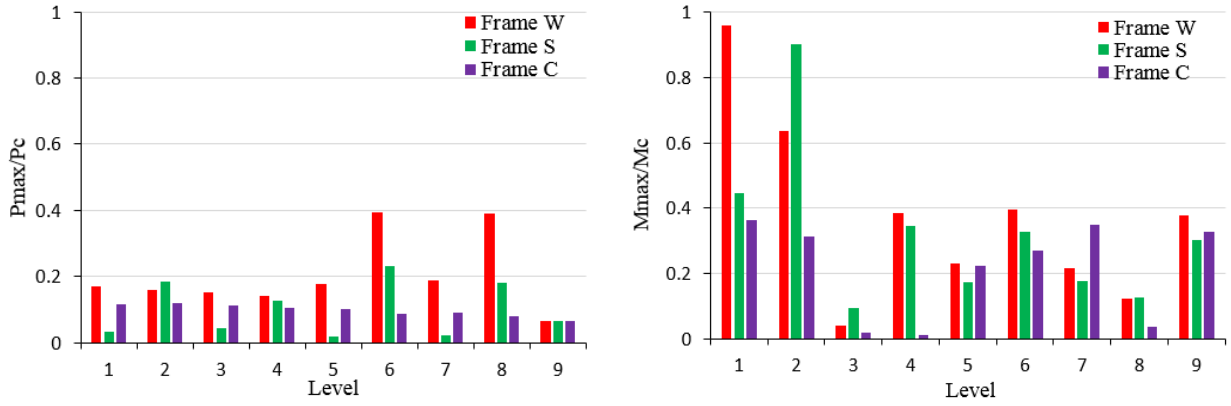

Figure 80: Axial force and flexural demand ratio on the girders at 2% SDR under GM11.

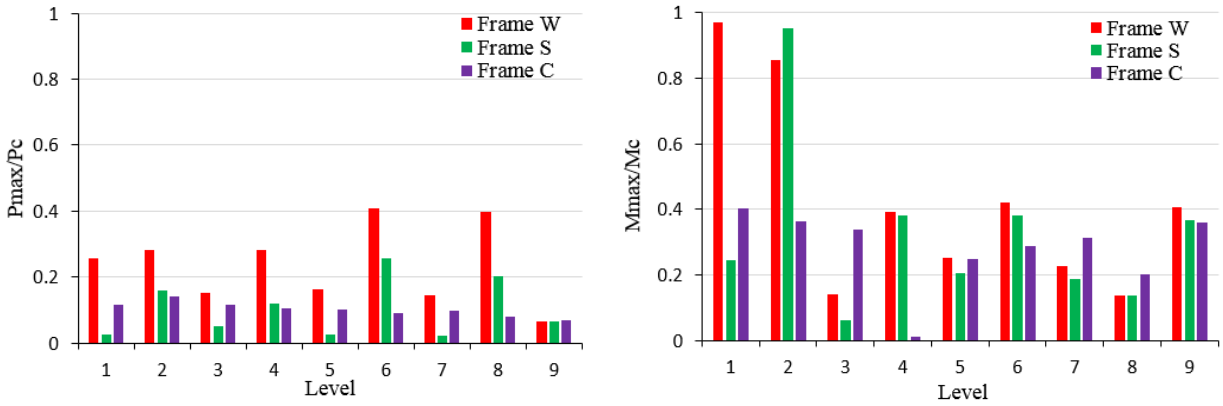

Figure 81: Axial force and flexural demand ratio on the girders at 3% SDR under GM11.

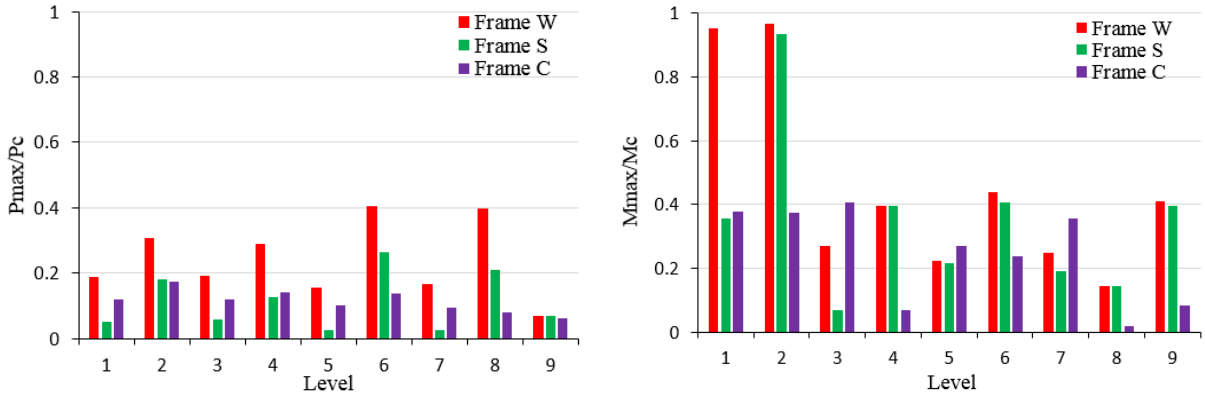

Figure 82: Axial force and flexural demand ratio on the girders at 4% SDR under GM11.

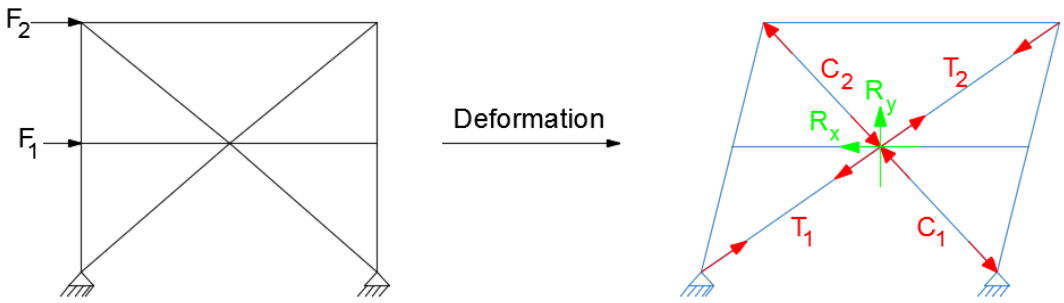

Figure 83: Unbalanced forces applied to the braced-intersected girders in TSXBFs.

Figure 84 presents the total demand on the beams of the frames S, W, and C. The total demand/capacity presented in this figure can be calculated by adding the axial force demand/capacity ratio to the flexural demand/capacity ratio. The total demand/capacity should be smaller than one to be considered in the safe zone, as shown in Figure 85. It should be noted that the peak total demand on the beams might occur at a different time than the peak axial force or flexural demand, so the total demand presented in Figure 84 is not necessarily equal to the summation of Figure 80, Figure 81, and Figure 82. Based on Figure 84, following comments can be made:

i) Similarly to the previous discussion, total demand on the first and second levels of the frame W reaches one, meaning that the beams in these stories experience yielding. Although the demand on the first level girder of the frame S is similar to the one on the chevron frame and substantially smaller than the girder demand on frame W, the total demand on the girders at the second level of frame W and S are close to one another due to the identical beam section and identical beam-to-column connection used in these frames, so it can be concluded that the new approach for designing of the braced-intersected beams is effective in reducing the beam

demand. However, second-story beams still must be strengthened (or a heavier section should be used) to reduce the demand/capacity.

ii) Total demand on the beams of the chevron frame remains almost constant after increasing the lateral displacement of the frame. The peak demand on the girders of frame C also occurs in the first level beam and is around 0.5. Based on our limited observations on the results of GM11, it seems that a lighter section can be used for the girders with chevron frames. This conclusion will be further investigated when the results from simulations of the twenty ground motions are presented.

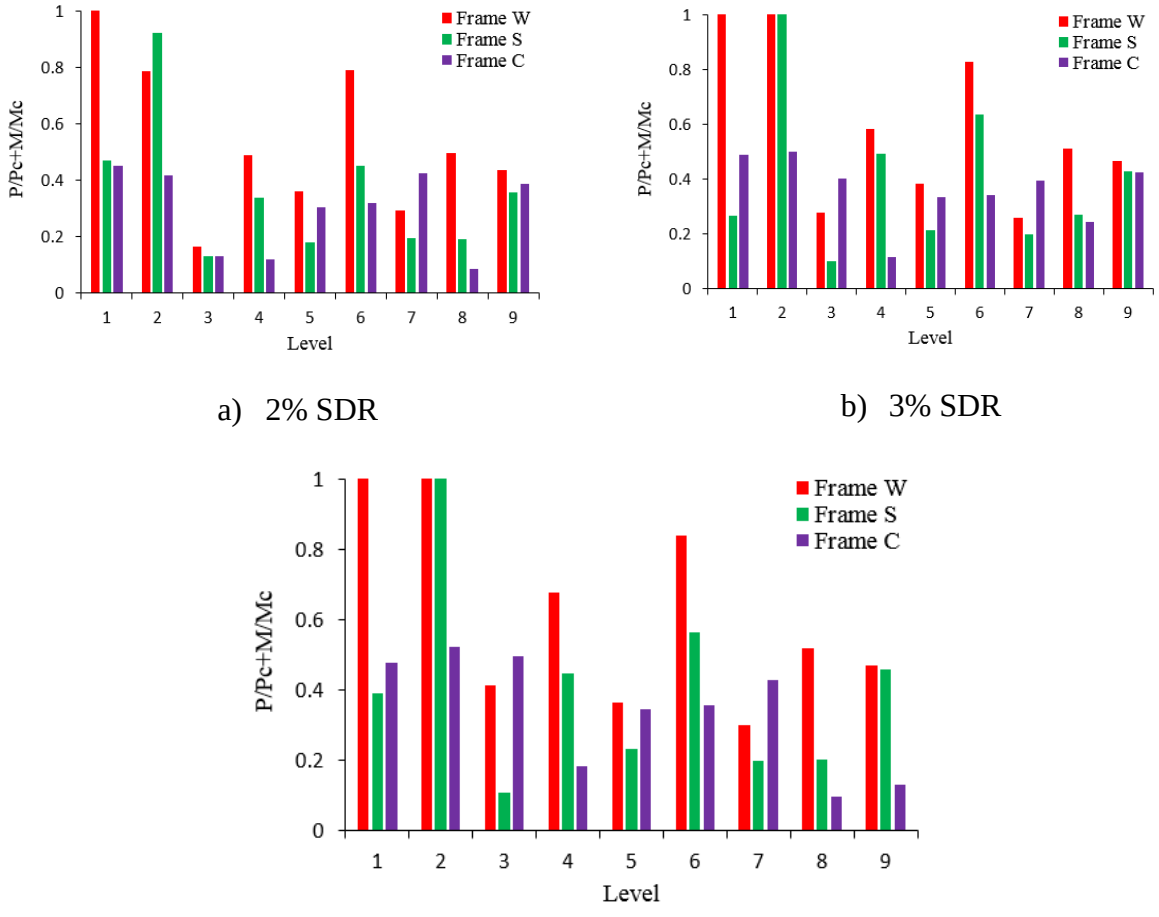

a) 2% SDR

b) 3% SDR

c) 4% SDR

Figure 84: Total demand on the girders under GM11.

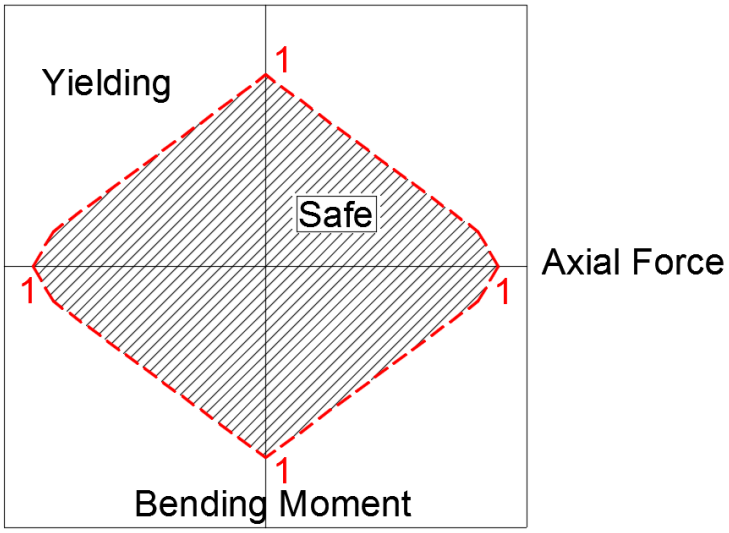

Figure 85: Axial-flexure interaction diagram.

4.7.3. Seismic Demand on the Columns

Behavior of the columns as the most important structural members is investigated in this section. Figure 86, Figure 87, and Figure 88 present the axial force and flexural demand/capacity ratio of the frames at 2%, 3%, and 4% SDR values, respectively. From these figures the following observations can be made:

i) Axial force demand/capacity ratios on the columns of the frames are similar to one another. It seems that bracing configuration and beam strength have no substantial impact on the axial force demand of columns in SCBFs.

ii) Based on the limited results regarding the axial force demand on columns under GM11 provided in Figure 86 through Figure 88, it can be concluded that axial force in the SCBFs column is not sensitive to the SDR and the demand on the columns remains constant with increasing SDR. This conclusion will be further investigated when simulation results from the twenty ground motions are presented.

iii) Unlike axial force demand, flexural demand of columns seems to be sensitive to the SDR. Comparing the figures leads to the conclusion that increasing the SDR results in larger flexural demand on columns. This phenomenon can be explained by taking into account the overall deformation of a frame. The larger the lateral displacement, the more prone are columns to bend, leading to greater flexural demand on columns.

iv) In early stages of the analysis (prior to 3% SDR), flexural demand on columns of frames W, S, and C were similar to each other, but at large SDRs, bending moment in columns of 1st and 2nd stories of the frame S is larger than that for other frames due to the deeper beam and rigid connections used in this frame. Deep beams sustain larger bending moments transferred to the columns through rigid connections, so it can be concluded that, while employing deeper beams in TSXBFs reduces the brace and beam ductility, it has a detrimental effect on the flexural demand of columns.

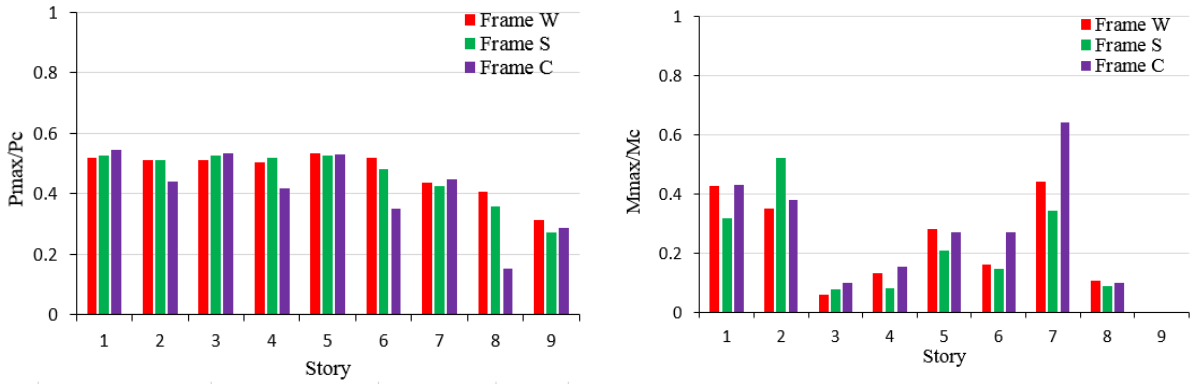

Figure 86: Axial force and flexural demand ratio on the columns at 2% SDR under GM11.

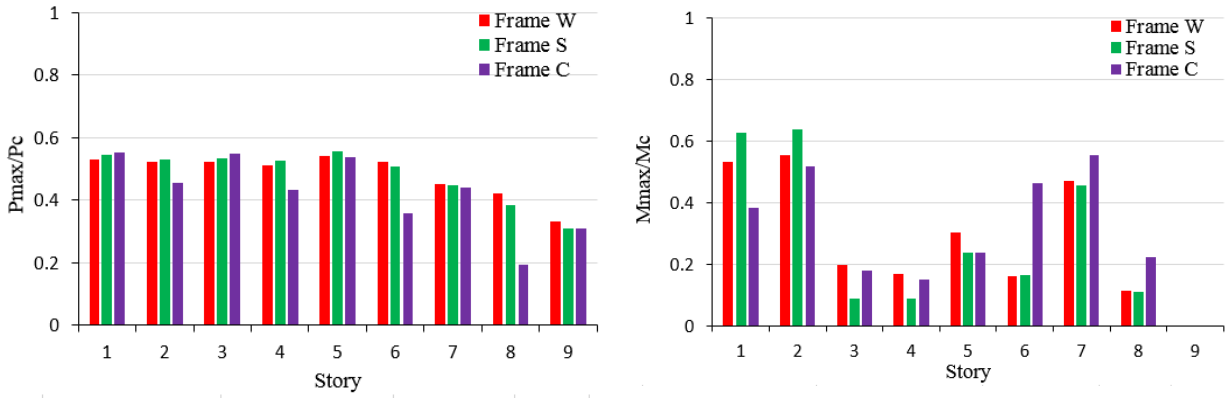

Figure 87: Axial force and flexural demand ratio on the columns at 3% SDR under GM11.

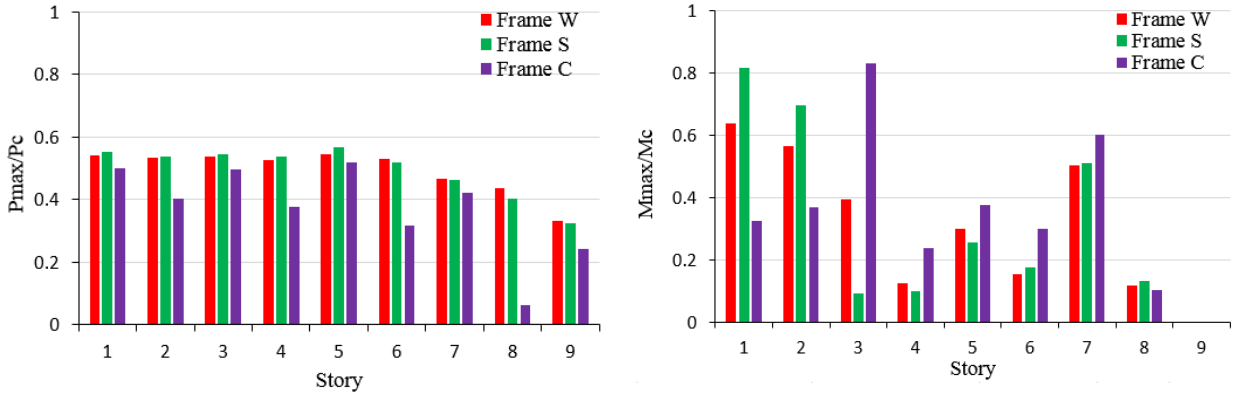

Figure 88: Axial force and flexural demand ratio on the columns at 4% SDR under GM11.

Figure 89 presents the total demand on columns of frames W, S, and C. Based on these results, the following conclusions can be drawn:

i) Columns experience yielding at 4% SDR and the total demand/capacity on a column is as large as 0.9 at 3% SDR in frame W. It should once again be mentioned that columns are required to remain elastic during an earthquake. Similar results can be observed in the columns of frame S.

ii) Increasing the lateral displacement of the frames causes total demand on the columns to increase, as can be observed in Figure 89. This increase is due to the flexural portion of the demand since axial force demand is almost constant at different SDRs, as previously discussed.

iii) Total demand on columns of frames W and S are similar to one another as shown in Figure 89. It seems that beam strength has little influence on the demand on the columns. On the contrary, total demand on the chevron frame columns is less than that for the other cases in most of the stories and at different SDRs, so it can be concluded that bracing configuration can be effective at large SDRs and demand on the columns of chevron configuration is smaller than for TSXBFs.

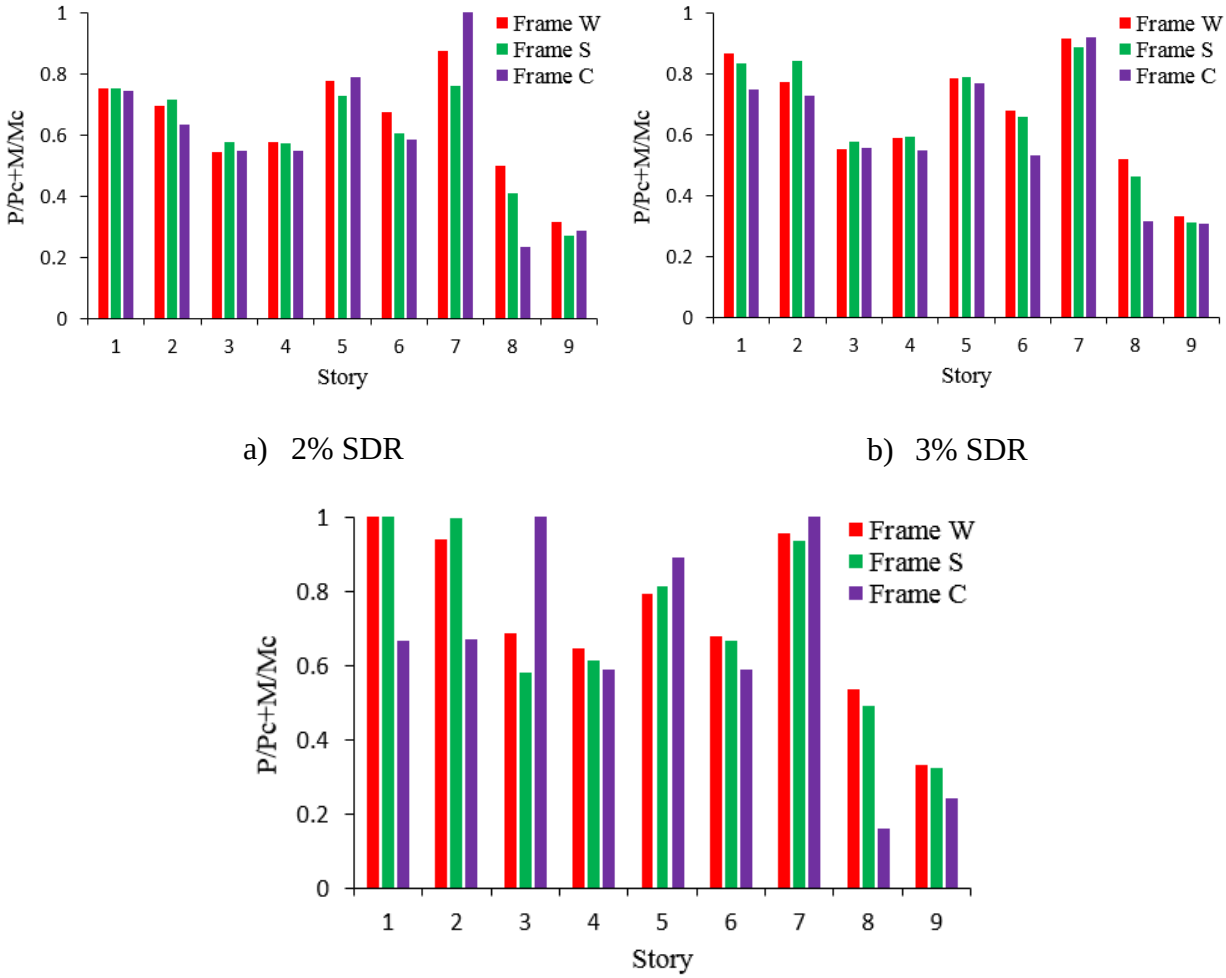

a) 2% SDR

b) 3% SDR

c) 4% SDR

Figure 89: Total demand on the columns under GM11.

4.7.4. Seismic Demand on the Braces

Brace ductility demand of the frames is presented in Figure 90. Based on previous experimental results, brace ductility bars can be divided into three regions and the following observations can be made:

i) At 2% SDR, braces are less likely to experience fracture except for the first story brace in the second region. When SDR increases to 3%, brace ductility in frame W is in region II and braces are likely to fracture. At 4% SDR, first-story brace ductility in frame W is in region III and is more likely to experience the fracture while peak brace ductility in frame S and C are in region II.

ii) Increasing the SDR results in a rise in brace ductility of the lower stories of the frames while having no major impact on the braces in the upper stories. This phenomenon can be explained by studying the deformation of the frame at 4% SDR. As seen in Figure 91, lateral displacement of the frame under this specific ground motion accumulates in the lower stories of the frame and increasing the lateral displacement of the frame would increase the lateral displacement of the lower stories while the SDR of the upper stories remain constant, so the effect of any increase in SDR is more significant in lower than in upper stories.

iii) Largest brace ductility demand occurs in the 1st and 2nd stories of the frame, as seen in Figure 91. As previously discussed, concentration of the lateral displacement of the frame is the main reason for this behavior.

iv) As mentioned earlier, peak brace ductility of frame W is larger than the one in frames S and C due to the yielding of the braced-intersected beam that results in

additional vertical displacement of the beam that imposes unpredicted larger deformation on the brace.

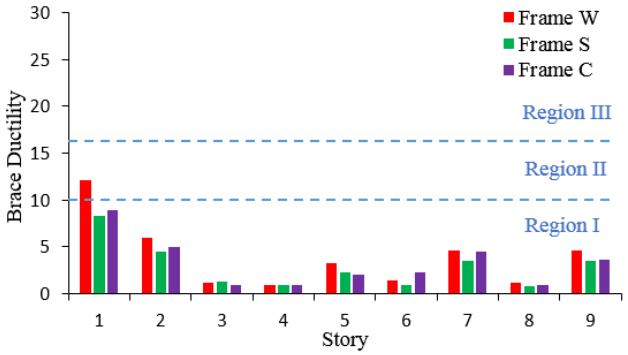

a) 2% SDR

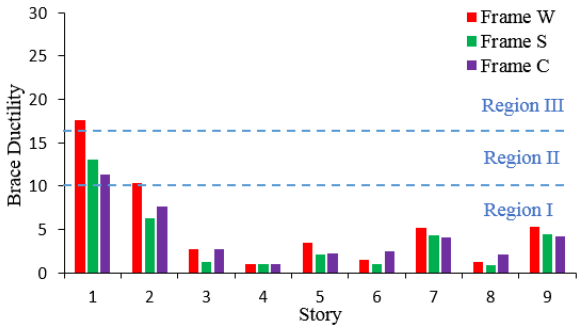

b) 3% SDR

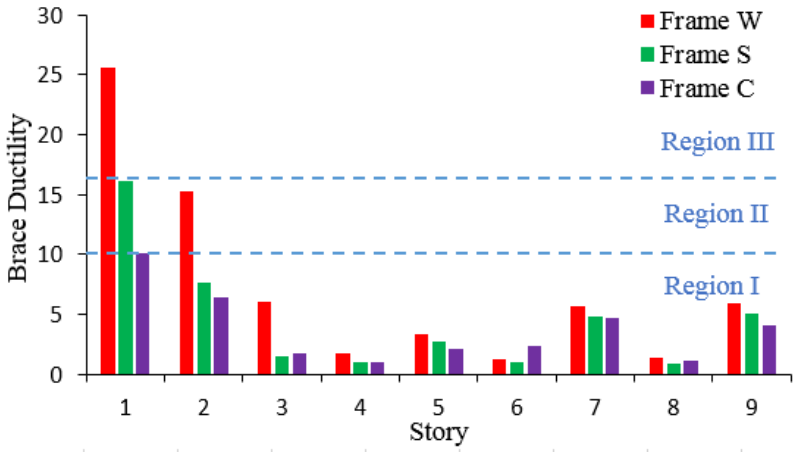

c) 4% SDR

Figure 90: Brace ductility demand on braces under GM11.

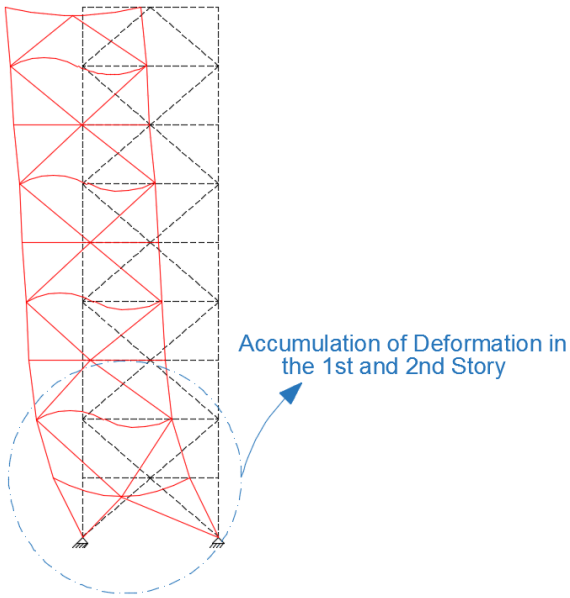

Figure 91: Concentration of the deformation in the first two stories of the frame W under GM11 at 4% SDR.

Figure 92 and Figure 93 show the axial force versus axial displacement of the braces in the first and second story of frame W and frame S, respectively. Response of the braces at the time peak beam ductility occurs is investigated. If the vertical deflection of the brace-intersected girders is neglected, axial displacement in both braces of the same story should be equal to $\Delta.Cos\alpha$, where Δ is the lateral displacement of the story and α is the angle between the brace and horizontal line. However, as can be seen in Figure 92, axial displacement of the left brace when peak beam ductility occurs is 2.4 inch, while the displacement on the right brace is 1.1 inch. This inequality can be explained by taking into account the vertical displacement of the beam that imposes additional shortening to the compressive brace and reduces elongation of the tensile brace. On the other hand, as presented in Figure 93, axial displacements of the braces in the first story of the frame S, are almost equal, showing the negligible effect of the vertical deflection of the beam, so it can be concluded that, unlike the current design approach implemented in the design code, it seems necessary to consider the vertical deflection of the beam in the design procedure if a weak

beam is going to be used. Thus, contrary to the current design approach, SDR cannot be used as the sole index for evaluating the behavior of SCBFs. It is interesting to notice that peak demand on the beam and braces occur at two different times, mainly because of the complex behavior of the four braces intersecting at the beam mid-point. At each moment of the analysis, any of the four braces might be in a different state, as shown in the Figure 94. This complex behavior hardens the prediction of the performance of the CBFs, so it is not necessarily true that peak demand in the beams and columns occur at the same time as peak SDR or peak brace ductility.

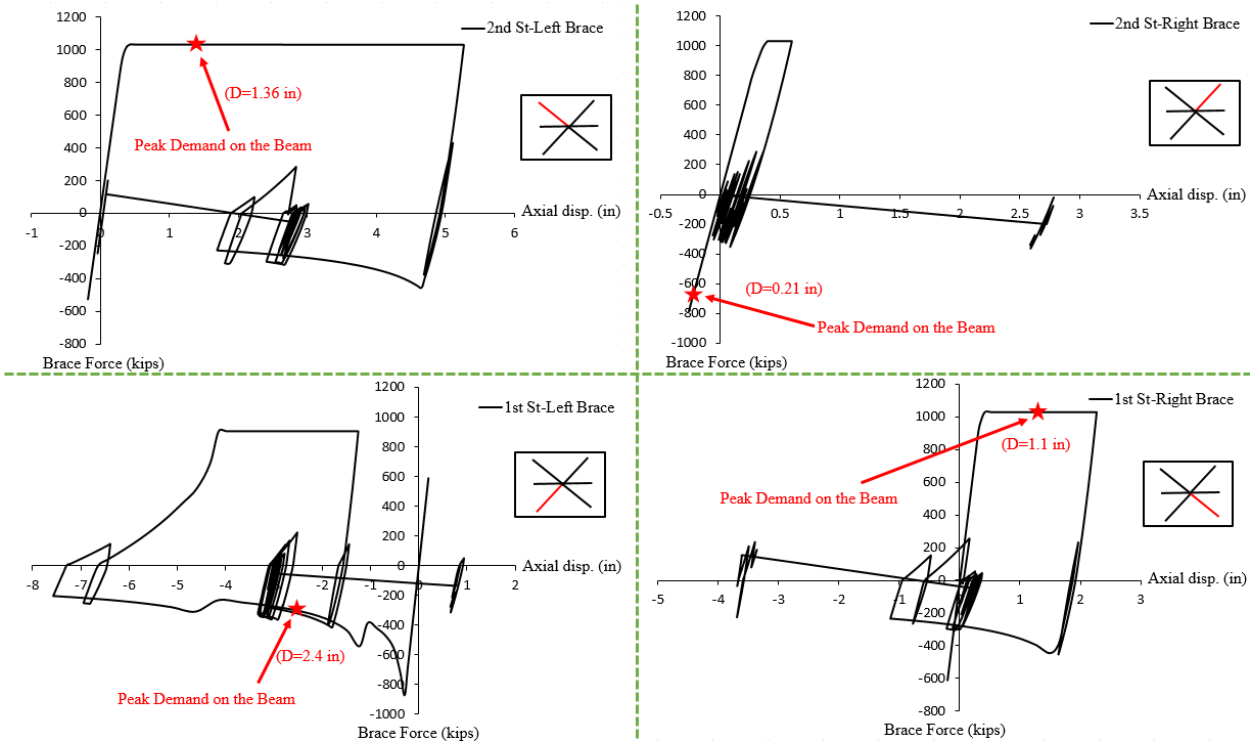

Figure 92: Axial force vs. axial displacement of the braces in Frame W at 4% SDR under GM11.

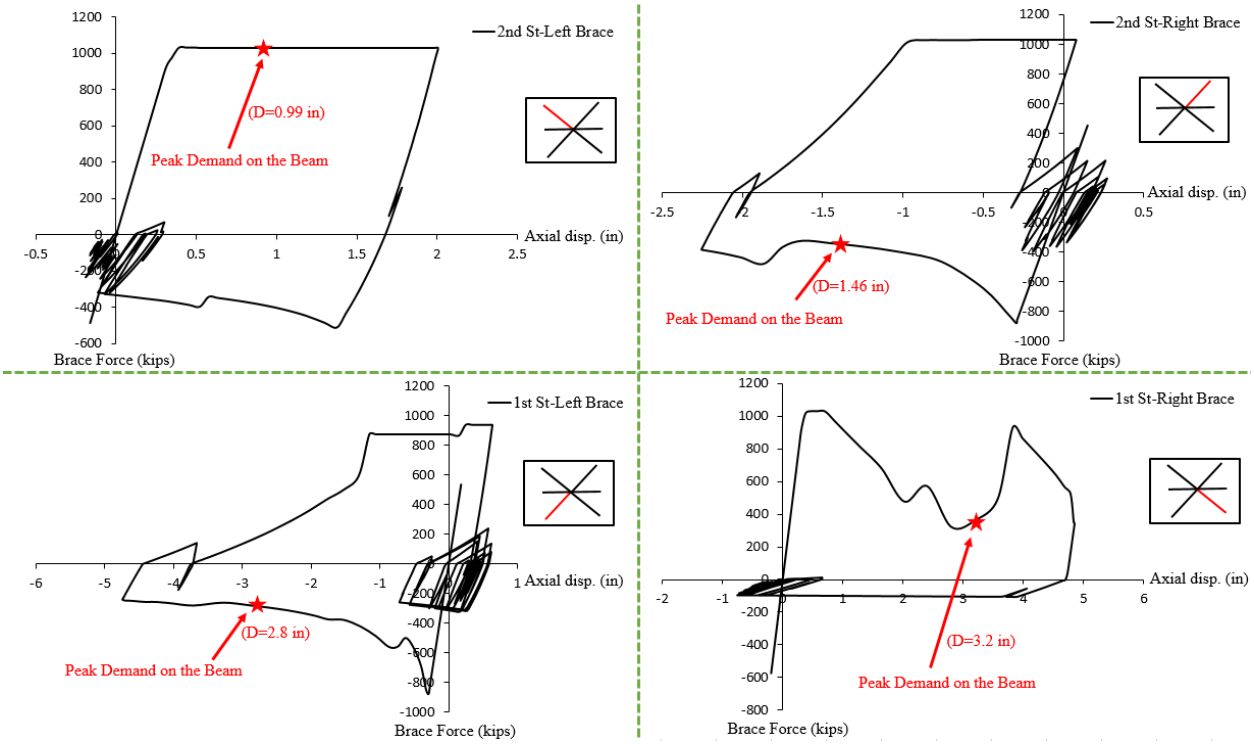

Figure 93: Axial force vs. axial displacement of the braces in Frame S at 4% SDR under GM11.

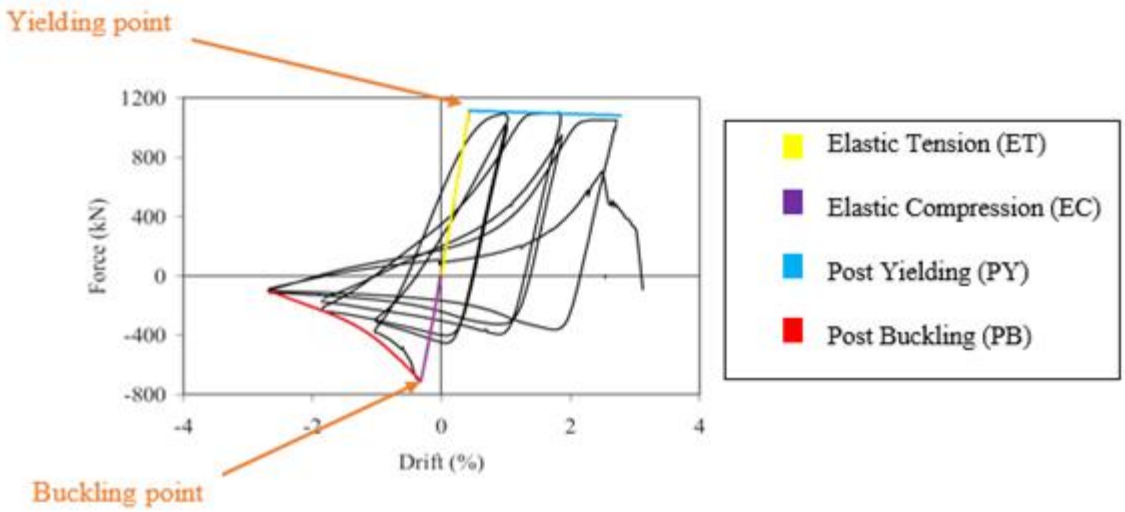

Figure 94: Different states of braces.

4.7.5. Seismic Response of the frames in Terms of Column Rotation

As mentioned earlier, columns tend to bend due to differences between the lateral displacements of the consecutive stories, so flexural demand on a column is related to the rotation

of the column as defined in Figure 95. In this figure, it is assumed that columns remain in a straight line between two stories and rotation of the column in each story can be calculated by dividing the story drift by story height (SDR), so column rotation at each joint can be calculated by adding or subtracting the SDRs of two consecutive stories. The sign of the previously-given formula can be determined based on the deformation mode shape of the frame. If the first mode deformation occurs in the frame (displacement in one direction), SDRs should be subtracted from one another; otherwise they should be added.

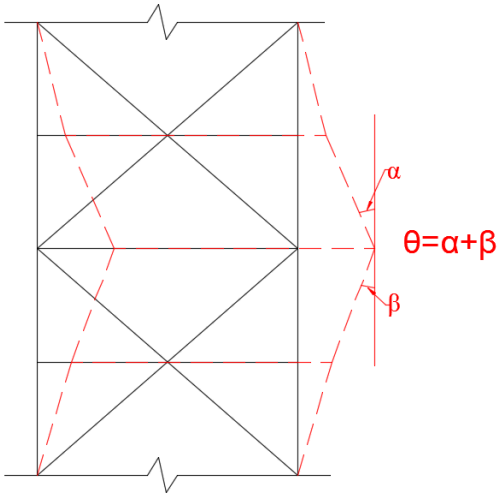

Figure 95: Definition of the relative rotation in columns.

Figure 96 plots the flexural demand of the columns versus their rotations. Based on this figure, the following observations can be made:

i) As expected, increasing the column rotation results in increasing the flexural demand of columns.

ii) According to the limited results achieved from GM11, it can be concluded that relative rotational demand in columns of frame C is significantly smaller than for

TSXBFs. This conclusion will further be investigated when results of simulations of twenty ground motions are discussed.

iii) As observed earlier, large relative rotation results in a flexural demand as large as 0.8. However, effect of this flexural demand on columns in SCBFs is completely neglected in the current design code (AISC341-10). According to the results presented, it seems more conservative for flexural demand on the columns to be considered in design procedures.

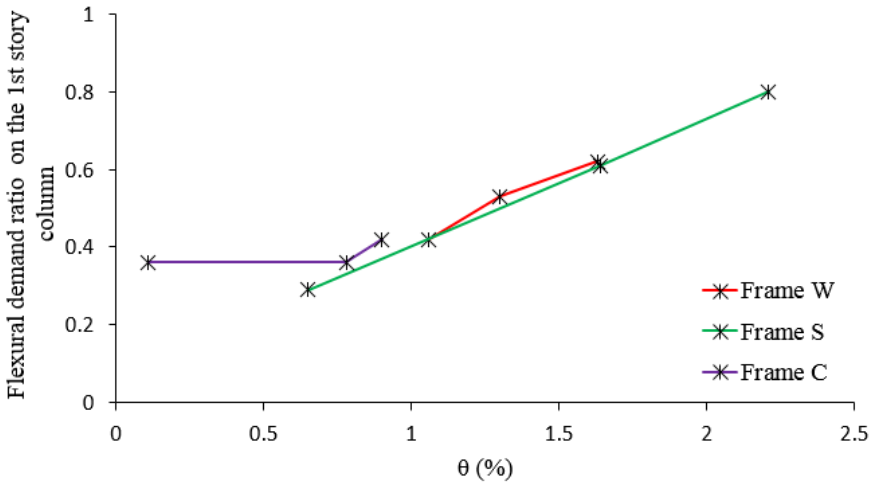

Figure 96: Flexural demand ratio vs. relative rotation in columns under GM11.

4.8. Deformation of the Frame under Seismic Loads

According to the current design code (AISC 341-10), first mode deformation should be considered for designing the SCBFs as shown in Figure 97. However, results of the analysis under GM01 shows that different deformation patterns might occur in the braced frame at different times of analysis, as shown in Figure 98. Results from the previous section have proven that larger relative rotation in the columns results in a more substantial flexural demand on column, so it seems that some of the deformation patterns presented in Figure 98 might lead to more critical results than the one suggested by AISC 341-10, and it may not be safe to use the first mode

deformation as the only possible deformation for designing of TSXBFs. Effects of the different loading patterns on the TSXBFs will be further investigated in Chapter 6.

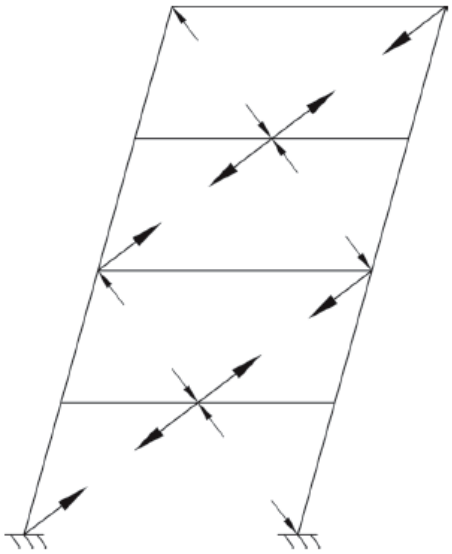

Figure 97: Anticipated deformation for designing of TSXBFs (AISC341-10).

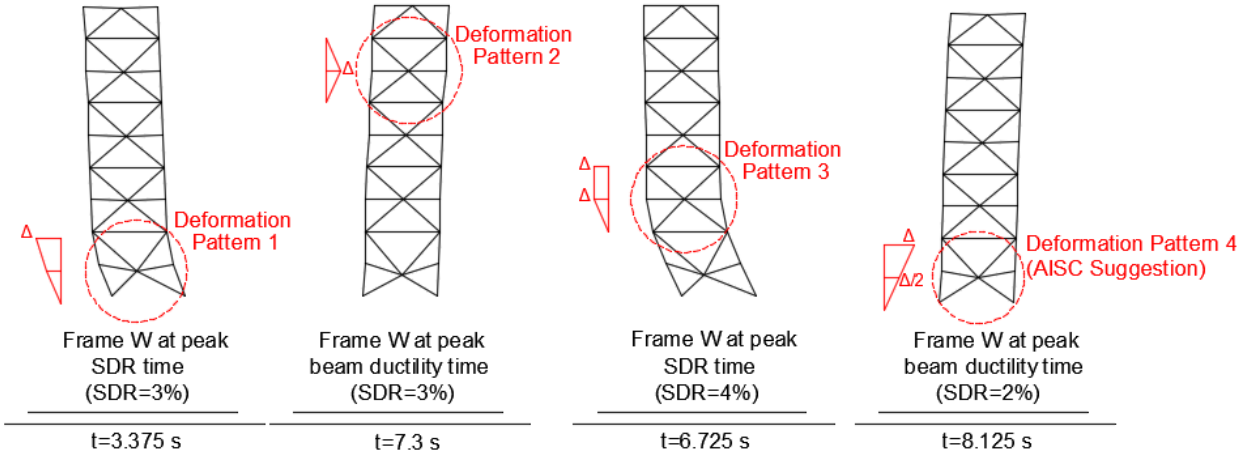

Figure 98: Different possible deformation patterns in TSXBFs under GM01.

4.9. Seismic Response of 9-Story Frames under 20 Ground Motions

Seismic behavior of 9-story steel braced frames under GM11 was investigated in previous sections. In the current section, an ensemble of twenty ground motions was applied to the 9-story braced frames and their seismic performance was evaluated through inelastic dynamic time history

analyses. Seismic response of the frame in terms of story drift ratio, beam ductility, brace ductility, and beam and column demand will be presented and discussed in this section.

4.9.1. IDA Curves under 20 Ground Motions

Incremental dynamic analysis was performed on the 9-story braced frames under twenty ground motions with intensity of all the ground motions increased until peak SDR in the frames reached 4%. Figure 99 presents the spectral acceleration of the ground motions versus the frames' peak SDR. Based on the response of the frames provided in this figure, it can be concluded that:

i) Beam strength has no significant effect on the seismic response of the braced frames in terms of story drift ratio.

ii) SDR of the frames is not sensitive to the bracing configuration, and if the braces from Two-Story X-bracing are changed to chevron, the resulting SDRs follow the same trend and are similar to one another.

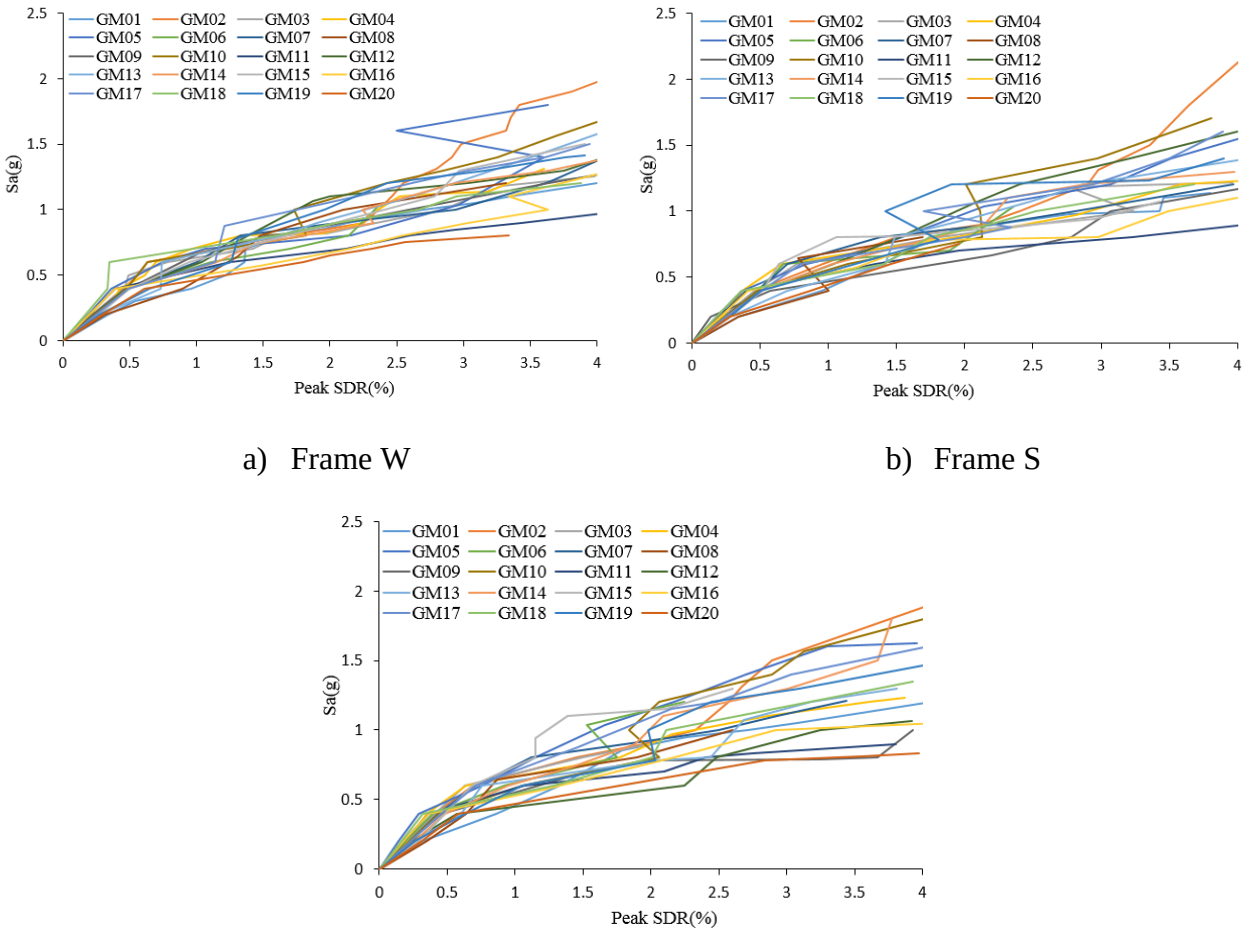

a) Frame W

b) Frame S

c) Frame C

Figure 99: Spectral acceleration vs. peak SDR in 9-Story frames under 20 ground motions.

Unlike the peak SDR that was almost identical for all frames, peak brace ductilities of the frames differ significantly from one another. Spectral acceleration of the ground motions versus peak brace ductility of the frames is shown in Figure 100, from which it can be observed that:

i) Beam strength plays an important role in reducing the brace ductility demand. Peak brace ductility in frame W to 34, while it is 17 in frame S.

ii) Brace response of frames S and C are similar to one another, demonstrating that bracing configuration has little impact on brace ductility demand in SCBFs.

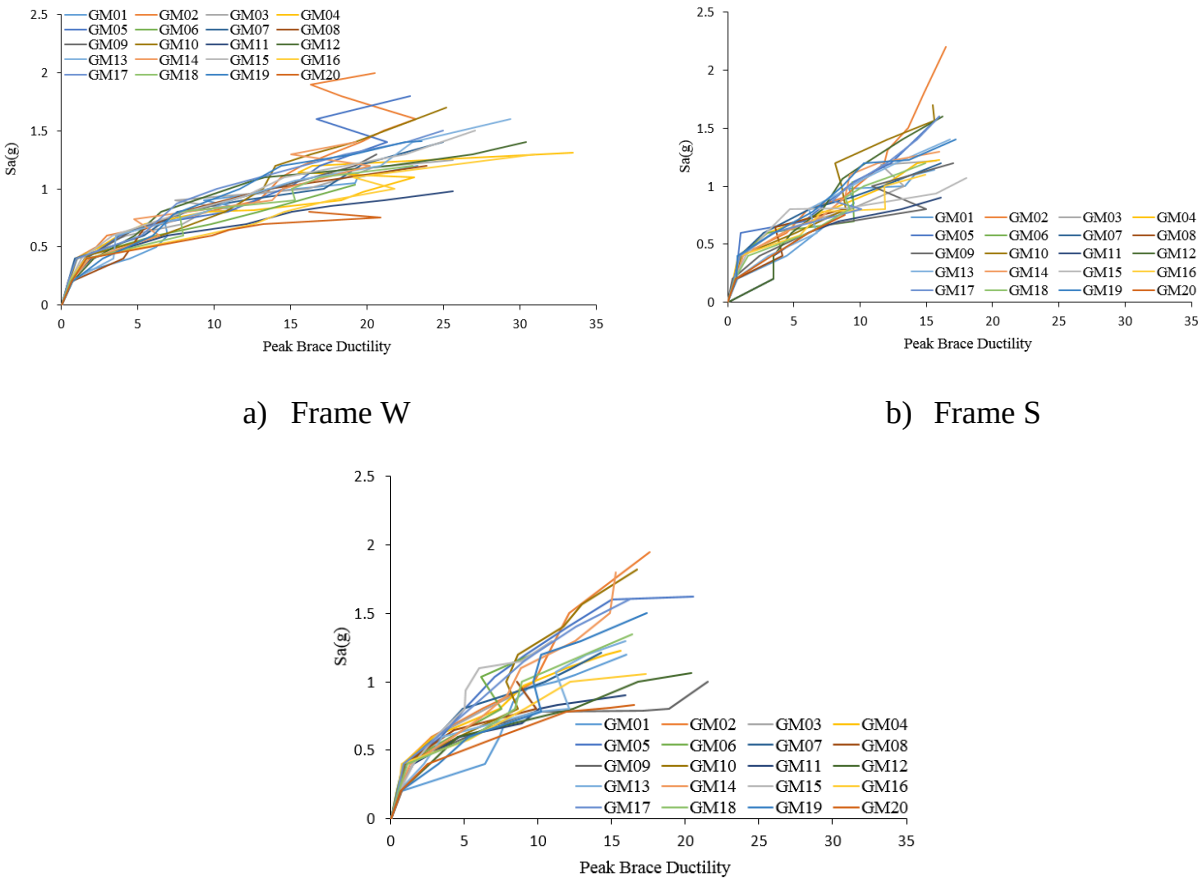

a) Frame W

b) Frame S

c) Frame C

Figure 100: Spectral acceleration vs. peak brace ductility in 9-story frames under 20 ground motions.

Similar to the brace ductility response of the frames, peak beam ductility of frames W, S, and C were compared under twenty ground motions with results given in Figure 101. As can be seen in this figure, peak beam ductility in frame W can be as large as 4.2, while maximum beam ductility in frames S and C are close to 0.8 and 0.7, respectively, so it can be concluded that beam strength substantially reduces the beam ductility demand/capacity. In addition, beam ductility response of the frames S and C are similar to one another, implying that bracing configuration is not an important parameter in beam response if a beam with sufficient strength is utilized in the frame.

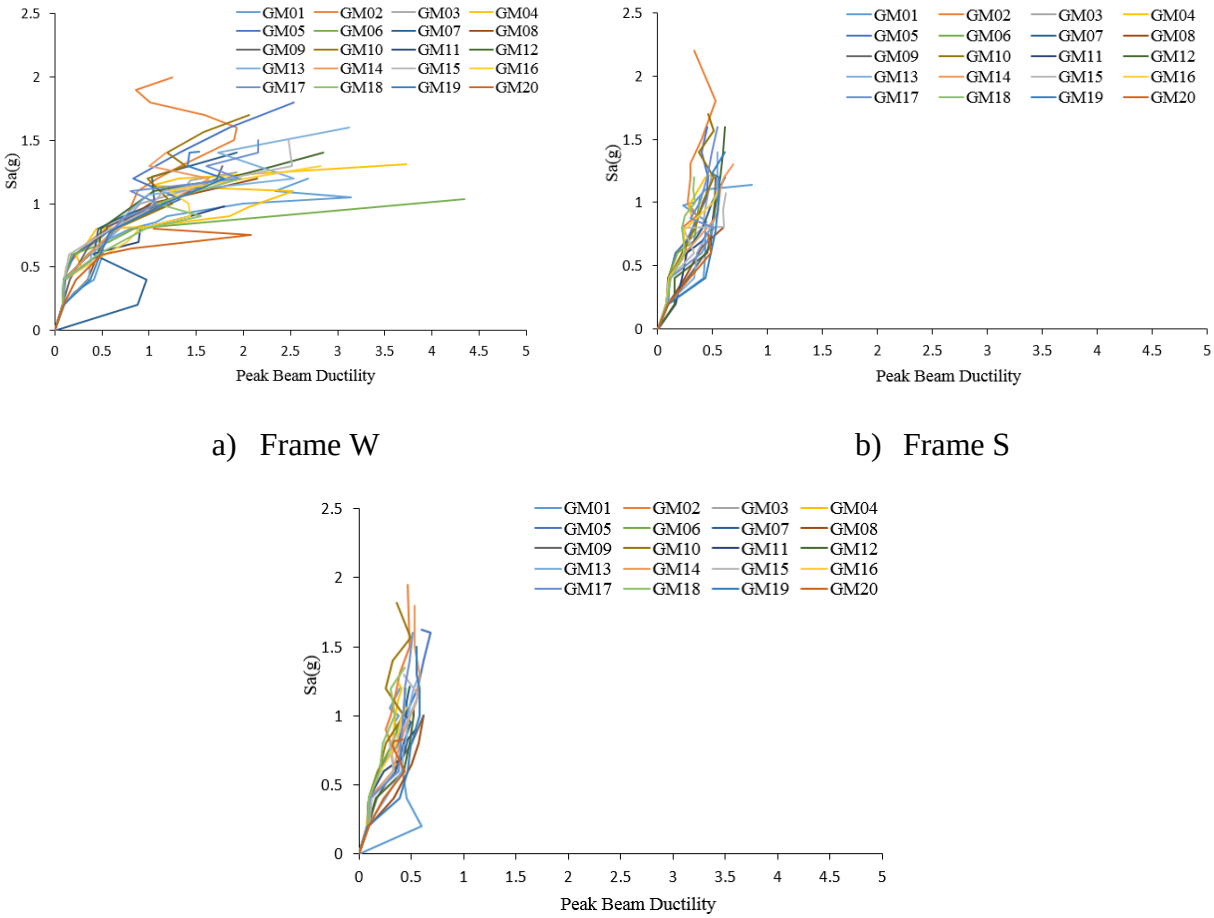

a) Frame W

b) Frame S

c) Frame C

Figure 101: Spectral acceleration vs. peak beam ductility in the 9-story frames under 20 ground motions.

Figure 102 gives a plot of the peak SDR of the frames vs. peak brace ductility. Based on this figure, the following observations can be made:

i) At 2% SDR, brace ductility in frame W varies from 10 to 15, placing it in region II, so braces are likely to experience fracture. However, at this SDR, peak brace ductility in frame S is between 6 and 11, mostly lying in region I, and braces are less likely to fracture. Similarly, brace ductility range in frame C at 2% SDR is between 7 and 10 and braces lie in region I.

ii) At 3% SDR, brace ductility in frame W is larger than 16 and is in region III, meaning that it is more likely to fracture. However, brace ductility ranges from 10 to 15 in frames S and C, lying in region II.

iii) At 4% SDR, brace ductility in frame W is still in region III and almost two times larger than the peak brace ductility in frames S and C. Braces in these frames lie in region II at 4% SDR.

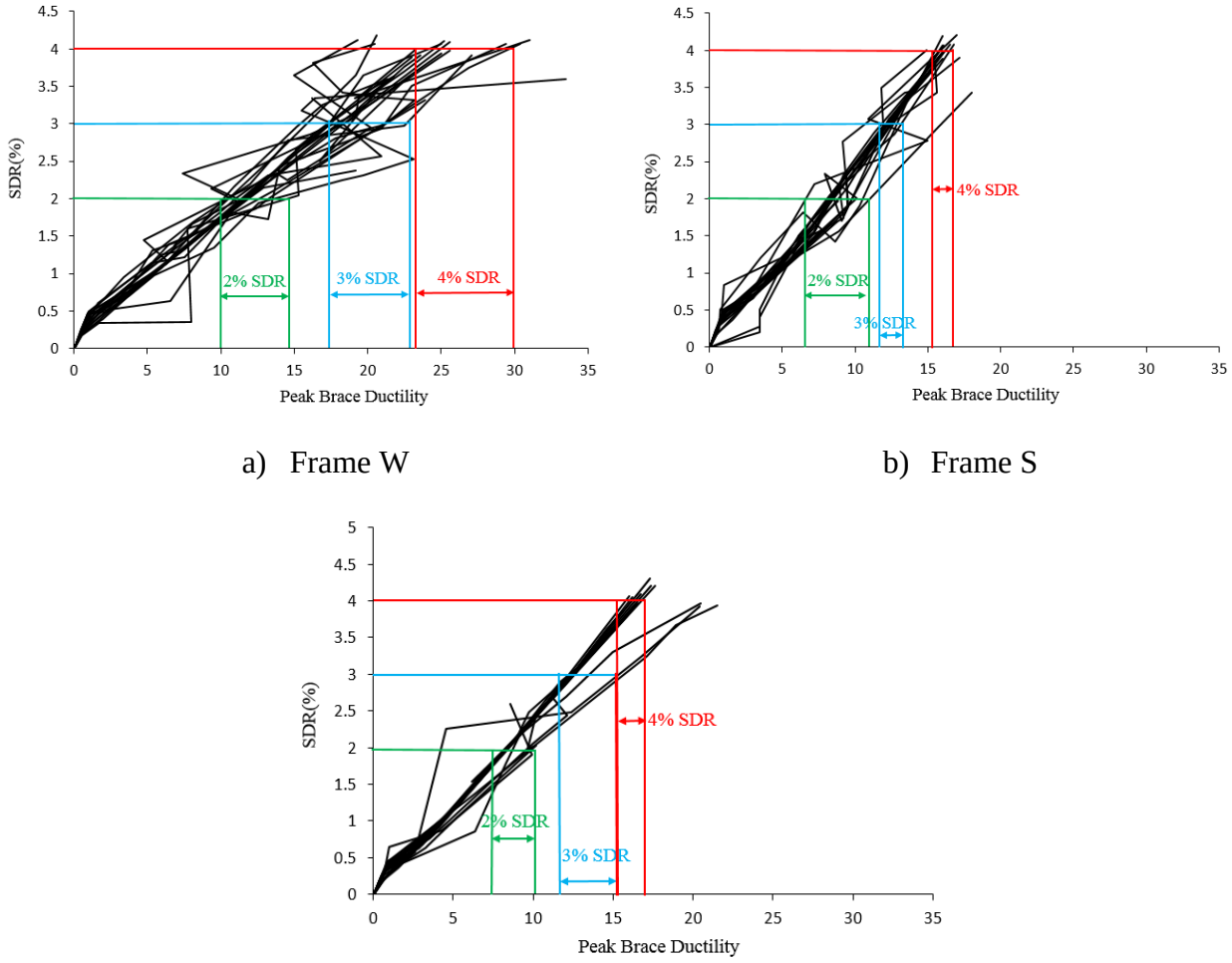

a) Frame W

b) Frame S

c) Frame C

Figure 102: SDR vs peak brace ductility of the 9-story frames under 20 ground motions.

4.9.2. Seismic Demand on the Beams and Columns of Frame W

Seismic response of the beams and column of the 9-story frame under GM11 has been described in previous sections. In this section, study of axial force and flexural demand/capacity of the beams and columns of frame W under twenty ground motions is discussed. Figure 103, Figure 104, and Figure 105 present the demand/capacity ratio of the beams and columns at 2%, 3%, and 4% SDR, respectively. It should be noted that 9-story frame was highly unstable under some of the ground motions at large SDRs, so results of the some of the ground motions are removed from this figure due to instability of the simulated frames. Based on these figures, the following conclusions can be drawn:

i) At 2% SDR, while axial force effect on the 1st level girder under all of the ground motions is small, impact of the bending moment on this beam is substantial and almost all the flexural capacity of the girder is used at this stage.

ii) Girders experienced yielding under 17 ground motions at 2% SDR (design level). This was unexpected and not conforming to the current design code (AISC341-10).

iii) Axial force demand/capacity ratio in the 1st story column of the frame at 2% SDR was almost constant (close to 0.5) under all of the ground motions.

iv) At 2% SDR, influence of the axial force on the 1st story column is more significant than that flexural effects.

v) Columns of the first story remained elastic under all the ground motions until 2% SDR was reached.

vi) At 3% SDR, axial force demand/capacity ratio in the 1st level girder was larger than the one at 2% SDR. An increase in the SDR results is reflected in the larger axial force demand on brace-intersected girders.

vii) Unlike axial force demand, flexural demand on the 1st level girder at 3% SDR is similar to that at 2% SDR. This insensitivity to SDR increase can be due to the fact that most of the flexural capacity of the beam is used until 2% SDR and the beam cannot sustain more flexural load above this value.

viii) At 3% SDR, braced-intersected girder in the first story of the frame experienced yielding under all twenty ground motions, i.e., a plastic hinge formed in the middle of the girder.

ix) Axial force demand/capacity ratio in the columns remains around 0.5 at 3% SDR and increasing the lateral displacement of the frame has little influence on the axial force demand in the 1st story column.

x) Unlike the axial force demand, flexural demand on the columns of the first story increases with rising SDR. At 3% SDR, flexural demand/capacity ratio in the 1st story column is close to the axial force ratio.

xi) At 3% SDR, columns are close to yielding under most of the ground motions, so it seems that both beams and columns assumed to remain elastic during an earthquake will experience yielding at 3% SDR.

xii) At 4% SDR, axial force demand/capacity ratio in the first story braced-intersected girder can be as large as 70% of the total demand. Comparing Figure 103 through Figure 105 leads to the conclusion that if SDR grows, axial force demand in the girder increases.

xiii) Similar to the 3% SDR case, flexural demand on the first level girder at 4% SDR remains almost identical to the one at 2% SDR. It seems that girders reach their

flexural capacity at 2% SDR and increasing the SDR has no major impact on the flexural demand on columns after 2%.

xiv) Axial force demand/capacity ratio in the column of the 1st story is about 0.5 at 4% SDR, so it can be concluded that axial force demand on the column is equal to half of the column capacity during an earthquake. Thus, in order to prevent yielding in columns, flexural demand in the columns should be limited to 0.5.

xv) Flexural demand on the 1st story column of the braced frame slightly increases when SDR grows from 3% to 4%. It seems that flexural demand/capacity ratio in the column is around 0.7 for all of the ground motions at 4% SDR.

xvi) Total demand/capacity ratio in the 1st story column reaches one under most of the ground motions, further affirming the fact that columns are yielding at this moment.

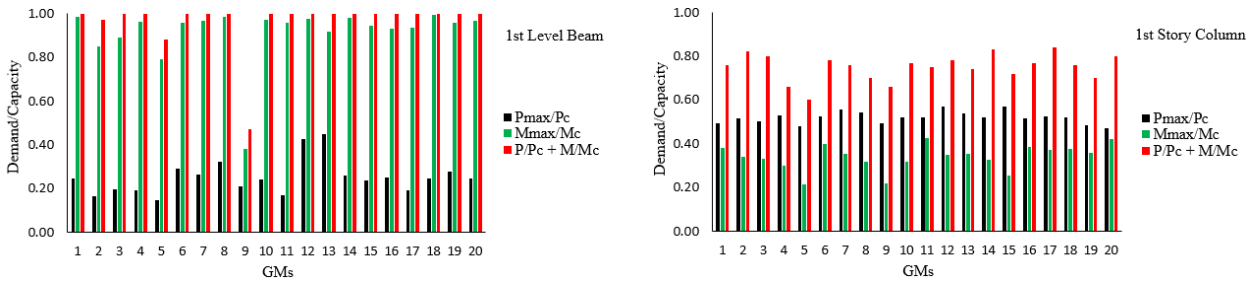

Figure 103: Axial force and flexural demand/capacity of the 1st story girder and column of frame W under 20 ground motions at 2% SDR.

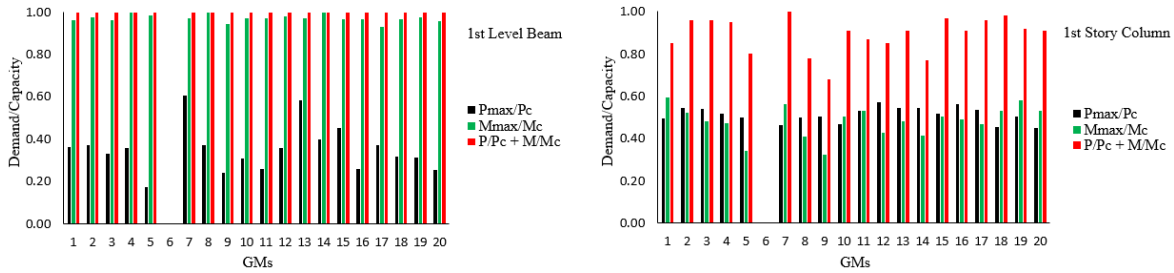

Figure 104: Axial force and flexural demand/capacity of the 1st story girder and column of frame W under 20 ground motions at 3% SDR.

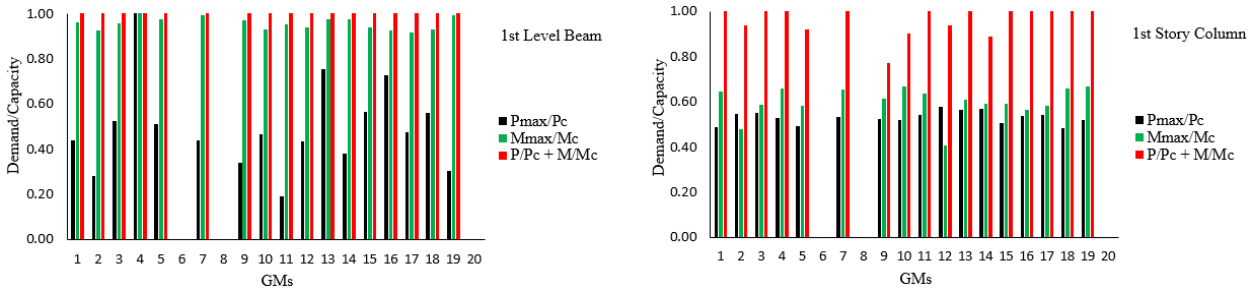

Figure 105: Axial force and flexural demand/capacity of the 1st story girder and column of frame W under 20 ground motions at 4% SDR.

4.9.3. Seismic Demand on the Beams and Columns of Frame S

In this section, results of seismic behavior of frame S are described in terms of beam and column demand. Figure 106, Figure 107, and Figure 108 present the axial force and flexural demand/capacity of the 1st level girder and 1st story column of frame S at 2%, 3%, and 4%, respectively. Based on these figures, the following observations can be made:

i) Axial force demand/capacity in the 1st story girder of frame S is negligible at 2% SDR.

ii) The major portion of the demand on the 1st level girder is due to flexural load acting on the beam. The flexural demand/capacity ratio in the 1st level beam is much larger than the axial force value at 2% SDR, as can be seen in Figure 106.

iii) Girders at the 1st level do not experience yielding at 2% SDR under any of the ground motions. Peak demand/capacity occurs under GM13 and is about 0.7.

iv) Axial force demand/capacity ratio in the 1st story column of frame S is about 0.5 at 2% SDR, similar to that for frame W.

v) Flexural demand on the 1st story column is smaller than the axial force demand at 2% SDR. A similar trend was observed for frame W, as discussed in the previous section.

vi) Total demand on the columns of the first story in frame S is smaller than the one at 2% SDR, i.e., none of the columns experienced yielding at this stage.

vii) At 3% SDR, axial force demand on the 1st level girder is small and similar to the one at 2% SDR.

viii) Flexural demand on the 1st level beam at 3% SDR is similar to the one at 2% SDR. It seems that growing the SDR has no considerable impact on the flexural demand on the beam.

ix) Total demand/capacity on the beam at 3% SDR is smaller than one, as can be seen in Figure 107. In other words, the heavy beam used in frame S does not yield at this stage.

x) Axial force demand/capacity on the column of the first story at 3% SDR is close to 0.5, similar to the one at 2% SDR, so increasing the lateral displacement of the frame has no significant impact on the axial force demand of columns.

xi) Bending moment demand on the first story column of frame S increases when the SDR grows from 2% to 3%. The flexural demand/capacity at this stage (3% SDR) is as large as the axial force demand/capacity, as can be observed in Figure 107.

xii) At 3% SDR, total demand on the column of the first story of frame S is still smaller than one, so columns in frame S remain elastic until 3% SDR value is reached.

xiii) Axial force demand in the first level girder of frame S at 4% SDR is similar to that at 2% and 3% SDR, so it can be concluded that axial force in the braced-intersected girders in frame S is almost constant and, regardless of the SDR, it has a value of about 0.05.

xiv) Flexural demand on the braced-intersected girder in frame S at 4% SDR is similar to that at 2% or and 3% SDR, so it can be concluded that flexural demand on the beams in frame S is not sensitive to the lateral displacement of the frame.

xv) Total demand on the first story braced-intersected girder at 4% SDR is smaller than one and the beams exhibit no yielding even after reaching 4% SDR. Also, the total demand at this stage is similar to the one at 2% and 3% SDR values.

xvi) At 4% SDR, axial force demand/capacity in first-story column is still about 0.5, similar to previous stages. As a result, it can be concluded that increasing the SDR has no significant effect on the axial force demand in first-story column.

xvii) Flexural demand on the first-story column of the frame reaches 0.9 at 4% SDR. Increasing the SDR results in an increase in flexural demand on columns of frame S.

xviii) Total demand on the first story column of frame S reaches one at 4% SDR and the column experiences yielding at this stage.

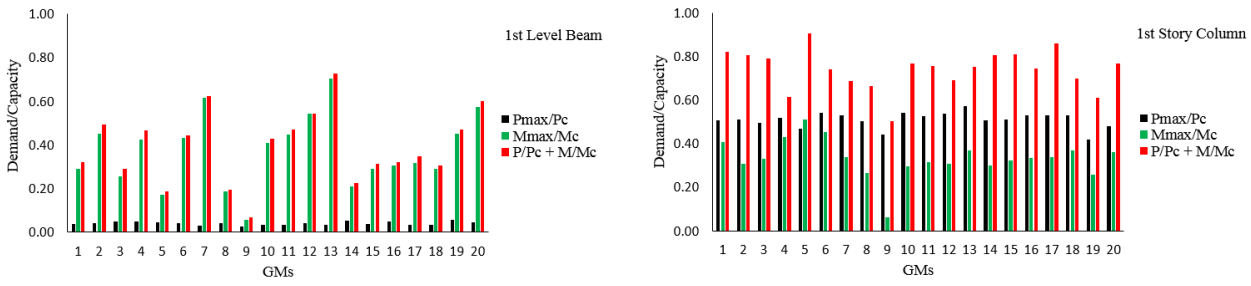

Figure 106: Axial force and flexural demand/capacity of the 1st story girder and column of frame S under 20 ground motions at 2% SDR.

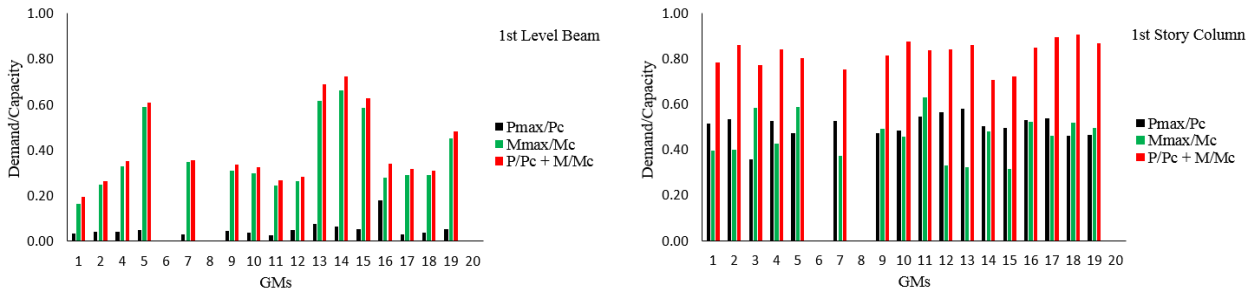

Figure 107: Axial force and flexural demand/capacity of the 1st story girder and column of frame S under 20 ground motions at 3% SDR.

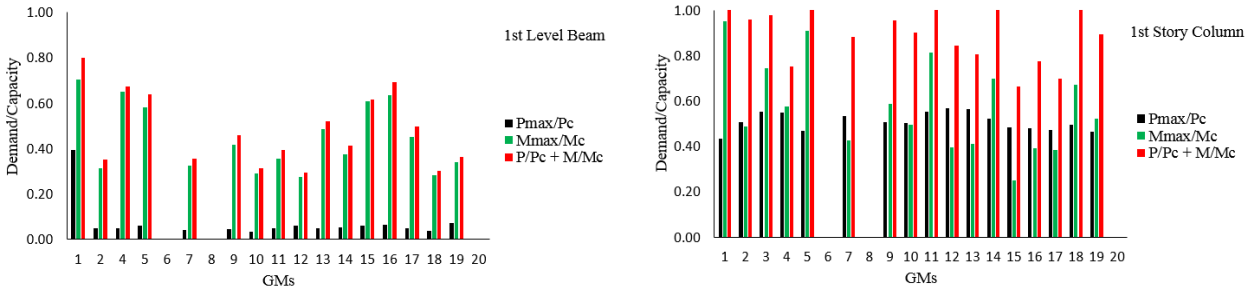

Figure 108: Axial force and flexural demand/capacity of the 1st story girder and column of frame S under 20 ground motions at 4% SDR.

4.9.4. Seismic Demand on the Beams and Columns of Frame C

Incremental dynamic analysis was performed on frame C under the previously-described twenty ground motions and response of the frame at three stages (2%, 3%, and 4% SDR) is discussed in this section in terms of beam and column demand/capacity. From Figure 109, Figure 110, and Figure 111, the following observations can be made:

i) Axial force demand/capacity in the 1st level beam of frame C at 2% SDR is almost constant at about 0.1under all ground motions.

ii) Flexural demand/capacity of the 1st level girder were similar for all twenty ground motions. The ratio is around 0.4, as can be seen in Figure 109.

iii) Total demand on the beam of the first story of the frame C does not reach one and the girder does not experience yielding at 2% SDR.

iv) At 2% SDR, axial force demand/capacity in the first story column of frame C is constant under all of the ground motions at about 0.5.

v) Flexural demand on the column of frame C is smaller than the axial force demand, and the effect of the axial force is more significant than the flexural impact at 2% SDR.

vi) Total demand on the 1st story column of the frame C is smaller than one at 2% SDR, so columns experience no yielding at this stage.

vii) Similar to the 2% stage, axial force demand/capacity in the 1st story braced-intersected girder is identical under all the ground motions. This ratio is around 0.1.

viii) Similar to the 2% SDR stage, flexural demand on the 1st level girder is identical under all the ground motions. The demand/capacity ratio is about equal to the one at 2% SDR. It seems that an increase in the SDR has no considerable influence on the flexural demand of the beam.

ix) Total demand of the 1st level braced-intersected girder is close to one at 2% SDR and the beam does not yield until 3% SDR.

x) Similar to the 2% SDR stage, axial force demand/capacity ratio in the 1st story column of the frame C is close to 0.5, and increasing the SDR has no major influence on the axial force demand.

xi) Flexural demand on the column of the first story at 3% SDR is increased in comparison to the one at 2% SDR.

xii) The first-story column in frame C does not yield under any of the ground motions, as can be seen in Figure 110. In other words, total demand/capacity is smaller than one.

xiii) Axial force demand/capacity ratio in the first story beam is close to 0.1 (except for one ground motion). It seems that, regardless of SDR, the axial force demand on the girder remains constant.

xiv) Similar to the axial force demand, flexural demand at 4% SDR is also similar to the one at 3% SDR, as can be seen in Figure 111. In other words, it can be observed that flexural demand is not affected by an SDR increase.

xv) Braced-intersected girder in the first story of frame C experienced no yielding under any of the ground motions.

xvi) Axial force demand on the column of the first story at 4% SDR is similar to the one at 2% and 3% at about 0.5. As for the girder, increasing the SDR does not affect the axial force demand of column.

xvii) Unlike the sensitivity of flexural demand of column to the SDR in the early stages of the analysis (from 2% to 3% SDR), it can be observed in Figure 111 that increasing the SDR from 3% to 4% has no significant impact on the flexural demand of column in the first story of the frame and flexural demand/capacity at 4% SDR is virtually the same as that at 3% SDR.

xviii) Total demand of the 1st story column shows that columns are still in the elastic range at 4% SDR, satisfying the current design code criteria.

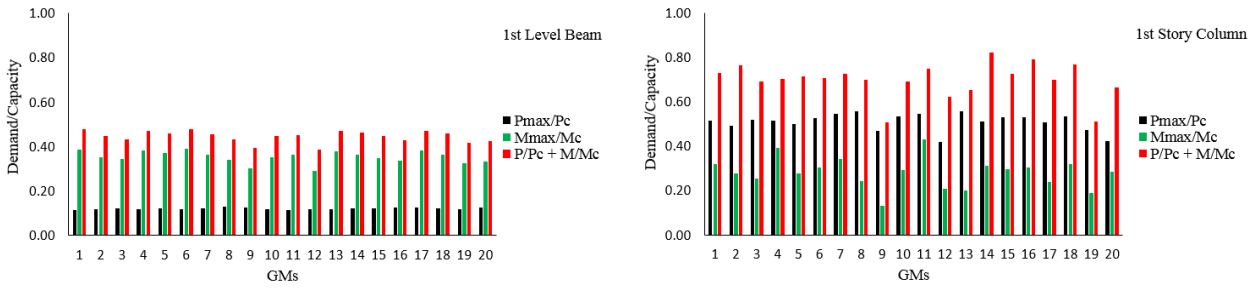

Figure 109: Axial force and flexural demand/capacity of the 1st story girder and column of frame C under 20 ground motions at 2 % SDR.

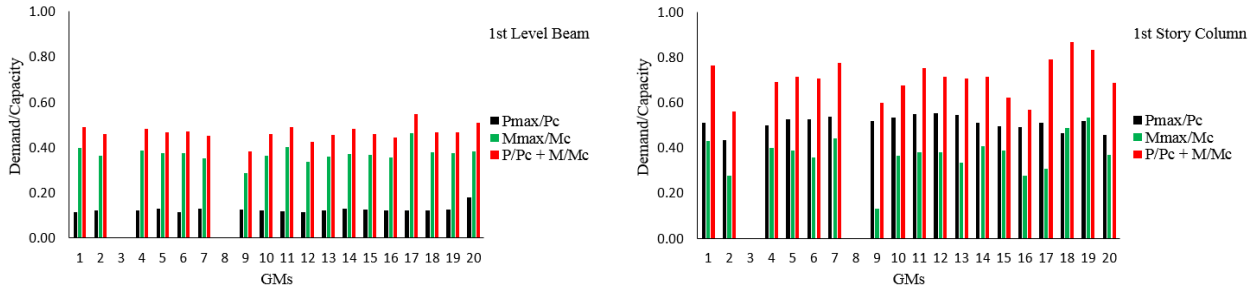

Figure 110: Axial force and flexural demand/capacity of the 1st story girder and column of frame C under 20 ground motions at 3 % SDR.

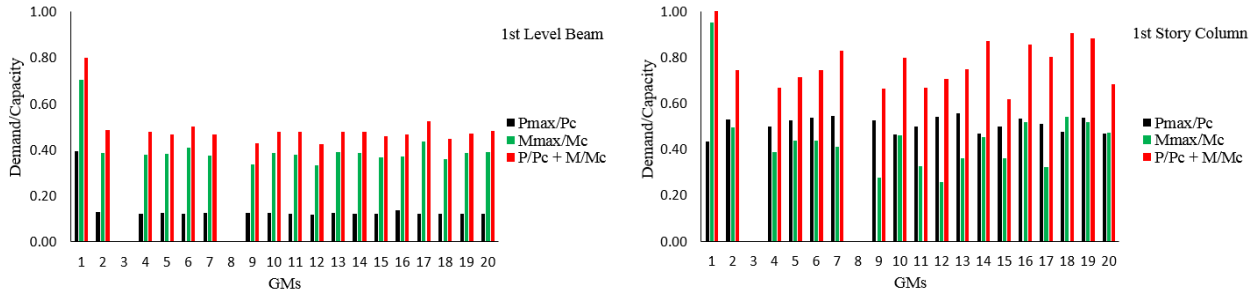

Figure 111: Axial force and flexural demand/capacity of the 1st story girder and column of frame C under 20 ground motions at 4 % SDR.

4.9.5. Seismic Demand on the Braces

Figure 112 describes the brace ductility demand in frames W, S, and C at 2%, 3%, and 4% SDR values under twenty ground motions. Comparing these figures leads to the following conclusions:

i) Due to the yielding of the beam in frame W, brace ductility in this frame is significantly larger (almost two times) than for the other frames, so, similarly to previously-stated conclusions based on GM11 results, it can be observed that beam strength plays an important role in brace ductility demand. The shallower the braced-intersected girder, the larger the brace ductility demand.

ii) Regardless of beam strength and bracing configuration, brace ductility demand increases with increased SDR. Since the lateral displacement of the frame is directly related to the brace ductility, it is to be expected that any increase in the lateral displacement results in increasing the brace ductility demand.

iii) Peak brace ductility values in frames S and C are similar to one another and both frames follow the same trends in term of brace behavior, so it can be concluded that bracing configuration has an inconsiderable effect on the brace ductility demand.

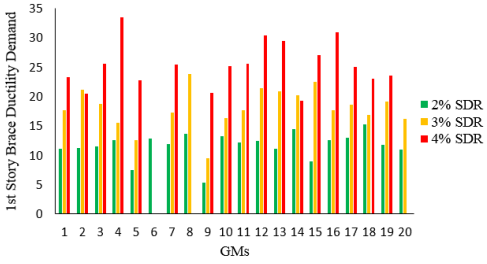

a) Frame W

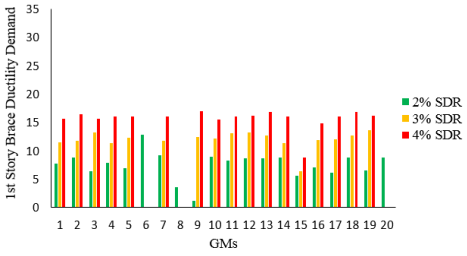

b) Frame S

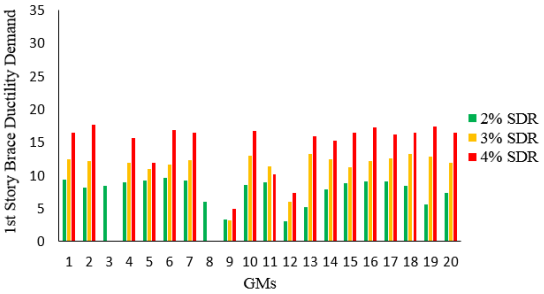

c) Frame C

Figure 112: 1st story brace ductility demand under 20 ground motions.

4.9.6. Flexural Demand-Rotation in Columns of SCBFs

As mentioned earlier, flexural demand on the columns is directly related to the rotation of the columns resulting from the differences between the lateral displacements of the consecutive stories, as shown in Figure 95. Figure 113 is a plot of the flexural demand/capacity ratio of the first-story column of frames W, S, and C versus the earlier-defined relative rotation (θ) each point in this figure represents peak flexural demand on the 1st story column of the frame at a specific SDR. Each figure contains about 60 data point (results of 20 ground motions at three stages, 2%, 3%, and 4% SDR) and a linear M-θ equation is fitted to these points. Based on this figure, the following observations can be made:

i) Flexural demand-relative rotation relation (M-θ) in frames W and S are similar to one another and the same equation can be used for both frames. Similar results were observed in previous sections when behavior of the columns was evaluated with respect to strength.

ii) Unlike the similar behaviors of frames W and S, frame C is different from the previous cases in that the slopes of the equations derived for frame C are significantly smaller than for TSXBFs. In other words, any increase in the relative rotation of the columns in TSXBF results in larger flexural demand than that for the chevron frame, so it can be concluded that brace configuration has a considerable impact on the flexural demand of the columns in SCBFs, and it seems that chevron bracing is advantageous when compared to the TSXBFs.

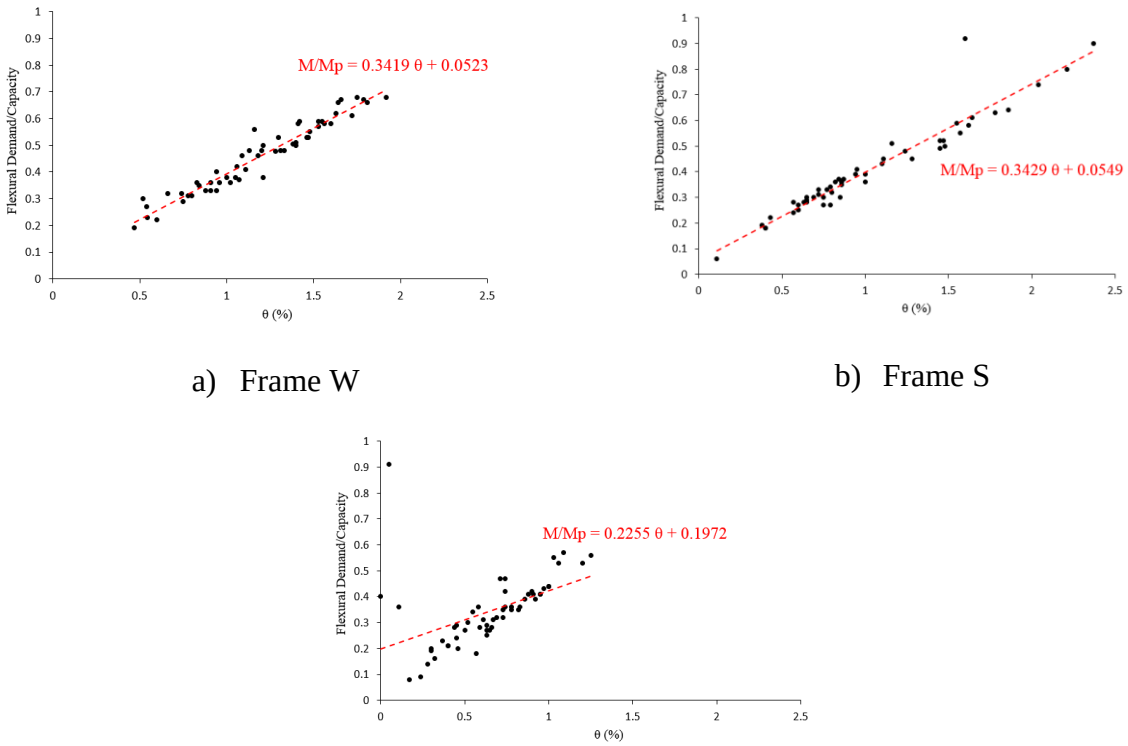

a) Frame W

b) Frame S

c) Frame C

Figure 113: Flexural Demand-relative rotation relationship in 1st story columns.

4.9.7. Comparison of the Response of the Frames W, S, and C and Conclusions

In this section, results for frames W, S, and C are compared and a summary of the important conclusions of this chapter is presented.

i) Brace ductility in frame W can be as large as twice that in frames S and C. Brace ductility demand in frame W lies in region 3 at 4% SDR and likely to result in fracture.

ii) Increasing the SDR results in an increase in axial force demand in the 1st level girder in frame W, while the axial force demand/capacity in frames S and C are independent from the SDR and virtually constant.

iii) Increasing the SDR leads to a rise in flexural demand in the braced-intersected girder of the frames W and S, while flexural demand on the first story beam of the chevron frame is independent of the SDR.

iv) Based on the results, it can be concluded that total demand on the braced-intersected girder in the first story of the chevron frame is insensitive to an increase in the lateral displacement of the frame.

v) Regardless of the bracing configuration, utilizing a deep girder in the concentrically braced frames prevents beam yielding and additional demand on the braces can be avoided.

vi) Yielding of the shallow beam in TSXBF is initiated at a SDR value of about 2% that is the design level and therefore unexpected. It should be recalled that, according to AISC 341-10, beams should not experience yielding during an earthquake, but results of the analyses demonstrate that this provision cannot be met in TSXBF designs based on current design codes.

vii) Regardless of the bracing configuration and beam strength, axial force demand/capacity in the columns of the special concentrically braced frames was always close to 0.5. It should be emphasized that increasing the SDR has an inconsiderable effect on the axial force demand on the columns.

viii) Flexural demand on the first story column of chevron frame is significantly smaller than that of the TSXBFs.

ix) The first-story column of the chevron frame does not yield at any stage, while the TSXBF column start to yield at about 3% SDR. It should be mentioned that the

current design code (AISC 341-10) assumes that columns remain elastic during an earthquake.

CHAPTER 5. SEISMIC BEHAVIOR OF BCBFs UNDER EARTHQUAKE GROUND MOTIONS

5.1. Introduction

Seismic behavior of conventional ductile CBFs was investigated in the previous chapter by deploying an ensemble of ground motions applied to three different frames with various bracing configurations and different beam strengths. Frame performance results were presented in terms of ductility, strength, displacement and deformation, and it was observed that TSXBF designed based on the current design codes does not meet expectations. In addition, large seismic demand on the columns due to the considerable flexural demand resulted in unexpected yielding in the columns. The following is a summary of these issues:

i) Braces: braces in frames W are most likely to experience fracture.

ii) Girders: Braced-intersected girders experience yielding in frame W, even though they should remain elastic.

iii) Columns: Columns unexpectedly experience yielding under several ground motions.

iv) Deformation: Deformation of the frame accumulates in one story due to soft story phenomena after yielding/buckling of the braces.

All these issues clarify the need to find a method for improving the seismic performance of the SCBFs.

In this chapter, study of the effect of the BCBs on the behavior of frames W, S, and C is described, and seismic performance of previously-designed SCBFs is compared with seismic response of BCBFs (SCBFs incorporating BCBs). Conclusions of this study are presented at the end of the chapter.

5.2. Modeling of BCBFs

Buckling-controlled braces were introduced in Chapter 3 of this study. Cyclic behavior of these braces is presented in Figure 36, where it can be observed that tensile and compressive capacity of the BCBs are similar, a significant advantage when compared to conventional braces. In this chapter, all the braces modeled in RUAUMOKO have been modified to simulate BCBs, and symmetrical bilinear behavior is used to simulate the actual behavior of the braces. Figure 114 shows the behavior of the modeled braces under tension and compression. All the other parameters in the frames are the same as those used for conventional frames.

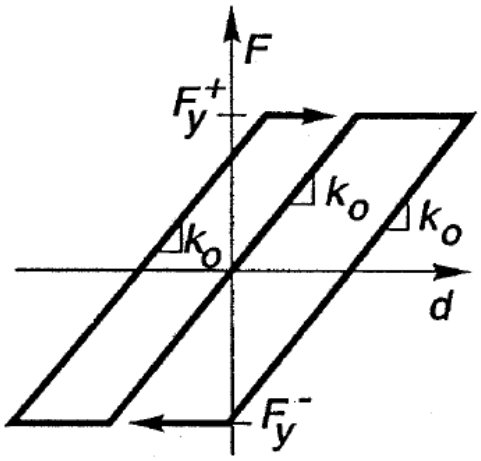

Figure 114: Behavior of BCB under tension and compression.

Since comparison of the behavior of SCBFs and BCBFs in large SDR is the purpose of this chapter, the scale factor resulting in 4% SDR in conventional frames has been used for the ground motions applied to the frames. Details of the simulated frames in RUAUMOKO are presented in Appendix B.

5.3. Seismic response of SCBFs and BCBFs in terms of SDR

A group of twenty ground motions were applied to the frames W, S, and C incorporating BCB. Seismic response of these frames in terms of SDR is investigated in this section. As can be seen in Figure 115, the story-drift ratio demand on SCBF is reduced by utilizing BCBs as bracing members and the peak story drift ratio demand in frame W is reduced from 4% to 2-3.5% by using BCBs. It should also be noted that BCBs have more significant effect on the SDRs of frames S and C. The SDR reduction in these frames is considerable and peak SDR decreases from 4% to 1.5-3% in frames S and C.

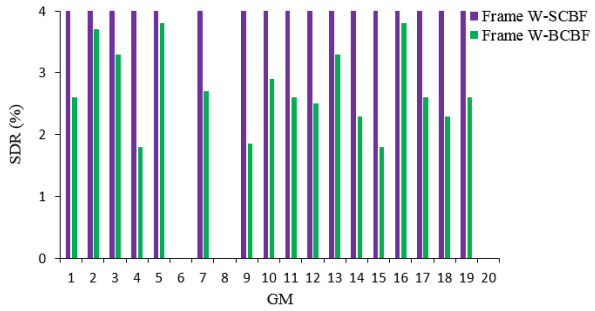

a) Frame W

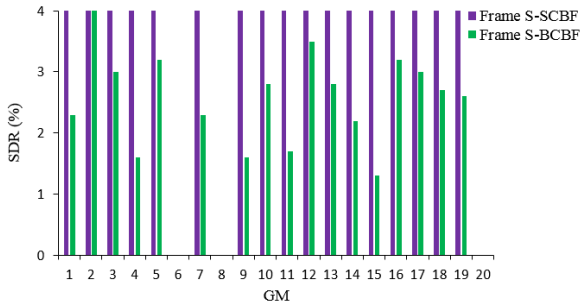

b) Frame S

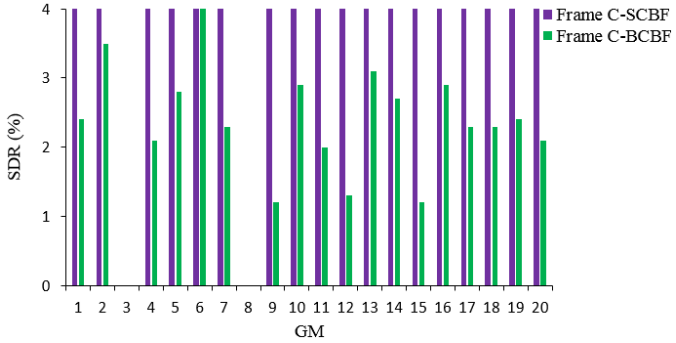

c) Frame C

Figure 115: Comparison of SDR in SCBFs and BCBFs.

The previously-mentioned SDR reduction is due to the influence of BCBs on the deformation of the frames. Figure 116 presents the SDR time history of frames W, S, and C both with and without BCBs under GM11. It can be observed that SDR in the first story of the

conventional frames is considerably larger than for the other stories. In other words, lateral displacement accumulates in the first story due to soft-story phenomena. However, in BCBFs, SDR in all the stories are closer to one another and it can be concluded that lateral displacement in the BCBFs is distributed uniformly along the height of the frame.

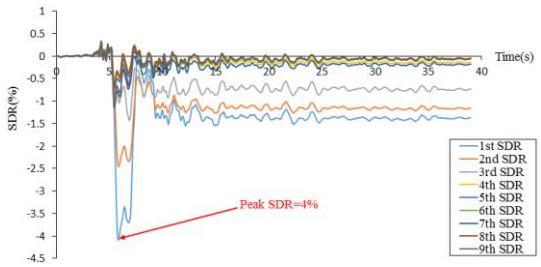

a) Frame W-SCBF

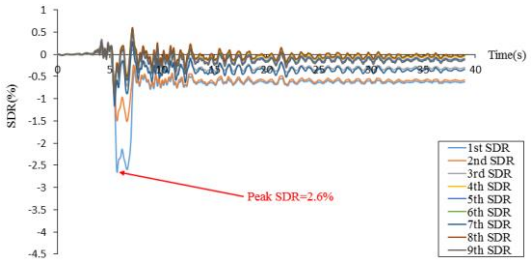

b) Frame W-BCBF

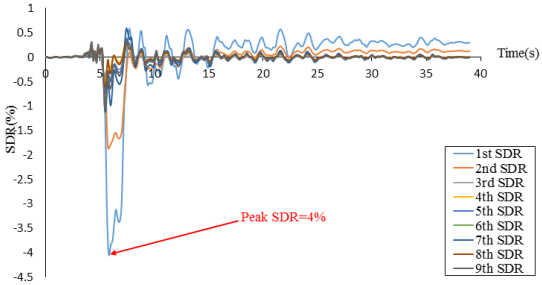

c) Frame S-SCBF

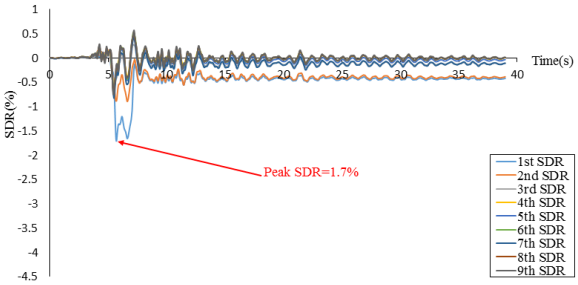

d) Frame S-BCBF

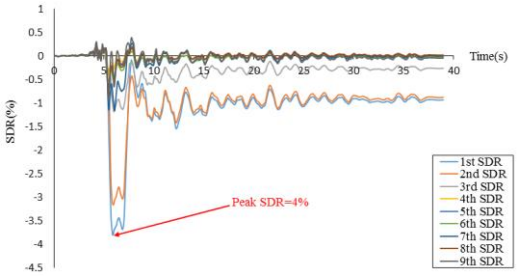

e) Frame C- SCBF

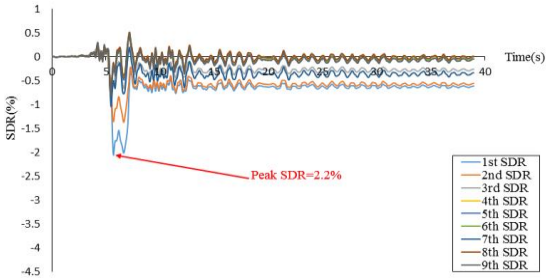

f) Frame C-BCBF

Figure 116: Comparison of SDR history between SCBFs and BCBFs under GM11.

Deformation of conventional frame W is shown in Figure 117 at 4% SDR for the time at which peak SDR occurs. Deformation of frame W incorporating BCB is also shown in this figure for the sake of comparison. As can be seen in the figure, while a considerable lateral displacement

is concentrated in the first two stories of the SCBF resulting in large brace ductility demand, the lateral displacement of the BCBF is nearly linear along the height, one of the advantages of this system.

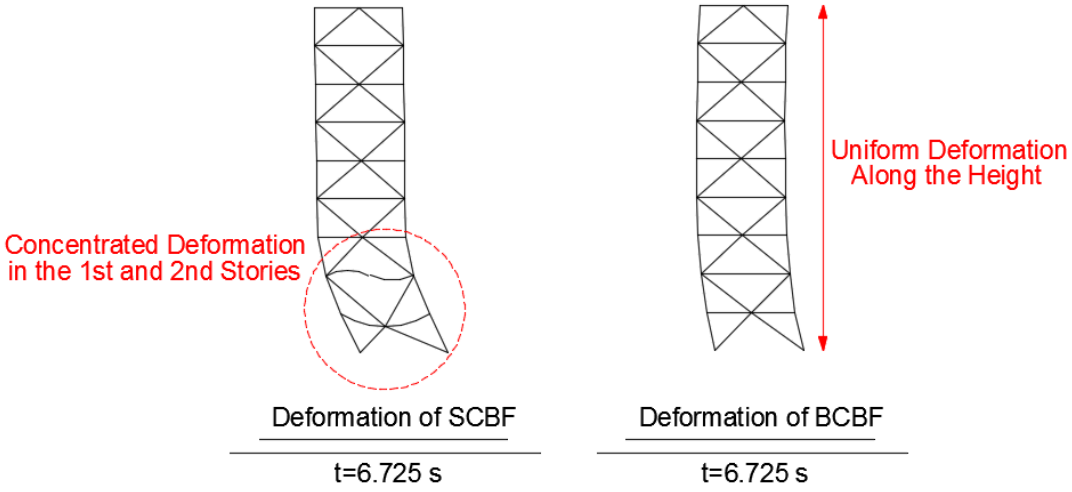

Figure 117: Comparison of the deformation of the SCBF and BCBF.

5.4. Seismic response of SCBFs and BCBFs in terms of beam behavior

In the previous chapter, seismic performance of the beams in the conventional SCBF under 20 ground motions was investigated. It was observed that 1st and 2nd story beams in frame W experience yielding at 2% SDR, and it was also found that the 1st story braced-intersected girder remains elastic in frames S and C. In this section, performance of the beams in SCBFs and BCBFs will be compared.

Comparison of the axial force demand/capacity of frames W, S, and C both with and without BCBs is presented in Figure 118. Because of the instability of the conventional frames under some of the ground motions, results of them are left blank in this figure. Based on Figure 118, the following conclusions can be drawn:

i) Axial force demand/capacity in frame W will become slightly larger if conventional braces are replaced with BCB, as can be explained by considering the higher-modes effect shown in Figure 119. While in the first mode deformation, the axial force of the braces almost cancel one another, resulting in small axial force demand on the braced-intersected girders, in the higher modes axial force of the braces will be added together, resulting in larger axial force demand. Therefore, because the compression capacity in the BCBs is larger than the one in conventional braces, the unbalanced horizontal force that will be applied to the girder in higher modes will be larger and result in greater demand, as can be seen in Figure 118.

ii) Unlike for frame W, axial force demand/capacity in frames S and C is not significantly changed by replacing the braces, and the negligible effect can be due to the considerable strength of the beam that keeps the demand/capacity ratio relatively small.

iii) Axial force demand/capacity in BCBF and SCBF does not exceed 0.3 in the frames, so it can be concluded that axial force demand on the beams is relatively small.

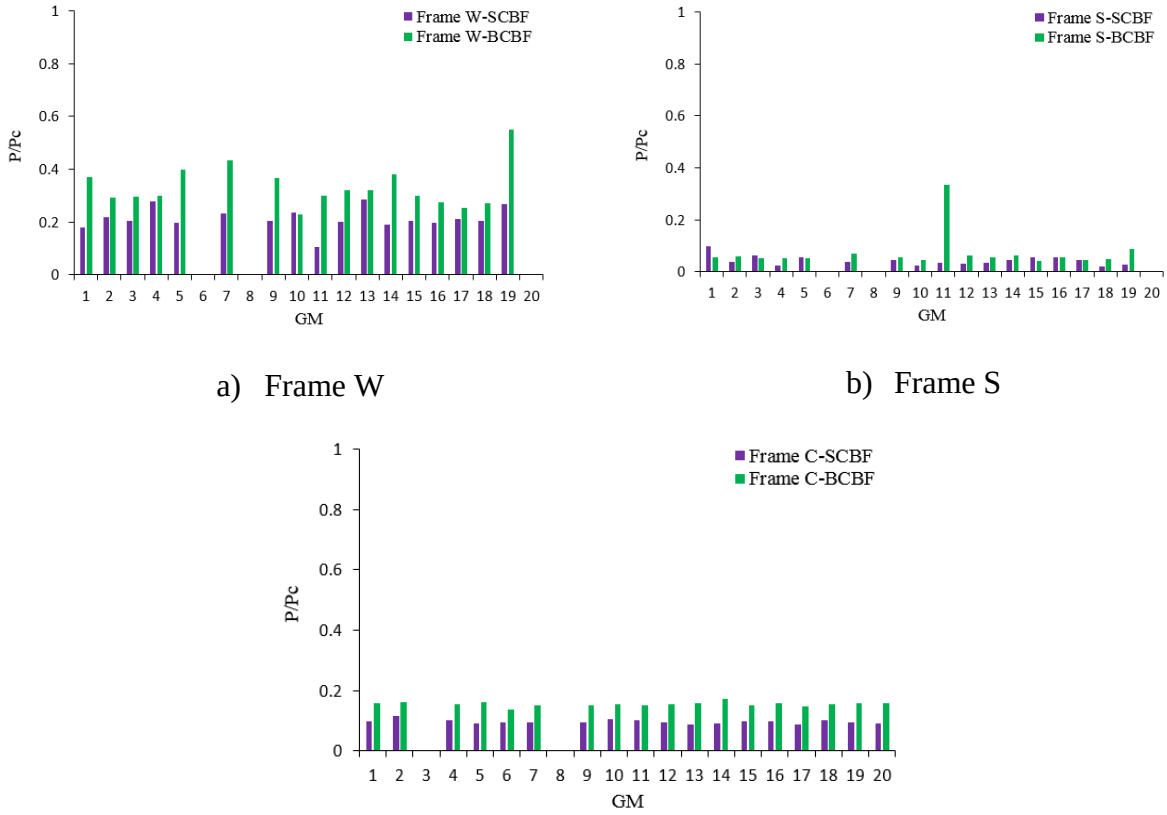

a) Frame W

b) Frame S

c) Frame C

Figure 118: Axial force demand/capacity on the 1st level braced-intersected girder in SCBF vs BCBF.

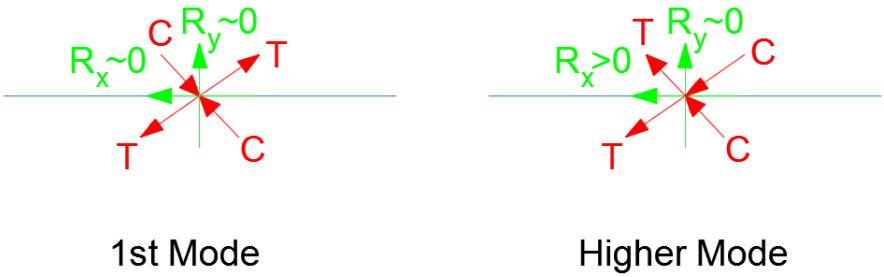

Figure 119: Unbalanced forces in different deformation modes.

Flexural demand/capacity in the first-story braced-intersected girders of frames W, S, and C is shown in Figure 120. From this figure, the following observations can be made:

i) While flexural demand/capacity in conventional SCBF can be as large as 0.9, it can be seen that flexural demand in the braced-intersected girder is substantially reduced by substituting for conventional braces with BCBs.

ii) Utilizing BCB with symmetrical cyclic behavior results in zero unbalanced vertical load on the braced-intersected girder, leading to zero bending moment in the beam, as can be seen in Figure 120.

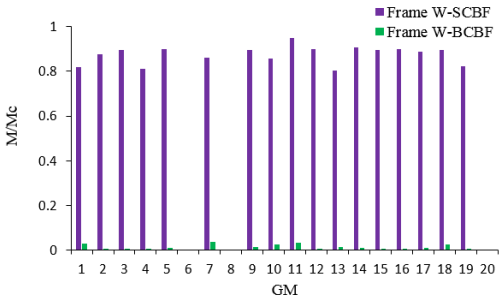

a) Frame W

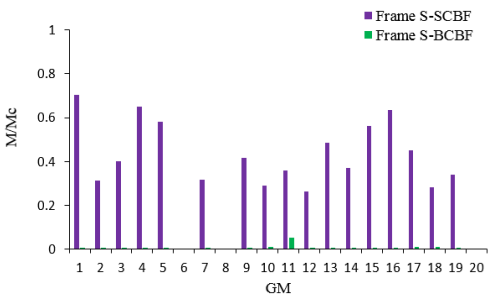

b) Frame S

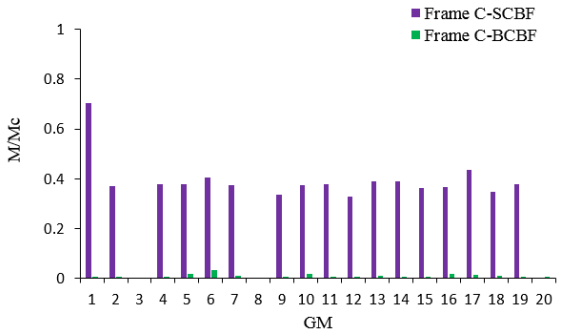

c) Frame C

Figure 120: Flexural demand/capacity on the 1st level braced-intersected girder in SCBF vs BCBF.

Total demand/capacity in the braced-intersected girder of frames W, S, and C are shown in Figure 121. Based on the frame response presented in this figure, the following conclusions can be drawn:

i) Although the first-story girder in frame W experienced yielding in conventional frames under all the ground motions, replacing the braces with BCBs reduced the demand substantially. The peak demand/capacity in the BCBF in frame W is about 0.4, 60% smaller than for conventional SCBF.

ii) Total demand/capacity in frames S and C is smaller than 0.2 if BCBs are incorporated, but can be as large as 0.8 in conventional frames.

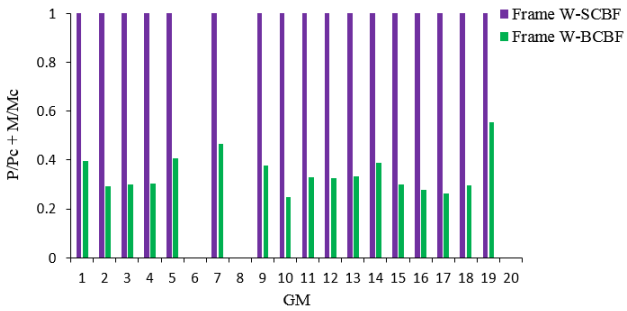

a) Frame W

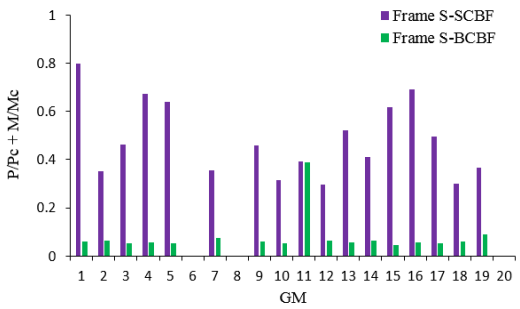

b) Frame S

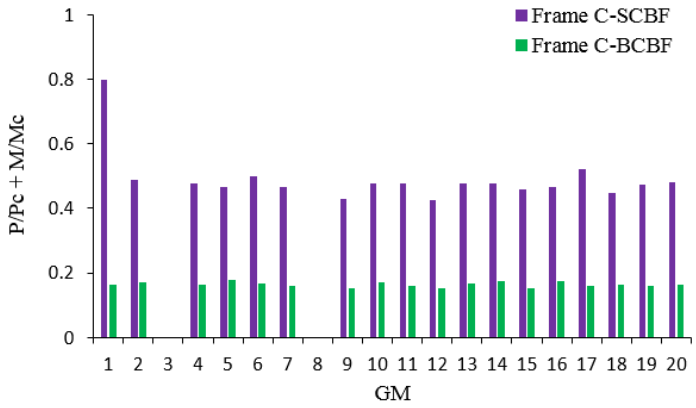

c) Frame C

Figure 121: Total demand/capacity on the 1st level braced-intersected girder in SCBF vs BCBF.

5.5. Seismic response of SCBFs and BCBFs in terms of column behavior

Seismic behavior of the columns in SCBFs was studied in the previous chapter. Columns in TSXBF experienced yielding under most of the ground motions, and the demand/capacity ratio

in columns of the chevron frame was about 0.7. In the current section, performance of columns in BCBFs are evaluated when conventional braces are replaced with BCBs.

Axial force demand/capacity of the columns of frames W, S, and C incorporating conventional braces and BCBs is presented in Figure 122, where it can be observed that axial force demand in BCBF is slightly larger than SCBF in all the frames, as would be expected. This can be explained by considering the fact that, because of buckling of the braces, larger forces will be applied to the structures and axial force demand on the columns will be larger.

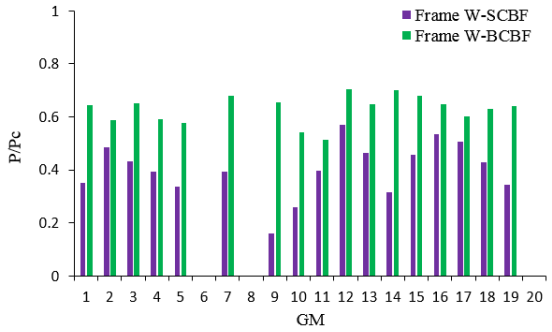

a) Frame W

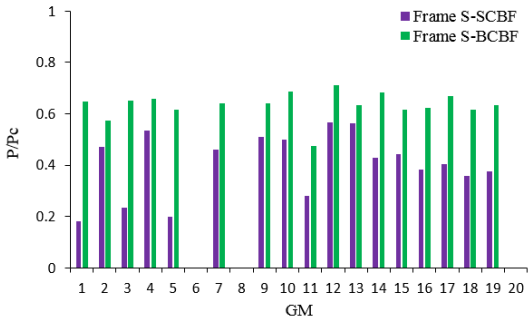

b) Frame S

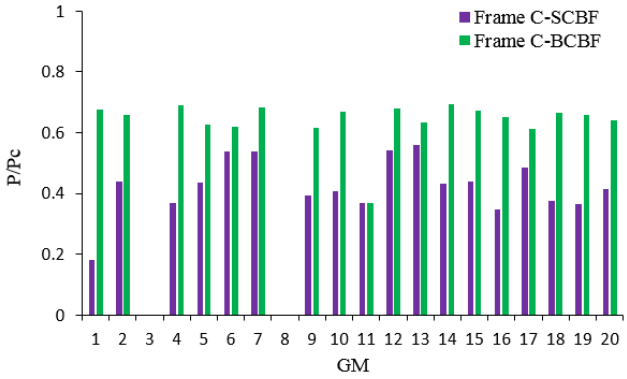

c) Frame C

Figure 122: Axial force demand/capacity on the 1st story column in SCBF vs BCBF.

Unlike the axial force demand, the flexural demand of the columns in SCBFs is reduced in BCBFs, as shown in Figure 123. The smaller flexural demand is due to the reduction in SDR that

results in a decrease in the relative rotation of the columns, causing the bending moments of the columns will be smaller.

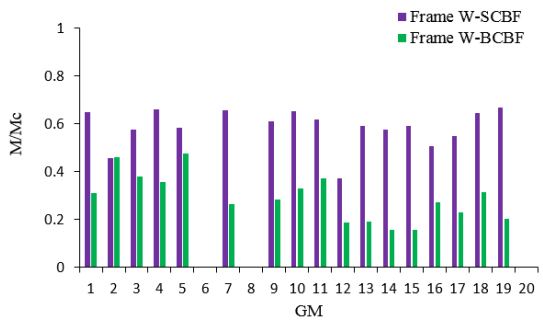

a) Frame W

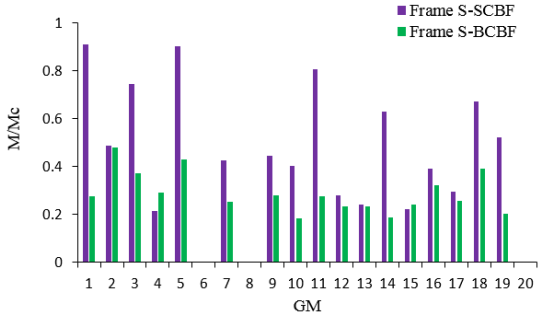

b) Frame S

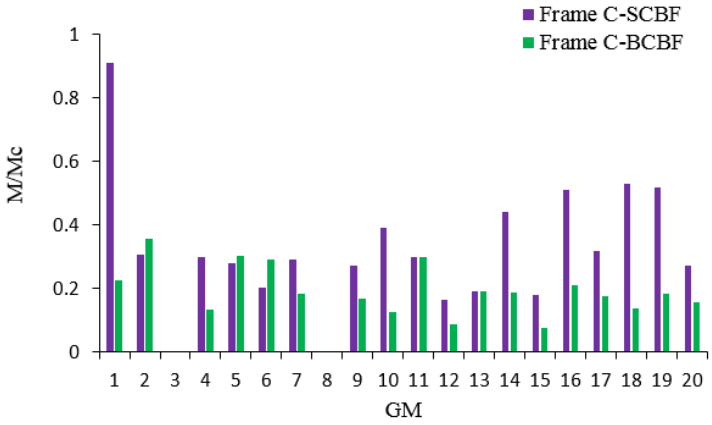

c) Frame C

Figure 123: Flexural demand/capacity on the 1st story column in SCBF vs BCBF.

Figure 124 shows a comparison of the total demand/capacity of the column in SCBFs and BCBFs. Based on this figure, it can be concluded that BCBs insignificantly affect the seismic response of the columns in braced frames. Total demand on the columns is almost similar in frames both with and without BCBs and columns experience yielding under some of the ground motions.

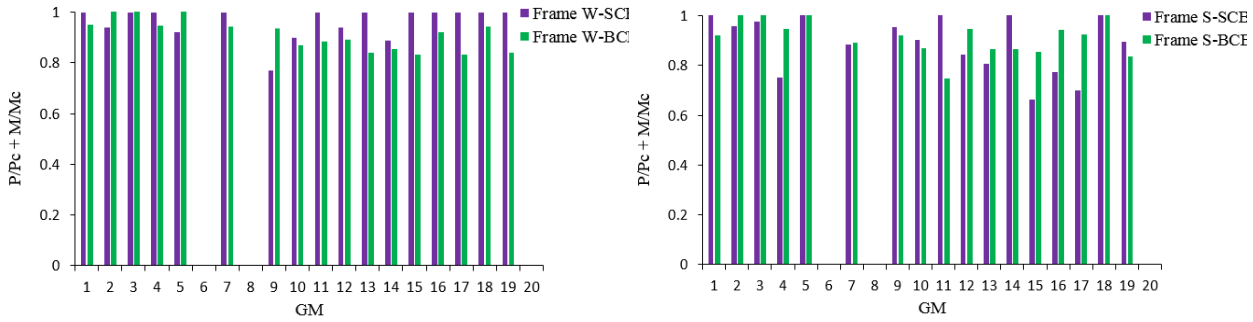

a) Frame W

b) Frame S

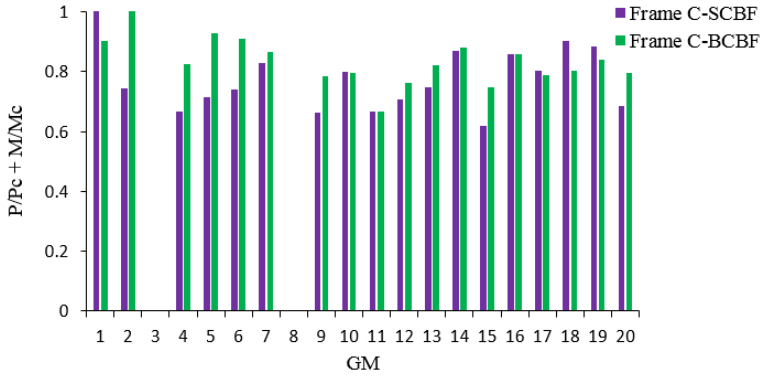

c) Frame C

Figure 124: Total demand/capacity on the 1st story column in SCBF vs BCBF.

5.6. Seismic response of SCBFs and BCBFs in terms of brace ductility

Seismic behavior of conventional braces in ductile braced frames was investigated in the previous chapter where it was observed that braces in frame W are likely to experience fracture and their ductility is in region III. In the current section, brace ductility demand in SCBFs and BCBFs are compared.

Brace ductility demand on the 1st story braces of the frames W, S, and C is presented in Figure 125. It can be observed that ductility demand on the 1st story brace in frame W can be significantly reduced by incorporation of BCBs in SCBFs. The considerable reduction in the brace ductility is due to the smaller vertical deflection of the beam in BCBF. In the previous section, it was shown that 1st story beam of BCBF in frame W does not experience yielding, in subsequent

vertical displacement of the beam is substantially smaller. On the other hand, impact of the BCBs on the brace ductility in frames S and C is less significant. From Figure 125 it can be concluded that peak brace ductility in BCBFs, regardless of the bracing configuration, is less than 16 (region II).

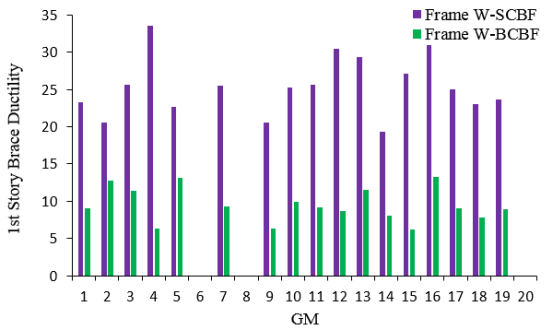

a) Frame W

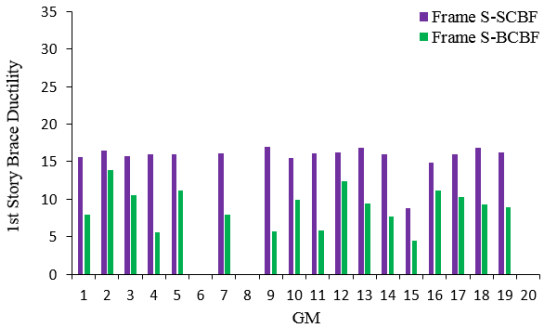

b) Frame S

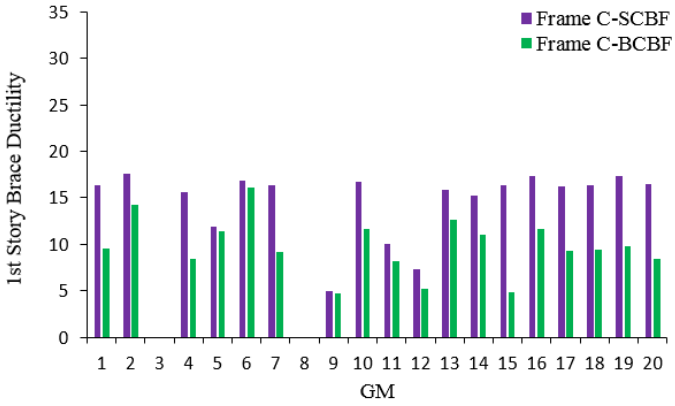

c) Frame C

Figure 125: Brace ductility demand in SCBF vs BCBF.

5.7. Effect of bracing configuration and beam strength on seismic response of BCBFs

Three buckling-controlled braced frames with different bracing configurations and beam strengths were modeled in RUAUMOKO and their seismic behavior investigated under twenty ground motions; the frame responses are compared in this section.

Seismic demand on the 1st story braced-intersected girder of frames W, S, and C is shown in Figure 126, from which it can be observed that:

i) Axial force demand/capacity in frame W is larger than for frames S and C, while using a deep beam in a two-story X-braced system results in the smallest axial force demand.

ii) Flexural demand in the 1st story girder is almost zero in all the frames, so it seems that, regardless of the beam strength and bracing configurations, flexural demand on the braced-intersected girders in BCBFs is negligible.

iii) Total demand on the first story girder in BCBF is smaller than 0.4 and the smallest demand occurs in TSXBF with strong beams.

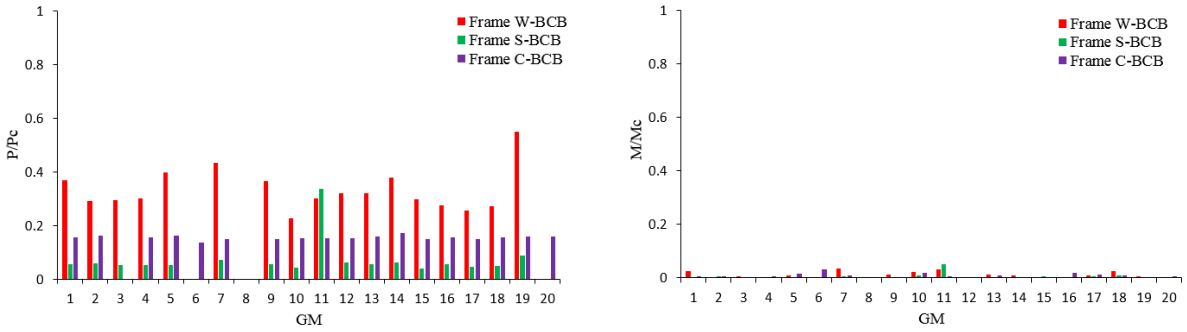

a) P/Pc b) M/Mc

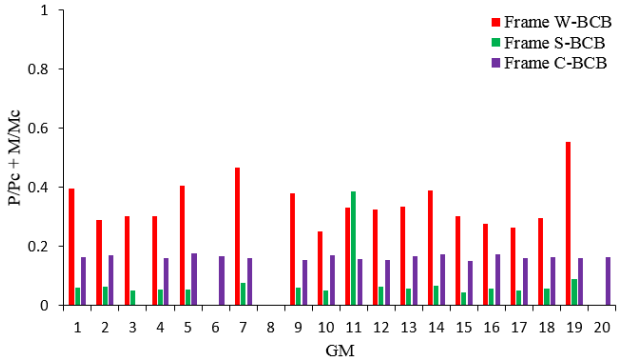

c) P/Pc + M/Mc

Figure 126: Demand/capacity in the 1st level braced-intersected girder.

Unlike for the first-story beam, axial force demand on the second-story girder is relatively small and the effect of the bracing configuration and beam strength is insignificant. Conversely, flexural demand on the second-story beams is considerably large. As can be seen in Figure 127, the beam experiences yielding in the TSXBF while the demand on the beams in the chevron frame is almost zero. The great flexural demand on the beams in TSXBFs is due to the lateral displacement of the frame created through rigid connections. It should be mentioned that beam sections used at the 2nd level are identical in frames W and S, and it should also be noted that, due to the significant bending moment, 2nd level beams yield under most of the ground motions.

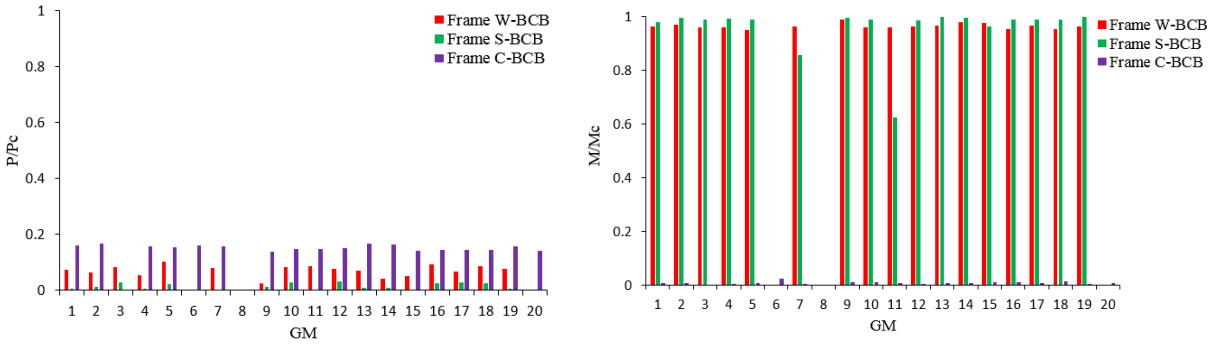

a) P/Pc

b) M/Mc

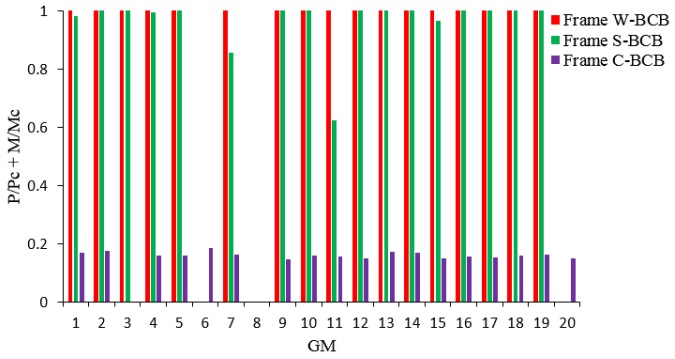

c) P/Pc + M/Mc

Figure 127: Demand/capacity in the 2nd level girder.

Seismic demand on the 1st story columns of frames W, S, and C are compared in Figure 128, from which it can be concluded that:

i) Axial force demand on the columns is similar to each other regardless of the bracing configuration and beam strength. It is also worth mentioning that axial force demand/capacity in the column is about 0.6, slightly larger than the one in SCBF, under all the ground motions.

ii) Similar to axial force demand, flexural demand on the columns of frames W, S, and C are similar to each other. The flexural demand/capacity is about 0.3, slightly smaller than for the SCBFs.

iii) Total demand values on the columns in all the frames are close to one other, so bracing configuration and beam strength have no significant impact on the seismic response of columns in BCBFs.

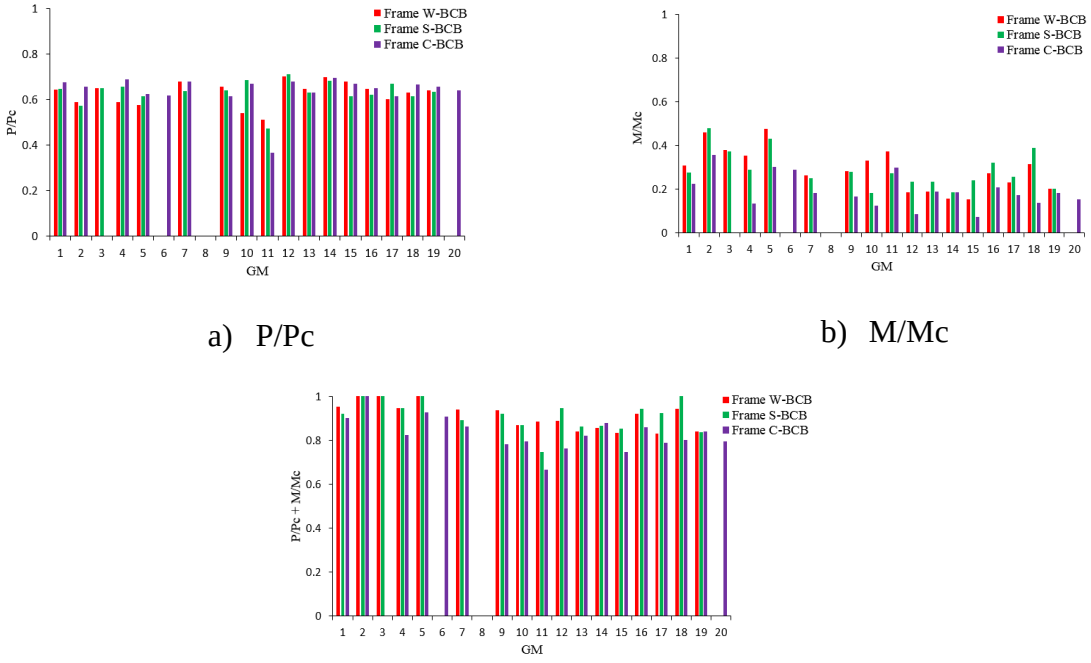

a) P/Pc

b) M/Mc

c) P/Pc + M/Mc

Figure 128: Demand/capacity in the 1st story column.

1st story brace ductility demand in BCBFs presented in Figure 129 shows that brace ductility in different frames are similar to each other and they are mostly in region I which is the safe zone based on the experienced results.

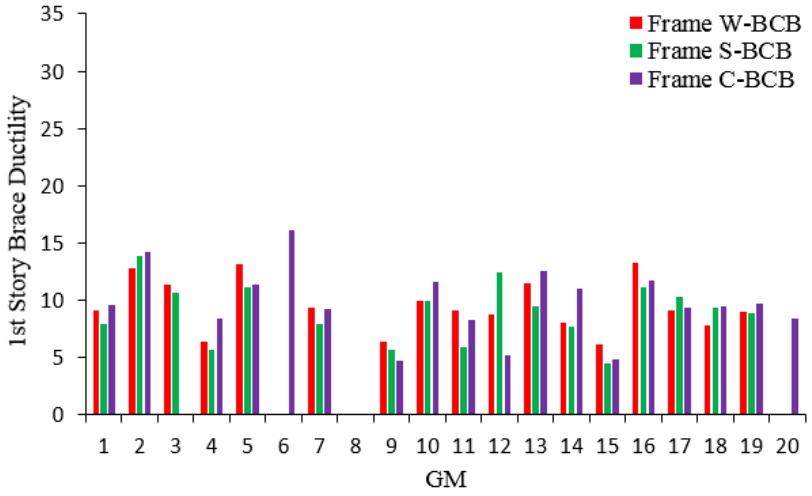

Figure 129: Brace ductility demand on the 1st story braces.

5.8. Conclusions

This chapter describes investigation of seismic performance of ductile concentrically braced frames incorporating buckling-controlled braces. Seismic response of the BCBF was compared with that of the SCBF and advantages of the BCB system were demonstrated and discussed. A summary of the conclusions of this chapter is as follows:

i) Peak SDR demand in the BCBFs is significantly smaller than for conventional SCBFs and it can be as low as 1.5% in comparison to 4% for SCBFs.

ii) A soft-story occurs in SCBFs and lateral displacement of these frames accumulates in one story, while it is uniformly distributed along the height of the BCBFs.

iii) While seismic demand on the braced-intersected girders in BCBFs is substantially smaller than for conventional braced frames and yielding of the girders can be

avoided, in TSXBFs seismic demand on the non-intersected girders cannot be improved by utilizing BCBs.

iv) Substituting for conventional braces with BCBs does not improve the seismic demand of columns in ductile braced frames.

v) Brace ductility in BCBFs is considerably smaller than for SCBFs and brace fracture is likely to be avoided in BCBs.

vi) Bracing configuration and beam strength have no major impact on brace ductility demand, column demand, and braced-intersected girder demand in BCBFs, and seismic demand on the girders in even stories with chevron frames is smaller than TSXBFs.

CHAPTER 6. EFFECT OF LOADING PATTERN ON THE BEHAVIOR OF TSXBF

6.1. Frame Simulation

Even though, according to AISC 341-10, SCBFs should be designed for the first mode of deformation, results of the dynamic analyses have shown that higher-mode deformation might occur in taller buildings and might be more critical than the ones suggested by AISC. To assess the effects of the loading pattern on TSXBFs, the frame tested by Uriz and Mahin has been simulated in ABAQUS. Braces of the second story are inverted to create a TSXBF and because the square HSS used in the tested frame in UC Berkley does not satisfy the compactness criteria of the current code, the braces were replaced with a section with a slenderness ratio and a critical axial force close to the original section. Two different girders, a strong beam (W24x117) and a weak beam (W16x57), are also used in the frame to study the effect of beam strength. Figure 130 shows the details of the simulated TSXBF, and the properties of the new brace are presented in Table 19.

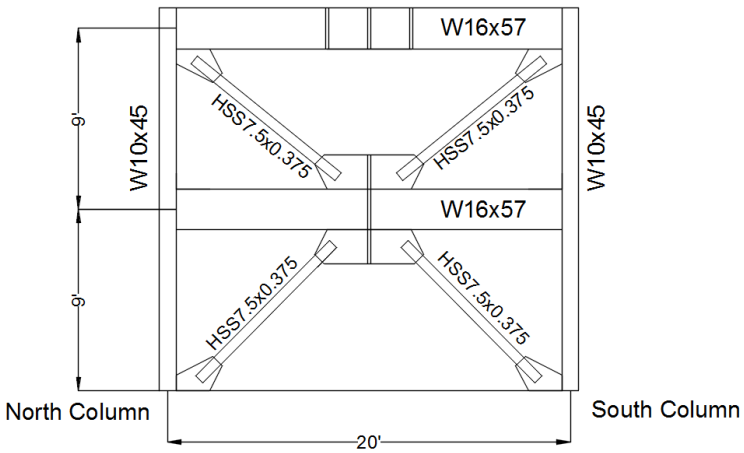

Figure 130: Simulated TSXBF in ABAQUS.

Table 19: Properties of the braces.

Member	Section	L_b (in)	KL/r	b/t or D/t	λ_{hd}
Brace	HSS7.5x0.375	113	50	18.4	26.2

The nominal strength provided in Table 20 was used to simulate the TSXBF. A static general analysis was conducted on each model using a full Newton method as the solution technique. Geometric nonlinearity was taken into account and a dissipated energy fraction of 0.0003 was used to avoid numerical problems. Moreover, a hard contact was used as the normal interaction between the elements, an essential step to prevent penetration, especially in the beam-column connections. Lateral supports were applied to the middle portion of the beams and beam-to-column connections in the first story. C3D8R elements were also used in all the members and a mesh size of 2 inches was used in the models (except for the braces). Because of the fact that capturing the accurate buckling of the braces was desired in this study, choice of a proper mesh size was absolutely necessary, so a mesh size about 0.6% times the length of the member is used in the braces, i.e., a mesh size equal to 0.5 inch was used in the braces to get the reliable deformation results. It should also be noted that two layers of elements were used in the braces to accurately capture local and global buckling. Figure 131 shows the mesh details of one of the braces. 8 nodes, each with 16 processors (a total of 128 processors), in an Iowa State University supercomputer, were used to analyze the two cases of this study.

Table 20: Material Properties.

Member	Specified Min. Stress	
	F_y (ksi)	F_u (ksi)
Beams and Columns	50	65
Round Braces	42	58
Square Outer Tube	46	58
Gusset Plates and Plate Stiffeners	36	58

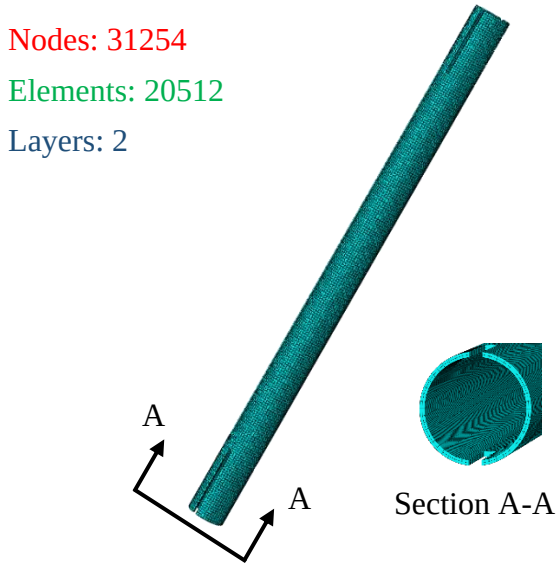

Figure 131: The mesh adopted for braces.

6.2. Loading Patterns and beam sizes

Four different loading patterns were used to assess the performance of the frame under different deformation shapes. Loading patterns were chosen based on the deformation of the frame under GM01 in dynamic time-history analyses results. Deformation of the frame and loading patterns are shown in Figure 132.

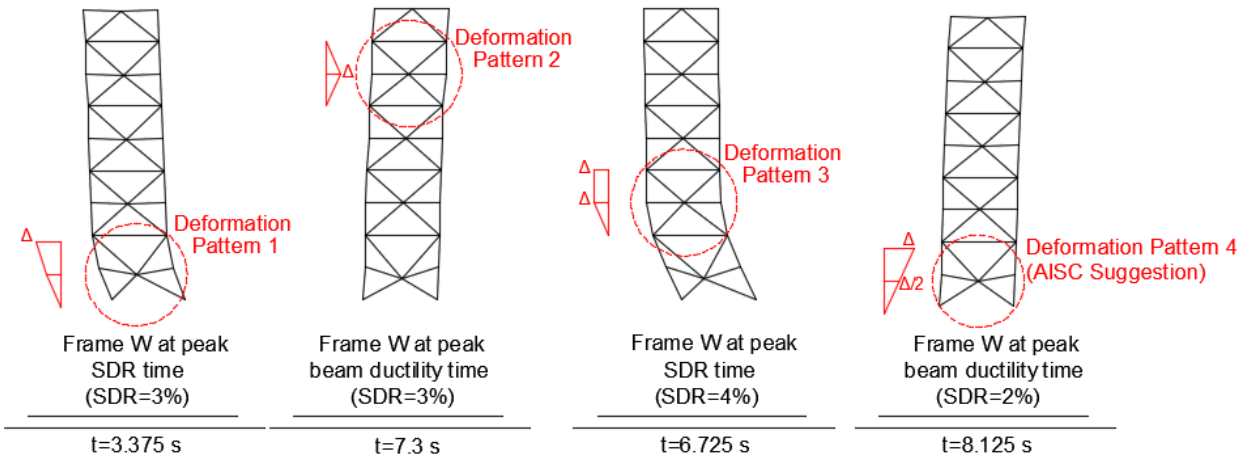

Figure 132: Loading patterns applied to TSXBF.

To create the first loading pattern, the cyclic loading shown in Figure 133 was applied to the roof and the frame was pushed until a 3% ODR was achieved.

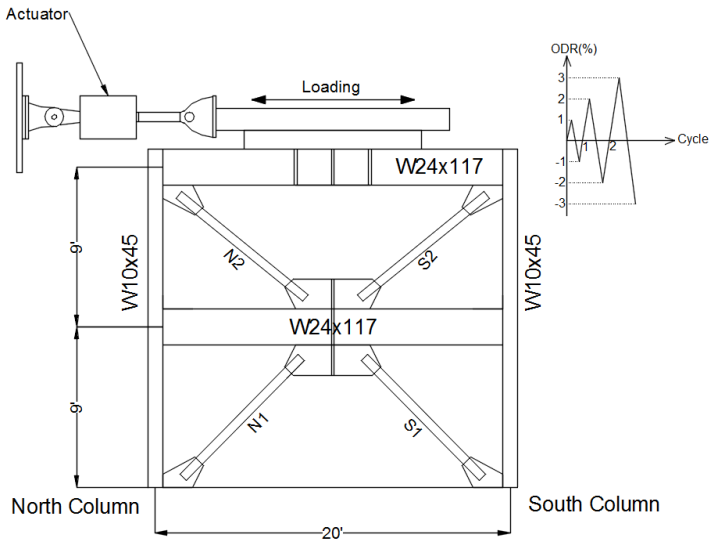

Figure 133: Loading pattern 1 (XSS case).

For the second case, to consider the effect of the higher modes of the deformation, cyclic loading was applied to the first story of the model and the frame was pushed until a 3% first SDR was achieved. Figure 134 shows this loading pattern.

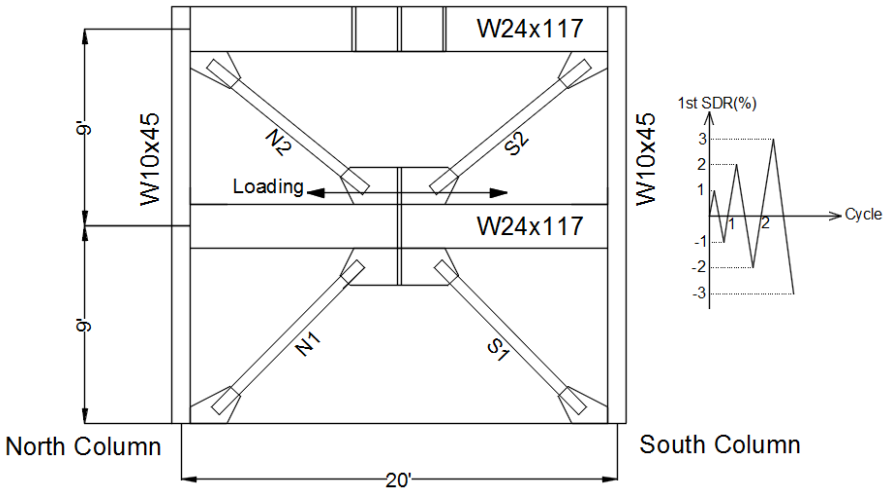

Figure 134: Loading pattern 2 (XFS case).

As shown in Figure 135, axial forces in the braces of two consecutive stories in the first mode of deformation are in opposite directions and the unbalanced force applied to the brace-intersected beam will be reduced. In an attempt to create the largest load in the beam, identical loading protocols were applied to the first and second levels to make the axial forces of the second story braces equal to zero; a maximum unbalanced force would be applied to the beam in this loading pattern. The third loading pattern is shown in Figure 136.

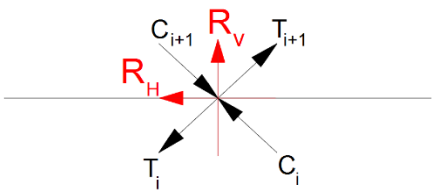

Figure 135: Free body diagram at brace intersected beam.

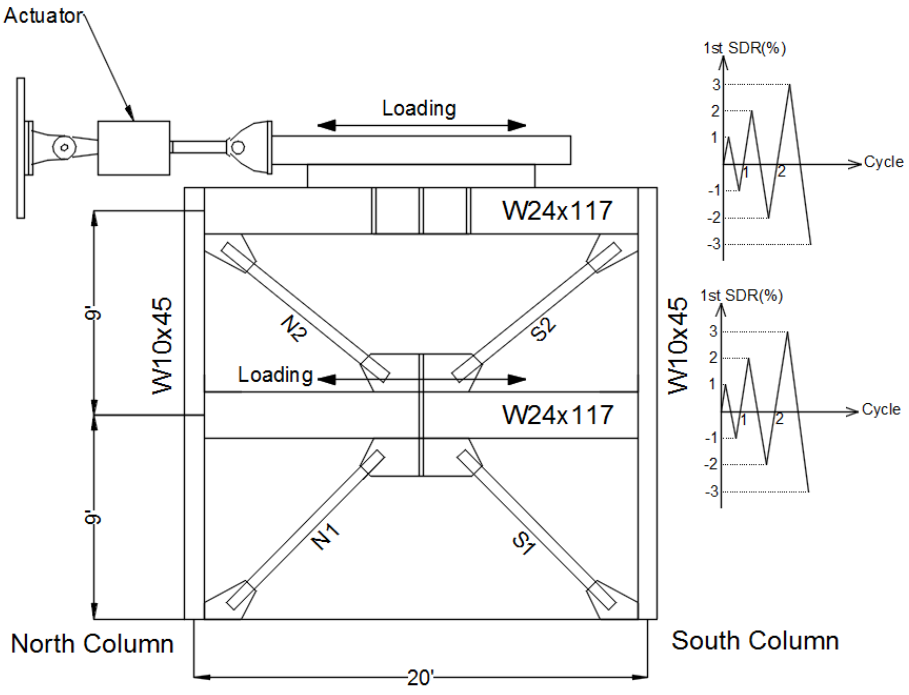

Figure 136: Loading pattern 3 (XBS case).

In the last case, the loading pattern suggested by the AISC 341-10 and shown in Figure 137 was applied to the frame to compare the results for the suggested loading pattern with the other cases.

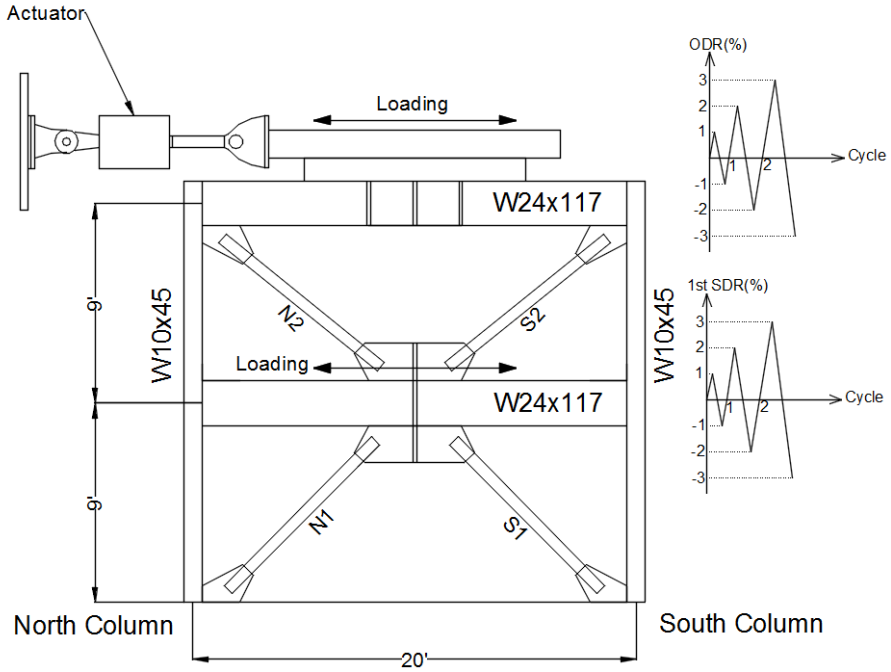

Figure 137: Loading pattern 4 (XLBS case).

Two different beam sizes are used in the simulation for each loading pattern to evaluate the influence of beam size on the behavior of the frame under different loading patterns. In the first case, the beam used in the tested frame by URIZ and Mahin (2008) was used in the simulation and considered to be a "strong" beam because it was designed based on the inverted V-type braced frames provisions that result in deep beams. In the second case, a "weak" beam as usually used in the TSXBFs was used. It should be mentioned that, because of the slight difference between beam depths in the two cases and the fact that length of the braces had to be identical, the difference was applied to the height of the columns so the story heights in the two cases were slightly different. Figure 138 shows the two simulated frames.

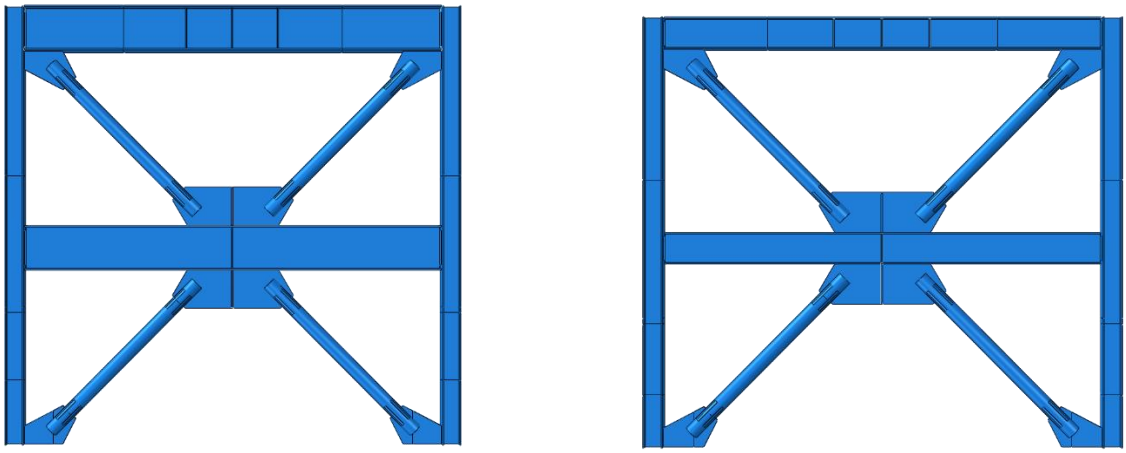

a) Strong beam (W24x117) b) Weak beam (W16x57)

Figure 138: Frames with different beam sizes.

6.3. Summary of the simulated cases

Eight different cases with different loading patterns and beam sizes were simulated in this study. Each model name was based on the frame type, loading pattern, and beam size, as shown on the next page:

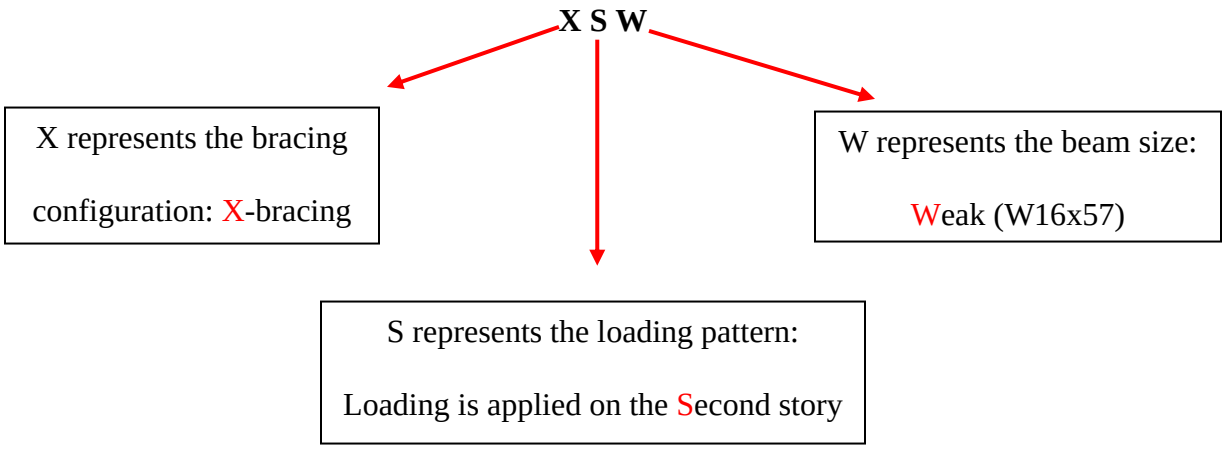

Table 21 represents all the simulated cases and their specifications.

Table 21: Simulation Cases.

#	Case Name	Frame type	Loading on	Beam size
1	XSS	X-Bracing	Second Story	Strong (W24x117)
2	XFS	X-Bracing	First Story	Strong (W24x117)
3	XBS	X-Bracing	Both Stories	Strong (W24x117)
4	XLBS	X-Bracing	Linear on Both Stories	Strong (W24x117)
5	XSW	X-Bracing	Second Story	Weak (W16x57)
6	XFW	X-Bracing	First Story	Weak (W16x57)
7	XBW	X-Bracing	Both Stories	Weak (W16x57)
8	XLBW	X-Bracing	Linear on Both Stories	Weak (W16x57)

6.4. Results

6.4.1. XSS and XSW

Stress distribution at 3% SDR is represented in Figure 139. It can be concluded that using a shallow beam results in higher stress in the gusset plates and in the middle portion of the beam, an expected result considering that the capacity of the beam in XSW is smaller than the one in the XSS case. Higher stress can also be seen in the 2nd story beam in the XSW case.

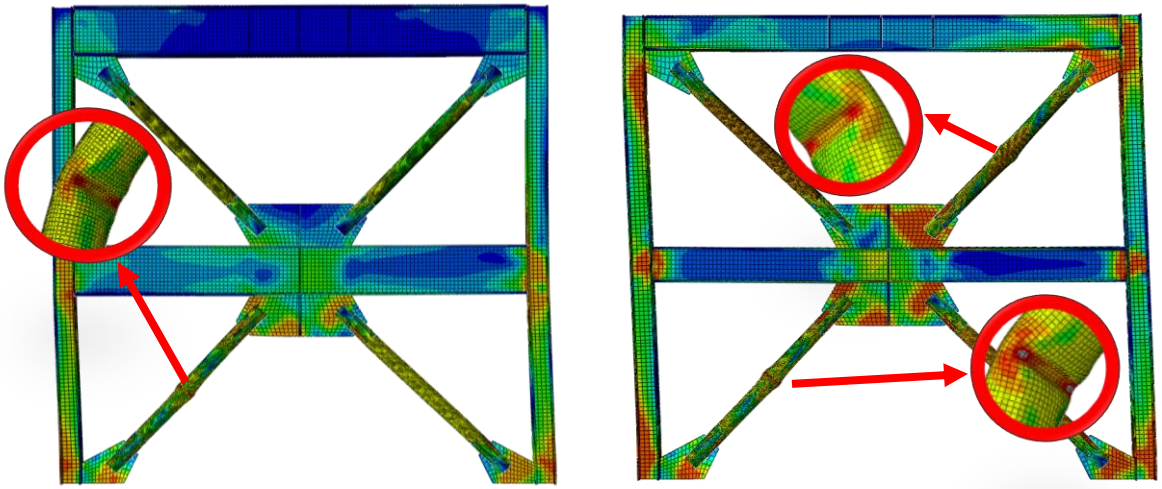

a) XSS at 3% 1st SDR

b) XSW at 3% ODR

Figure 139: Stress distribution in XSS and XSW models.

Force versus SDR for each story in the frames are shown in Figure 140. Although both cases have similar overall behavior, as shown in Figure 140c, a significant difference can be seen in each story response, mainly due to the large concentrated story drift in the first story of the XSS model, mainly due to the difference between the brace lengths in the 1st and 2nd story of the XSS frame. During the same analysis step, braces in the first story of the XSS case undergo larger axial displacement that resulted in earlier buckling. It will be shown that this conclusion is a function of loading pattern and not necessarily true for higher-mode deformations.

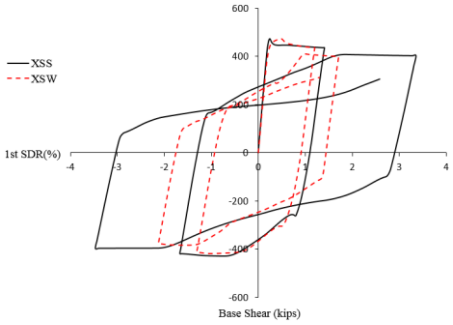

a) Base shear vs 1st SDR

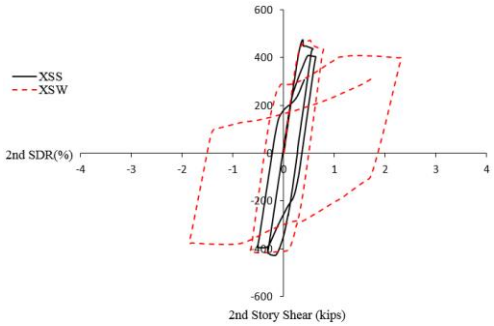

b) 2nd story shear vs 2nd SDR

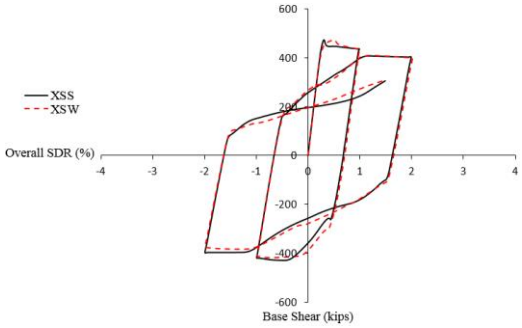

c) Base shear vs ODR

Figure 140: Forces vs. story drift ratios.

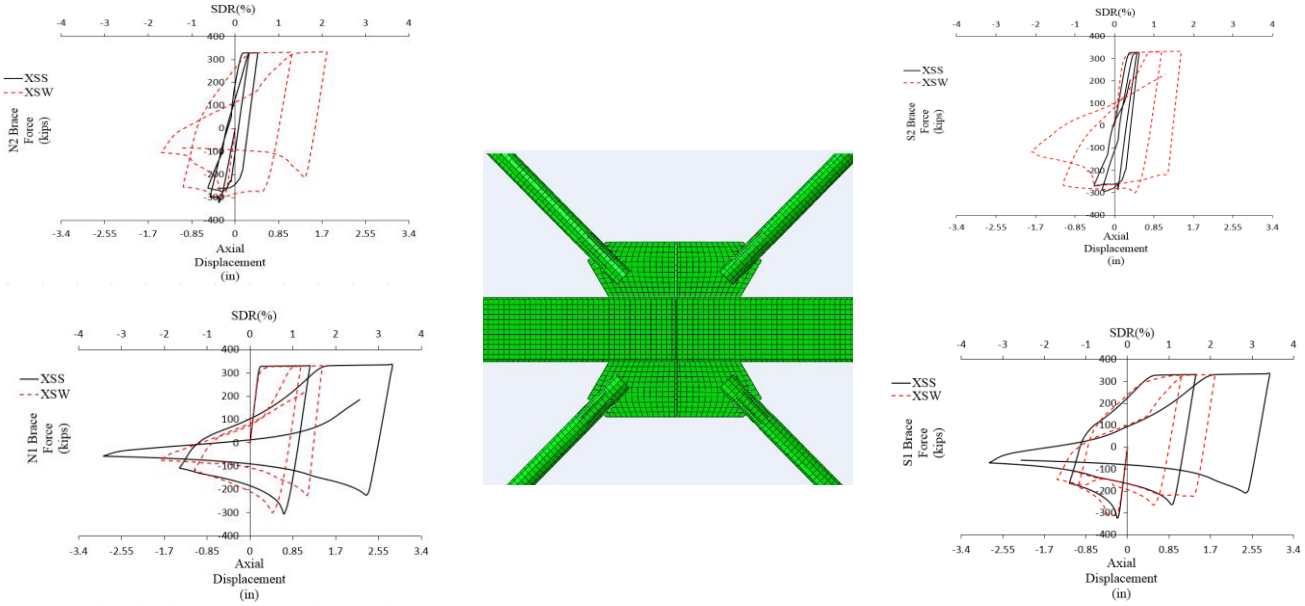

Figure 141: XSS and XSW braces' forces comparison.

The axial force and flexural demand/capacity of the beam in the first story is shown in Figure 142, with the internal forces extracted from the edge of the middle gusset plates. Because major deformation is concentrated in the first story of the XSS case, internal forces in the second story braces are relatively small, so it is to be expected that if the overall drift ratio increases from 1% to 2%, internal forces develop in the beam. To shed more light on this concept, it should be noted that, according to Figure 143 that shows the behavior of a brace tested by Fell, et al., (2009) under tension and compression, after reaching the buckling point, an increase in the story drift will result in a decrease in the compression axial force of the first story brace, while the tension force is constant. Therefore, based on Figure 143, the difference between the forces in the first story braces will grow and result in larger unbalanced forces on the beam. It should be mentioned that, in cycles with the same story drift, the ratio does not follow a general rule and might raise or drop.

In the XSW case, during the first two cycles of the loading (1% ODR), only first-story braces buckled and the maximum ratio was captured during the second cycle of 1% ODR. The high flexural demand/capacity ratio is the result of the significant difference between the compressive-brace forces in the two stories. After the second cycle, buckling was observed in the second story braces, so axial forces in the compressive braces get closer to one another and a decreasing ratio can be seen in the following cycles. It is important to note that, when loading is applied on the second story of TSXBFs, regardless of the beam size, the major portion of the ratio is derived from the bending moment and the axial force is negligible.

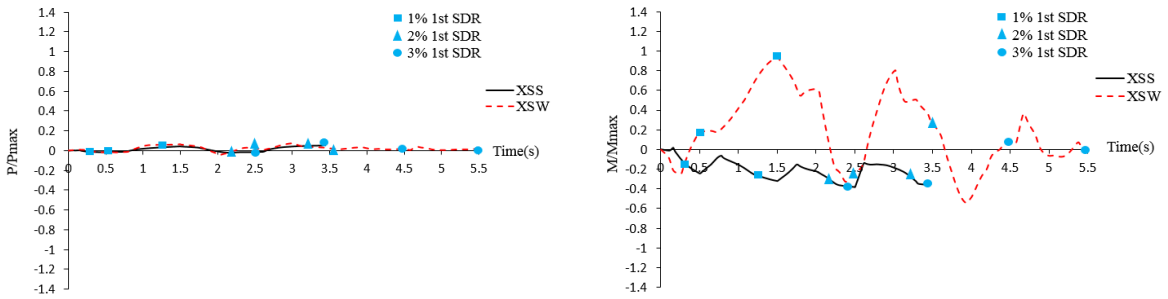

a) Axial force ratio. b) Bending moment ratio.

Figure 142: XSS and XSW beam internal forces ratios.

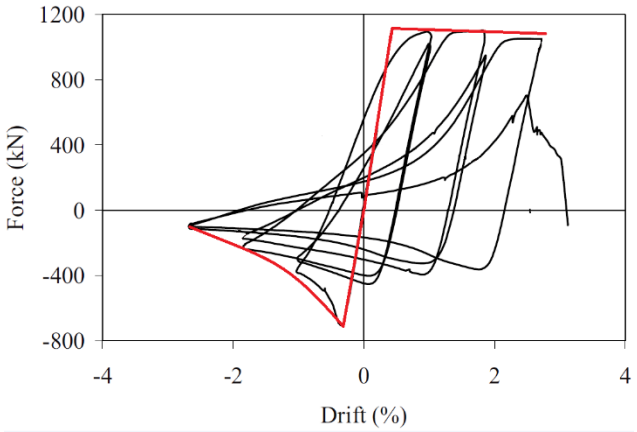

Figure 143: Cyclic behavior of a brace tested by Fell et al (2009).

In addition to the beams, axial force and flexural demand/capacity in the columns was also investigated, so internal forces in a section below the bottom flange of the beam was extracted to evaluate the demand/capacity ratio of the column at each step of the analysis. Based on Figure 144, in the XSS case the bending moment ratio is equal to one at the 3% first SDR, representing an unexpected early-stage demand in the column that is the most important member in a frame expected to remain elastic.

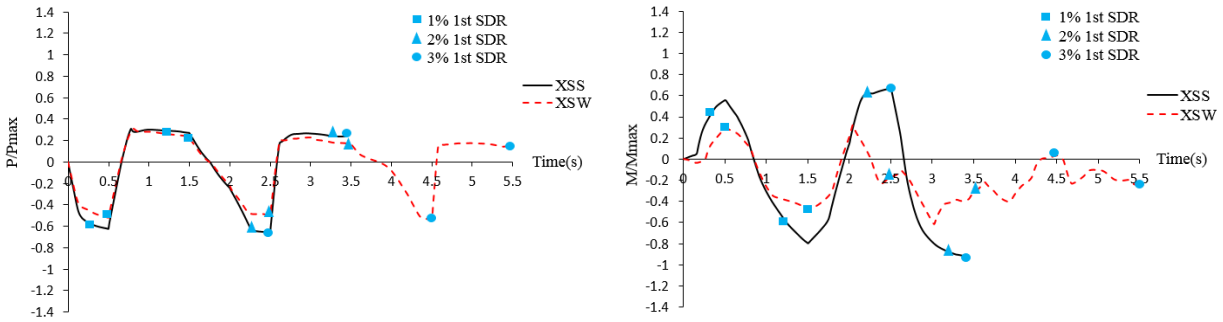

a) Axial force ratio

b) Bending moment ratio

Figure 144: XSS and XSW column internal forces ratios.

6.4.2. XFS and XFW

Stress distribution comparison between XFS and XFW cases is provided in Figure 145. Nearly identical stress distributions can be seen in the second story of the both frames, while a larger stress in the gusset plate of the first story of XFW case can be seen.

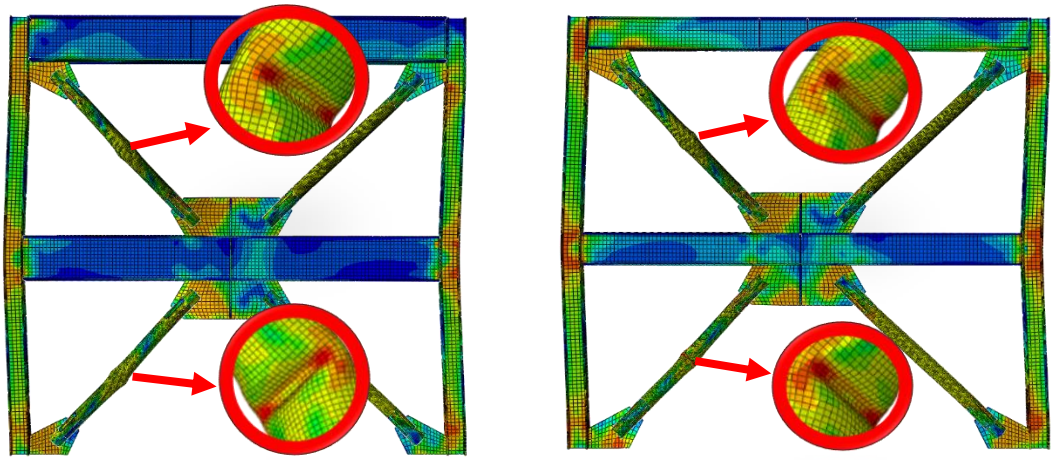

a) XFS

b) XFW

Figure 145: Stress distribution at 3% 1st SDR.

Similar hysteresis diagrams are achieved for XFS and XFW cases, as shown in Figure 146. Identical brace forces are also obtained for these models, as shown in Figure 147. From these results, it can be stated that local stress in the connections and middle portion of braced-intersected beam is affected by the size of the beam.

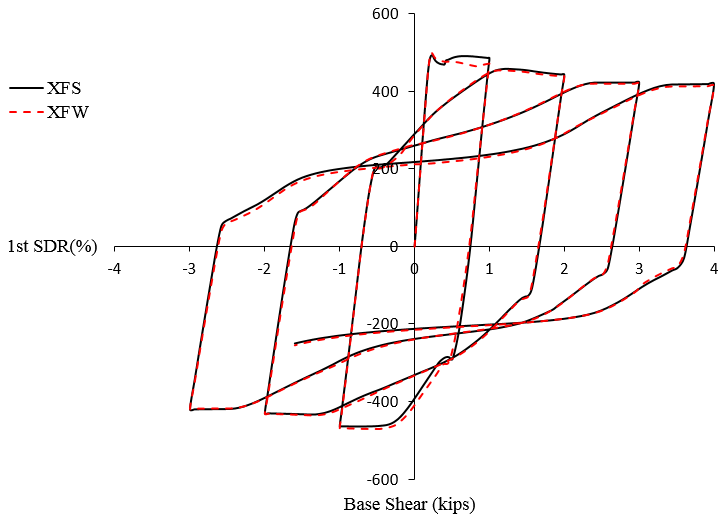

Figure 146: Base shear vs 1st SDR in XFS and XFW cases.

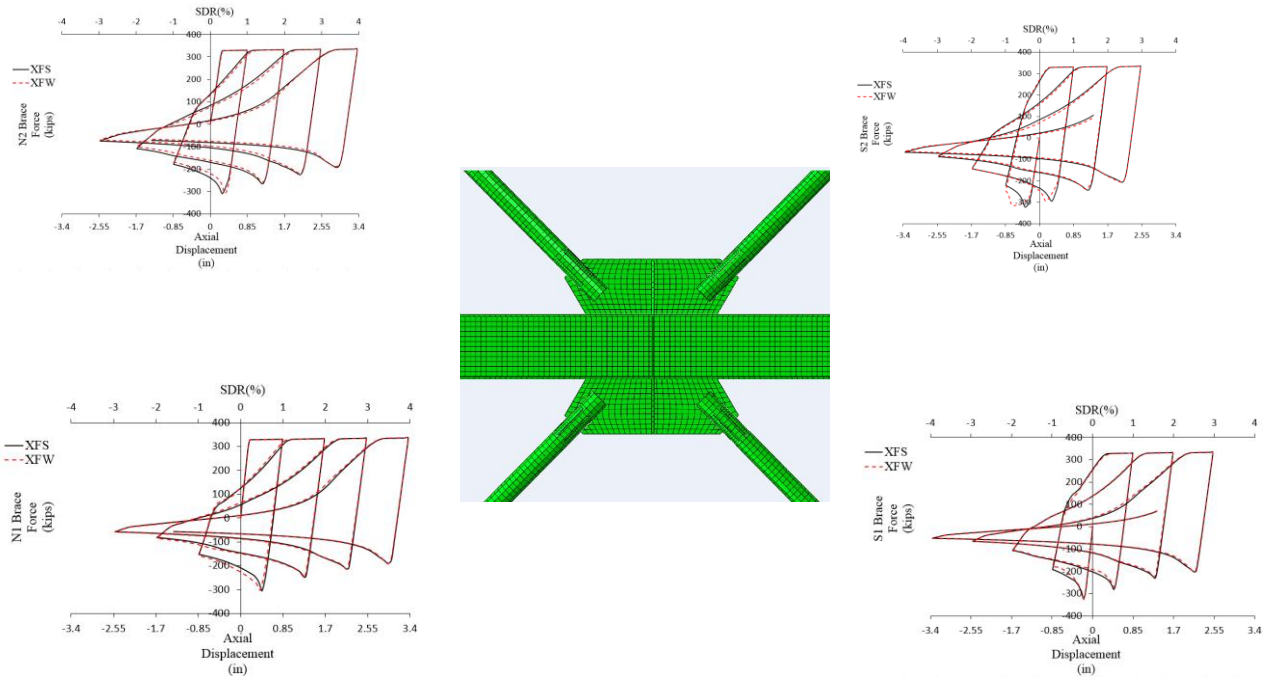

Figure 147: XFS and XFW braces' forces comparison.

Demand/capacity curves in the XFS and XFW cases are shown in Figure 148. Because a similar boundary condition is applied to the base and roof level of these cases, identical story drift is achieved in both stories, so an identical axial force that should result in zero vertical load and

moment in the beam is carried by the braces. However, due to in-plane buckling of the braces, an extra moment is applied to the beam, creating normal stresses in an opposite direction to the normal stress induced by axial force so, although the loading is applied to the first-story beam and a large axial force is therefore expected in that beam, a small axial-force demand/capacity ratio can be seen in the figure because of the in-plane buckling of the braces, a consequence of using a shallow beam, is sufficient to provide this type of loading. It should be noted that restraining the buckling of the braces might increase the ratio in the beam because the normal stress alleviation due to in-plane buckling of the braces will be eliminated.

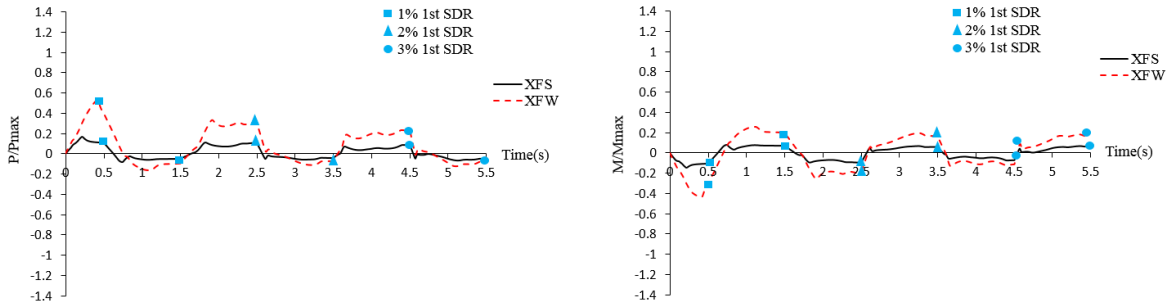

a) Axial force ratio. b) Bending moment ratio.

Figure 148: XFS and XFW beam internal forces ratios.

A comparison of the demand/capacity ratios in the columns used in these cases is presented in Figure 149. The bending-moment ratio is nearly one at the 1% first SDR value in both cases, representing a large demand on the column. This comparison proves that beam size has no significant effect on the column response and the column experiences yielding under this loading pattern.

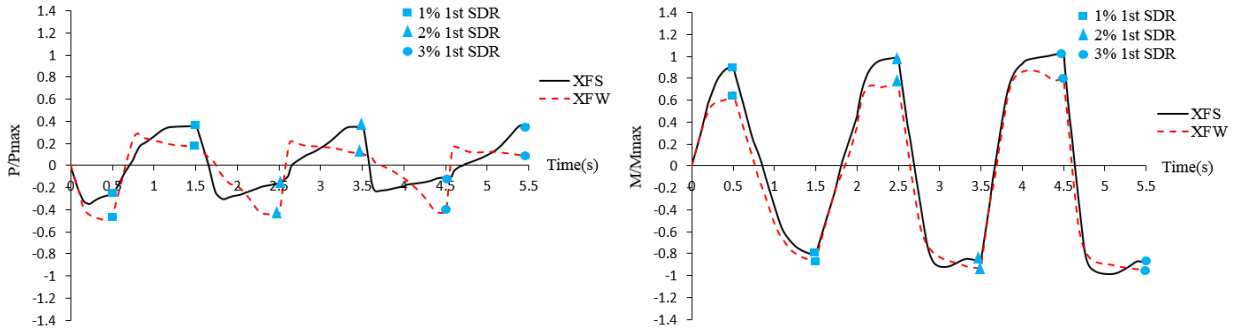

a) Axial force ratio b) Bending moment ratio

Figure 149: XFS and XFW column internal forces ratios.

6.4.3. XBS and XBW

Since identical loading protocols are applied to both stories of the frames, axial force in the second story braces of the frames remain at zero until buckling occurs in the braces in the first story. Beam vertical displacement, which was due to the brace buckling in the first story, induced an axial force in the second story braces. Stress distribution in the first story of the both of the cases are similar to one another as can be seen in Figure 150, and negligible stress is observed in the second story of the frame as expected.

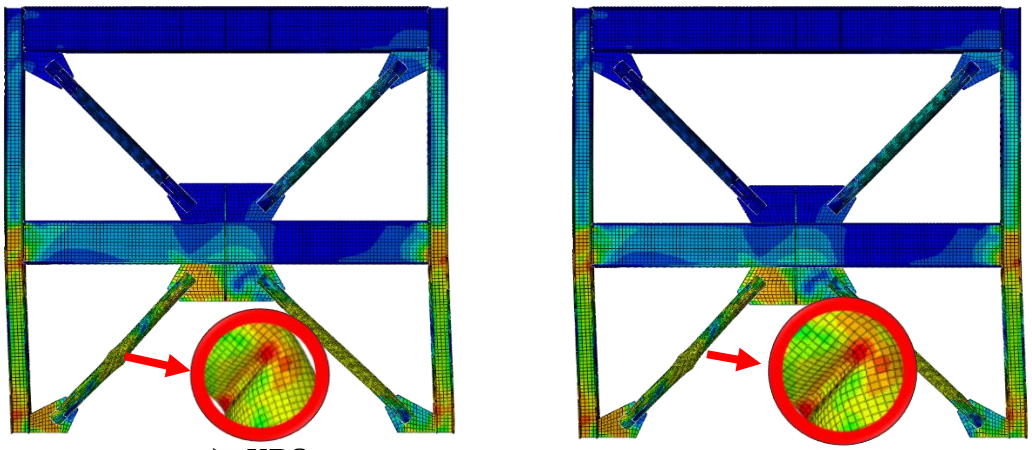

a) XBS b) XBW

Figure 150: Stress distribution at 3% 1st SDR.

Identical results for the two cases shown in Figure 151 and Figure 152 show that overall performance of the frame is not affected by changing the beam size under this type of the loading pattern, and that the axial force of the 2nd story braces are nearly zero in both frames as expected.

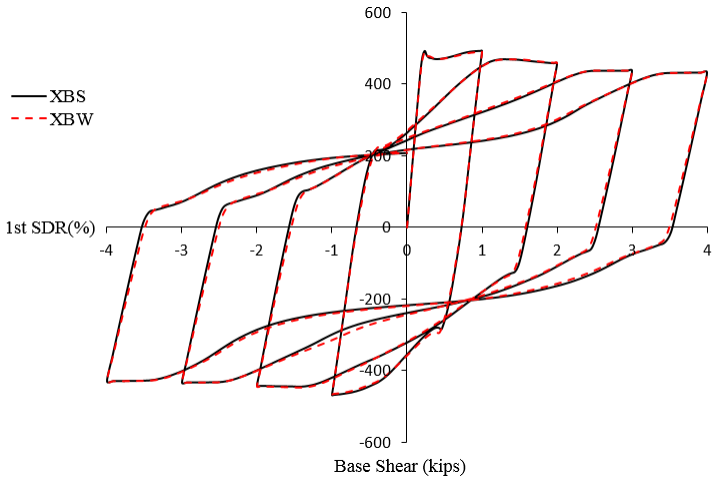

Figure 151: Base shear vs 1st SDR in XBS and XBW cases.

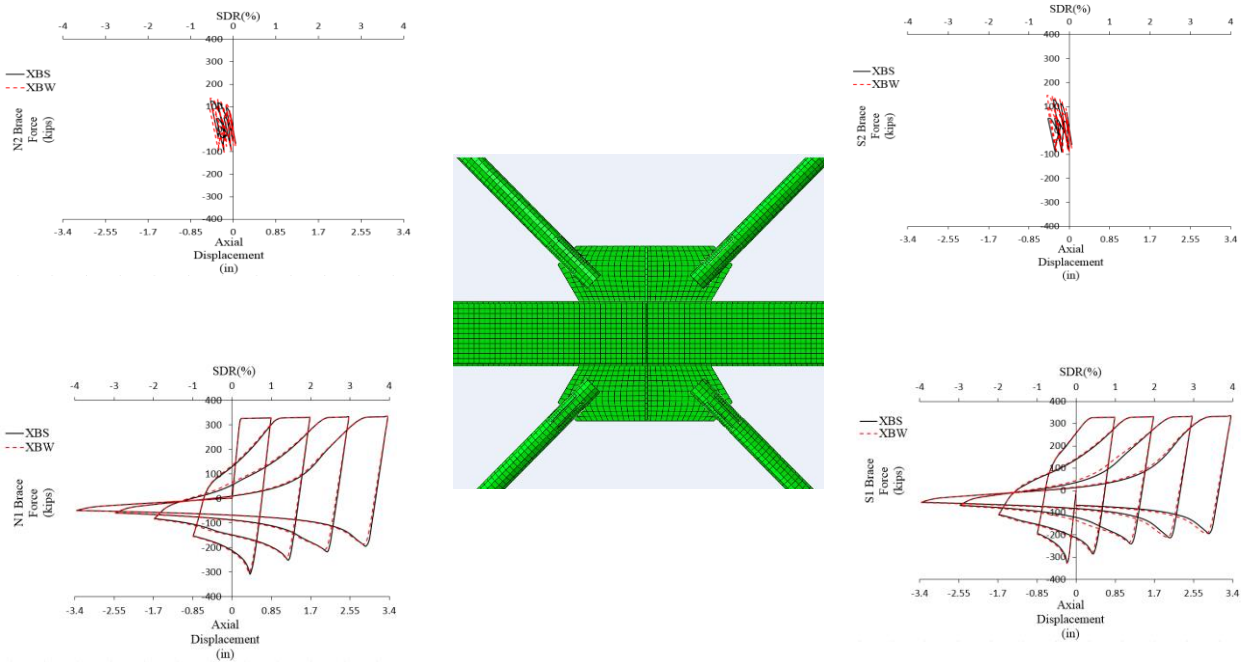

Figure 152: XBS and XBW braces' forces comparison.

Axial force and flexural demand/capacity of the beams presented in Figure 153 shows that the demand in the girder is relatively small and the beams remain elastic under this loading pattern.

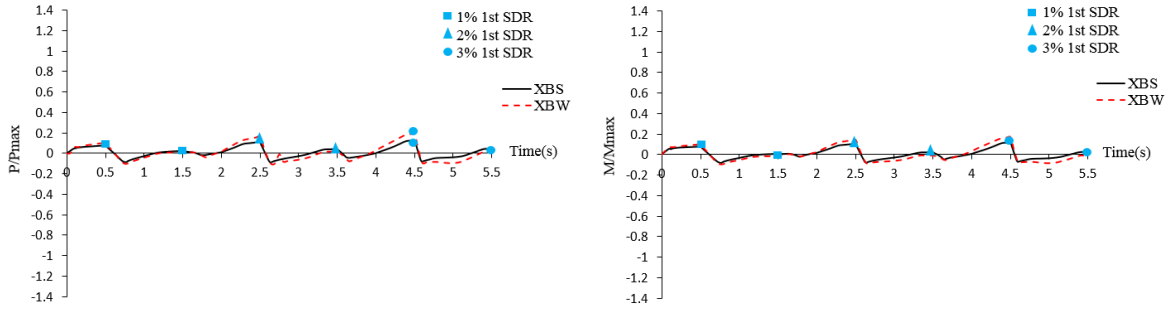

a) Axial force ratio. b) Bending moment ratio.

Figure 153: XBS and XBW beam internal forces ratios.

Unlike for beams, demand/capacity ratios in the columns of both of these cases, presented in Figure 154, are quite large. Similar to previous cases, the bending moment demand/capacity ratio in the column is close to one at 2% first SDR. The difference between the ratios in the strong and weak beam cases is negligible under this loading pattern and nearly identical results are achieved.

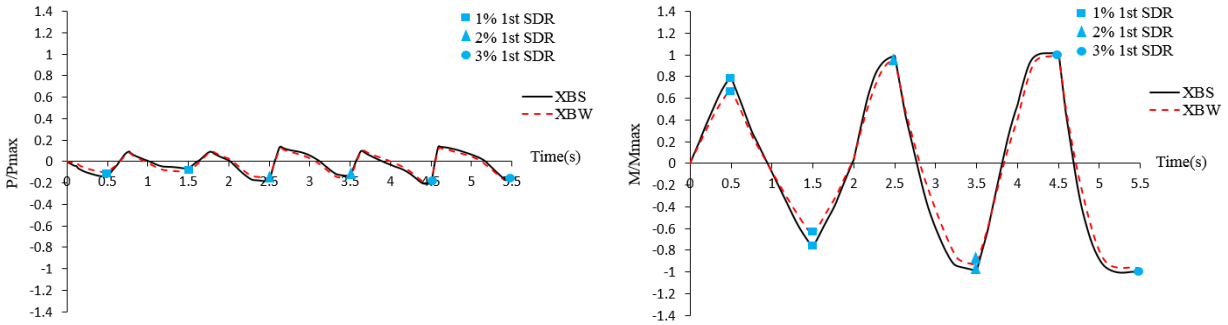

a) Axial force ratio b) Bending moment ratio

Figure 154: XBS and XBW column internal forces ratios.

6.4.4. XLBS and XLBW

In this section, a linear loading pattern, as suggested by AISC 341-10, was applied to the frames with different beam sizes, and the resulting stress distribution in the frames is shown in Figure 155. The frame with shallower beam has higher stress in the middle portion of the brace-intersected beam as expected, and higher stress in the gusset plates of the XLBW can be seen in comparison to the XLBS case.

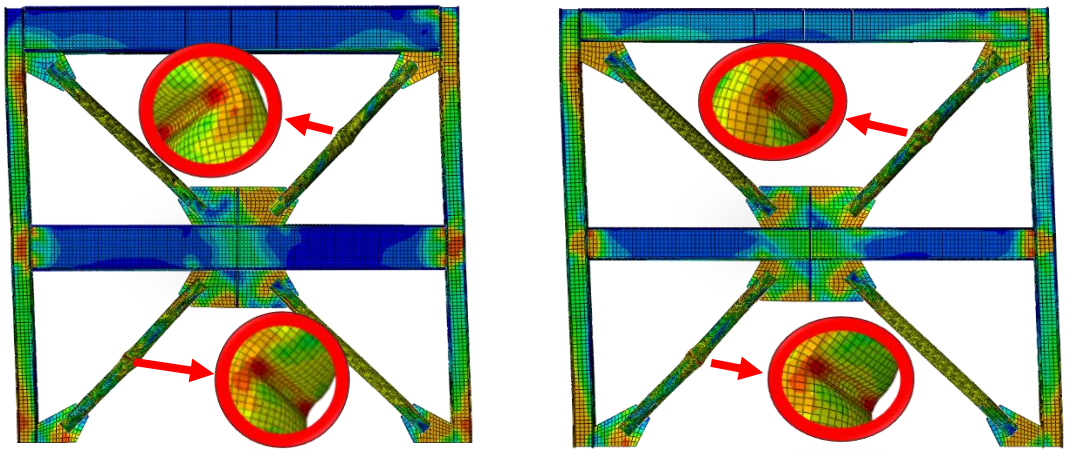

a) XLBS b) XLBW

Figure 155: Stress distribution at 3% 1st SDR.

Identical responses are achieved from both frames, either in terms of story drifts or in terms of overall drift, as shown in Figure 156. Comparison of the axial forces on the braces is shown in Figure 157.

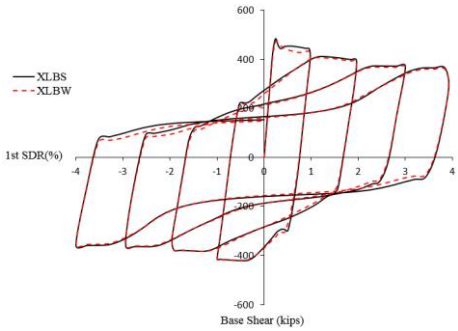

a) Base shear vs 1st SDR

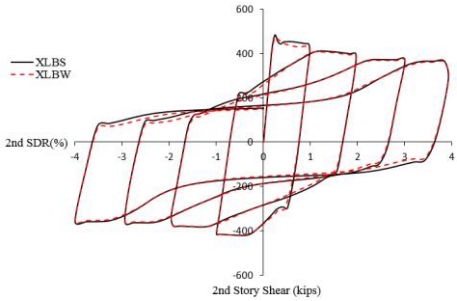

b) 2nd story shear vs 2nd SDR

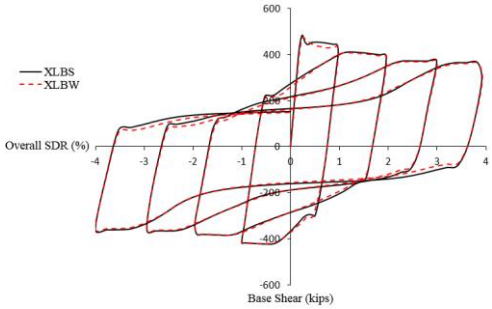

c) Base shear vs ODR

Figure 156: Forces vs. story drift ratios.

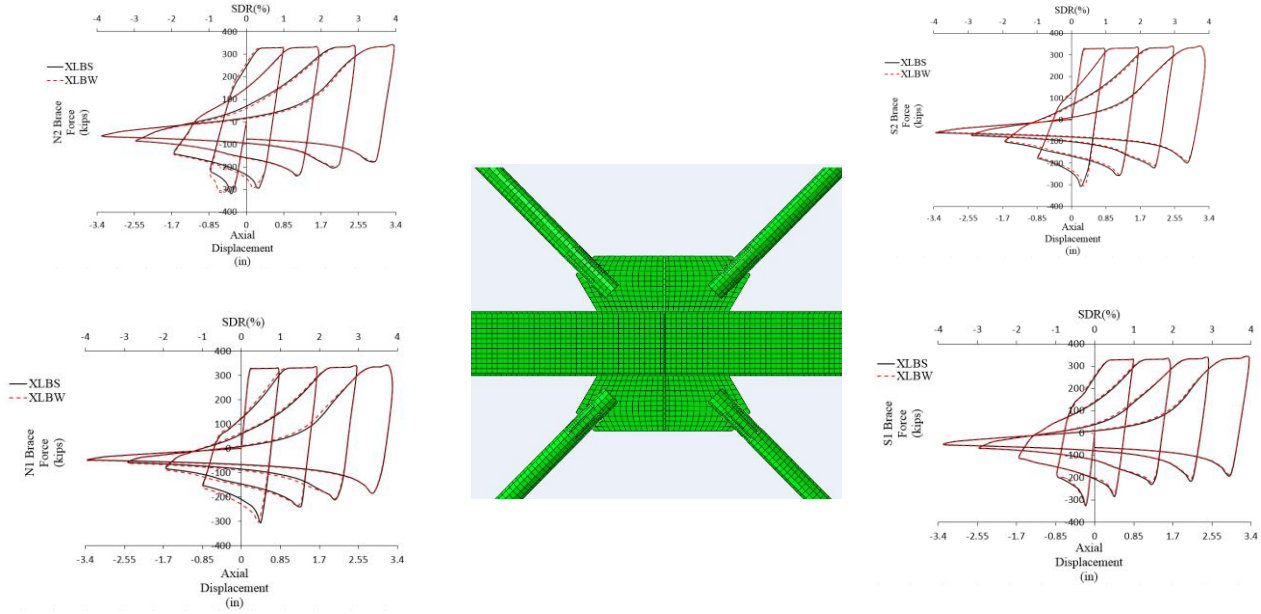

Figure 157: XLBS and XLBW braces' forces comparison.

Small demand/capacity ratios in the first story beams were observed in both cases during the analysis, as shown in Figure 158.

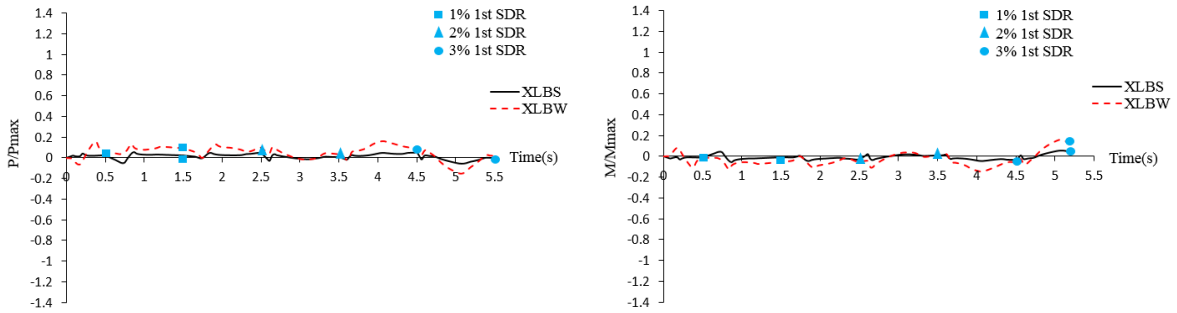

a) Axial force ratio. b) Bending moment ratio.

Figure 158: XLBS and XLBW beam internal forces ratios.

Similar to the demand/capacity ratio in the beam, the ratio for the columns of both cases are much smaller than for the other cases, as can be seen in Figure 159. Peak axial force demand/capacity in the column is about 0.5, and the maximum flexural demand/capacity is about 0.25 in the XLBS frame.

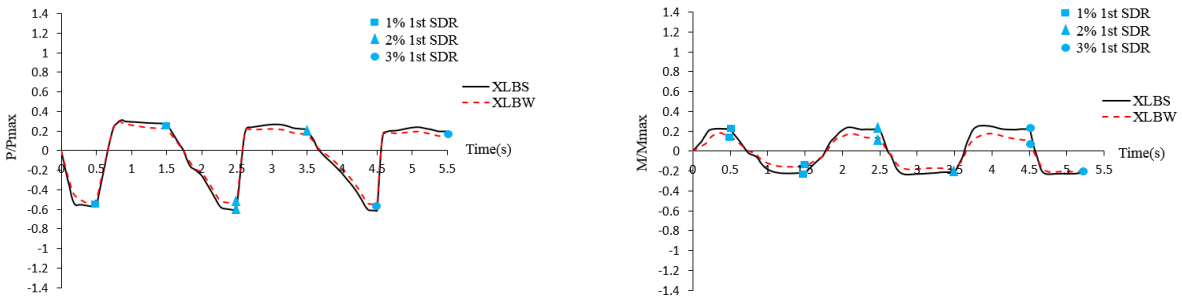

a) Axial force ratio. b) Bending moment ratio.

Figure 159: XLBS and XLBW column internal forces ratios.

6.4.5. Comparison of Frame Responses

In this section, response of the TSXBF under four different loading patterns are compared, and axial force and flexural demand/capacity of both beams and columns of the eight frames are presented. Response of the 1st story girder of the frame with strong beams is presented in Figure 160, where it can be seen that demand/capacity in the beam is smaller than 0.4 and the beam experiences no yielding. Similar results were achieved in the previous chapters, and the beam in frame S remains elastic.

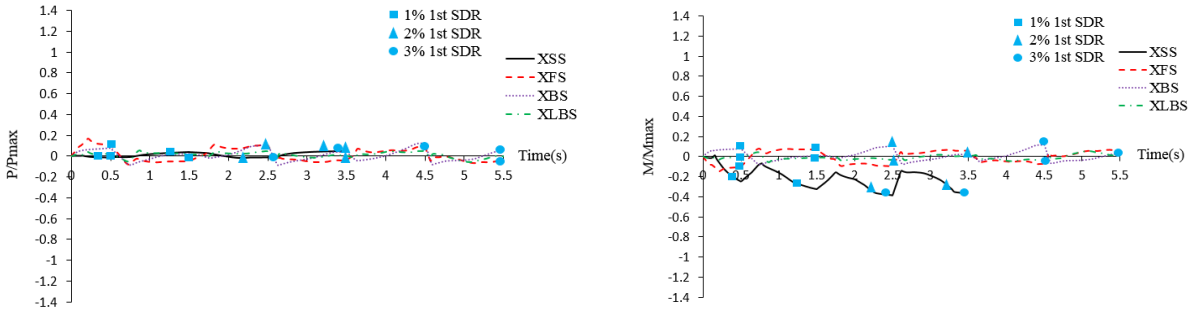

a) Axial force demand/capacity

b) Bending moment demand/capacity

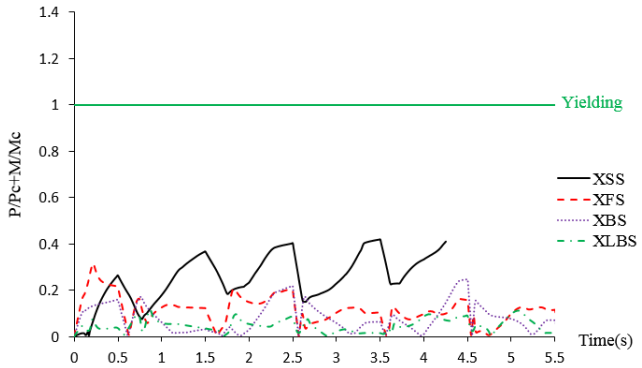

c) Total demand/capacity

Figure 160: Demand/capacity in the 1st story girder in frame S.

Axial force and flexural demand/capacity in the 1st story column of the frame S is shown in Figure 162. It can be observed that columns experience yielding due to large flexural demand.

It should be noted that demand/capacity of the members can be as large as 1.3 due to strain hardening.

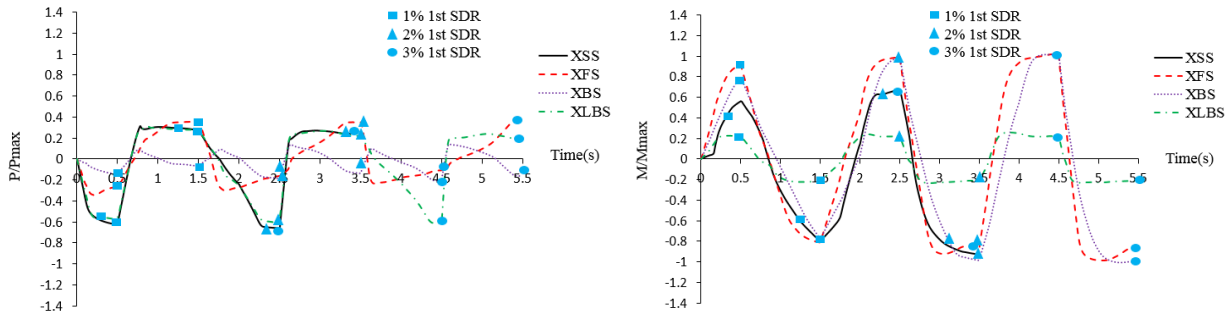

a) Axial force demand/capacity

b) Bending moment demand/capacity

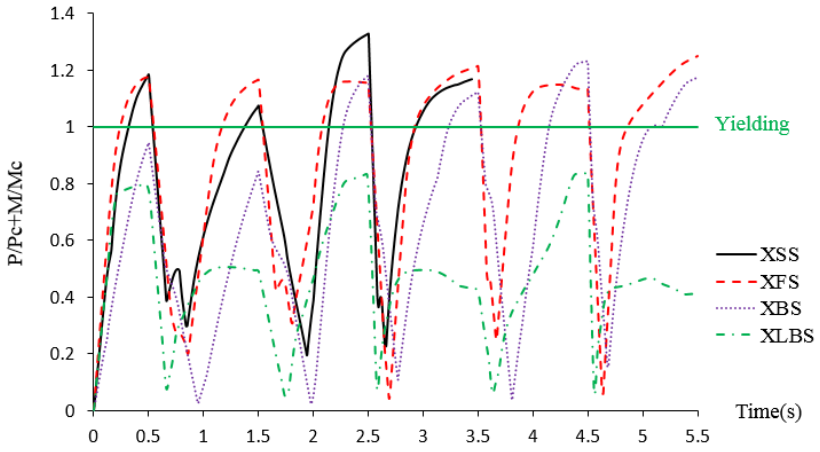

c) Total demand/capacity

Figure 161: Demand/capacity in the 1st story column in frame S.

Response of the 1st story girder in frame W under four loading patterns are compared in Figure 162. It can be observed that, unlike strong beams, weak girders experience yielding and the demand/capacity in both XFW and XSW cases are equal to one, while peak demand/capacity under the loading pattern suggested by AISC341 is about 0.3, the smallest response among the four loading patterns.

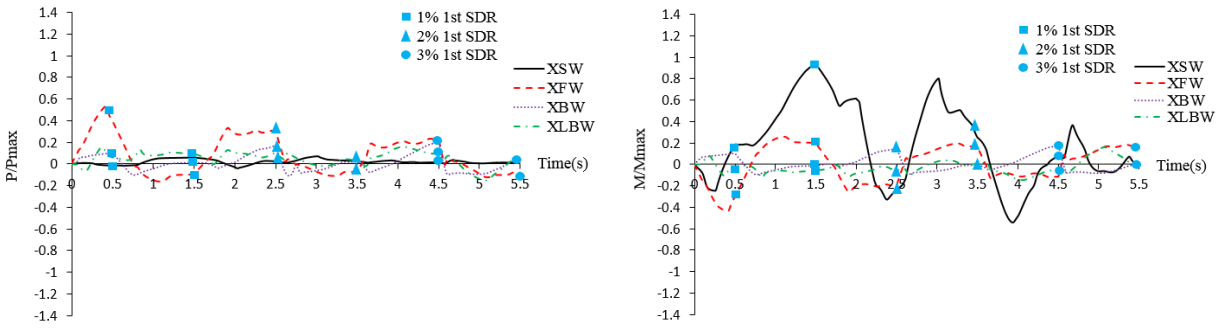

a) Axial force demand/capacity

b) Bending moment demand/capacity

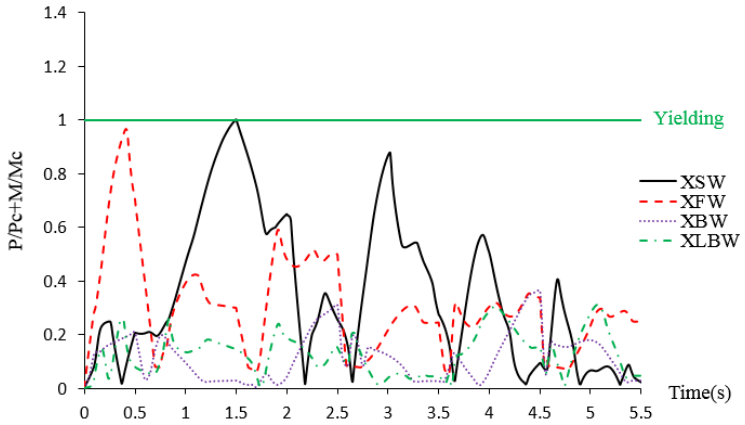

c) Total demand/capacity

Figure 162: Demand/capacity in the 1st story girder in frame W.

Axial force and flexural demand/capacity of the 1st story column of frame W are shown in Figure 163. As for the dynamic response of the frames, it can be observed that column responses in frames S and W are similar to one another and beam strength has no significant effect on the column response. Columns also experience yielding in both XFW and XBW cases, even though XLBW remains elastic as suggested by AISC341. It seems that higher mode deformation results in more critical responses in the frames and should be considered in the design procedure.

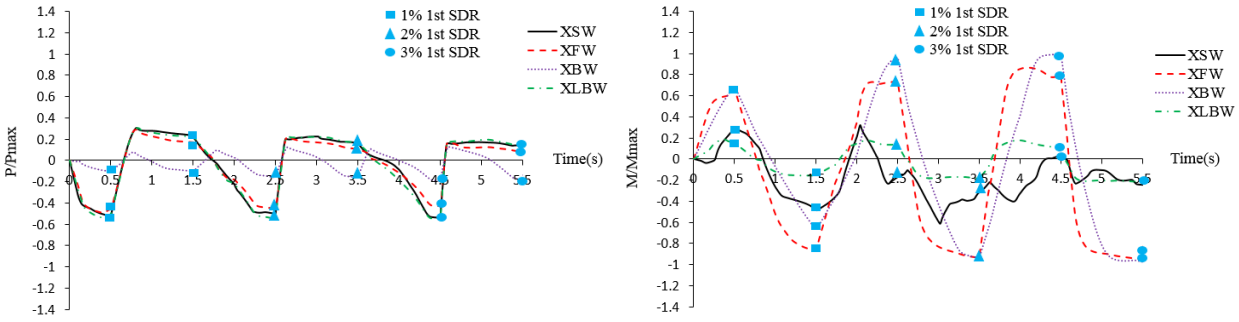

a) Axial force demand/capacity

b) Bending moment demand/capacity

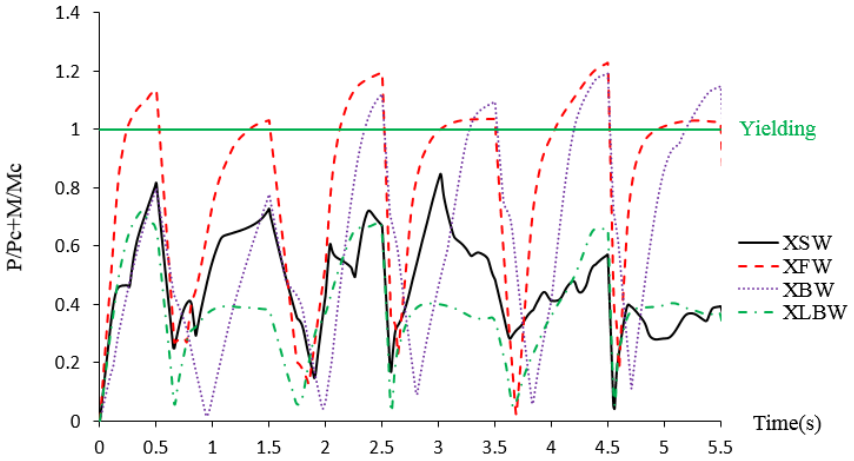

c) Total demand/capacity

Figure 163: Demand/capacity in the 1st story column in frame W.

6.5. Conclusions

Eight TSXBFs were simulated using general-purpose finite-element software to evaluate their behavior under various type of loading patterns and to assess their performance with different beam strengths. The impact of loading pattern and beam size on the stress distribution, frame deformation, demand in the beams and columns have been discussed and, based on the results presented, the following conclusions can be drawn:

i) Stress in the gusset plate of the frames with weak beams is larger than in frames with strong beams, so a thicker gusset plate might be necessary for the frames with light beams.

ii) Based on the results provided, it can be implied that loading patterns suggested by the current design code do not result in the highest possible demand in the beams, and frames must sustain larger demand under the higher-mode loading patterns.

iii) Results of the analyses prove that, regardless of beam strength, a column may experience yielding under different loading patterns. It should be noted that the demand on columns under the loading pattern suggested by AISC 341 is smaller than that for the other loading patterns.

CHAPTER 7. CONCLUSIONS AND RECOMMENDATIONS

7.1. General Remarks

SCBF is one of the most common lateral load resisting systems used in steel structures. In the present study, seismic performance of ductile CBFs was investigated through extensive non-linear dynamic analyses using two-dimensional dynamic analysis software, RUAUMOKO-2D. Behavior of steel braces and braced frames were evaluated under cyclic and seismic loading in Chapters 3 through 6 of this study that may be summarized as follows:

In Chapter 3, newly developed buckling-controlled braces were presented and cyclic behavior of the conventional braces was compared with BCB performance. Effects of various cross sections on the behavior of the BCBs were also assessed using non-linear finite element analyses. At the chapter conclusion, impact of BCBs on the cyclic behavior of ductile CBFs was examined.

In Chapter 4, seismic performance of conventional ductile CBFs under twenty ground motions was studied. Two different beam sections were used to evaluate the influence of beam strength on the behavior of two-story X-braced frames. Two different bracing configurations were also modeled to assess the effect of bracing type on frame response.

In Chapter 5, conventional HSS braces were replaced with buckling-controlled braces in the modeled braced frames, and response of the BCBFs under twenty ground motions were compared with the conventional ductile CBFs in terms of brace ductility, beam and column response, and frame deformation.

Finally, in Chapter 6, four different loading patterns achieved from SCBF response were applied to a two-story X-braced frame using finite-element software. Responses of the frames

under different loading patterns were compared with one another and critical deformation patterns were identified.

7.2. Conclusions

Based on the results presented in this investigation, the following conclusions can be drawn:

i) Round-in-square BCBs provide desirable performance either when the thickness ratio of the outer tube to inner tube is greater than one or when an enhanced gusset plate is employed. However, regardless of the thickness ratio in square-in-round BCBs, it was found necessary to utilize an enhanced gusset plate to achieve promising results.

ii) Experimental and numerical results demonstrate stable and symmetrical hysteretic behavior of BCBs until 3% SDR. It is observed that BCBs are significantly more ductile than conventional braces and the larger enclosed area of the cyclic loops in BCBs results in greater energy dissipation compared with conventional braces.

iii) The symmetrical cyclic behavior of BCBs results in substantial reduction in unbalanced forces applied to brace-intersected girders, with this reduction being as large as 80% at 3% story drift ratio.

iv) Unexpected yielding of the shallow beam in TSXBF initiates at about a 2% SDR value, the design level. It should be remembered that, according to AISC 341-10, beams should not experience yielding during an earthquake, and the results of this analysis demonstrates that this provision cannot be guaranteed in TSXBFs designed under current design codes.

v) Regardless of the bracing configuration and beam strength, axial force demand/capacity in the columns of special concentrically braced frames is always close to 0.5. It should be emphasized that increasing the SDR has an inconsiderable effect on the axial force demand on the columns.

vi) Peak story drift ratio and peak brace ductility demand in the BCBFs are significantly smaller than those in conventional SCBFs and can be as low as 1.5% and 15, respectively, compared to 4% and 30 in SCBFs.

vii) A soft story occurs in SCBFs and lateral displacement of these frames uniformly distributed along the height of BCBFs accumulates in one story.

viii) Seismic demand on the braced-intersected girders in BCBFs is substantially smaller than that in conventional braced frames, and yielding of girders can be avoided. However, in TSXBFs, seismic demand on non-intersected girders cannot be improved by utilizing BCBs. Similarly, substituting the conventional braces with BCBs does not improve the seismic demand of columns in ductile braced frames.

ix) The analysis implies that loading pattern suggested by the current design code does not reflect the highest possible demand in the beams, and they are likely to sustain larger demand under the higher-mode loading patterns.

x) Results of the analyses prove that, regardless of the beam strength, a column may experience yielding under different loading patterns. It should be noted that the demand on the columns under the loading pattern suggested by AISC 341 is smaller than the one in the other loading patterns.

7.3. Future Study

The major conclusions from the numerical and experimental studies are presented in the previous section. Although this investigation has elaborated on issues related to the current design procedure, and proposes a solution to overcome the problem, there is a remaining need to perform studies in this field seeking a comprehensive and well-established design procedure for ductile CBFs w/ and w/o brace controllers. Recommendations for potential future studies are as follows:

i) While all the simulations performed in the present study have been based on the conventional cyclic behavior of steel braces, based on the experimental tests on HSS sections, braces are likely to experience fracture during early cycles, so it would be helpful to simulate the fracture of the braces in to achieve a better understanding of the real-life performance of SCBFs.

ii) The analyses results in Chapter 6 show that higher mode deformation patterns might result in more critical response in two-story X-braced frames, so there is a need to propose a new design approach for current braced frames that not only takes into account the effect of the deformation in higher modes, but also includes brace ductility in the design approach rather than the story drift ratio.

iii) Although experimental studies on the isolated buckling-controlled braces have been carried out in this investigation, an experimental test on the ductile CBFs incorporating BCBs should be performed to verify the simulation results provided in this dissertation.

iv) Connections that connect the girders to the columns with a shear tab and two gusset plates were simulated in this study as rigid connections. Although the simulated

connections probably perform similarly to rigid connections, actual rigidity of these connections could be investigated, perhaps by simulating them as springs.

v) While seismic performance of several mid-rise SCBFs and BCBFs were investigated in the present research, applicability of the current findings to both low-rise and high-rise buildings should be examined in future studies to produce more thorough conclusions.

References

AISC (1997), Seismic Provisions for Structural Steel Buildings, American Institute of Steel Construction, IL 60601.

AISC (2005), Seismic Provisions for Structural Steel Buildings, ANSI/AISC 341-05, American Institute of Steel Construction, IL.

AISC (2010b), Seismic Provisions for Structural Steel Buildings, ANSI/AISC 341-10, American Institute of Steel Construction, IL.

AISC (2016), Seismic Provisions for Structural Steel Buildings, ANSI/AISC 341-16, American Institute of Steel Construction, IL.

ASCE 7 (2010), Minimum design loads for buildings and other structures, ASCE7-10. American Society of Civil Engineers, Virginia.

Astaneh-Asl, A., Goel, S.C., and Hanson, R.D. (1985), Cyclic out-of-plane buckling of double-angle bracing, *Journal of structural Engineering*, vol. 111, no. 5, pp. 1135-1153.

Architectural Institute of Japan, Steel committee of Kinki Branch (1995), Reconnaissance report on damage to steel building structures observed from the 1995 Hyogoken-Nanbu (Han-shin/Awaji) earthquake, AIJ, Tokyo, May, P. 167.

Black, R.G., and Wenger, W. (1980), Inelastic buckling of steel struts under cyclic load reversals, UCB/EERC-80/40, Earthquake Engineering Research Center, University of California, Berekeley.

Bosco, M., Ghersi, A., Marino, E., and Rossi, P. (2014), A Capacity Design Procedure for Columns of Steel Structures with Diagonals Braces, Open Construction and Building Technology Journal, vol. 8, no. 1, pp. 196-207.

Brandonisio, G., Toreno, M., Grande, E., Mele, E., and De Luca, A. (2012), Seismic design of concentric braced frames, Journal of Constructional Steel Research, vol. 78, pp. 22-37.

Carr, AJ, RUAUMOKO manual, vols. 1 and 2. Christchurch, New Zealand: University of Canterbury; 2004.

Chambers, J.J. and Ernst, C.J. (2005), Brace frame gusset plate research – phase 1 literature review, volumes 1 and 2, Department of Civil Engineering, University of Utah, Salt Lake City, UT.

Chen, C. (2010), Performance-based Seismic Demand Assessment of Concentrically Braced Steel Frame Buildings, Ph.D. dissertation, University of California, Berkeley, CA.

Clark, P., Aiken, I., Kasai, K., Ko, E., Kimura, I. (1999). Design Procedures for Buildings Incorporating Hysteretic Damping Devices, Proceedings, 68th Annual Convention, Santa Barbara, California Structural Engineers Association of California.

Eurocode 8 (EC8), 2005, Eurocode 8: Design of structures for earthquake resistance-part 1: general rules, seismic actions and rules for buildings.

Fell, B.V., Kanvinde, A.M., Deierlein, G.G., Myers, A.T., (2009), Experimental investigation of inelastic cyclic buckling and fracture of steel braces, Journal of Structural Engineering, 135, PP. 19-32.

Goggins, J., Broderick, B.M., Elghazouli, A., and Lucas, A. (2006), Behaviour of tubular steel members under cyclic axial loading, *Journal of Constructional Steel Research*, vol. 62, no. 1, pp. 121-131.

Han, S., Kim, W.T., Foutch, D.A. (2007), Tensile strength equation for HSS bracing members having slotted end connections, Earthquake Engineering and Structural Dynamics, 36, PP. 995-1008.

Hibbitt, Karlsson, and Sorensen (2001), ABAQUS/Standard user's manual: Hibbitt, Karlsson & Sorensen.

Hisatoku, T. (1995), "Reanalysis and repair of a high-rise steel building damaged by the 1995 Hyogoken-Nanbu earthquake, Proceedings, 64th Annual convention, Structural Engineers Association of California, Structural Engineers Assn. of California, Sacramento, CA, PP 21-40.

Jain, A.K., Goel, S.C., and Hanson, R.D. (1987), Inelastic response of restrained steel tubes, *Journal of the Structural Division*, vol. 104, no. ASCE 13832 Proc Paper.

Khatib, F., Mahin, S.A., and Pister, K.S. (1987), Seismic behavior of concentrically braced steel frames, UCB/EERC-88/01, Earthquake Engineering Research Center, University of California, Berkeley, CA.

Kim, H., and Goel, S. (1992), Seismic evaluation and upgrading of braced frame structures for potential local failures, UMCEE92-24, Dept. of Civil Engineering and Environmental Engineering, University of Michigan, Ann Arbor, Oct., P.290.

Koboevic, S., and Redwood, R. (1997), Design and seismic response of shear critical eccentrically braced frames, Canadian Journal of Civil Engineering, 24, PP.761-77.

Krawinkler, H, et al. (1996), Northridge earthquake of January 17, 1994: reconnaissance report, Vol. 2-steel buildings, Earthquake Spectra, 11, Suppl. C, Jan., pp.25-47.

Kumar, A., Anandm A., and Sahoo, D.R. (2017), Modified seismic design of concentrically braced frames considering flexural demand on columns, Earthquake Engineering & Structural Dynamics.

Lai, J., and Mahin, S. (2013), Experimental and analytical studies on the seismic behavior of conventional and hybrid braced frames, PEER-2013/20, Pacific Earthquake Engineering Research Center, University of California, Berkeley, CA.

Lee, K., and Bruneau, M. (2005), Energy Dissipation of compression members in concentrically braced frames: Review of experimental data, Journal of Structural Engineering, 131(4), PP. 552-9.

Leowardi, L.S., and Walpole, W.R. (1996), Performance of steel brace members: Department of Civil Engineering, University of Canterbury.

Lin, P.C., Tsai, K.C., Wang, K.J., Yu, Y.J., Wei, C.Y., Wu, A.C., Tsai, C.Y., Lin, C.H., Chen, J.C., and Schellenberg, A.H. (2012), Seismic design and hybrid tests of a full-scale three-story buckling-restrained braced frame using welded end connections and thin profile, Earthquake Engineering & Structural Dynamics, vol. 41, no. 5, pp. 1001-1020.

Ma, N., Wu, B., and Ou, J.P. (2011), Finite Element Analysis on Critical Constraint Ratio of All-Steel Buckling Restrained Brace. Advance Material Research, pp. 2126-2129.

MacRae, G. (1989), The seismic response of steel frames, Ph.D. dissertation, University of Canterburry, Christchurch, New Zealand.

MacRae, G., Kimura, Y., Roeder, C., (2004), Effect of column stiffness on braced frame seismic behavior, Journal of structural engineering, 130(3), PP. 381-91.

Marino, E.M., (2014), A unified approach for the design of high ductility steel frames with concentric braces in the framework of Eurocode 8, Earthquake Engineering & Structural Dynamics, vol. 43, no. 1, pp. 97-118.

McCormick, J., DesRoches, R., Fugazza, D., and Auricchio, F. (2007), Seismic assessment of concentrically braced steel frames with shape memory alloy braces, Journal of Structural Engineering, 133(6), PP. 862-70.

Momenzadeh, S., Seker, O., Shen, J., (2017), Observed seismic demand on columns in SCBFs, Architectural Engineering Institute, PP. 647-658, Oklahoma City.

Newell, J. and Uang, C.M. (2006), Cyclic behavior of steel columns with combined high axial load and drift demand, SSRP-06/22, University of California, San Diego.

Nip, K.H., Gardner, L., Elghazouli, A.Y. (2010), Cyclic testing and numerical modeling of carbon steel and stainless steel tubular bracing members, Engineering structures, 32, PP. 424-41.

Osteraas J. and Krawinkler, H. (1989), The Mexico Earthquake of September 19, 1985-behvaior of steel buildings, Earthquake Spectra, 5(1), pp. 51-88.

Palmer, K.D., Christopulos, A.S., Lehman, D.E., and Roeder, C.W. (2014), Experimental evaluation of cyclically loaded, large-scale, planar and 3-d buckling-restrained braced frames, Journal of Constructional Steel Research, vol. 101, pp. 415-425.

Park, Y.S., Park, S.J., Iwai, S., and Kang, S.H. (2004), Failure and damage of steel thin-plate elements and angle members due to very-low-cycle loading, *Engineering structures*, vol. 26, no. 11, pp. 1623-1632.

PEER, Peer.berekeley.edu/peer_ground_motion_database. Pacific Earthquake Engineering Research Center, 325 Davis Hall, University of California, Berkeley, CA 94720.

Popov, E., Bertero, V.V. and Chandramoulli, S. (1975), Hysteretic behavior of steel columns, UCB/EERC 75-11.

Richards, P. (2009), Seismic Column Demands in Ductile Braced Frames, Journal of Structural Engineering, 135(10, PP. 33-41.

Roeder, C., et al. (2010), Influence of gusset plate connections and braces on the seismic performance of X-braced frames, Earthquake Engineering & Structural Dynamics, 40(4), PP. 355-74.

Roeder, C., Lehman, D., Johnson, S., Herman, D., Yoo, J. (2006), Seismic Performance of SCBF Braced Frame Gusset Plate Connections, 4th International Conference on Earthquake Engineering, Taipei, Taiwan.

Sabelli, R. (2000), Research on improving the design and analysis of earthquake resistant steel braced frames, FEMA/EERI.

Sabelli, R., and Chunho, C. (2001), Investigation of the nonlinear seismic response of special concentric and buckling restrained braced frames and implications for design, FEMA/EERI Professional Fellowship Report.

Sabelli, R., Mahin, S., Chang, C. (2003), Seismic Demands on Steel Braced Frame Buildings with Buckling-Restrained Braces, Engineering Structures, 2, PP. 655-66.

Seker, O. (2016), Development of buckling-ontrolled braced frames for seismic design of steel buildings, Ph.D. Dissertation, Iowa State University.

Shaback, B., Brown, T. (2003), Behavior of square hollow structural steel braces with end connections under reversed cyclic axial loading, Canadian journal of civil engineering, 30, PP.745-53.

Shaw, S.M., Kanvinde, A.M. (2014), Seismic performance of partial joint penetration welds in column splices, Tenth U.S. National Conference on Earthquake Engineering, Anchorage, Alaska.

Shen, J., Seker, O., Akbas, B., Toru Seker, P., Momenzadeh, S., Faytarouni, M. (2017), Seismic Performance of Concentrically Braced Frames with and without Brace Buckling, Engineering Structures, 141, PP. 461-481.

Shen, J., Wen, R., Akbas, B., Doran, B., Uckan, E. (2014), Seismic Demand on brace-intersected beams in two-story X-braced frames, Engineering Structures, 76, PP. 295-312.

Shen, J., Wen, R., Akbas, B. (2015), Mechanisms in two-story X-braced frames, Journal of Constructional Steel Research, 106, 258-77.

Tremblay R. (2002), Inelastic Seismic Response of Bracing Members, Journal of constructional Steel Research, 58, PP. 665-701.

Tremblay, R., Archambault, M.H., and Filiatrault, A. (2003), Seismic Response of Concentrically Braced Steel Frames Mde with Rectangular Hollow Bracing Members, ASCE Journal of Structural Engineering, 129(12), PP. 1626-36.

Tremblay, R., et al. (1995), Performance of steel structures during the 1994 Northridge earthquake, Canadian Journal of Civil Engineering, 22(2), pp. 338-360.

Tremblay, R., et al. (1996), Seismic design of steel buildings: lessons from the 1995 Hyogo-ken Nanbu earthquake, Canadian Journal of Civil Engineering, 23(3), pp. 727-756.

Tremblay, R., Haddad, M., Martinez, G., Richard, J., Moffatt, K. (2008), Inelastic cyclic testing of large size steel bracing members, The 14th World Conference on Earthquake Engineering, Beijing, China.

Uriz, P. (2005), Towards Earthquake Resistant Design of Concentrically Braced Steel Structures, Ph.D. Dissertation, University of California, Berkeley, CA.

Uriz, P., and Mahin, S. (2008), Towards Earthquake Resistant Design of Concentrically Braced Steel Structures, PEER-2008/08, Pacific Earthquake Engineering Research Center, University of California, Berkeley, CA.

Usami, T., Wang, C., and Funayama, J. (2011), Low-cycle fatigue tests of a type of buckling restrained braces, Procedia Engineering, vol. 14, pp. 956-964.

Yang F., and Mahin, S.A. (2005), Limiting net section fracture in slotted tube braces, Steel Tips Series, Structural Steel Education Council, Moraga, CA.

Zhao, J., Wu, B., and Ou, J. (2011), A novel type of angle steel buckling-restrained brace: Cyclic behavior and failure mechanism, Earthquake Engineering & Structural Dynamics, vol. 40, no. 10, pp. 1083-1102.

APPENDIX A.
TIME HISTORIES OF GROUND MOTIONS

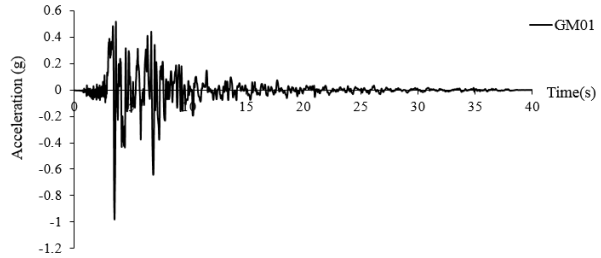

Figure A1. GM01

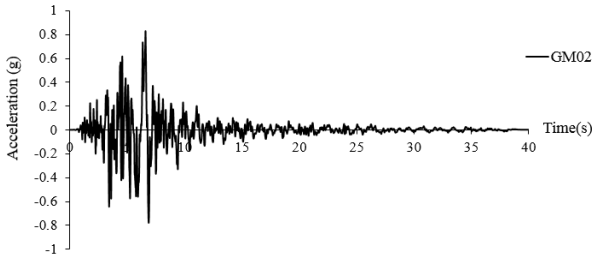

Figure A2. GM02

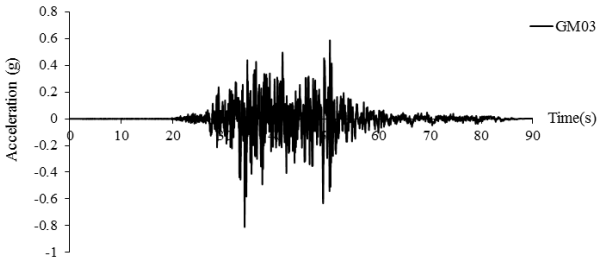

Figure A3. GM03

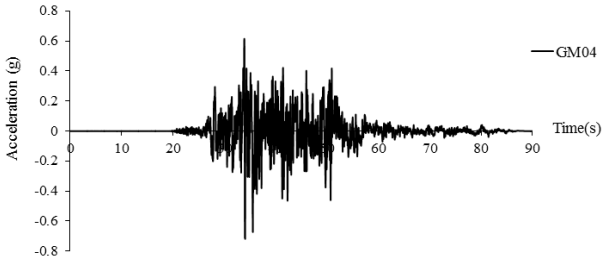

Figure A4. GM04

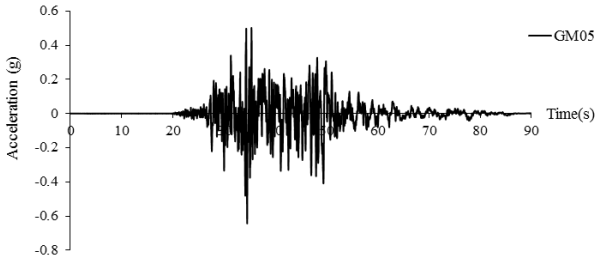

Figure A5. GM05

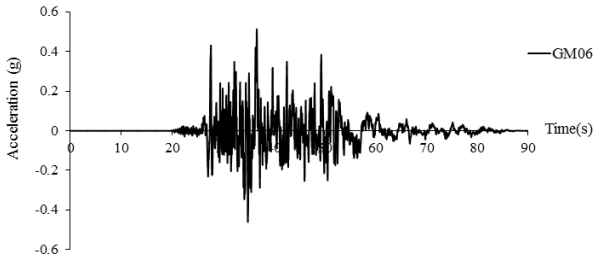

Figure A6. GM06

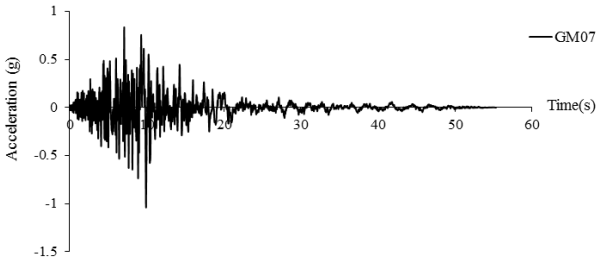

Figure A7. GM07

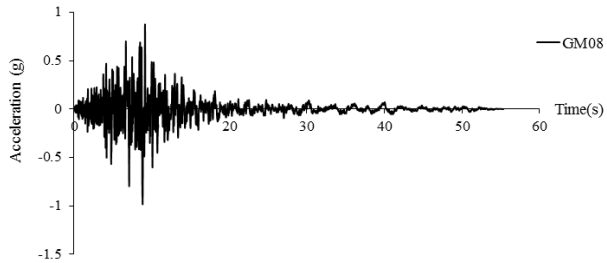

Figure A8. GM08

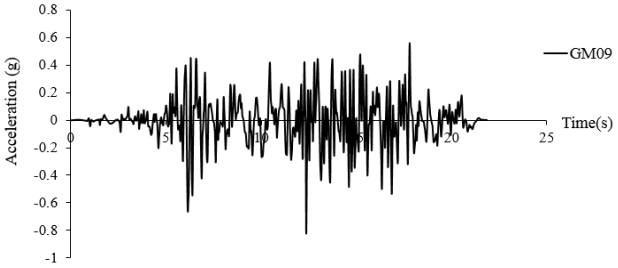

Figure A9. GM09

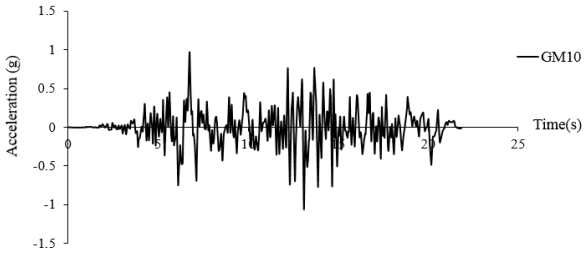

Figure A10. GM10

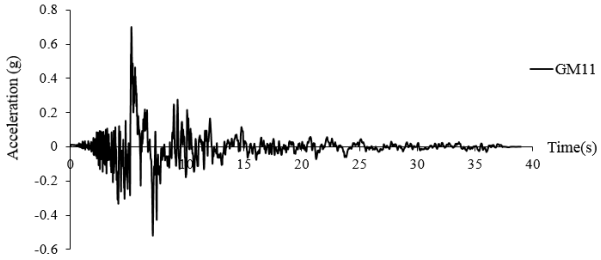

Figure A11. GM11

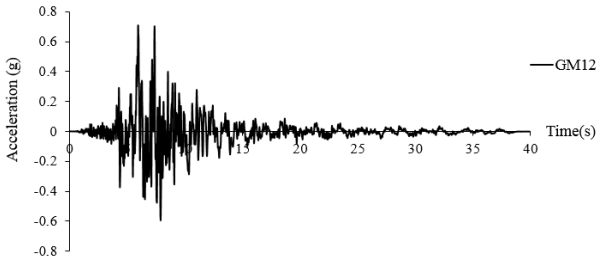

Figure A12. GM12

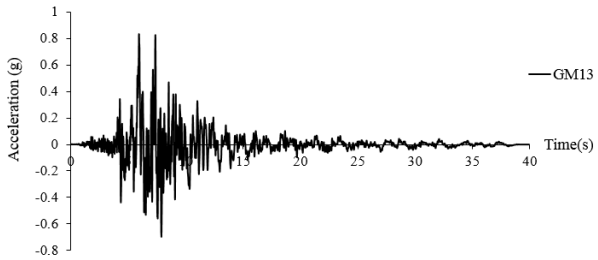

Figure A13. GM13

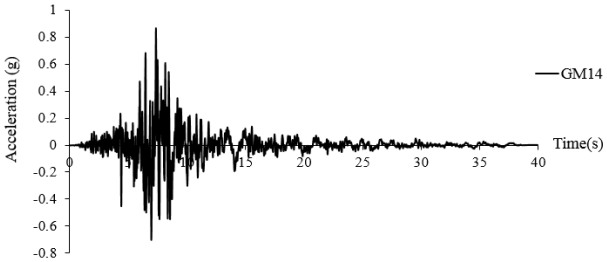

Figure A14. GM14

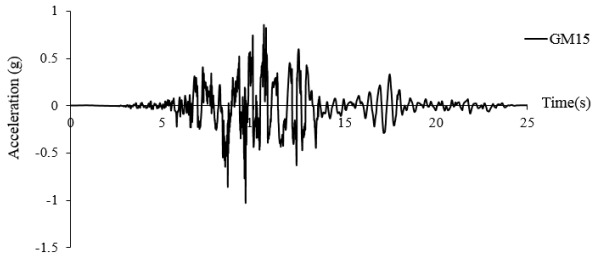

Figure A15. GM15

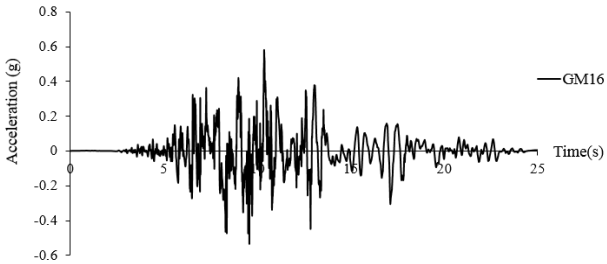

Figure A16. GM16

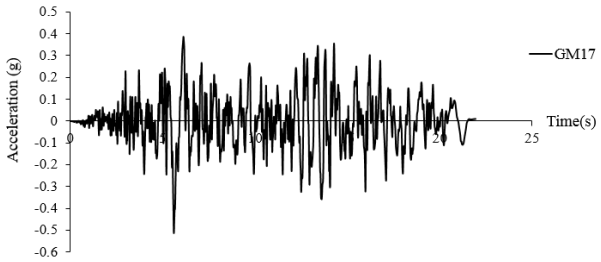

Figure A17. GM17

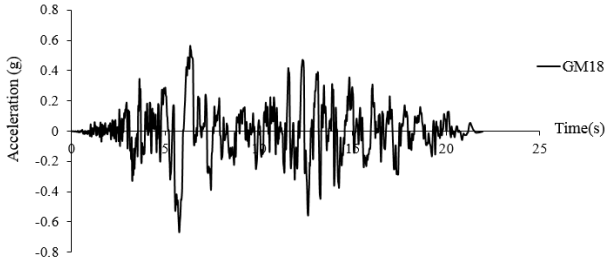

Figure A18. GM18

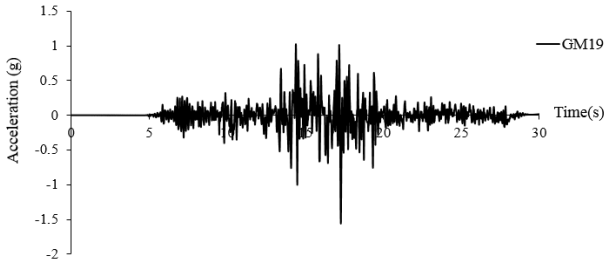

Figure A19. GM19

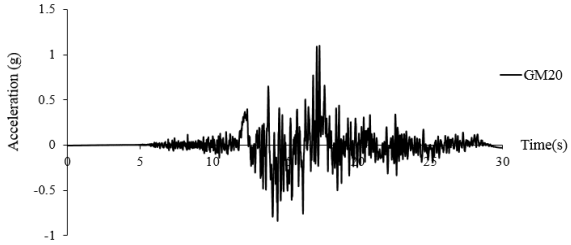

Figure A20. GM20

APPENDIX B.
DETAILS OF THE SIMULATIONS.

(1) Verification of Fell et al. (2009) Experimental Test

```
Verification-Fell                          !Analysis Descriptions
8 0 1 1 0 -1 0 1 1 0 0                     !Analysis Options
2 1 1 1 1 1 386 0 0 0.0001 30 1.0          !Frame Control Parameters (Unit: kips, inch)
0 200 200 0 1.0                            !Output and Plotting Control Parameters
5 0 0.000001                               !Iteration Control

NODES
1      0   0 1 1 0  0 0 0 0
2  117.5   0 0 1 0 -1 0 0 0

ELEMENTS
1 1 1 2 0 0 0

PROPS
1 FRAME                                    !HSS4x4x1/4
3 0 0 24 0 0 0 0
29000 11154 3.37 3.37 7.80 0.00 0.0 0.0 0.0 0.0
0.0 0.0 0.0 0.0
-157    -31.4    312.4   347.06 49.4     312.4   247      0
7.80 3.90 0.7 1.0 1.4 0.000 0.20 0.4 1.20 0.25 1 3

WEIGHT
1 0 0 0
2 0 0 0

LOADS
1 0 0 0
2 0 0 0

EQUAKE
3 1 0.01 1.0

START
1         0         0.00
2         1         0.11811
3         2         0.00
4         3         -0.11811
5         4         0.00
6         5         0.11811
```

7	6	0.00
8	7	-0.610
9	8	0.00
10	9	0.610
11	10	0.00
12	11	-0.610
13	12	0.00
14	13	0.610
15	14	0.00
16	15	-1.09843
17	16	0.00
18	17	1.09843
19	18	0.00
20	19	-1.09843
21	20	0.00
22	21	1.09843
23	22	0.00
24	23	-1.59055
25	24	0.00
26	25	1.59055
27	26	0.00
28	27	-1.59055
29	28	0.00
30	29	1.59055
31	30	0.00

(2) Verification of Tested Frame by Uriz (2005)

```
Uriz and Mahin Frame Experimental Test  !Analysis Descriptions
2 0 1 1 0 0 1 2 0 0 0                   !Analysis Options
8 12 8 5 1 2 386.4 5 5 0.0005 40 1.1675 !Frame Control Parameters
0 50 20 0 1.0 1.0                       !Output and Plotting Control Parameters
5 0 0.000001                            !Iteration Control

NODES
1    0    0  1 1 1   0 0 0  0
2   240   0  1 1 1   0 0 0  0
3    0   120  0 0 0   0 0 0  0
4   120 120  0 0 0   0 0 0  0
5   240 120  0 0 0   0 0 0  0
6    0   228  0 0 0   0 0 0  0
7   120 228  0 0 0   0 0 0  0
8   240 228  0 0 0   0 0 0  0
```

ELEMENTS
1 1 1 3 0 0 0
2 7 1 4 0 0 0
3 7 2 4 0 0 0
4 1 2 5 0 0 0
5 2 3 6 0 0 0
6 8 3 7 0 0 0
7 8 5 7 0 0 0
8 2 5 8 0 0 0
9 3 3 4 0 0 0
10 4 4 5 0 0 0
11 5 6 7 0 0 0
12 6 7 8 0 0 0

PROPS
1 Frame !W10x45-10ft_1st Level Column (Steel Beam-Column Element, Rigid-Rigid Ends)
3 0 0 1 0 0 0 0
29000 11153 13.3 0.0 248 0.0 0.0 0.0 0.0 0.0
0.0 0.0 0.0 0.0
-571.64 -114.33 2717.6 3019.56 146.3 2717.6 731.5 0

2 Frame !W10x45-9ft_2nd Level Column (Steel Beam-Column Element, Rigid-Rigid Ends)
3 0 0 1 0 0 0 0
29000 11153 13.3 0.0 248 0.0 0.0 0.0 0.0 0.0
0.0 0.0 0.0 0.0
-592.8 -118.6 2717.63019.56 146.3 2717.6 731.5 0

3 Frame !W21x117x10ft_1st st-Left Beam (Steel Beam-Column Element, Pin-Rigid Ends)
3 0 0 1 0 0 0 0
29000 11153 34.4 0.0 3540 0.0 0.0 0.0 0.0 0.0
0.0 0.0 0.0 0.0
-1822 -364.4 16189 17988 364.4 16189 1822 0

4 Frame !W21x117x10ft_1st st-Right Beam (Steel Beam-Column Element, Rigid-Pin Ends)
3 0 0 1 0 0 0 0
29000 11153 34.4 0.0 3540 0.0 0.0 0.0 0.0 0.0
0.0 0.0 0.0 0.0
-1822 -364.4 16189 17988 364.4 16189 1822 0

5 Frame !W21x117x10ft_2nd st-Left Beam (Steel Beam-Column Element, Pin-Rigid Ends)
3 1 0 1 0 0 0 0
29000 11153 34.4 0.0 3540 0.0 0.0 0.0 0.0 0.0
0.0 0.0 0.0 0.0
-1822 -364.4 16189 17988 364.4 16189 1822 0

6 Frame !W21x117x10ft_2nd st-Right Beam (Steel Beam-Column Element, Rigid-Pin Ends)
3 2 0 1 0 0 0 0
29000 11153 34.4 0.0 3540 0.0 0.0 0.0 0.0 0.0
0.0 0.0 0.0 0.0
-1822 -364.4 16189 17988 364.4 16189 1822 0

7 Frame !HSS6x6x3/8_1st Level Brace (Steel Beam-Column Element, Pin-Pin Ends)
3 3 0 24 0 0 0 0
29000 11153 7.58 0.0 39.5 0.0 0.0 0.0 0.0 0.0
0.0 0.0 0.0 0.0
-452.5 -90.5 861.73 957.48 90.5 861.73 452.5 0
39.5 13.2 0.7 1.25 1.3 0 0.2 0.25 1.2 1.4 0 3

8 Frame !HSS6x6x3/8_2nd Level Brace (Steel Beam-Column Element, Pin-Pin Ends)
3 3 0 24 0 0 0 0
29000 11153 7.58 0.0 39.5 0.0 0.0 0.0 0.0 0.0
0.0 0.0 0.0 0.0
-466.6 -93.32 861.73 957.48 91.86 861.73 459.34 0
39.5 13.2 0.7 1.25 1.3 0 0.2 0.25 1.2 1.4 0 3

WEIGHT
1 0.0 0.0 0.0
3 812.1 0.0 0.0
5 812.1 0.0 0.0
6 812.1 0.0 0.0
8 812.1 0.0 0.0

LOADS
1 0.0 0.0 0.0

EQUAKE
6 1 0.005 1.0 -1 0.0 0.0 1.0

(3) Simulation of 9-Story SCBF

```
9 story Weak Frame Seismic Analysis     !Analysis Descriptions
2 0 1 1 0 0 1 2 0 0 0                   !Analysis Options
45 78 24 5 1 2 386.4 5 5 0.0005 40 1.2  !Frame Control Parameters
0 50 20 0 1.0 1.0                       !Output and Plotting Control Parameters
5 0 0.000001                            !Iteration Control

NODES
1    0       0  1 1 0     0 0 0  0
2    360     0  1 1 0     0 0 0  0
3    0     156  0 0 0     0 0 0  0
4    180   156  0 0 0     0 0 0  0
5    360   156  0 0 0     3 0 0  0
6    0     312  0 0 0     0 0 0  0
7    360   312  0 0 0     0 0 0  0
8    0     468  0 0 0     0 0 0  0
9    180   468  0 0 0     0 0 0  0
10   360   468  0 0 0     8 0 0  0
11   0     624  0 0 0     0 0 0  0
12   360   624  0 0 0     0 0 0  0
13   0     780  0 0 0     0 0 0  0
14   180   780  0 0 0     0 0 0  0
15   360   780  0 0 0    13 0 0  0
16   0     936  0 0 0     0 0 0  0
17   360   936  0 0 0     0 0 0  0
18   0    1092  0 0 0     0 0 0  0
19   180  1092  0 0 0     0 0 0  0
20   360  1092  0 0 0    18 0 0  0
21   0    1248  0 0 0     0 0 0  0
22   360  1248  0 0 0     0 0 0  0
23   0    1404  0 0 0     0 0 0  0
24   180  1404  0 0 0     0 0 0  0
25   360  1404  0 0 0    23 0 0  0
26   720     0  1 1 1     0 0 0  0
27   720   156  0 0 1     3 0 0  0
28   720   312  0 0 1     0 0 0  0
29   720   468  0 0 1     8 0 0  0
30   720   624  0 0 1     0 0 0  0
31   720   780  0 0 1    13 0 0  0
32   720   936  0 0 1     0 0 0  0
33   720  1092  0 0 1    18 0 0  0
```

34 720 1248 0 0 1 0 0 0 0
35 720 1404 0 0 1 23 0 0 0
36 155 156 0 0 0 0 0 0 0
37 205 156 0 0 0 0 0 0 0
38 155 468 0 0 0 0 0 0 0
39 205 468 0 0 0 0 0 0 0
40 155 780 0 0 0 0 0 0 0
41 205 780 0 0 0 0 0 0 0
42 155 1092 0 0 0 0 0 0 0
43 205 1092 0 0 0 0 0 0 0
44 155 1404 0 0 0 0 0 0 0
45 205 1404 0 0 0 0 0 0 0

ELEMENTS

1 1 1 3 0 0 0
2 10 1 4 0 0 0
3 10 2 4 0 0 0
4 1 2 5 0 0 0
5 2 3 6 0 0 0
6 10 4 6 0 0 0
7 10 4 7 0 0 0
8 2 5 7 0 0 0
9 3 6 8 0 0 0
10 10 6 9 0 0 0
11 10 7 9 0 0 0
12 3 7 10 0 0 0
13 20 8 11 0 0 0
14 10 9 11 0 0 0
15 10 9 12 0 0 0
16 20 10 12 0 0 0
17 4 11 13 0 0 0
18 11 11 14 0 0 0
19 11 12 14 0 0 0
20 4 12 15 0 0 0
21 21 13 16 0 0 0
22 11 14 16 0 0 0
23 11 14 17 0 0 0
24 21 15 17 0 0 0
25 5 16 18 0 0 0
26 12 16 19 0 0 0
27 12 17 19 0 0 0
28 5 17 20 0 0 0
29 22 18 21 0 0 0

30 12 19 21 0 0 0
31 12 19 22 0 0 0
32 22 20 22 0 0 0
33 6 21 23 0 0 0
34 13 21 24 0 0 0
35 13 22 24 0 0 0
36 6 22 25 0 0 0
37 7 3 36 0 0 0
38 8 37 5 0 0 0
39 9 6 7 0 0 0
40 7 8 38 0 0 0
41 8 39 10 0 0 0
42 9 11 12 0 0 0
43 7 13 40 0 0 0
44 8 41 15 0 0 0
45 16 16 17 0 0 0
46 7 18 42 0 0 0
47 8 43 20 0 0 0
48 17 21 22 0 0 0
49 18 23 44 0 0 0
50 19 45 25 0 0 0
51 14 26 27 0 0 0
52 14 27 28 0 0 0
53 14 28 29 0 0 0
54 14 29 30 0 0 0
55 14 30 31 0 0 0
56 14 31 32 0 0 0
57 14 32 33 0 0 0
58 14 33 34 0 0 0
59 14 34 35 0 0 0
60 15 5 27 0 0 0
61 15 7 28 0 0 0
62 15 10 29 0 0 0
63 15 12 30 0 0 0
64 15 15 31 0 0 0
65 15 17 32 0 0 0
66 15 20 33 0 0 0
67 15 22 34 0 0 0
68 15 25 35 0 0 0
69 23 36 4 0 0 0
70 23 4 37 0 0 0
71 23 38 9 0 0 0
72 23 9 39 0 0 0

73 23 40 14 0 0 0
74 23 14 41 0 0 0
75 23 42 19 0 0 0
76 23 19 43 0 0 0
77 24 44 24 0 0 0
78 24 24 45 0 0 0

PROPS
1 Frame !W14x550x13ft_1st Level Braced Column (Steel Beam-Column Element, Rigid-Rigid Ends)
3 0 0 1 0 0 0 0
29000 11153 162 0.0 9430 0.0 0.0 0.0 0.0 0.0
0.0 0.0 0.0 0.0
-7411 -1482 53100 59000 1620 53100 8100 0

2 Frame !W14x550x13ft_2nd Level Braced Column (Steel Beam-Column Element, Rigid-Rigid Ends)
3 0 0 1 0 0 0 0
29000 11153 162 0.0 9430 0.0 0.0 20.0 0.0 0.0
0.0 0.0 0.0 0.0
-7411 -1482 53100 59000 1620 53100 8100 0

3 Frame !W14x370x13ft_3rd Level Braced Column (Steel Beam-Column Element, Rigid-Rigid Ends)
3 0 0 1 0 0 0 0
29000 11153 109 0.0 5440 0.0 20.0 0.0 0.0 0.0
0.0 0.0 0.0 0.0
-4944 -989 33120 36800 1090 33120 5450 0

4 Frame !W14x233x13ft_5th Level Braced Column (Steel Beam-Column Element, Rigid-Rigid Ends)
3 0 0 1 0 0 0 0
29000 11153 68.5 0.0 3010 0.0 20.0 0.0 0.0 0.0
0.0 0.0 0.0 0.0
-3078 -616 19620 21800 685 19620 3425 0

5 Frame !W14x132x13ft_7th Level Braced Column (Steel Beam-Column Element, Rigid-Rigid Ends)
3 0 0 1 0 0 0 0
29000 11153 38.8 0.0 1530 0.0 20.0 0.0 0.0 0.0
0.0 0.0 0.0 0.0
-1711.11 -342.2 10530 11700 388 10530 1940 0

6 Frame !W14x48x13ft_9th Level Braced Column (Steel Beam-Column Element, Rigid-Rigid Ends)
3 0 0 1 0 0 0 0
29000 11153 14.1 0.0 484 0.0 20.0 0.0 0.0 0.0
0.0 0.0 0.0 0.0
-433.3 -86.7 3528 3920 141 3528 705 0

7 Frame !W18x65x15ft_Left Beam (Steel Beam-Column Element, Pin-Rigid Ends)
3 1 0 1 0 0 0 0
29000 11153 19.1 0.0 1070 0.0 0.0 0.0 0.0 0.0
0.0 0.0 0.0 0.0
-776.15 -155.23 5985 6650 191 5985 955 0

8 Frame !W18x65x15ft_Right Beam (Steel Beam-Column Element, Rigid-Pin Ends)
3 2 0 1 0 0 0 0
29000 11153 19.1 0.0 1070 0.0 0.0 0.0 0.0 0.0
0.0 0.0 0.0 0.0
-776.15 -155.23 5985 6650 191 5985 955 0

9 Frame !W21x111x30ft_ Beam (Steel Beam-Column Element, Rigid-Rigid Ends)
3 0 0 1 0 0 0 0
29000 11153 32.6 0.0 2670 0.0 30.0 30.0 0.0 0.0
0.0 0.0 0.0 0.0
-1519.16 -303.83 12555 13950 326 12555 1630 0

10 Frame !1st Level Brace HSS14x0.625
3 3 0 24 0 0 0 0
29000 11153 24.5 0.0 552 0.0 0.0 0.0 0.0 0.0
0.0 0.0 0.0 0.0
-882.4 -176.5 3969 4410 206 3969 1029 0
552 105 0.7 1.0 1.0 0.00 0.20 0.25 1.20 1.4 0 3

11 Frame !5th Level Brace HSS10.0x10.0x5/8
3 3 0 24 0 0 0 0
29000 11153 21 0.0 304 0.0 0.0 0.0 0.0 0.0
0.0 0.0 0.0 0.0
-743 -149 3030.5 3367 193 3030.5966 0
304 73.2 0.7 1.0 1.0 0.00 0.20 0.25 1.20 1.4 0 3

12 Frame !7th Level Brace HSS10.0x0.62500
3 3 0 24 0 0 0 0
29000 11153 17.2 0.0 191 0.0 0.0 0.0 0.0 0.0
0.0 0.0 0.0 0.0
-529 -106 1951 2167 144.5 1951 722 0
191 51.6 0.7 1.0 1.0 0.00 0.20 0.95 1.20 0.25 0 3

13 Frame !9th Level Brace HSS8.625x0.375
3 3 0 24 0 0 0 0
29000 11153 9.07 0.0 77.8 0.0 0.0 0.0 0.0 0.0
0.0 0.0 0.0 0.0
-254.4 -51 903.4 1004 76 903.4 381 0
77.8 23.9 0.7 1.0 1.0 0.00 0.20 0.95 1.20 0.25 0 3

14 Frame !W14x550x13ft_P-delta Column (Steel Beam-Column Element, Pin-Pin Ends)
3 3 0 1 0 0 0 0
29000 11153 162 0.0 9430 0.0 0.0 0.0 0.0 0.0
0.0 0.0 0.0 0.0
-7411 -1482 53100 59000 1620 53100 8100 0

15 Frame !Rigid Links For Beams
1 3 0 0 0 0 0 0
29000000 11153000 100 0.0 100 0.0 0.0 0.0 0.0 0.0

16 Frame !W21x93x30ft_ Beam (Steel Beam-Column Element, Pin-Pin Ends)
3 0 0 1 0 0 0 0
29000 11153 27.3 0.0 2070 0.0 30.0 30.0 0.0 0.0
0.0 0.0 0.0 0.0
-1145.9 -229.19 9945 11050 273 9945 1365 0

17 Frame !W18x86x30ft_ Beam (Steel Beam-Column Element, Pin-Pin Ends)
3 0 0 1 0 0 0 0
29000 11153 25.3 0.0 1530 0.0 30.0 30.0 0.0 0.0
0.0 0.0 0.0 0.0
-1081.2 -216.2 8370 9300 253 8370 1265 0

18 Frame !W30x211x30ft_ Left Beam (Steel Beam-Column Element, Pin-Rigid Ends)
3 1 0 1 0 0 0 0
29000 11153 62.3 0.0 10300 0.0 0.0 0.0 0.0 0.0
0.0 0.0 0.0 0.0
-2967.2 -593.4 33795 37550 623 33795 3115 0

19 Frame !W30x211x30ft_ Right Beam (Steel Beam-Column Element, Rigid-Pin Ends)
3 2 0 1 0 0 0 0
29000 11153 62.3 0.0 10300 0.0 0.0 0.0 0.0 0.0
0.0 0.0 0.0 0.0
-2967.2 -593.4 33795 37550 623 33795 3115 0

20 Frame !W14x370x13ft_4th Level Braced Column (Steel Beam-Column Element, Rigid-Rigid Ends)
3 0 0 1 0 0 0 0
29000 11153 109 0.0 5440 0.0 0.0 20.0 0.0 0.0
0.0 0.0 0.0 0.0
-4944 -989 33120 36800 1090 33120 5450 0

21 Frame !W14x233x13ft_6th Level Braced Column (Steel Beam-Column Element, Rigid-Rigid Ends)
3 0 0 1 0 0 0 0
29000 11153 68.5 0.0 3010 0.0 0.0 20.0 0.0 0.0
0.0 0.0 0.0 0.0
-3078 -616 19620 21800 685 19620 3425 0

22 Frame !W14x132x13ft_8th Level Braced Column (Steel Beam-Column Element, Rigid-Rigid Ends)
3 0 0 1 0 0 0 0
29000 11153 38.8 0.0 1530 0.0 0.0 20.0 0.0 0.0
0.0 0.0 0.0 0.0
-1711.11 -342.2 10530 11700 388 10530 1940 0

23 Frame !W18x65x15ft_Middle Beam(Rigid) (Steel Beam-Column Element, Rigid-Rigid Ends)
3 0 0 1 0 0 0 0
2900000 11153000 1910 0.0 10700 0.0 0.0 0.0 0.0 0.0
0.0 0.0 0.0 0.0
-776.15 -155.23 59850 66500 191 5985 955 0

24 Frame !W30x211x30ft_ Middle Beam(Rigid) (Steel Beam-Column Element, Rigid-Rigid Ends)
3 0 0 1 0 0 0 0
2900000 11153000 6230 0.0 10300 0.0 0.0 0.0 0.0 0.0
0.0 0.0 0.0 0.0
-2967.2 -593.4 33795 37550 623 33795 3115 0

WEIGHT
1 0.0 0.0 0.0
27 450 0.0 0.0
28 450 0.0 0.0
29 450 0.0 0.0
30 450 0.0 0.0
31 450 0.0 0.0
32 450 0.0 0.0
33 450 0.0 0.0
34 450 0.0 0.0
35 450 0.0 0.0

LOADS

1	0.0	0.0	0.0
3	0.0	-45.0	0.0
5	0.0	-45.0	0.0
6	0.0	-45.0	0.0
7	0.0	-45.0	0.0
8	0.0	-45.0	0.0
10	0.0	-45.0	0.0
11	0.0	-45.0	0.0
12	0.0	-45.0	0.0
13	0.0	-45.0	0.0
15	0.0	-45.0	0.0
16	0.0	-45.0	0.0
17	0.0	-45.0	0.0
18	0.0	-45.0	0.0
20	0.0	-45.0	0.0
21	0.0	-45.0	0.0
22	0.0	-45.0	0.0
23	0.0	-45.0	0.0
25	0.0	-45.0	0.0
27	0.0	-456.0	0.0
28	0.0	-456.0	0.0
29	0.0	-456.0	0.0
30	0.0	-456.0	0.0
31	0.0	-456.0	0.0
32	0.0	-456.0	0.0
33	0.0	-456.0	0.0
34	0.0	-456.0	0.0
35	0.0	-456.0	0.0

EQUAKE

6 1 0.005 1.0 -1 0.0 0.0 1.0

(4) Simulation of 9-Story BCBF

```
9 story Weak BCBF Seismic Analysis     !Analysis Descriptions
2 0 1 1 0 0 1 2 0 0 0                  !Analysis Options
45 78 24 5 1 2 386.4 5 5 0.0005 40 1.2 !Frame Control Parameters
0 50 20 0 1.0 1.0                      !Output and Plotting Control Parameters
5 0 0.000001                           !Iteration Control

NODES
1    0       0  1 1 0     0 0 0  0
2   360      0  1 1 0     0 0 0  0
3    0     156  0 0 0     0 0 0  0
4   180    156  0 0 0     0 0 0  0
5   360    156  0 0 0     3 0 0  0
6    0     312  0 0 0     0 0 0  0
7   360    312  0 0 0     0 0 0  0
8    0     468  0 0 0     0 0 0  0
9   180    468  0 0 0     0 0 0  0
10  360    468  0 0 0     8 0 0  0
11   0     624  0 0 0     0 0 0  0
12  360    624  0 0 0     0 0 0  0
13   0     780  0 0 0     0 0 0  0
14  180    780  0 0 0     0 0 0  0
15  360    780  0 0 0    13 0 0  0
16   0     936  0 0 0     0 0 0  0
17  360    936  0 0 0     0 0 0  0
18   0    1092  0 0 0     0 0 0  0
19  180   1092  0 0 0     0 0 0  0
20  360   1092  0 0 0    18 0 0  0
21   0    1248  0 0 0     0 0 0  0
22  360   1248  0 0 0     0 0 0  0
23   0    1404  0 0 0     0 0 0  0
24  180   1404  0 0 0     0 0 0  0
25  360   1404  0 0 0    23 0 0  0
26  720      0  1 1 1     0 0 0  0
27  720    156  0 0 1     3 0 0  0
28  720    312  0 0 1     0 0 0  0
29  720    468  0 0 1     8 0 0  0
30  720    624  0 0 1     0 0 0  0
31  720    780  0 0 1    13 0 0  0
32  720    936  0 0 1     0 0 0  0
33  720   1092  0 0 1    18 0 0  0
```

34 720 1248 0 0 1 0 0 0 0
35 720 1404 0 0 1 23 0 0 0
36 155 156 0 0 0 0 0 0 0
37 205 156 0 0 0 0 0 0 0
38 155 468 0 0 0 0 0 0 0
39 205 468 0 0 0 0 0 0 0
40 155 780 0 0 0 0 0 0 0
41 205 780 0 0 0 0 0 0 0
42 155 1092 0 0 0 0 0 0 0
43 205 1092 0 0 0 0 0 0 0
44 155 1404 0 0 0 0 0 0 0
45 205 1404 0 0 0 0 0 0 0

ELEMENTS

1 1 1 3 0 0 0
2 10 1 4 0 0 0
3 10 2 4 0 0 0
4 1 2 5 0 0 0
5 2 3 6 0 0 0
6 10 4 6 0 0 0
7 10 4 7 0 0 0
8 2 5 7 0 0 0
9 3 6 8 0 0 0
10 10 6 9 0 0 0
11 10 7 9 0 0 0
12 3 7 10 0 0 0
13 20 8 11 0 0 0
14 10 9 11 0 0 0
15 10 9 12 0 0 0
16 20 10 12 0 0 0
17 4 11 13 0 0 0
18 11 11 14 0 0 0
19 11 12 14 0 0 0
20 4 12 15 0 0 0
21 21 13 16 0 0 0
22 11 14 16 0 0 0
23 11 14 17 0 0 0
24 21 15 17 0 0 0
25 5 16 18 0 0 0
26 12 16 19 0 0 0
27 12 17 19 0 0 0
28 5 17 20 0 0 0
29 22 18 21 0 0 0

30 12 19 21 0 0 0
31 12 19 22 0 0 0
32 22 20 22 0 0 0
33 6 21 23 0 0 0
34 13 21 24 0 0 0
35 13 22 24 0 0 0
36 6 22 25 0 0 0
37 7 3 36 0 0 0
38 8 37 5 0 0 0
39 9 6 7 0 0 0
40 7 8 38 0 0 0
41 8 39 10 0 0 0
42 9 11 12 0 0 0
43 7 13 40 0 0 0
44 8 41 15 0 0 0
45 16 16 17 0 0 0
46 7 18 42 0 0 0
47 8 43 20 0 0 0
48 17 21 22 0 0 0
49 18 23 44 0 0 0
50 19 45 25 0 0 0
51 14 26 27 0 0 0
52 14 27 28 0 0 0
53 14 28 29 0 0 0
54 14 29 30 0 0 0
55 14 30 31 0 0 0
56 14 31 32 0 0 0
57 14 32 33 0 0 0
58 14 33 34 0 0 0
59 14 34 35 0 0 0
60 15 5 27 0 0 0
61 15 7 28 0 0 0
62 15 10 29 0 0 0
63 15 12 30 0 0 0
64 15 15 31 0 0 0
65 15 17 32 0 0 0
66 15 20 33 0 0 0
67 15 22 34 0 0 0
68 15 25 35 0 0 0
69 23 36 4 0 0 0
70 23 4 37 0 0 0
71 23 38 9 0 0 0
72 23 9 39 0 0 0

73 23 40 14 0 0 0
74 23 14 41 0 0 0
75 23 42 19 0 0 0
76 23 19 43 0 0 0
77 24 44 24 0 0 0
78 24 24 45 0 0 0

PROPS
1 Frame !W14x550x13ft_1st Level Braced Column (Steel Beam-Column Element, Rigid-Rigid Ends)
3 0 0 1 0 0 0 0
29000 11153 162 0.0 9430 0.0 0.0 0.0 0.0 0.0
0.0 0.0 0.0 0.0
-7411 -1482 53100 59000 1620 53100 8100 0

2 Frame !W14x550x13ft_2nd Level Braced Column (Steel Beam-Column Element, Rigid-Rigid Ends)
3 0 0 1 0 0 0 0
29000 11153 162 0.0 9430 0.0 0.0 20.0 0.0 0.0
0.0 0.0 0.0 0.0
-7411 -1482 53100 59000 1620 53100 8100 0

3 Frame !W14x370x13ft_3rd Level Braced Column (Steel Beam-Column Element, Rigid-Rigid Ends)
3 0 0 1 0 0 0 0
29000 11153 109 0.0 5440 0.0 20.0 0.0 0.0 0.0
0.0 0.0 0.0 0.0
-4944 -989 33120 36800 1090 33120 5450 0

4 Frame !W14x233x13ft_5th Level Braced Column (Steel Beam-Column Element, Rigid-Rigid Ends)
3 0 0 1 0 0 0 0
29000 11153 68.5 0.0 3010 0.0 20.0 0.0 0.0 0.0
0.0 0.0 0.0 0.0
-3078 -616 19620 21800 685 19620 3425 0

5 Frame !W14x132x13ft_7th Level Braced Column (Steel Beam-Column Element, Rigid-Rigid Ends)
3 0 0 1 0 0 0 0
29000 11153 38.8 0.0 1530 0.0 20.0 0.0 0.0 0.0
0.0 0.0 0.0 0.0
-1711.11 -342.2 10530 11700 388 10530 1940 0

6 Frame !W14x48x13ft_9th Level Braced Column (Steel Beam-Column Element, Rigid-Rigid Ends)
3 0 0 1 0 0 0 0
29000 11153 14.1 0.0 484 0.0 20.0 0.0 0.0 0.0
0.0 0.0 0.0 0.0
-433.3 -86.7 3528 3920 141 3528 705 0

7 Frame !W18x65x15ft_Left Beam (Steel Beam-Column Element, Pin-Rigid Ends)
3 1 0 1 0 0 0 0
29000 11153 19.1 0.0 1070 0.0 0.0 0.0 0.0 0.0
0.0 0.0 0.0 0.0
-776.15 -155.23 5985 6650 191 5985 955 0

8 Frame !W18x65x15ft_Right Beam (Steel Beam-Column Element, Rigid-Pin Ends)
3 2 0 1 0 0 0 0
29000 11153 19.1 0.0 1070 0.0 0.0 0.0 0.0 0.0
0.0 0.0 0.0 0.0
-776.15 -155.23 5985 6650 191 5985 955 0

9 Frame !W21x111x30ft_ Beam (Steel Beam-Column Element, Rigid-Rigid Ends)
3 0 0 1 0 0 0 0
29000 11153 32.6 0.0 2670 0.0 30.0 30.0 0.0 0.0
0.0 0.0 0.0 0.0
-1519.16 -303.83 12555 13950 326 12555 1630 0

10 Frame !1st Level Brace HSS14x0.625
3 3 0 1 0 0 0 0
29000 11153 24.5 0.0 552 0.0 0.0 0.0 0.0 0.0
0.0 0.0 0.0 0.0
-1029 -206 3969 4410 206 3969 1029 0

11 Frame !5th Level Brace HSS10.0x10.0x5/8
3 3 0 1 0 0 0 0
29000 11153 21 0.0 304 0.0 0.0 0.0 0.0 0.0
0.0 0.0 0.0 0.0
-966 -193 3030.5 3367 193 3030.5966 0

12 Frame !7th Level Brace HSS10.0x0.62500
3 3 0 1 0 0 0 0
29000 11153 17.2 0.0 191 0.0 0.0 0.0 0.0 0.0
0.0 0.0 0.0 0.0
-722 -144.5 1951 2167 144.5 1951 722 0

13 Frame !9th Level Brace HSS8.625x0.375
3 3 0 1 0 0 0 0
29000 11153 9.07 0.0 77.8 0.0 0.0 0.0 0.0 0.0
0.0 0.0 0.0 0.0
-381 -76 903.4 1004 76 903.4 381 0

14 Frame !W14x550x13ft_P-delta Column (Steel Beam-Column Element, Pin-Pin Ends)
3 3 0 1 0 0 0 0
29000 11153 162 0.0 9430 0.0 0.0 0.0 0.0 0.0
0.0 0.0 0.0 0.0
-7411 -1482 53100 59000 1620 53100 8100 0

15 Frame !Rigid Links For Beams
1 3 0 0 0 0 0 0
29000000 11153000 100 0.0 100 0.0 0.0 0.0 0.0 0.0

16 Frame !W21x93x30ft_ Beam (Steel Beam-Column Element, Pin-Pin Ends)
3 0 0 1 0 0 0 0
29000 11153 27.3 0.0 2070 0.0 30.0 30.0 0.0 0.0
0.0 0.0 0.0 0.0
-1145.9 -229.19 9945 11050 273 9945 1365 0

17 Frame !W18x86x30ft_ Beam (Steel Beam-Column Element, Pin-Pin Ends)
3 0 0 1 0 0 0 0
29000 11153 25.3 0.0 1530 0.0 30.0 30.0 0.0 0.0
0.0 0.0 0.0 0.0
-1081.2 -216.2 8370 9300 253 8370 1265 0

18 Frame !W30x211x30ft_ Left Beam (Steel Beam-Column Element, Pin-Rigid Ends)
3 1 0 1 0 0 0 0
29000 11153 62.3 0.0 10300 0.0 0.0 0.0 0.0 0.0
0.0 0.0 0.0 0.0
-2967.2 -593.4 33795 37550 623 33795 3115 0

19 Frame !W30x211x30ft_ Right Beam (Steel Beam-Column Element, Rigid-Pin Ends)
3 2 0 1 0 0 0 0
29000 11153 62.3 0.0 10300 0.0 0.0 0.0 0.0 0.0
0.0 0.0 0.0 0.0
-2967.2 -593.4 33795 37550 623 33795 3115 0

20 Frame !W14x370x13ft_4th Level Braced Column (Steel Beam-Column Element, Rigid-Rigid Ends)
3 0 0 1 0 0 0 0
29000 11153 109 0.0 5440 0.0 0.0 20.0 0.0 0.0
0.0 0.0 0.0 0.0
-4944 -989 33120 36800 1090 33120 5450 0

21 Frame !W14x233x13ft_6th Level Braced Column (Steel Beam-Column Element, Rigid-Rigid Ends)
3 0 0 1 0 0 0 0
29000 11153 68.5 0.0 3010 0.0 0.0 20.0 0.0 0.0
0.0 0.0 0.0 0.0
-3078 -616 19620 21800 685 19620 3425 0

22 Frame !W14x132x13ft_8th Level Braced Column (Steel Beam-Column Element, Rigid-Rigid Ends)
3 0 0 1 0 0 0 0
29000 11153 38.8 0.0 1530 0.0 0.0 20.0 0.0 0.0
0.0 0.0 0.0 0.0
-1711.11 -342.2 10530 11700 388 10530 1940 0

23 Frame !W18x65x15ft_Middle Beam(Rigid) (Steel Beam-Column Element, Rigid-Rigid Ends)
3 0 0 1 0 0 0 0
2900000 11153000 1910 0.0 10700 0.0 0.0 0.0 0.0 0.0
0.0 0.0 0.0 0.0
-776.15 -155.23 59850 66500 191 5985 955 0

24 Frame !W30x211x30ft_ Middle Beam(Rigid) (Steel Beam-Column Element, Rigid-Rigid Ends)
3 0 0 1 0 0 0 0
2900000 11153000 6230 0.0 10300 0.0 0.0 0.0 0.0 0.0
0.0 0.0 0.0 0.0
-2967.2 -593.4 33795 37550 623 33795 3115 0

WEIGHT
1 0.0 0.0 0.0
27 450 0.0 0.0
28 450 0.0 0.0
29 450 0.0 0.0
30 450 0.0 0.0
31 450 0.0 0.0
32 450 0.0 0.0
33 450 0.0 0.0
34 450 0.0 0.0
35 450 0.0 0.0

LOADS
1 0.0 0.0 0.0
3 0.0 -45.0 0.0
5 0.0 -45.0 0.0
6 0.0 -45.0 0.0
7 0.0 -45.0 0.0

8 0.0 -45.0 0.0
10 0.0 -45.0 0.0
11 0.0 -45.0 0.0
12 0.0 -45.0 0.0
13 0.0 -45.0 0.0
15 0.0 -45.0 0.0
16 0.0 -45.0 0.0
17 0.0 -45.0 0.0
18 0.0 -45.0 0.0
20 0.0 -45.0 0.0
21 0.0 -45.0 0.0
22 0.0 -45.0 0.0
23 0.0 -45.0 0.0
25 0.0 -45.0 0.0
27 0.0 -456.0 0.0
28 0.0 -456.0 0.0
29 0.0 -456.0 0.0
30 0.0 -456.0 0.0
31 0.0 -456.0 0.0
32 0.0 -456.0 0.0
33 0.0 -456.0 0.0
34 0.0 -456.0 0.0
35 0.0 -456.0 0.0

EQUAKE
6 1 0.005 1.0 -1 0.0 0.0 1.0